



---

# Precast, Prestressed Concrete Bent Caps: Volume 1 Preliminary Design Considerations and Experimental Test Program

Technical Report 0-6863-R1-Vol1

---

Cooperative Research Program

TEXAS A&M TRANSPORTATION INSTITUTE  
COLLEGE STATION, TEXAS

in cooperation with the  
Federal Highway Administration and the  
Texas Department of Transportation  
<http://tti.tamu.edu/documents/0-6863-R1-Vol1.pdf>



1. Report No. FHWA/TX-18/0-6863-R1-Vol1		2. Government Accession No.		3. Recipient's Catalog No.	
4. Title and Subtitle PRECAST, PRESTRESSED CONCRETE BENT CAPS: VOLUME 1 PRELIMINARY DESIGN CONSIDERATIONS AND EXPERIMENTAL TEST PROGRAM				5. Report Date Published: April 2018	
				6. Performing Organization Code	
7. Author(s) Anna C. Birely, John B. Mander, Ju Dong Lee, Codi D. McKee, Kevin J. Yole, and Usha R. Barooah				8. Performing Organization Report No. Report 0-6863-R1-Vol1	
9. Performing Organization Name and Address Texas A&M Transportation Institute College Station, Texas 77843-3135				10. Work Unit No. (TRAIS)	
				11. Contract or Grant No. Project 0-6863	
12. Sponsoring Agency Name and Address Texas Department of Transportation Research and Technology Implementation Office 125 E. 11 <sup>th</sup> Street Austin, Texas 78701-2483				13. Type of Report and Period Covered Technical Report: January 2015–November 2017	
				14. Sponsoring Agency Code	
15. Supplementary Notes Project performed in cooperation with the Texas Department of Transportation and the Federal Highway Administration. Project Title: Develop Strong and Serviceable Details for Precast, Prestressed Concrete Bent Cap Standards That Can Be Implemented on Everyday Bridge Construction Projects URL: <a href="http://tti.tamu.edu/documents/0-6863-R1-Vol1.pdf">http://tti.tamu.edu/documents/0-6863-R1-Vol1.pdf</a>					
16. Abstract Precast prestressed concrete bent caps may provide significant benefits by enabling accelerated construction of bridge substructures and improve longevity by reducing the propensity for cracking. The Texas Department of Transportation enables the use of precast reinforced concrete (RC) bent caps through standard connection details that allow contractors the option of cast-in-place or precast caps. A largely unrealized benefit of precast caps is the use of prestressing to enable additional fabrication options and to reduce or eliminate cracking. To enable widespread use, the design and behavior of pretensioned bent caps is explored through a comprehensive study consisting of a literature review, a design study, experimental tests, and with a discussion of the results. Design for flexure is based upon the concept of zero tensile stresses under dead loads, thereby ensuring any cracks close upon removal of live loads. A modified pocket connection is designed to improve constructability and minimize the potential negative effects of prestressing at the reduced cross-section. Full-scale bent caps were tested under indeterminate loads representative of those in multicolumn bents. An RC specimen was designed, constructed, and tested to serve as a performance baseline. Pretensioned caps investigate the spacing of shear spacing, use of voids, and void detailing. Pretensioned caps exhibit significantly reduced flexure cracking, with the ability to fully close upon removal of live load. Bent caps with voids were susceptible to minor shear cracking under design loads, with minimal impact of void detailing. Pocket connections provided adequate performance under design loads. The experimental findings validate the design and construction concepts, which may be useful in developing design and construction recommendations.					
17. Key Words Pretensioned Concrete, Bent Caps, Pier Caps, Pocket Connections, Interior Void, Serviceability, Full-Scale			18. Distribution Statement No restrictions. This document is available to the public through NTIS: National Technical Information Service Alexandria, Virginia <a href="http://www.ntis.gov">http://www.ntis.gov</a>		
19. Security Classif.(of this report) Unclassified		20. Security Classif.(of this page) Unclassified		21. No. of Pages 318	22. Price



**PRECAST, PRESTRESSED CONCRETE BENT CAPS: VOLUME 1  
PRELIMINARY DESIGN CONSIDERATIONS AND EXPERIMENTAL  
TEST PROGRAM**

by

Anna C. Birely, Ph.D.  
Assistant Professor  
Zachry Department of Civil Engineering  
Assistant Research Scientist  
Texas A&M Transportation Institute

John B. Mander, Ph.D.  
Zachry Professor of Design and Construction Integration  
Zachry Department of Civil Engineering  
Research Scientist  
Texas A&M Transportation Institute

and

Ju Dong Lee, Codi D. McKee, Kevin J. Yole, and Usha R. Barooah  
Graduate Assistant Researchers  
Texas A&M Transportation Institute

Report 0-6863-R1-Vol1  
Project 0-6863

Project Title: Develop Strong and Serviceable Details for Precast, Prestressed Concrete Bent Cap  
Standards That Can Be Implemented on Everyday Bridge Construction Projects

Performed in cooperation with the  
Texas Department of Transportation  
and the  
Federal Highway Administration

Published: April 2018

TEXAS A&M TRANSPORTATION INSTITUTE  
College Station, Texas 77843-3135



## **DISCLAIMER**

This research was performed in cooperation with the Texas Department of Transportation (TxDOT) and the Federal Highway Administration (FHWA). The contents of this report reflect the views of the authors, who are responsible for the facts and the accuracy of the data presented herein. The contents do not necessarily reflect the official view or policies of the FHWA or TxDOT. This report does not constitute a standard, specification, or regulation.

This report is not intended for construction, bidding, or permit purposes. The researcher in charge of the project was Anna C. Birely. The United States Government and the State of Texas do not endorse products or manufacturers. Trade or manufacturers' names appear herein solely because they are considered essential to the object of this report.

## **ACKNOWLEDGMENTS**

This project was conducted in cooperation with TxDOT and FHWA under Project 0-6863 with Darrin Jensen serving as project director. The authors would like to thank the input of the project monitoring committee, including Christopher Miller, Courtney Holle, Graham Bettis, Todd Speck, Jason Tucker, Manuel Pardon Jr., Susana Ceballos, Frank Estrada III, Dennis Johnson, and Roger Lopez.

Pretensioned bent caps were fabricated by Bexar Concrete Works in San Antonio, Texas. The contributions of Jorge Hinojosa and his staff are greatly appreciated. Ready-mix concrete was provided by Martin Marietta Materials in Bryan, Texas. The assistance of Johnny Salinas is greatly appreciated.

The project was conducted at Texas A&M University through the Texas A&M Transportation Institute. The authors would like to thank the support of Maria Medrano and Kanchan Pandey. Experimental tests were conducted in the High Bay Structural and Materials Testing Laboratory, with assistance from Dr. Peter Keating, Matthew Potter, Charles Droddy, and Ramiro Vanoye-Trevino. The support of graduate and undergraduate student workers in fabricating, instrumenting, and testing the bent caps is greatly appreciated. These students include Alexis Velazquez, Nick Danney, Josh Ortiz, Benito Soto, Ricardo Espinoza, Brandon Oxley, Vanessa Hernandez, John Teets, Walker Needles, Jacob Page, J. Bryce Martin, Daniel Kruzick, Natasha Boger, Sun Hee Park, and Jilong Cui.



# TABLE OF CONTENTS

	<b>Page</b>
<b>List of Figures</b> .....	<b>xi</b>
<b>List of Tables</b> .....	<b>xv</b>
<b>1. Introduction</b> .....	<b>1</b>
1.1. Overview.....	1
1.2. Objectives .....	2
1.3. Research Tasks.....	2
1.3.1. Task 1 – Literature Review.....	2
1.3.2. Task 2 – Design Considerations and Preliminary Design.....	3
1.3.3. Task 3 – Experimental Test Program.....	3
1.3.4. Task 4 – Design Recommendations.....	3
1.4. Overview of Reports.....	4
<b>2. Literature Review</b> .....	<b>5</b>
2.1. Overview.....	5
2.2. Precast Bent Caps in Texas.....	5
2.3. Design and Performance of Bent Caps .....	7
2.4. Shear Design and Analysis .....	8
2.4.1. AASHTO Sectional Design .....	8
2.4.2. Strut-and-Tie Models.....	10
2.5. Alternative Shear Reinforcement.....	12
2.5.1. Welded Wire Fabric.....	13
2.5.2. Steel Fiber Reinforced Concrete .....	15
2.5.3. Wire Rope .....	17
2.5.4. Rectangular Spiral Reinforcement.....	17
2.6. Methods to Reduce Bent Cap Weight.....	18
2.6.1. U-shaped Shell Beams .....	18
2.6.2. Box Beam Bent Caps.....	20
2.6.3. Concrete Blockouts.....	22
2.6.4. Multiple Bent Cap Segments .....	25
2.7. Connections.....	27
2.7.1. Overview of Column-To-Bent Cap Connections.....	27
2.7.2. Discussion of Connection Details.....	30
<b>3. Design Considerations</b> .....	<b>59</b>
3.1. Introduction.....	59
3.2. TxDOT Reinforced Concrete Bent Caps .....	59
3.3. Design Objectives for Pretensioned Bent Caps .....	61
3.4. Flexural Design.....	61
3.4.1. Proposed Design Procedure .....	62
3.4.2. Alternate Design Approach.....	67
3.4.3. Effect of Strand Configuration.....	67
3.4.4. Reduced Weight Section.....	69
3.5. Overview of TxDOT Standard Bridge Inventory .....	70
3.5.1. Bridge Characteristics.....	71
3.5.2. Loads and Analysis.....	73
3.5.3. Summary of Demands .....	73
3.6. Flexural Design for Standard Bridge Inventory.....	77

3.6.1.	Number of Stands .....	77
3.6.2.	Minimum Concrete Strength.....	78
3.6.3.	Service and Ultimate Stresses.....	78
3.6.4.	Factor of Safety.....	82
3.6.5.	Comparison to RC Designs.....	85
3.7.	Shear Design for Standard Bridge Inventory.....	88
3.7.1.	Application of AASHTO Provisions to Bridge Inventory.....	88
3.7.2.	Deficiency of Application of AASHTO Shear Provisions for Pretensioned Bent Caps... 91	
3.8.	End Region Detailing.....	92
3.8.1.	Stresses in End Regions of PSC Beams.....	93
3.8.2.	AASHTO and Research Recommendations .....	95
3.8.3.	Application to Pretensioned Bent Caps .....	96
3.9.	Pocket Connections.....	98
3.9.1.	Discussion of Current Practice and Previous Research .....	98
3.9.2.	Alternative Connections .....	100
3.9.3.	Connection Demands .....	102
3.9.4.	Moment Capacity of the Pocket Connection .....	105
3.9.5.	Pipe Thickness .....	107
3.9.6.	Connection Performance under Collision Loads .....	111
3.10.	Summary .....	114
<b>4.</b>	<b>Experimental Test Program: Overview .....</b>	<b>117</b>
4.1.	Overview.....	117
4.2.	Design .....	122
4.2.1.	Flexural Design.....	122
4.2.2.	Prototype Selection.....	124
4.2.3.	Shear Design.....	128
4.2.4.	End Region .....	133
4.2.5.	Column and Connection .....	136
4.3.	Test Matrix.....	137
4.4.	Test Specimen Construction .....	143
4.4.1.	RCS-16-12 .....	144
4.4.2.	Pretensioned Bent Caps .....	147
4.4.3.	Pretesting Damage .....	162
4.4.4.	Support Columns .....	164
4.4.5.	Assembly of Specimens.....	166
4.5.	Experimental Test Setup.....	170
4.5.1.	Connection Details – Installation of Reaction Towers to Strong Floor.....	174
4.5.2.	Connection Details – 10-ft × 7-ft Base Plate .....	175
4.5.3.	Column Rocker Foundation.....	175
4.5.4.	Connection Details – Actuators .....	177
4.6.	Instrumentation .....	180
4.6.1.	Strain Gauges.....	180
4.6.2.	Linear Variable Differential Transformers .....	182
4.6.3.	Linear String Potentiometers .....	182
4.6.4.	Optotrak Motion Capture System .....	183
4.7.	Material Properties.....	184
4.7.1.	Concrete Mix Designations.....	184
4.7.2.	Concrete Material Properties .....	187
4.7.3.	Steel Material Properties.....	193
4.8.	Expected Strengths.....	193

4.8.1.	Flexural Strength.....	193
4.8.2.	Shear Strength.....	196
<b>5.</b>	<b>Experimental Test Program: Results .....</b>	<b>199</b>
5.1.	Specimen Loading .....	199
5.2.	Overview of Experimental Results .....	203
5.2.1.	Phase 1 .....	210
5.2.2.	Phase 2 .....	215
5.3.	Comparison of Design Parameters.....	217
5.3.1.	Impact of Prestressing.....	217
5.3.2.	Impact of Shear Reinforcement .....	220
5.3.3.	Impact of Interior Void. ....	224
5.3.4.	Impact of Number of Strands.....	228
5.3.5.	Impact of Void Details.....	230
5.3.6.	Impact of Pocket Connection Details .....	234
5.3.7.	Impact of Overhang Geometry and Details .....	236
5.4.	Evaluation of Cracking in Pretensioned Bent Caps .....	238
5.5.	General Findings.....	240
<b>6.</b>	<b>Summary and Conclusions .....</b>	<b>243</b>
6.1.	Summary .....	243
6.2.	Conclusions.....	243
6.2.1.	Detailing and Fabrication.....	243
6.2.2.	Pocket Connection Construction and Behavior .....	244
6.2.3.	Flexure Design and Behavior.....	245
6.2.4.	Shear Design and Behavior.....	246
6.3.	Research Needs.....	246
	<b>References.....</b>	<b>249</b>
	<b>Appendix A: Construction Timeline .....</b>	<b>A-1</b>
	<b>Appendix B: Design Drawings.....</b>	<b>B-1</b>
	<b>Appendix C: Thermocouple and Temperature Data .....</b>	<b>C-1</b>
	<b>Appendix D: Instrumentation Plans .....</b>	<b>D-1</b>
	<b>Appendix E: Load Sequence .....</b>	<b>E-1</b>



## LIST OF FIGURES

	<b>Page</b>
Figure 2.1. Standard TxDOT Bent Cap-to-Column Connection for 36-in. Diameter Column (TxDOT Standard Drawing).....	7
Figure 2.2. Pretensioned Precast Concrete U-Beam (Park 1995).....	19
Figure 2.3. Cap Box Beam Used in Bridge in Honduras (Zhenqiang and Leiva 2010).....	21
Figure 2.4. Edison Bridge, Florida DOT (Culmo 2009).....	22
Figure 2.5. Straddle Bents with Styrofoam in the Cap (SHRP 2013).....	24
Figure 2.6. Connection between Multiple Pier Cap Segments (WisDOT Standard Drawing).....	25
Figure 2.7. PCI Northeast Bridge Tech Committee (Culmo 2009).....	26
Figure 2.8. Grouted Pocket Connection (Matsumoto et al. 2001).....	32
Figure 2.9. Carolina Bays Parkway Project South Carolina DOT (Culmo 2009).....	32
Figure 2.10. Escambia Bay Bridge Project- Florida DOT (Culmo 2009).....	33
Figure 2.11. St. George Island Bridge- Florida DOT (Culmo 2009).....	34
Figure 2.12. Scaled (40 Percent) Specimen Connection Tested by Pang et al. (2008).....	38
Figure 2.13. Lake Belton Project- TxDOT (Culmo 2009).....	39
Figure 2.14. Lake Hubbard Project TxDOT (Culmo 2009).....	39
Figure 2.15. Grouted Vertical Duct Connection in Washington State (Project 20-68A).....	40
Figure 2.16. Pretensioned Precast Cap (Miller et al. 2014).....	40
Figure 2.17. Reinforcement in CPLD (Top) and CPF (Below) (Restrepo et al. 2011).....	42
Figure 2.18. Boone County IBRC Project Iowa DOT (Culmo 2009).....	43
Figure 2.19. Bridge over BNSF Railway Project, Wyoming DOT (Culmo 2009).....	46
Figure 2.20. Utah DOT (Culmo 2009).....	49
Figure 2.21. South Carolina DOT (Culmo 2009).....	51
Figure 2.22. Louisiana DOT (Culmo 2009).....	51
Figure 2.23. Conventional Hybrid Connection (Tobolski 2010).....	54
Figure 2.24. Concrete Filled Pipe Hybrid Connection (Tobolski 2010).....	54
Figure 2.25. Dual Steel Shell Hybrid Connection (Tobolski 2010).....	55
Figure 2.26. Design Based on DAD (Mander and Cheng 1997).....	56
Figure 2.27. Precast, Pretensioned Rocking Column (Stanton et al. 2014).....	58
Figure 3.1. Stresses Under Dead Load: No Tension.....	64
Figure 3.2. Stresses under Service Load and Establish Minimum Concrete Strength.....	66
Figure 3.3. Ultimate Strength Capacity.....	66
Figure 3.4. General Strand Layouts.....	68
Figure 3.5. Moment Curvature Response of 42-in. Square Bent Cap with Top and Side Strand Configuration.....	68
Figure 3.6. Nominal Strength vs Area of Prestressing.....	69
Figure 3.7. Moment Curvature up to Yield for Bent Cap with 18 Strands, Side Configuration.....	70
Figure 3.8. Bent Configurations in Bridge Inventory.....	72
Figure 3.9. Bending Moment Diagram under Dead Load for 80-ft Span Length.....	75
Figure 3.10. Minimum Strands Configuration.....	78
Figure 3.11. Maximum Tensile Stress vs. Number of Strands for 42-in. Bent Cap.....	80

Figure 3.12. Maximum Tensile Stress vs. Number of Strands for 48-in. Bent Cap. ....	81
Figure 3.13. Factor of Safety vs. Number of Strands for 42-in. Bent Cap. ....	83
Figure 3.14. Factor of Safety vs. Number of Strands for 48-in. Bent Cap. ....	84
Figure 3.15. Cracking of 40-ft, 42-in. Bent Cap (Maximum Span).....	87
Figure 3.16. Cracking of 40-ft, 48-in. Bent Cap (Maximum Span).....	87
Figure 3.17. Bent Caps with I-Girder (BIG Type).....	90
Figure 3.18. Bent Caps with X-Beam (BXB Type).....	90
Figure 3.19. Bent Caps with Box-Beam (BXB Type).....	91
Figure 3.20. Crack Angle for RC and PSC Bent Cap Designs Following the AASHTO Sectional Design Method for Shear Design.....	92
Figure 3.21. Local Effects of Applied Prestressing Forces (adapted from Uijl 1983). ....	93
Figure 3.22. Stress Trajectories due to Applied Prestress. ....	94
Figure 3.23. Transverse Stresses due to Applied Prestress.....	94
Figure 3.24. Strut and Tie Model to Assess Reinforcement Requirement. ....	95
Figure 3.25. Application of End Region Detailing Provisions. ....	97
Figure 3.26. Preliminary Options for Pocket Connection for 36-in. Diameter Connection around Standard TxDOT Bar Configuration. ....	101
Figure 3.27. Geometry of 21-in. Diameter Pocket Connection with 6-#11 Dowel Bars.....	102
Figure 3.28. Example Pocket Connections to Handle Misalignment of Column. ....	102
Figure 3.29. Evaluation of Joint Forces and Shear Force Diagram. ....	105
Figure 3.30. Calculation of Moment Capacity.....	106
Figure 3.31. Corrugated Pipe Thickness Required to Minimize Stress Concentrations.....	110
Figure 3.32. Failure Mechanism Due to Vehicle Collision Load. ....	113
Figure 4.1. Prototype Bridge Shear and Moment Diagrams.....	118
Figure 4.2. Specimen Shear and Moment Diagrams. ....	119
Figure 4.3. Elevation View of Test Specimens.....	121
Figure 4.4. RC Bent Cap Cross-Section. ....	123
Figure 4.5. Strand Layout. ....	124
Figure 4.6. Phase 1 Prototype Bridge Configuration.....	125
Figure 4.7. Phase 2 Prototype Bent Cap Schematic.....	126
Figure 4.8. Phase 2 Prototype and Specimen Demands.....	127
Figure 4.9. Shear Force Diagram and Three Shear Critical Section Locations in BIG-32 and BIG-40 Prototypes in Phase 1. ....	129
Figure 4.10. Shear Force Diagram and Three Shear Critical Section Locations in Phase 2 Specimen. ....	133
Figure 4.11. Pretensioned Specimens Battered End Detailing. ....	135
Figure 4.12. RC Specimen End Region Detailing. ....	136
Figure 4.13. Steel Corrugated Pipe Connection.....	137
Figure 4.14. Specimen Geometry and Interior Void Placement. ....	140
Figure 4.15. Interior Void Cross-Sections. ....	141
Figure 4.16 Pretensioned Specimens End Region Detailing Options.....	142
Figure 4.17. Pretensioned Specimens Pocket Connection Detailing.....	143
Figure 4.18. RCS-16-12 Bent Cap Formwork. ....	144
Figure 4.19. Fabrication of RCS-16-12 Bent Cap. ....	146
Figure 4.20. RCS-16-12 Honeycombing and Honeycombing Repair. ....	147
Figure 4.21. Prestressing Bed Layout. ....	148

Figure 4.22. Initial (Black) and Final (Red) Prestressing Strand Layout. ....	148
Figure 4.23. Placement of Initial Strands and End Formwork (Phase 2). ....	149
Figure 4.24. Square End Actuator Load Assembly. ....	150
Figure 4.25. Corrugated Steel Pipe Installation. ....	151
Figure 4.26. PSV-28B Polystyrene Forming Block.....	152
Figure 4.27. Polystyrene Forming Blocks Installed.....	152
Figure 4.28. PVC Drain Pipe Installation. ....	153
Figure 4.29. Interior Void Polystyrene Forming Block Anchorage. ....	154
Figure 4.30. Strands Through Pocket Connection (Phase 2). ....	154
Figure 4.31. Strain Gauged Reinforcement. ....	155
Figure 4.32. PSV-28B Mild Steel Hoop Installation. ....	155
Figure 4.33. Phase 1 and Phase 2 Thermal Couple Plans. ....	156
Figure 4.34. Concrete Batch Distribution. ....	158
Figure 4.35. Concrete Placement and Consolidation.....	158
Figure 4.36. PSV-28B Polystyrene Void Shifting. ....	158
Figure 4.37. Concrete Finishing and Curing.....	159
Figure 4.38. Torch Cutting Prestressing Strands. ....	159
Figure 4.39. Strand Release Pattern.....	160
Figure 4.40. Measured Temperature Difference.....	161
Figure 4.41. Phase 2 Pretesting Cracks (Top of Bent Cap). ....	162
Figure 4.42. End Region Pretesting Cracks. ....	163
Figure 4.43. Column Base Octagonal Formwork Plan. ....	165
Figure 4.44. Column Base Construction.....	165
Figure 4.45. Column Reinforcement and Formwork.....	166
Figure 4.46. Column Construction.....	166
Figure 4.47. Installation of Bent Cap onto Column.....	167
Figure 4.48. HDPE Shim Installation. ....	168
Figure 4.49. Bedding Layer Formwork and Air Vents.....	169
Figure 4.50. Casting of the Bedding Layer.....	169
Figure 4.51. Honeycombing in Bedding Layer (RCS-16-12).....	169
Figure 4.52. General Laboratory Experimental Setup – 3D Rendition. ....	171
Figure 4.53. Phase 1 Experimental Test Setup. ....	172
Figure 4.54. Phase 2 Experimental Test Setup. ....	173
Figure 4.55. Vertical Reaction Towers. ....	174
Figure 4.56. Horizontal Reaction Frames. ....	174
Figure 4.57. 10-ft × 7-ft Base Plate. ....	175
Figure 4.58. Rocker Foundation (Pegs Removed prior to Testing).....	176
Figure 4.59. Rocker Foundation Assembly. ....	177
Figure 4.60. Horizontal Actuator Connections. ....	178
Figure 4.61. Elastomeric Bearing Pad Locations.....	178
Figure 4.62. Top Actuator Load Assembly. ....	179
Figure 4.63. Vertical Actuator Connections. ....	179
Figure 4.64. Strain Gauge Layout.....	181
Figure 4.65. LVDT Locations.....	182
Figure 4.66. Optotrak LED Marker Layout. ....	184
Figure 4.67. Concrete Compressive Strength vs. Age.....	190

Figure 4.68. 28-Day Bent Cap Concrete Stress-Strain Curves.....	192
Figure 4.69. Full Moment-Curvature Response for Phases 1 and 2.....	196
Figure 5.1. Moment Region Location.....	199
Figure 5.2. Schematic Drawing of Specimen with Actuator Forces.....	200
Figure 5.3. Load Pattern Moment Diagrams.....	201
Figure 5.4. Visual Observation at Failure (Back Face).....	205
Figure 5.5. Visual Observation at Failure (Failed region).....	206
Figure 5.6. Crack Maps of Phase 1 Specimens.....	207
Figure 5.7. Crack Maps of Voided Specimen Crack Damage Summary.....	208
Figure 5.8. Pocket Crack Propagation.....	209
Figure 5.9. Crack Patterns – Joint Opening and Joint Closing Demands.....	212
Figure 5.10. Crack Progression Comparison for RC (RCS-16-12) and PSC (PSS-16-12).....	218
Figure 5.11. Crack Width Envelopes (RCS-16-12 vs. PSS-16-12).....	219
Figure 5.12. Crack Progression Comparison of PSC Bent Caps with Different Shear Spacing; 12-in. Spacing (PSS-16-12) and 24-in. Spacing (PSS-16-24).....	221
Figure 5.13. Log Scale Crack Width Comparison (PSS-16-12 vs. PSS-16-24).....	222
Figure 5.14. Shear Strength and Shear Damage Summary of PSS-16-12 and PSS-16-24.....	223
Figure 5.15. Crack Progression Comparison for Specimens with No Void (PSS-16-12) and Void (PSV-16-12).....	224
Figure 5.16. Damage at Failure (PSS-16-12 vs. PSV-16-12).....	225
Figure 5.17. Crack Width Comparison (PSS-16-12 vs. PSV-16-12).....	226
Figure 5.18. Shear Strength and Shear Damage Summary of PSS-16-12 and PSV-16-12.....	227
Figure 5.19. Comparison of Shear Cracks in Span Region of PSV-28A and PSV-28B at ULS and 140 Percent ULS Demands.....	231
Figure 5.20. Comparison of Formation of Shear Cracks in Square End of PSV-28A and PSV-28B under $V_{max}$ of Square End.....	232
Figure 5.21. Comparison of Damage at Failure in Negative Moment Region of PSV-28A and PSV-28B.....	233
Figure 5.22. Loss of Concrete in Negative Moment Region of Phase 2 Specimens during Maximum Negative Moment Demands.....	233
Figure 5.23. Comparison of Cracking in Negative Moment Region of Pretensioned Specimens with Different Pocket Connection Details <sup>†</sup> under ULS and 140 percent ULS Demands.....	235
Figure 5.24. Comparison of Damage in Overhangs with Different Lengths and Void Details under ULS and 140 Percent ULS Demands.....	237
Figure 5.25. Comparison of Overhang Damage of Solid (PSV-28A) and Voided (PSV-28B) Overhang at Negative Moment Region Failure.....	238



## LIST OF TABLES

	<b>Page</b>
Table 3.1. Scenarios at Which Span Moment Controls Design or Evaluation of Bent Cap.....	76
Table 3.2. Summary of Maximum Moment Demands in 42-in. and 48-in. Bent Cap. ....	76
Table 3.3. Summary of Maximum Shear Demands in 42-in. and 48-in. Bent Cap.....	76
Table 3.4. Comparison of Strength between RC and PSC for the 40-ft Bent Cap. ....	85
Table 3.5. Joint Moment and Column Axial Forces in 32-ft Roadway, 80-ft Span. ....	103
Table 4.1. Prototype Bridges Phases 1 and 2.....	122
Table 4.2. Summary of Flexural Strength and Lab Capacity. ....	124
Table 4.3. Summary of Demands and Shear Design Results for RC and PSC Bent Caps Phase 1. ....	130
Table 4.4. Key Values for Shear Spacing Selection. ....	131
Table 4.5. Summary of Demands and Shear Design Results for a Section with 26-in. Square Void.....	132
Table 4.6. Summary of Demands and Shear Design Results for Phase 2 Specimen.....	133
Table 4.7. Test Matrix Overview.....	139
Table 4.8. Pretensioned Specimens Pocket and End Region Detailing Matrix. ....	141
Table 4.9. Summary of Strain Gauges.....	180
Table 4.10. Concrete Mix Designation. ....	186
Table 4.11. Standard Class C Concrete. ....	187
Table 4.12. Modified Class C Concrete for Mix P-1.....	187
Table 4.13. Concrete Compressive Strength Results.....	189
Table 4.14. Modulus of Elasticity, Indirect Tensile, and Modulus of Rupture Results.....	191
Table 4.15. Steel Tensile Test Results.....	193
Table 4.16. Summary of Expected Moment Strengths. ....	195
Table 4.17. Expected Cracking and Nominal Shear Strengths Using Actual Material Properties for All Specimens. ....	198
Table 5.1. Actuator Control Pattern.....	201
Table 5.2. Summary of Crack Formation and Crack Widths in Phase 1 Specimens.....	213
Table 5.3. Summary of Crack Formation and Crack Widths in Phase 2 Specimens.....	216
Table 5.4. Flexure Cracking Summary (RCS-16-12 vs. PSS-16-12). ....	217
Table 5.5. Summary of Shear Strength and Damage in Span (PSS-16-12 vs. PSS-16-24).....	223
Table 5.6. Shear Strength and Damage in Square End (PSS-16-12 vs. PSS-16-24). ....	223
Table 5.7. Comparison of Voided Specimens at Equivalent Load (Negative Moment Region).....	229
Table 5.8. Comparison of Voided Specimens at Equivalent Load (Positive Moment Region).....	229
Table 5.9. Comparison of Voided Specimens at Equivalent Load (Span Region).....	230
Table 5.10. Cracking Moment Summary in Negative Moment Region. ....	239
Table 5.11. Cracking Moment Summary in Positive Moment Region.....	239
Table 5.12. Cracking Shear Summary .....	240

# 1. INTRODUCTION

## 1.1. OVERVIEW

Multicolumn bents are the most common substructure in Texas bridges. Bent caps must be capable of supporting loads prior to placement of the superstructure, thus the bent cap construction can become a critical event in the construction timeline. With hundreds of new and replacement bridges constructed every year, efficiency of the substructure construction becomes especially critical, particularly in high traffic areas and in locations where significant detours exist when a bridge is under construction. For construction over roads or water, substructure construction exposes workers to additional hazards.

To decrease construction time and improve worker safety, precast bent caps can be used in place of cast-in-place (CIP) bent caps. The Texas Department of Transportation (TxDOT) first began exploring the use of precast bent caps in the mid-1990s. Since then, the practice has evolved, with precast bent caps having been used in unique projects and in standard bridges. Currently, contractors have the option of selecting CIP or precast reinforced concrete (RC) bent caps. This construction option is enabled by a standard connection detail developed by TxDOT through experience on individual projects and experimental tests performed for TxDOT Project 0-1748.

The next stage in evolution of precast bent caps in TxDOT bridges is the use of precast, prestressed caps. Prestressed caps can be built by precast fabricators, eliminating the need for on-site construction of the bent caps. This can be particularly beneficial where there is limited on-site space for precast fabrication or where ready-mix concrete is not readily available. Other benefits to prestressed bent caps are the possibility for improved resistance to cracking as a result of the prestressing force and reduced weight through the use of interior voids.

To avoid costly mistakes and to fully realize the performance benefits of pretensioned bent caps over RC bent caps, it is necessary to establish a thorough understanding of the behavior of pretensioned bent caps for multicolumn substructures, to address any detailing concerns, and to establish appropriate design procedures. From a performance standpoint, validation of improved resistance to cracking is needed, along with stress limits for use in design. For shear, the American Association of State Highway and Transportation Officials (AASHTO) LRFD sectional design procedures were developed for thin-web girders, and while they may lead to reasonable shear

reinforcement design for RC bent caps, their appropriateness for pretensioned bent caps must be assessed. The introduction of prestressing can lead to the potential for end-region cracking, for which adequate detailing must be validated. Finally, cap-to-column connection options must be assessed to determine the best option for pretensioned bent caps. To address these concerns, TxDOT initiated project 0-6863. This report documents the results of the project.

## **1.2. OBJECTIVES**

This project investigated the use of precast, pretensioned bent caps to enable implementation in multicolumn bridges. Specific technical objectives are to:

- Evaluate the overall behavior and serviceability of precast, pretensioned bent caps through large-scale experimental testing.
- Evaluate precast cap connections and develop connections ideal for pretensioned bent caps.
- Evaluate the use of interior voids to reduce substructure weight and enhance constructability.
- Develop details and design recommendations to enable implementation in multicolumn substructures.

## **1.3. RESEARCH TASKS**

The investigation of the precast, pretensioned bent caps was conducted via four tasks aimed at meeting the technical objectives.

### **1.3.1. Task 1 – Literature Review**

A literature review was conducted to provide a solid foundation for the overall project objectives. Topics reviewed were selected with the specific intent of determining how current practice and the results of previous research can support the understanding of pretensioned bent caps and the development of design and detailing recommendations. Topics include performance of RC bent caps; performance issues in the end-zone of precast, pretensioned bridge components; prestressed concrete (PSC) shear design and analysis; pretensioned concrete with interior voids; and connection details for precast bent caps.

### **1.3.2. Task 2 – Design Considerations and Preliminary Design**

Prior to design of an experimental test program, it was necessary to identify potential design challenges and opportunities for improvements in design efficiency. Design objectives were identified, with the primary objectives being to reduce or eliminate cracks and to ensure that any cracks that do form close under removal of live load. Flexure and shear design procedures were implemented for a suite of standard TxDOT bridges to assess the ability to achieve the design objectives. Recommendations were made for end-region detailing. Finally, recommendations were made for a pocket connection that allows for improved construction of precast bent caps.

### **1.3.3. Task 3 – Experimental Test Program**

A full-scale experimental test program was used to evaluate the serviceability and overall behavior of precast bent caps. Sub-assemblages consisted of the upper portion of an exterior column and the bent cap from the end to the second inflection point. The test setup applied multiple load configurations including one that allowed for demands representative of the indeterminate demands in a multicolumn bent cap. Subsequent load configurations generated higher demands on the connection, positive moment region, and negative moment region. The test matrix consisted of one RC bent cap and five pretensioned bent caps. Pretensioned bent caps investigated the amount of shear reinforcement, the amount of pretensioning, and the use of interior voids. Several end region details were explored, along with detailing of interior voids. All six tests used the proposed pocket connection detail.

### **1.3.4. Task 4 – Design Recommendations**

The results of the experimental test program informed the development of design and detailing recommendations for pretensioned bent caps. The recommended flexural design procedure is based on the philosophy of zero tension under dead loads to ensure that any cracks that form close under removal of live loads. For design of most bent caps, it is practical to achieve no cracking under service loads by modifying AASHTO service stress limits to proposed limits. For shear design, implementation of AASHTO sectional design procedures for pretensioned bent caps can result in kinematic inadmissibility of crack angles, thus, a modified sectional design procedure is recommended. An additional set of design recommendations is made to allow for a conversion of a RC bent cap design to a pretensioned concrete design. A suite of design examples is provided to

demonstrate implementation of the design recommendations and to illustrate how pretensioned bent caps can be used to economize design.

#### **1.4. OVERVIEW OF REPORTS**

The work in this project was conducted under TxDOT project 0-6863. The final report consists of two volumes. This volume (Volume 1) documents the results of Tasks 1–3. Chapter 2 presents the literature review. In Chapter 3, preliminary design considerations are discussed. Chapter 4 presents an overview of the experimental test program, including fabrication details. The results of the six full-scale tests are presented in Chapter 5. Volume 1 concludes in Chapter 6 with a summary of findings, with emphasis on those which impact future design and implementation, as well as identification of future research needs.

Volume 2 provides design recommendations based on the outcomes of the experimental test program, along with design examples to demonstrate how the design recommendations can be implemented for future construction.

## **2. LITERATURE REVIEW**

### **2.1. OVERVIEW**

This chapter presents the results of a literature review conducted to provide a foundation for the project objective of enabling the use of pretensioned concrete bent caps in multicolumn bridges. Section 2.2 provides background on the use of precast bent caps in Texas. Section 2.3 summarizes research on the performance of reinforced bent caps, with an emphasis on those studies influencing bent cap design by TxDOT. Section 2.4 summarizes shear design and analysis. Section 2.5 summarizes literature to support consideration for the potential use of alternative shear reinforcement. Section 2.6 summarizes potential methods for reducing bent cap weight. Finally, Section 2.7 provides an in-depth review of the state-of-the art and the state-of-the-practice of cap-to-column connections to support the development of a connection for pretensioned bent caps.

### **2.2. PRECAST BENT CAPS IN TEXAS**

The use of precast bent caps in Texas began in the mid-1990s, generally at the request of contractors wishing to facilitate unique construction projects. One of the earliest documented uses of precast bent caps by TxDOT was the Pierce Street Elevated Project in 1996, which needed replacement of 113 superstructure spans and bent caps. Connections between precast bent cap and columns were made with post-tensioned bars embedded in the column and projected from the column top to corrugated ducts built in the precast bent cap. The ducts were grouted and the bars were anchored at the cap top. The Red Fish Bay and Morris & Cummings Cut Bridges built in 1994 involved use of rectangular precast bent caps to minimize casting over water. The connection between precast bent caps and precast trestle piles consisted of two U-shaped reinforcing bars epoxy grouted into ducts at the top of precast piles, and projected into two voids built along the full depth of the bent cap. Concrete was placed into the voids after placement of the cap (Freeby et al. 2003).

As part of TxDOT Project 0-1748, Matsumoto et al. (2001) formally investigated four connection types. Follow-up project 0-4176 (Brenes et al. 2006) further investigated one of these connection types. These research projects resulted in the current TxDOT precast connection option for standard bent caps. Two options exist, one for square piles and one for round columns. The standard TxDOT connection detail specifies that the column longitudinal and spiral reinforcement

be terminated at the top of the column and that additional #11 bars be embedded into the column cross-section, as shown in Figure 2.1. These embedded bars extend above the top of the column and provide the connection with the bent cap. The precast bent cap is built with individual 4-in. diameter vertical steel ducts that align with the extended reinforcing bars. Reinforcing ties are placed around the group of ducts. Following placement of the caps, the vertical ducts are grouted. Discussion with TxDOT representatives provided information that the current connection presents a number of challenges. These challenges include successful grouting operations that use properly mixed grout and avoiding the formation of voids. Additionally, the use of the grouted duct connection requires tight tolerances for alignment of bars for the ducts, so there is minimal room for accidental misalignment of the columns or dowel bars. This project on pretensioned precast bent caps provides the opportunity to develop an alternative connection, so an evaluation of the literature and state-of-the-practice is provided in Section 2.7.

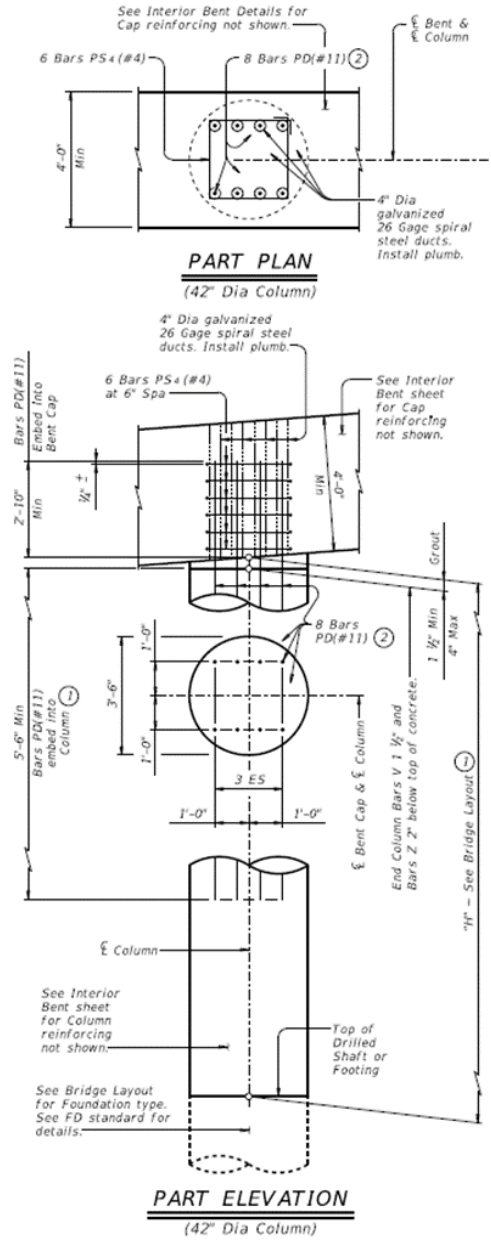


**Figure 2.1. Standard TxDOT Bent Cap-to-Column Connection for 36-in. Diameter Column (TxDOT Standard Drawing).**

### 2.3. DESIGN AND PERFORMANCE OF BENT CAPS

Research to investigate the performance of Texas bent caps and to improve the design detailing precedes efforts to develop options for precast bent caps. Ferguson (1964) investigated bent caps using an experimental test program of 36 specimens that varied parameters such as the shear span dimensions, anchorage length of longitudinal steel in the end regions, web reinforcement, and material properties. Key outcomes of the study included recommendations for minimum extension



of reinforcing bars and recommendations for calculating the strength of the bent caps. In particular, Ferguson commented on the limited contribution of shear reinforcement at small shear span ratios. Ferguson made important observations on the distribution of strains in the connection region and the importance of adequate skin steel to minimize side cracks.

For TxDOT project 0-1851, Bracci et al. (2001) conducted 16 tests of full-scale bent caps. The project was initiated in response to the observation of unexpected cracking in the bent cap joint region. Field investigations indicated typical crack patterns consisted of small flexural cracks within the width of the column support and large shear or flexure-shear cracks within the shear span region. The experimental tests investigated parameters such as shear reinforcement detailing, skin reinforcement, and embedment length of longitudinal reinforcement in the overhang region of the cap. Additionally, they evaluated the appropriate critical section for design and found it to be in the column on account of its similar size to the bent cap. The experimental crack patterns were similar to that in the field, and results indicate the importance of using, what was at the time, new design recommendations for the amount of skin steel to reduce the presence of web cracks. Other key observations included that flexural reinforcement layout did not impact cracking and the use of overlapping stirrups reduced flexure-shear cracking at higher loads.

Research on the performance of RC bent caps has also been conducted outside Texas. Fonseca et al. (2003) tested deteriorated RC rectangular bent caps that were significantly deteriorated while in service in Utah. For the bent caps tested, flexural response was found to dominate the response (no D-regions existed) but the damage did not compromise the load capacity on account of the fact that corrosion had not occurred. A number of studies (e.g., Restrepo et al. 2011) have evaluated performance of bent caps under earthquake loading, either evaluation of existing bridges, retrofit, or the development of designs for new construction; these studies are not summarized here.

## **2.4. SHEAR DESIGN AND ANALYSIS**

### **2.4.1. AASHTO Sectional Design**

Hawkins and Kuchma (2006) recommended changes to the AASHTO shear provisions (AASHTO 1998) that resulted in the Modified LRFD Sectional Design Method. The LRFD model is based on the Modified Compression Field theory (MCFT). However, in light of the inconvenience of

iterating calculations to determine values of  $\beta$  and  $\theta$ , the authors proposed incorporating provisions similar to those from the 2004 Canadian Standards Association Code for the Design of Concrete Structures (CSA A23.3, 2004). Thus, the use of tables and repeated iteration would not be necessary and facilitate convenience of hand calculation. The LRFD model makes a few assumptions. The LRFD model assumes that the distribution of shear stress can be taken as the value at mid-depth of the cross-section whereas there is variation (that is not necessarily uniform) along the depth. The compressive stress-strain response is assumed to be a parabolic relation, peaking at  $-0.002$ . For members satisfying the minimum transverse reinforcement requirement, the crack spacing is assumed to be 12-in., conservatively. The model has several shortcomings related to its basis in MCFT. This approach does not model individual behavior of cracks, and crack angles are assumed to overlap with the diagonal compressive strut. MCFT was a method developed for members having uniform stress distributions; however, the LRFD model applies this method to flanged members and other sections that have non-uniform stress distributions.

Research conducted by Shioya et al. (1990) indicated that the depth of concrete members without reinforcement affects the shear capacity at failure. Results showed that shear capacity decreased as depth increased in the unreinforced beams. Collins and Kuchma (1999), however, found that there was an insignificant effect on beams with transverse reinforcement. The minimum shear reinforcement requirement ensures that the concrete continues to perform at the calculated capacity after diagonal shear cracks begin to form. Greater amounts of reinforcement (and smaller crack spacing) allow shear stress to be transferred across cracks and help reduce the effect of member depth on shear capacity. Since the minimum steel requirement is based on the concrete strength, assurance of shear behavior comes at the cost of purely economic design for members with high strength concrete. Researchers found that the proposed simplified approach was the most conservative for continuous members while the proposed modified LRFD, CSA, and AASHTO Standard Specification methods (AASHTO 1996) were more unconservative.

Hawkins and Kuchma evaluated six design examples using the non-iterative method and compared with the iterative design methods. The examples included RC bent caps and prestressed girders, but did not include a prestressed bent cap or other structural member with similar characteristics. Based on the design examples explored by the Hawkins and Kuchma, the proposed simplified method was the most conservative method for calculating the required amount of shear

reinforcement. The AASHTO Standard Specifications (AASHTO 2002) had the lowest required reinforcement and was the least conservative method. The LRFD and CSA methods showed similar results falling between the other two methods.

Reineck et al. (2003) assembled a database of shear tests for RC members that have no shear reinforcement. These data can be reviewed and used to evaluate shear design criteria. This database was used by Hawkins and Kuchma to evaluate their design models. The tests do not seem to resemble the dimensions and shear stress demands of typical TxDOT bent caps.

Higgs et al. (2015) compared experimental results for high-strength concrete girders to AASHTO calculated values. Parameters compared included residual prestressing force, shear capacity, and flexural capacity. The authors concluded that the AASHTO calculations are good predictors of girder behavior.

Avendaño and Bayrak (2013) analyzed experimental results from the University of Texas Prestressed Concrete Shear Database (UTPCSD). The objective of this analysis was to evaluate the design specifications for minimum shear reinforcement and maximum shear strength. Sections needed to display a certain reserve shear strength (RSS). RSS is an index describing the ratio between the maximum shear and the cracking shear. RSS was determined to be affected by the shear reinforcement index ( $\rho_v f_y$ ) indicating the tensile stress that can be resisted by the shear reinforcement, the tensile strength of concrete (by affecting the amount of transverse steel required), prestressing (by delaying diagonal cracking and affecting the amount of transverse steel required), and detailing for anchorages and spacing.

Nakamura et al. (2013) expanded the contents of the UTPCSD to include more shear tests. These data sets have been used to evaluate different shear design models. While there are many full-scale model tests in the UTPCSD, none of the tests closely resemble the shape or scale of the TxDOT standard bent caps.

#### **2.4.2. Strut-and-Tie Models**

Experimental data from TxDOT 0-1851 (Bracci et al. 2001) were used by Scott et al. (2012a; 2012b) to demonstrate the use of compatibility strut-and-tie models (C-STM) as a simplistic computational means of predicting experimental behavior.

Strut-and-tie models (STM) are a method used to calculate the behavior of disturbed regions and deep beams. TxDOT projects that have explored STM include: TxDOT 0-5997 and TxDOT 0-4371. The AASHTO LRFD Bridge Design Specifications note that STM can approximate force interactions between shear, flexure, and torsion. STM defines nodal zones at the loading and support points. These points are joined (and forces are allowed to be transmitted) through compressive struts and tension ties. In this way, STM aims to estimate and predict the flow of forces throughout an element. However, conventional STM only accounts for force equilibrium. The critical failure mechanism may not truly be calculated since nonlinear material effects are not adequately estimated. STM has been found to predict unconservative capacities for beams subjected to alkali silica reaction (ASR) and delayed ettringite formation (DEF) damage. A C-STM that evaluates nonlinear material characteristics may be a more favorable alternative to analysis of bent caps.

Kim and Mander (1999) explored the application of truss models to RC combined shear-flexure behavior. Both constant angle and variable angle truss models were found to be viable methods for determination of shear stiffness. While a piecewise linear elastic approach to material modeling provided a good response, nonlinear material models were more refined. TxDOT 0-4371 (Brown et al. 2006) evaluated the application of STM to RC members. Their findings indicated that the shear span-to-depth ratio was a prominent parameter in consideration of shear capacity. Struts that formed at shallower angles experienced reduced ultimate capacities. They also found that cracking loads were unaffected by reinforcement crossing over cracks. Additionally, direct struts between the point of load application and a support were found to be a good representation of behavior for  $a/d < 2$ .

Deschenes et al. (2009) tested six large scale bent caps for behavior subjected to ASR and DEF damage. Two specimens used non-reactive concrete to form a control group, and the remaining four test specimens were created using reactive concrete, which would deteriorate more severely when exposed to high temperatures during the curing process. Deschenes et al. found that there was expansion from ASR deterioration parallel to the casting direction and suggested that modeling of ASR deterioration should consider that accordingly. Temperature control during curing was found to be a very important factor in controlling both ASR and DEF deterioration. Deschenes et al. found that AASHTO requirements for both sectional and strut-and-tie methods

would not be adequate to resist ASR and DEF deterioration. Additional confining reinforcement would be required. At service level loads, however, the provided transverse steel adequately restrained cracking. The authors noted that diagonal cracking in an ASR deteriorated bent cap indicated impending failure.

Scott et al. (2012a) formulated C-STM as a means to simply and accurately predict the behavior of experimental specimens. C-STM incorporates the interaction behavior between truss mechanisms and shear resisting arch stresses. C-STM includes stress contributions from both concrete and steel in diagonal compression members. C-STM also accounts for material softening of cracked concrete (in particular, for diagonal struts). The C-STM model accounts for the behavior of disturbed regions well.

Scott et al. (2012b) also analyzed experimental data to test C-STM using SAP2000. The analysis procedure is as follows: definition of nodal zones, assignment of element properties, assignment of nonlinear constitutive relationships, load case definition, analysis execution, and post-analysis investigations. Post-analysis investigations involve evaluating axial forces and displacements. Based on the application of C-STM to experimental data, C-STM provides a suitable computational prediction of the force-deformation response with a reasonable degree of accuracy (in particular for deep beams and disturbed regions).

TxDOT 0-5997-1 (Mander et al. 2012) evaluated a C-STM approach for bridge piers with ASR and DEF damage. The authors modeled ASR/DEF effects as prestress forces acting at nodal zones. The results of the analytical model were similar to the experimental results. Additionally, results from the C-STM analysis agreed well with experimental results from specimens without ASR/DEF damage. TxDOT 0-5997-2 (Mander et al. 2015) continued the previous study by studying damage in beams damaged over a long time period to explore heavier levels of damage. The results of C-STM analysis on these specimens agreed well with the failure behavior and non-linear behavior of the heavily damaged specimens.

## **2.5. ALTERNATIVE SHEAR REINFORCEMENT**

The most common method of reinforcing concrete structures to resist shear is the use of stirrups made of mild reinforcing steel. Stirrups are commonly #3, #4, #5, or #6 bars with two or more vertical legs that contribute to the shear strength of the beam and help to strain the opening of

cracks. Stirrups spacing is determined based on that need to provide adequate strength and to ensure that diagonal shear cracks cross at least one stirrup. In standard TxDOT bent caps, #5 bars are used at spacing ranging from 4 in. to 12 in. The use of prestressing is expected to enable reconsideration of the amount of shear reinforcement used, either in reduction of the spacing used or alternative reinforcement. While vertical stirrups are commonly accepted shear reinforcement, placement of the steel can be time consuming, particularly when the spacing is needed relatively close for crack control. A number of alternatives that may improve the constructability, serviceability, and/or strength of bent caps in shear include welded wire fabric (WWF), steel fibers, wire rope, and rectangular spiral. An overview of each of these alternatives is presented in the following sections.

### **2.5.1. Welded Wire Fabric**

WWF is a convenient alternative option to conventional transverse reinforcement. This type of transverse steel is easily constructible. The relatively close spacing of wires in the fabric mesh has been shown to reduce crack spacing. Research projects exploring the use of WWF as a means of shear reinforcement include both RC and PSC. Mansur et al. (1987), Robertson and Durani (1987), and Pinchiera et al. (1989) discussed the comparison between experimental strength and predicted strength. Results for static tests showed greater capacities than building code provisions, but results for cyclic loading performed by Pinchiera indicated that building code requirements were lacking.

Mansur et al. (1987) evaluated the performance of deformed WWF reinforcement in RC beams. Their general findings indicated a consistent crack progression. Flexural cracks first formed at the bottom face of the specimens underneath the applied loads. As the loads increased, the flexural cracks began to turn in a more horizontal direction and more (shear-related) diagonal cracks formed. Eventually, one crack widened to the point of failure. Additionally, the diagonal cracks were observed to be the largest at the mid-depth of the beam specimens. While the rate of crack growth in the deformed WWF reinforced specimens were similar to that in a conventionally reinforced beam, the maximum crack widths were smaller, indicating improved crack control. The WWF reinforced specimens also achieved their required ultimate shear strength capacities, showing that deformed WWF reinforcement can be adequate for shear capacity. Experimental data showed better performance over predicted values based on the American Concrete Institute (ACI)

Building Code. However, the authors noted that the actual yield strength was greater than that which was suggested by the code provisions.

Robertson and Durani (1987) investigated the use of WWF reinforcement to resist shear in PSC T-beams. Thirteen prestressed T-beams were evaluated with a combination of bonded and unbonded tendon bundles for a shear span-to-depth ratio of 2.75. Shear failure was independent of the tendons being bonded or unbonded. The experiments indicated that WWF reinforcement showed adequate performance as compared to conventional stirrups. Anchorage provided by two wires at the top and bottom was sufficient for development and provided safety against any weaknesses in the welds (the quality of which is important). The authors found that the shear capacity contribution of concrete was 40 percent higher than that which was prescribed by the ACI Building Code. Crack angles were found to typically fall within  $30^\circ$  angles. Additionally, yield strength of the wires was found to be higher than the suggested values in the code.

Xuan et al. (1988) evaluated the use of WWF reinforcement in pretensioned T-beams for static loading cases. The authors measured and compared the point of first cracking, the crack pattern, the crack width, and the ultimate strength for the tested specimens. The six pretensioned single T-beam specimens had equal shear span-to-depth ratios of 2.9 and identical amount and configuration of flexural reinforcement. The transverse reinforcement, however, was varied between no web reinforcement, double leg stirrups (to simulate conventional practices), smooth WWF, deformed WWF, and deformed WWF with extra longitudinal wire at mid-depth. The deflection of all types of beams was similar until the specimens began to crack. Afterward, the smooth WWF provided a similar response to that of conventional steel. Deformed WWF failed at lower load and deflection values, which the authors suggest may be attributed to a lack of ductility in the reinforcement type. Addition of the extra longitudinal wire in the second deformed WWF specimen provided slightly increased strength and additional ductility. Shear capacity in the WWF reinforced specimens was found to be sufficiently adequate compared to the conventionally reinforced specimen. All specimens failed by shear with cracks propagating between  $45^\circ$  and  $65^\circ$ . With the exception of deformed WWF without extra wire, all transversely reinforced specimens yielded before failing in shear. The specimen with deformed WWF failed by fracture of the wires crossing a diagonal crack. Crack spacing was similar for the conventionally reinforced specimen and the smooth WWF specimen. The deformed WWF specimens had the most uniform crack

spacing but also had the most cracks. Additionally, the presence of two horizontal wires at the top and the bottom provided adequate anchorage for development.

Pinchiera et al. (1989) assessed the viability of WWF reinforcement as shear reinforcement under cyclic loading cases. The authors tested nine beams with a mixture of prestressed and RC specimens. Transverse reinforcement was varied between conventional stirrups, smooth WWF, and deformed WWF. As mentioned previously, adequate anchorage was provided by two horizontal wires at both the top and the bottom of the specimen. The experimental results indicated that WWF reinforcement had slightly better control of the diagonal cracking than either single or double-legged conventional reinforcement. Deformed WWF reinforcement was shown to not perform as well as conventional reinforcement (i.e., lower ultimate strength for RC specimens and fewer number of cycles for PSC specimens).

### **2.5.2. Steel Fiber Reinforced Concrete**

Steel fiber reinforced concrete (SFRC) is another alternative to traditional reinforcing methods and can either enhance or replace conventional transverse steel. The ACI 318 allows designers to not provide minimum transverse reinforcement if the height of the beam is less than 24-in.  $V_u \leq 2\sqrt{f'_c} b_w d$ , and  $f'_c \leq 6,000$  psi (among other requirements for material properties). Parra-Montesinos (2006) supported the use of deformed steel fibers as an alternative to conventional minimum shear reinforcement. Specifically, the author suggested this would be effective for shear demands ranging from  $\sqrt{f'_c} b_w d$  to  $2\sqrt{f'_c} b_w d$ . The shear stress demands of TxDOT bent caps fall within the range shear stresses contained in the database included in that report. However, the tested beam dimensions do not closely resemble those of a typical TxDOT bent cap. Lequesne et al. (2013) investigated high performance fiber reinforced concrete (HPFRC) and their applications in buildings. The authors found that using HPFRC increased the ductility of coupling beams. Results also indicated that (for an aspect ratio of 1.75) the amount of beam diagonal reinforcement could be significantly reduced. The shear and confinement requirements of the 2008 ACI Building Code were found to be adequate for ensuring a flexural failure mechanism.

Mansur and Ong (1991) investigated the use of fiber reinforcement to resist shear in deep beams containing conventional reinforcement. Tension reinforcement consisted of four 16 mm deformed bars, and web reinforcement (both longitudinal and transverse) was comprised of 6 mm bars. They



found that the specimens showed elastic behavior at low loadings. As loading increased, diagonal cracks formed at mid-depth and gradually widened. Specimens with smaller shear span-to-depth ratios experienced less flexural cracking, but specimens with larger ratios sometimes experienced combined shear and flexure cracking. Larger fiber volume fractions decreased the rate of crack widening, decreased the deflections slightly, and added shear strength. The test results closely resembled predicted values calculated using a softened truss model for both ultimate strength and load-deformation response.

Kwak et al. (2002) studied the shear strength of concrete beams with steel fibers as the only transverse reinforcement. In this experiment, the fractional volume of fibers, the shear span-to-depth ratio, and the concrete compressive strength were evaluated for their effects on shear strength. The results indicated that the test beams without fibers experienced shear failure. Beams with 0.5 percent and 0.75 percent fractional fiber volumes experienced a combined flexure and shear failure mode. Additionally, as the fractional fiber volume increased, the crack spacing became closer. Both the ultimate shear strength and the cracking shear strength decreased as the shear span-to-depth ratio increased. Both the ultimate shear strength and the cracking shear strength increased with increases in the fractional volume of fibers and the concrete compressive strength. The increase in the fractional volume of fibers was more effective at increasing the ultimate shear strength, and the increase in the concrete compressive strength was shown to be more effective at increasing the cracking shear strength. The authors also noted that the methods to increase capacities were particularly effective for shear span-to-depth ratios around 2.

TxDOT 0-4819 (Dhonde et al. 2005) tested PSC I-beams with fiber reinforcement in the end regions. Both traditional FRC and self-consolidating FRC were tested. The increase in tensile capacity was greater for the self-consolidating concrete specimens on average. Optimal fiber content for the self-consolidating concrete specimens was 1.0 percent for short steel fibers and 0.5 percent for long steel fibers (for workability). Self-consolidating concrete was also found to be more workable, thereby improving the constructability. Fiber reinforcement was shown to control the width of cracks in the end zones. Fibers also controlled tensile strains during the curing process and prestress release. The presence of fibers increased beam strength, stiffness, crack resistance, ductility (more energy absorption), and flexural capacity.

Dinh et al. (2011) developed a shear strength model for SFRC beams basing the shear capacity on shear strength in the concrete compression zone and tensile resistance of the steel fibers acting over the shear cracks. This model based material performance of the steel fibers on ASTM 1609 four-point bending tests.

Chalioris (2013) conducted a study on SFRC beams under cyclic deformations. Seven beams with a shear span-to-depth ratio of 2 were tested. Chalioris tested a combination of plain concrete and SFRC with volume fraction of fibers equal to 0.5 percent and 0.75 percent. Steel fiber reinforced sections were shown to have improved shear strength, lower residual drifts (increased energy absorption), and more favorable cracking patterns than unreinforced sections.

### **2.5.3. Wire Rope**

Wound wire rope is another potential alternative method. Dutta et al. (1999) used wire rope reinforcement as an alternative method to conventional spirals for retrofitting damaged concrete columns. The wire rope was used in the plastic hinge zone of the column. Testing under seismic loads from a simulated foreshock, main shock, and aftershock indicated that the wire rope performed as intended and limited damage to the plastic hinge region.

Kim et al. (2007) tested 15 beams that failed in shear and had been retrofitted with wire rope to repair the damage or provide additional strength. Wire rope was shown to be effective in controlling cracking and increased the ultimate strength of the beams. Additionally, higher amounts of prestress in the wire ropes corresponded to higher values of shear strength.

### **2.5.4. Rectangular Spiral Reinforcement**

Karayannis and Chalioris (2013) compared the performance of continuous rectangular spiral reinforcement to conventional stirrups on simply supported RC beams. All experimental beams had a shear span-to-depth ratio of 2.67. The results showed that rectangular spirals that were oriented at a shear-favorable angle (i.e., closer to the horizontal) had better performance for ultimate shear strength. Small spacing improved the ductility of spirally reinforced specimens. The previously mentioned shear-favorable specimens also displayed increased ductility (and some improved flexural characteristics). Rectangular spirals were shown to increase shear capacity and somewhat lower crack angles.

Chalioris and Karayannis (2013) performed tests on 11 rectangular beams under torsion effects to ascertain the performance of rectangular spiral reinforcement. Two specimens had no transverse reinforcement, three had closed stirrups, and the remaining six had rectangular steel spirals. Torsional behavior was found to depend on the locking effects of the spiral reinforcement. Beams that used rectangular spiral reinforcement with locking characteristics showed better performance than those with conventional stirrups. Beams with unlocked rectangular spirals showed a decrease in performance.

De Corte and Boel (2013) evaluated the performance of spirally shaped stirrups for rectangular RC beams under a four-point bending test with shear span-to-depth ratios of 2.5 and 3. Both conventionally vibrated concrete and self-consolidating concrete were tested. For  $a/d = 2.5$ , spirals were less effective than conventional reinforcement. For  $a/d = 3$ , the spirals had comparably effective performance to conventional reinforcement with the exception of the specimens made with the second batch of conventionally vibrated concrete. Spiral reinforcement was not shown to have any significant effects on deflections. Self-consolidating concrete was found to improve the ultimate capacity and control crack widths but did not control deflection as well as conventional concrete. The authors noted that the cracks were not symmetrical on both sides of the beam, but the critical crack was symmetrical.

## **2.6. METHODS TO REDUCE BENT CAP WEIGHT**

TxDOT standard bent caps with rectangular cross sections and without skews range from 24-ft to 44-ft. A particular bridge project may require a longer bent cap to cope with a wider bridge deck. However, the length of bent cap is often limited by the restrictions in weight for shipping and erecting. This section provides information on different methods that could be used to avoid the problem of weight exceedance. Methods to alter the bent cap cross-section (U-shaped shell beams, box beams, and concrete blockouts in the bent cap) are described in Section 2.6.1 through Section 2.6.3. Methods for connecting individual bent caps are described in Section 2.6.4.

### **2.6.1. U-shaped Shell Beams**

Park (1995) presented general details of the widespread application of precast pretensioned shell beams as structural elements in New Zealand. The paper gives an overview of construction of

floors, moment resisting frames, and structural walls of buildings using PSC. One such application is in the use of precast concrete shell beam, as shown in Figure 2.2.

The shell beams are precast pretensioned U-shaped beams. After placing the beams in position, an additional reinforcing cage is placed within the hollow portion of the beam and then in filled with CIP concrete. The beam is designed for its low self-weight plus imposed construction loads. All external loads are carried by both the beam and the core concrete compositely. Reinforcement is not projected from either the beam or core concrete, and composite action is dependent on the bond developed at the roughened interface. Tests have been performed in New Zealand in moment resisting frames incorporating this system and subjected to seismic loading. Results from the tests showed that during severe seismic loading, plastic hinging in the beams is not concentrated only at the column faces, but plastic hinging also spreads along the RC core due to bond failure. Such a performance is not an issue for non-seismic performance of gravity dominated structures in Texas.

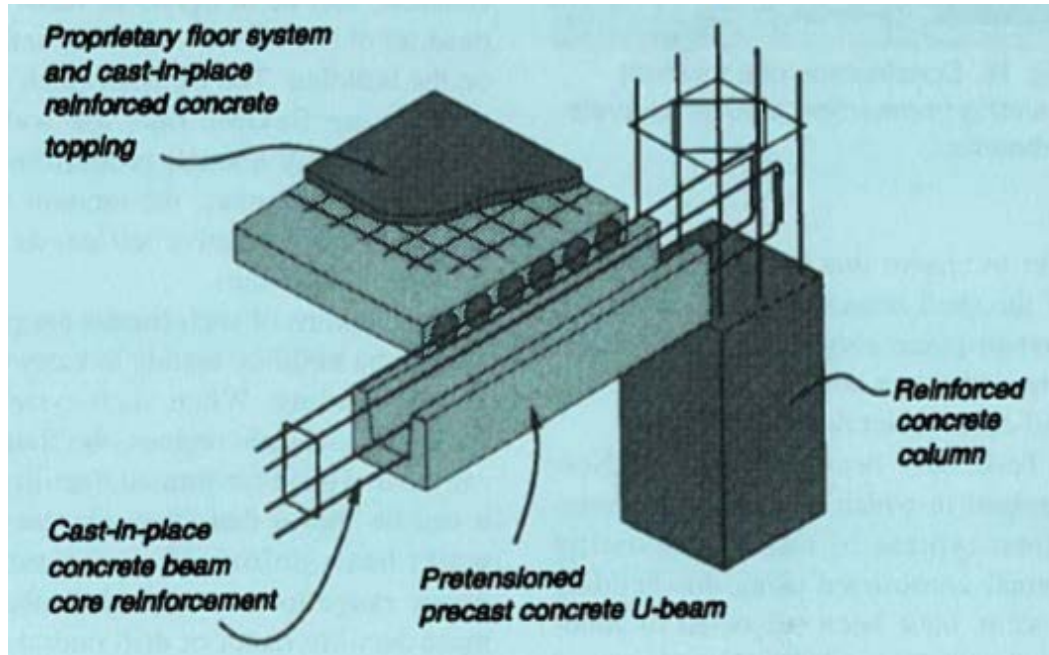
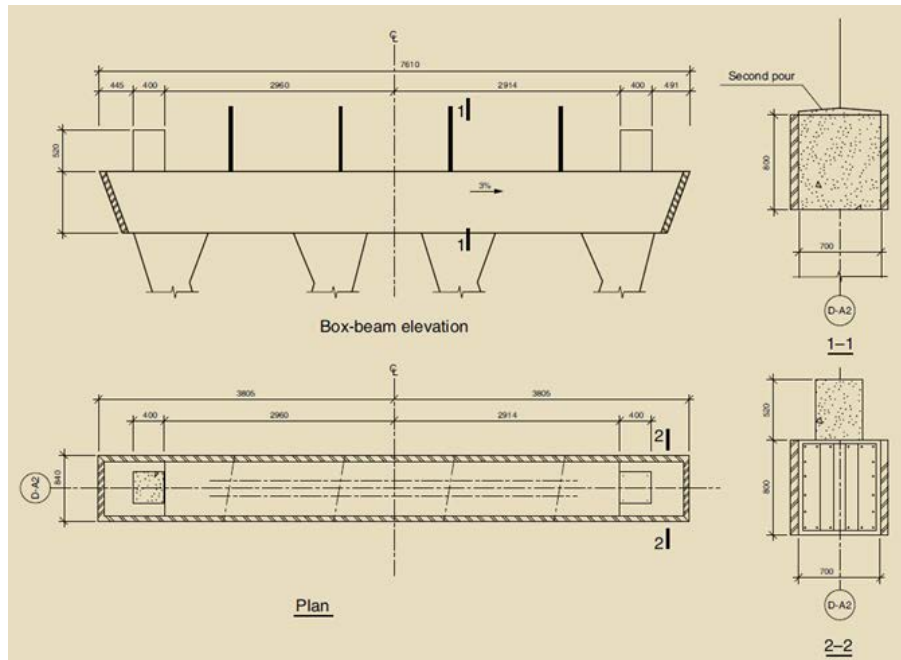


**Figure 2.2. Pretensioned Precast Concrete U-Beam (Park 1995).**

### **2.6.2. Box Beam Bent Caps**

Zhenqiang and Leiva (2010) discussed the use of precast concrete structures incorporated both in superstructure and substructure of an interchange bridge project in Honduras. The bridge had four spans with a total length of 213-ft. Each pier cap was composed of a precast concrete box beam and served as a stay-in-place formwork for the CIP concrete filled in the center of the box beams. These box units with dimensions of 3-ft width, 2.3-ft depth, and 26-ft length were prefabricated at a precast plant, and constructed using precast, PSC panels and reinforcing-steel cages. Figure 2.3 shows the design details of the cap box beam and the underside of the bridge.

A variation in this method of weight reduction is an inverted U-shaped beam. Florida DOT used an inverted U-shaped bent cap for weight reduction in the design of the Edison Bridge crossing the Caloosatchee River (Figure 2.4).



(a) Design Details of the Cap Box Beam



(b) The Underside of the Completed Bridge in Honduras

Figure 2.3. Cap Box Beam Used in Bridge in Honduras (Zhenqiang and Leiva 2010).

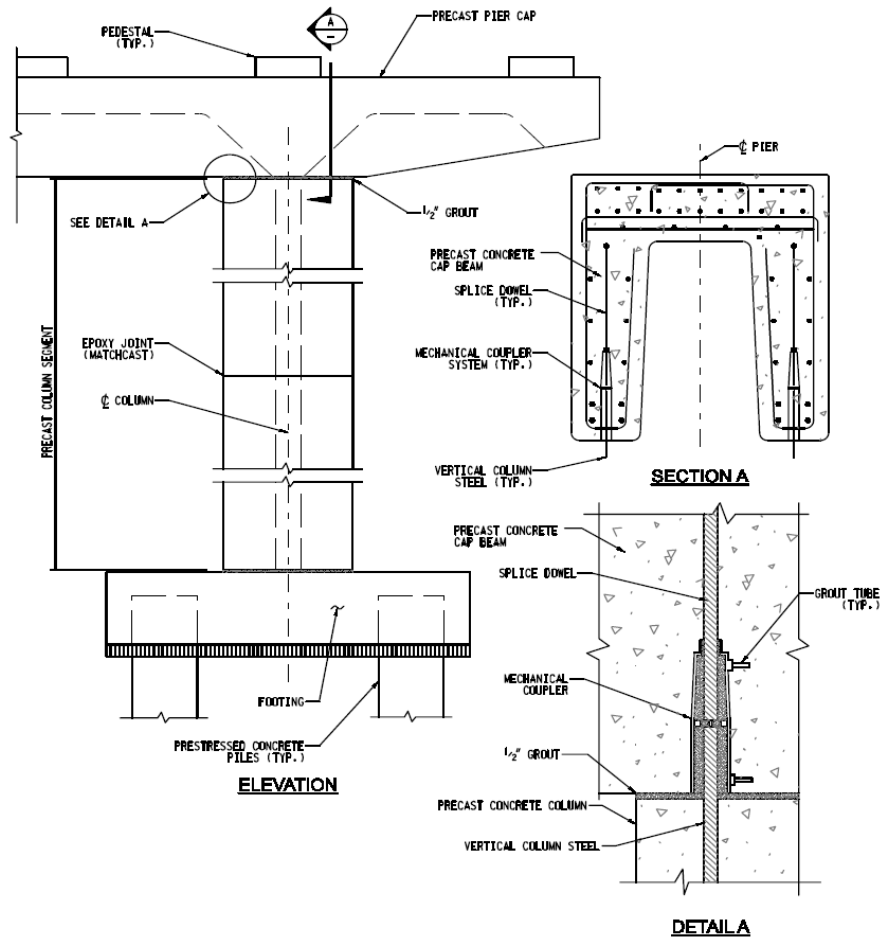


Figure 2.4. Edison Bridge, Florida DOT (Culmo 2009).

### 2.6.3. Concrete Blockouts

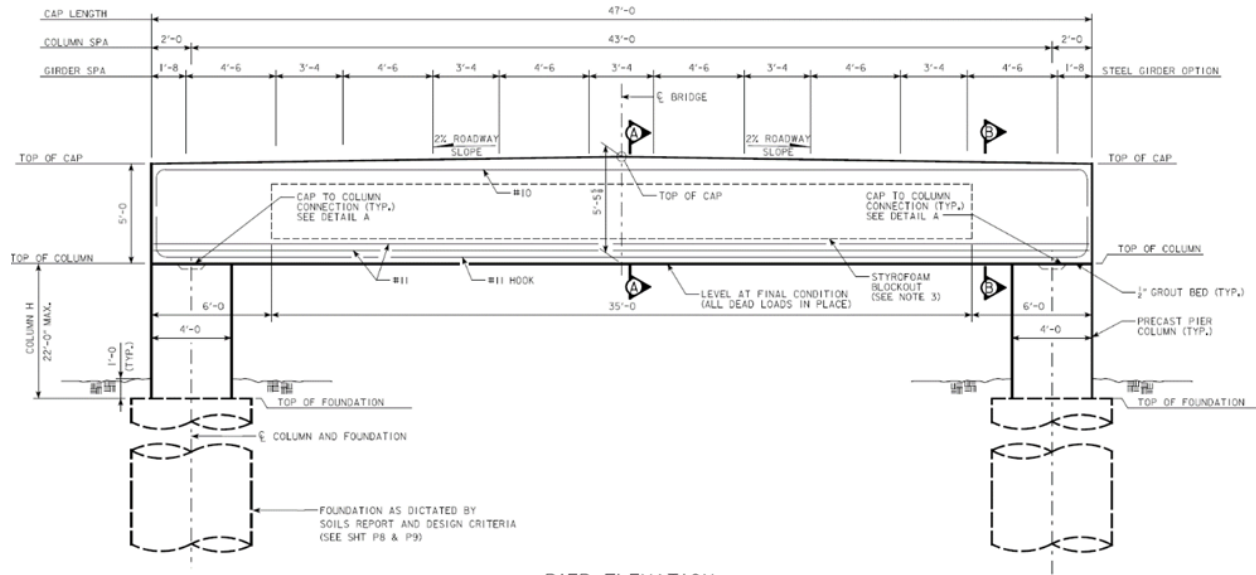
Strategic Highway Research Program (SHRP) 2 Report S2-R04-RR-2 (SHRP 2013) is focused on accelerated bridge construction (ABC) and using innovative techniques for bridge renewal. This report has provided an ABC toolkit offering design and implementation techniques for precast elements and their connections between those elements. One of the objectives for the widespread use of ABC includes developing standardized ABC systems. Two types of precast pier caps systems are illustrated: conventional pier bents and straddle pier bents. While in the conventional pier bent, the column foundations are constructed below the existing bridge, in a straddle pier bent the columns are at the ends of the cap. This enables the foundation to be constructed outside the footprint of an existing bridge and avoids disrupting traffic. For a pier cap with reasonable length to be supported by columns only at the ends, considerations about its weight need to be taken into consideration. The standard drawings for straddle bent in the report indicate hollow sections on

two sides from middle of the cap along its length by placing polystyrene blockouts, as can be seen in Figure 2.5. In addition, it is mentioned that light weight concrete can also be used in place of polystyrene blockouts to reduce weight of pier cap.

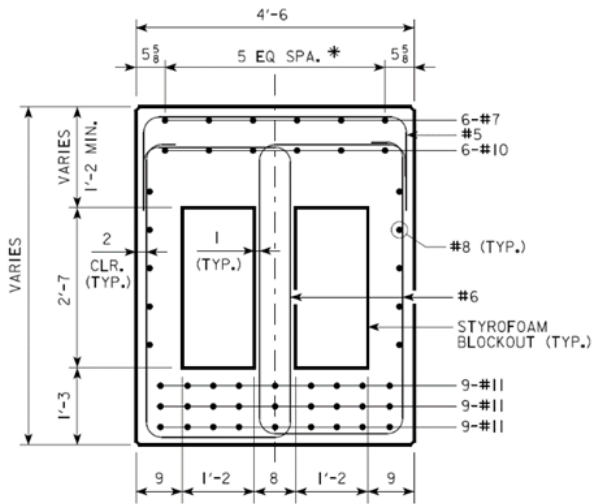
Billington et al. (1998) proposed a substructure system suitable for precast structures with the objective to reduce construction time and improve aesthetics of bridges. One of the two proposals of the system intended to reduce the weight of a bent cap by providing voids in the web of an inverted tee cap. This precast bent cap can be pretensioned, post-tensioned, or both.

Heiber et al. (2005) reported on the aspects of Billington et al. (1998) for reducing weight of cap beam by partial voids. These voids are made with forms that might increase the cost of fabrication. The author suggested that such voids should be introduced only if savings are achieved by its usage.



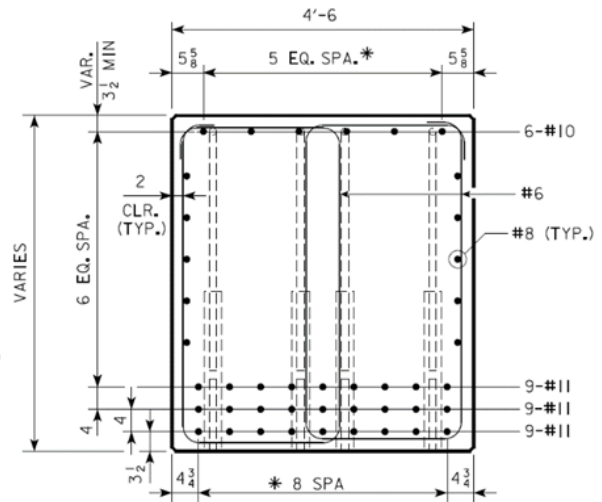


**PIER ELEVATION**  
(70' SPAN)



**SECTION A-A**  
**PRECAST PIER CAP**  
(70' SPAN)

\*SPACE REINFORCING TO CLEAR COUPLERS AND PROVIDE PROPER BAR CLEARANCE.



**SECTION B-B**  
**PRECAST PIER CAP**  
(70' SPAN)

\*SPACE REINFORCING TO CLEAR COUPLERS AND PROVIDE PROPER BAR CLEARANCE.

**Figure 2.5. Straddle Bents with Styrofoam in the Cap (SHRP 2013).**

#### 2.6.4. Multiple Bent Cap Segments

SHRP 2 Report S2-R04-RR-2 (SHRP 2013) proposed that limitation in the length of pier caps due to weight or shipping could be avoided by using a number of shorter caps and combining them together to form a straight pier cap.

Similar solutions of using multiple pier cap segments have also been addressed in the optional standard bent cap drawings prepared by Wisconsin Department of Transportation (WisDOT). Figure 2.6 shows the use of non-shrink grout to connect the individual segments. The WisDOT manual has standardized that if two or more segments compose a pier cap, each segment may be supported by two columns (WisDOT 2014).

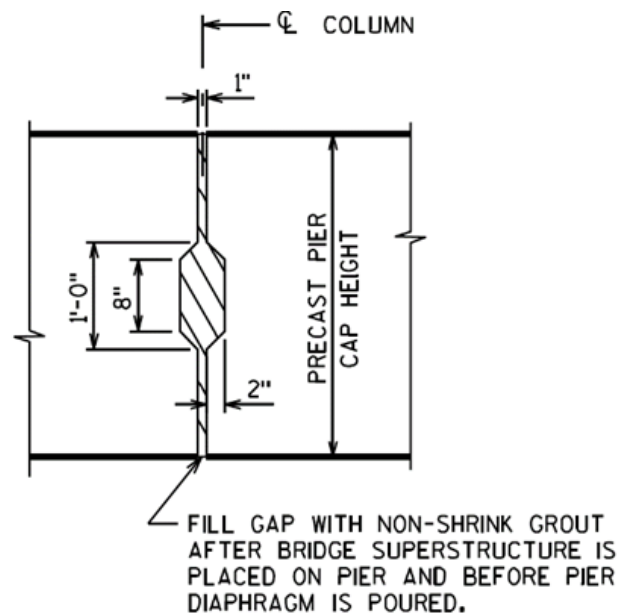


**Figure 2.6. Connection between Multiple Pier Cap Segments (WisDOT Standard Drawing).**

The Washington State Department of Transportation (WSDOT) has used multiple pier cap segments in a demonstration project that was a part of a Highway for Life project awarded by the Federal Highway Administration (FHWA), to test the constructability of a bent system that they developed before its implementation on site (Khaleghi et al. 2012). The pier cap was constructed in two stages. Since the bridge width was 84-ft, the first stage precast bent cap was built of two segments and then joined with a closure pour at mid width of the bridge. The bent cap system including the method of multiple pier cap segments was implemented in a Washington bridge

project in the replacement of the I-5 Grand Mound to Maytown Interchange, as reported by Stanton et al. (2012).

PCI Northeast Bridge Tech Committee conceptualized a detail for connecting adjacent precast cap beams (Culmo 2009). The Committee mentioned that this detail has already been in use in the building industry. As shown in Figure 2.7, bars projecting from the adjacent precast bent caps are connected by grouted sleeve couplers and CIP concrete is then poured.

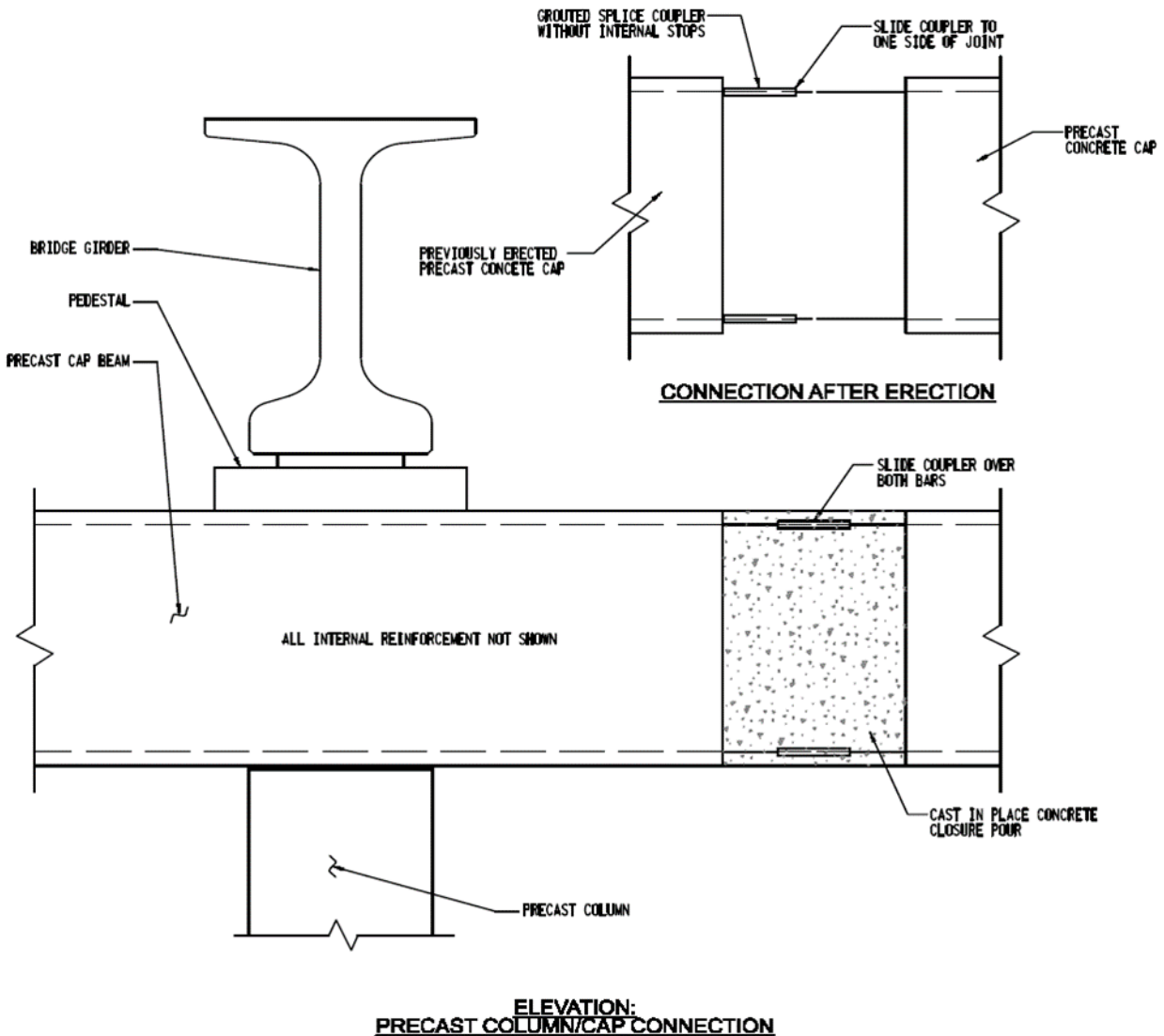


Figure 2.7. PCI Northeast Bridge Tech Committee (Culmo 2009).

## **2.7. CONNECTIONS**

Precast bent caps have been used in bridges in a number of projects by various state departments of transportation (DOTs) due to several advantages such as ABC, reduction of on-site hazards, improved economy, and reduction of cracking that leads to improved durability and quality. The main challenge in delivering a successful bridge project is in the design and construction of the connections between the precast cap and the pier columns whether they be CIP or precast.

This section of the literature review describes several types of cap beam-to-column connections that may be used as a part of the bridge pier. These connections have been classified into emulative and jointed connections. An informative description has been provided in Section 2.7.1. The use of precast connections in some of the early projects in Texas and the current TxDOT precast bent cap-to-column connections have been discussed in Section 2.7.2. Details of the different types of precast connections have been presented in Section 2.7.2, which includes a discussion of results of relevant research conducted and state-of-the practice used by many state DOTs.

### **2.7.1. Overview of Column-To-Bent Cap Connections**

For construction of traditional CIP bent caps, columns are constructed first with the longitudinal column reinforcement extended beyond the column top to form part of the connection of the column-to-cap joint. Following construction of the columns, the cap formwork is placed (typically on falsework), then the cap reinforcement is installed and finally the concrete is poured. As column reinforcement extending into the cap is bonded to the cap concrete, a monolithic (rigid) connection between the columns and cap beam is created.

The primary motivation for the use of precast bent caps is to facilitate improved construction, particularly to accelerate construction and to reduce worker exposure to potentially hazardous worksite conditions. Because the concrete for the bent cap is generally cast at an off-site location, a connection between column and cap needs to be formed on-site. In this study, the existing column-to-precast-cap connection types have been classified into two broad categories: emulative connections and jointed connections.

### 2.7.1.1. *Emulative Connections*

In emulative connections, a rigid connection is formed to emulate customary CIP concrete bridge piers described above. Most bridge piers built with precast bent caps have been constructed to date following an emulative style of construction. For emulative connections the cap beam is typically stronger than the column, particularly in seismic zones. Emulative connections include the following types:

- **Grouted pocket connection:** Reinforcing bars embedded into the column are projected above the top of column and inserted into pocket(s) built in the precast bent cap and then grouted. The pockets are unlined voids cast in the full depth of the bent cap. These pocket connections can have configurations in number of voids (e.g., single or double rectangular tapered pockets used in the tests by Matsumoto [2009]), and configurations in the cross-section of the voids throughout the bent cap, both of which are project specific.
- **Grouted vertical duct connection:** Reinforcing bars embedded into the column are projected above the top of the column to create a connection with the bent cap. The extended bars are each inserted into individual corrugated ducts built in the precast bent cap. The connection is then grouted. TxDOT uses this connection as a standard connection between precast bent caps and columns.
- **Pocket connection:** This connection is similar to the grouted vertical duct connection, but instead of individual ducts, a large corrugated pipe is built in the precast bent cap to which the column reinforcement projected from the top of the column is inserted and is then filled with CIP concrete.
- **Bolted connection:** This connection is also similar to the grouted vertical duct connections. The difference is that threaded bars or post-tensioning bars embedded in the column are extended from the top of the column into individual corrugated ducts present in the bent cap and are then anchored at the top of the cap with nuts. Alternatively, strands used in a precast column may be post-tensioned at the top of the cap.
- **Grouted sleeve coupler connection:** Sleeve couplers are embedded into a precast member (such as a bent cap) and reinforcing bars extended from an adjacent member (such as a column) are inserted into the sleeve and then grouted.

- **Socket connection:** The socket connection involves a member to be embedded to a certain length into an adjacent member. In a socket connection between precast bent cap and piles, a void is created at the bottom of the bent cap for the pile to be inserted. The void is then filled with grout. There is no reinforcement projecting from either member.

#### 2.7.1.2. *Jointed Connections*

Jointed connections are a relatively new concept and have had little field deployment. Nevertheless, considerable research has been conducted on jointed connections. Distinct from emulative constructions, the joints themselves are typically weaker than the adjoining columns and cap beam. Thus under either lateral load or differential settlement, the joint may slightly open or close, thereby protecting the adjoining members from damage. Jointed connections include the following types: partially prestressed (hybrid) connection, armored damage avoidance connections, and pretensioned rocking bridge bent:

- **Partially prestressed (hybrid) connection:** The partially prestressed connection has a combination of both mild steel reinforcement and unbonded post-tensioning strands. It is often referred to as a hybrid connection. Unlike damage avoidance design (DAD), the reinforcement or strands may not be terminated at the column top and continue to the top of the bent cap. Mild steel dissipates inelastic energy, unbonded post-tensioning strands remain elastic and enable controlled rocking at joints, thus leading to minimal residual lateral displacement.
- **DAD:** This is a design procedure to maximize post-earthquake serviceability requirements along with providing life safety. Reinforcement and post-tensioning strands (if used) are terminated at the column top, which enables controlled rocking of the column at the joints. A steel interface is used to strengthen the joint to prevent damage due to development of shear forces during rocking. Essentially no residual drift is observed after large earthquakes thus eliminating the need for post-earthquake repairs.
- **Pretensioned rocking bridge bent:** Similar to DAD, pretensioned rocking bridge bent design dissipates energy by controlled rocking of the column at the ends. This results in minimal residual damage after an earthquake. The columns have pretensioned strands that are unbonded in the central region and bonded at the ends, allowing the structure to return to its original position after an earthquake.

## **2.7.2. Discussion of Connection Details**

The connection types under emulative and jointed connections are described in this subsection and include important conclusions for associated research projects and a discussion of use in DOT projects. The results of research studies are drawn from the relevant references. Much of the discussion on implementation by DOTs is based on the work of Culmo (2009). Summary of the state-of-the-art practice of connection details between prefabricated elements in ABC projects conducted under US DOT and FHWA is presented in that report. The details were classified into three levels based on frequency of use and effectiveness. Information on performance rating by the agencies for constructability, durability, cost, maintenance of the connection has been included. Connection details between precast bents with CIP columns, precast columns, pile bents, and precast concrete caps have been presented. Additionally some of the connection details that are adopted by the state DOTs have been reproduced from the Scan Team report from Project 20-68A by Kapur et al. (2012) performed under the National Cooperative Highway Research Program (NCHRP).

### *2.7.2.1. Grouted Pocket Connection*

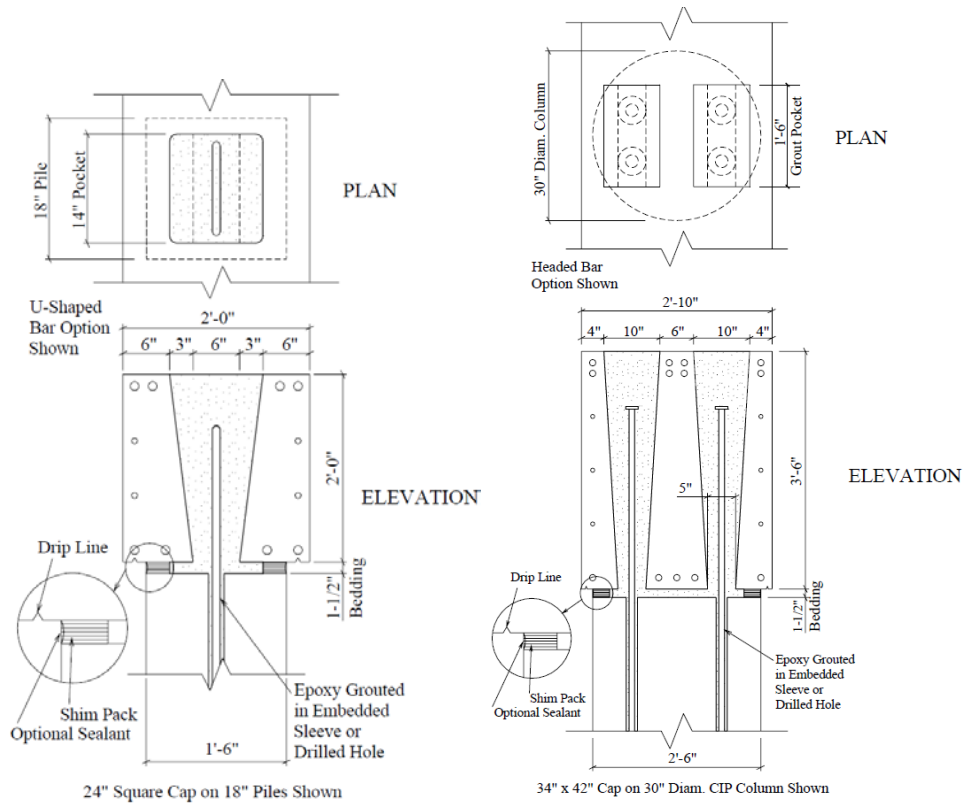
In the grouted pocket connections, column or pile longitudinal reinforcement or reinforcing bars embedded into the column are extended from the top of the column. Pockets are created in the precast bent cap. The noticeable difference between a grouted pocket and a grouted vertical duct connection is the absence of individual ducts in the grouted pocket connection. Tapered pocket shapes were used in the tests conducted by Matsumoto et al. (2001). A single pocket is used in a single line pocket connection, while two pockets are present in a double line pocket connection. The embedded rebars project from the column. During placing of the bent cap, the bars are inserted into the pocket and the connection is then grouted. A similar connection configuration was used in the Red Fish Bay Project by TxDOT, in which #9 U-bars were epoxy grouted into precast piles and inserted into double line pockets present in the precast cap beam.

Matsumoto et al. (2001) examined both single and double line connections (Figure 2.8), conducted pull out tests during Phase 1, and conducted full-scale bent cap to column connection tests in Phase 2 of their experimental program.

Phase 1 results established the embedment depths required for yielding of bars (#6 and #8 were used in the test) and generated the failure pattern of the connection while using different parameters in each of the 24 tests. Failure modes were recognized as 1) concrete breakout with possible yielding of reinforcement before concrete breakout, or 2) bar pullout in which the bar along with a conical grout mass would form a cone separate from rest of the grout. Confining reinforcement in the form of WWF and spirals were observed to increase ductility and capacity. In Phase 2, different combinations of loading and eccentricity for horizontal and vertical loading were applied. Phase 2 yielded results that indicated minor stress levels, limited tensile strains in connection reinforcement, and crack widths. Adequate ductility was confirmed by performance of reinforcement beyond yield strain. Overall performance established grouted pocket connection as an acceptable connection type. A Phase 3 test was also conducted in this program, which intended to confirm the constructability of the connection.

Figure 2.9 presents a grouted pocket connection as used by various state DOTs and described in the synthesis report by Culmo (2009). South Carolina DOT used this connection in the Carolina Bays Parkway Project. Also seen in Figure 2.9, four 1.25-in. diameter bars were inserted into each precast pile and continued to near the top of bent cap. An additional feature in this connection is the insertion of the pile into a recess created in the bottom of the precast bent cap. A significant variation from the grouted pocket connection is seen in the connection types of Florida DOT. The connection used in I-10 Escambia Bay Bridge in Florida was between precast pile cap and precast prestressed square pile. The difference as seen in Figure 2.10 is that all the column reinforcement has been carried until near the top of the pile cap through the precast voids in the cap. The pocket is filled with CIP concrete rather than grout used in the connections in the research and projects discussed earlier in this section. Although this connection detail is similar to the pocket connection type discussed later in this section, the difference from the pocket connection is in the absence of a corrugated steel pipe. These pipes that encase the void in the pocket connection act as a stay-in-place formwork and joint hoop reinforcement.





a) Single Line Grouted Pocket Connection      b) Double Line Grouted Pocket Connection

**Figure 2.8. Grouted Pocket Connection (Matsumoto et al. 2001).**

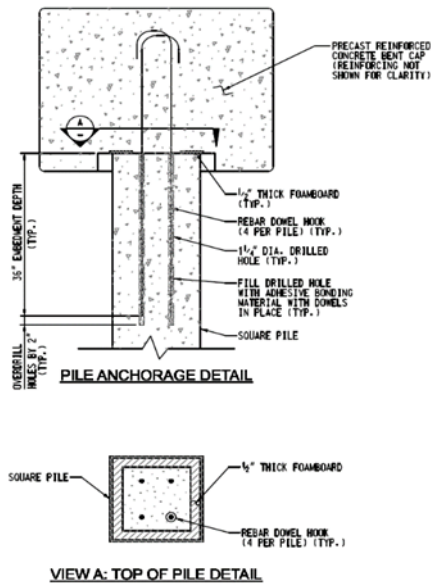


**Figure 2.9. Carolina Bays Parkway Project South Carolina DOT (Culmo 2009).**

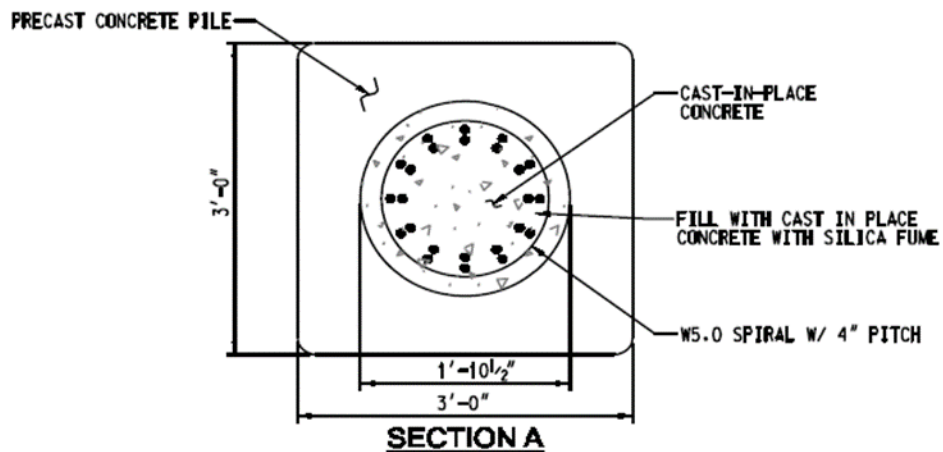
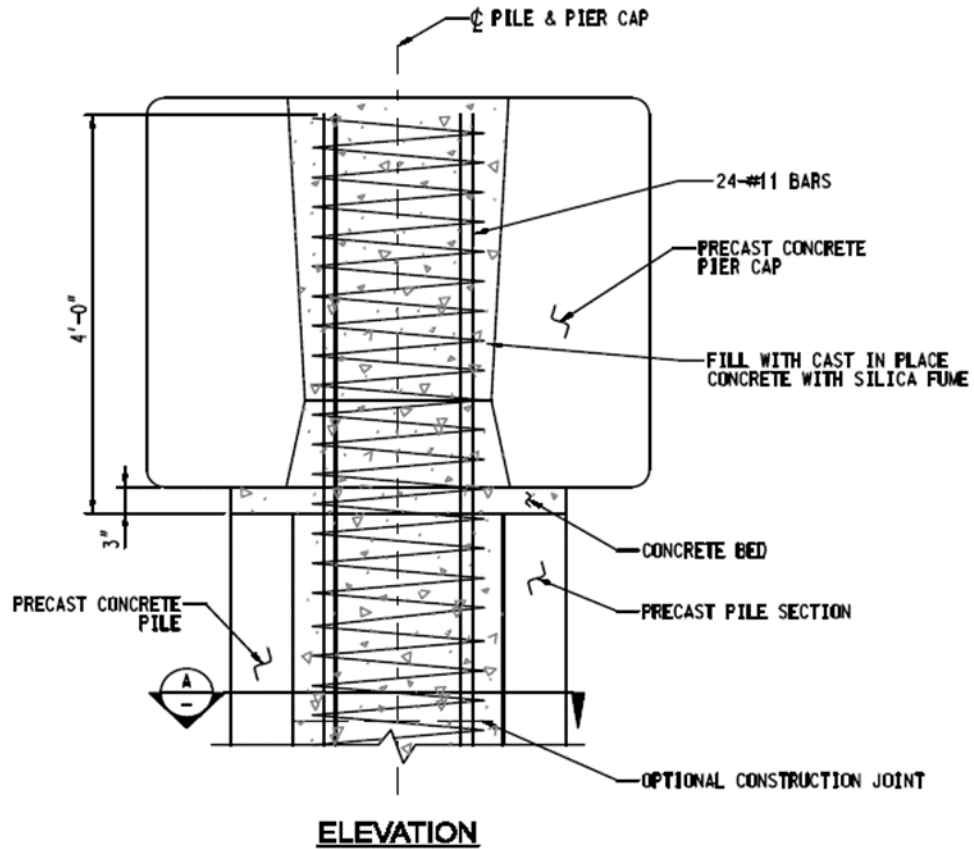


**Figure 2.10. Escambia Bay Bridge Project- Florida DOT (Culmo 2009).**

Figure 2.11 presents a grouted pocket connection used in St. George Island Bridge in Florida. Instead of reinforcing bars, a steel pipe embedded in the precast cylindrical pile continued to the top region of the pile cap and anchored at the round steel plate with a hole in the center.

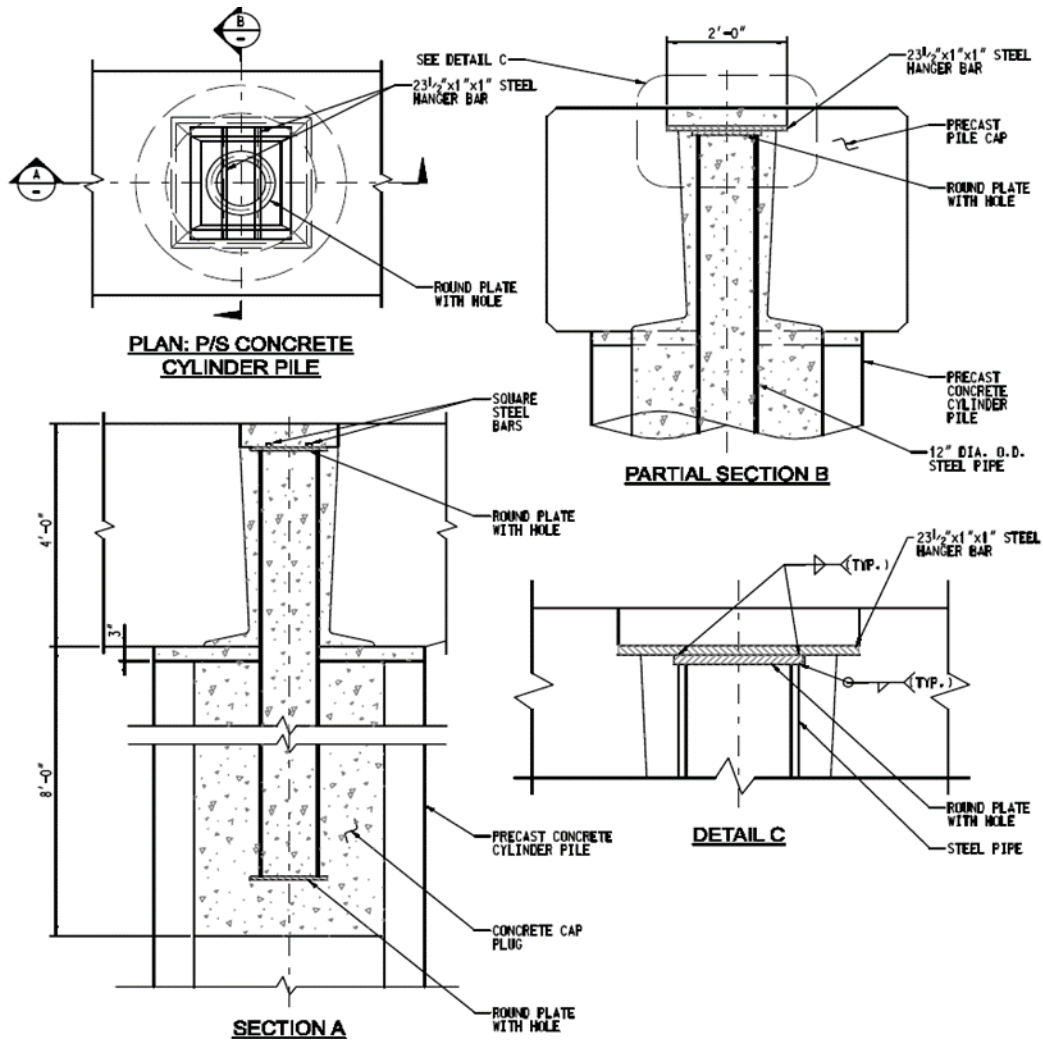


Figure 2.11. St. George Island Bridge- Florida DOT (Culmo 2009).

The grouted pocket connection allows large tolerances during construction. However, a number of considerably oversized pockets may not be preferable as it would reduce the effective area of the bent cap and pose an obstacle to placement of the longitudinal reinforcement in the cap beam. Significant grouting is required in the pockets depending upon the pocket size. Although an acceptable connection type, the focus of the research group is on a connection with minimal use of grout (as discussed earlier), which is in contrast to this connection.

#### 2.7.2.2. Grouted Vertical Duct Connection

##### 2.7.2.2.1. Description

The grouted vertical duct connection is used as a standard TxDOT connection. As discussed earlier in this section, this connection consists of reinforcing bars embedded into the column that

continues from the top of the column and projects into individual corrugated ducts built in the precast bent cap. The duct is then grouted.

This connection has been investigated and tested under several research studies. Matsumoto et al. (2001) examined behavior in pull out tests, gravity loads, and wind lateral loading. Brenes et al. (2006) also conducted pull out tests on this connection. Restrepo et al. (2011) studied the seismic behavior of the connection. Pang et al. (2008; 2010) investigated the seismic response of this connection built with large diameter bars such as #18 bars.

The experimental test program conducted by Matsumoto et al. (2001) was done in three phases. Phase 1 consisted of pull out tests that were performed on epoxy coated straight and headed bars to determine the influence of variable parameters on the connection response. The embedment depth required in grouted ducts could be easily accommodated in a typical bent cap. Both headed and straight bars showed pullout behavior in which a bar grout mass would be pulled out from rest of the grout inside the duct. Phase 2 of the test program involved testing full-scale bent cap-column specimens. Out of the four tests, one was conducted on a grouted vertical duct connection. Different combinations of loading and eccentricity were applied for vertical (gravity) and horizontal (wind) loads. Results showed that no cracking occurred in the grout surface as flexural cracks were restrained by ducts. Spiral reinforcement did not improve ductility and strength for large bar diameters and spacing, but the authors recommend the use of at least a minimum amount of spiral confining reinforcement. Although use of a grout with strength less than that of bent cap concrete did not affect response, the authors recommended using a grout with compressive strength greater than the surrounding concrete. Grouted vertical duct was found to be an acceptable connection type for use in precast bent caps. Phase 3 investigated the constructability of the connection by testing two bent systems in which one of the connections tested was a grouted vertical duct connection. The connection would be constructible on-site.

Brenes et al. (2006), under TxDOT Project 0-4176, researched grouted vertical duct connections widely used in Texas and tested 12 bent caps specimens for 32 pullout tests to understand the influence of a list of parameters. The results indicated that average bond was sensitive to duct material, effect of one or more bars tested simultaneously, and eccentric placement of bars within ducts. The use of polyethylene or polypropylene duct reduced capacity of bars to resist high bond

stress in comparison to the use of galvanized corrugated steel ducts. Eccentric placement of bars within each duct reduced the capacity of the bars. Testing of multiple bars in tension reduced bond strength. Bar coating, clear spacing between ducts, and transverse reinforcement did not influence connector response. Results showed that small spirals around individual ducts reduced connector response. The authors suggested that this might be due to low strength concrete around the ducts. Placing of concrete around the ducts might have been interfered by the small pitch of individual spirals or the small spacing between individual spirals and the ducts leading to low strength concrete, which affected the connector response. Therefore, the authors recommended not using single spirals around each corrugated duct. Also, a single spiral used to confine a group of connectors showed no increase in average bond strength.

As the two studies on grouted vertical ducts discussed above were confined to non-seismic regions such as Texas, it was considered necessary to assess the behavior of this connection under seismic loading and confirm its suitability for use in moderate to high seismic regions. Therefore, Restrepo et al. (2011) conducted 42 percent scaled tests to evaluate the seismic performance of this precast connection. Out of the 7 tests performed on different connections including grouted vertical duct connections, a CIP specimen was also tested. This was done for comparison between the precast connection and the CIP connection for confirmation of emulative behavior. The connection was made with reinforcing bars extending from the column into individual 1.75-in. diameter, 22-gage corrugated galvanized steel ducts in the bent cap. The voids were grouted with high strength, non-shrink, cementitious grout specified to be at least 0.5 ksi greater than compressive strength of concrete in the bent cap. The test specimen consisting of a bent cap, a column, and a footing was tested in an inverted position. Force controlled and displacement controlled loading was applied. Plastic hinges formed in the column, stable hysteretic response was exhibited, and joint shear deformation was minor. Failure occurred by low cyclic fatigue of the longitudinal reinforcement. The connection was deemed to achieve its intended emulative behavior.

To reduce construction time and thereby enhance ABC, research was necessary to assess the behavior of a grouted vertical duct connection with the use of fewer number of larger diameter bars. Pang et al. (2008) examined the seismic performance of this connection and compared it with a CIP connection. Column flexural reinforcing bars were terminated at the top of the column.

Connection to the cap was made using 6-#18 dowel bars embedded in the precast column and projected from the top of the column; bars were evenly spaced around the circumference of the column. Flexural reinforcement was terminated at the top of column. The bars were then extended to individual ducts made of 8.5-in. corrugated steel pipe placed in the precast bent cap. The spiral reinforcement in the column was continued along the depth of the bent cap. To design the connection with adequate ductility, bar yielding should precede other types of brittle failure. This necessitated knowledge of the embedment length required for #18 bars grouted in ducts. Prior tests to determine embedment lengths were either limited to small diameters or to bars that were not grouted. Consequently, Steuck et al. (2007) performed pull out tests to evaluate the required anchorage. Experimental results indicated that embedment depths of  $6d_b$  and  $14d_b$  were required for bar yield and fracture, respectively. An analytical model concluded that bar fracture could be achieved at an embedment depth of  $10d_b$ . The result indicates that embedment depth of bars grouted in ducts is less than that required in concrete and can easily be accommodated in a typical bent cap.

Using the results, tests were performed to evaluate the seismic performance of the proposed connection. The test assemblies consisted of columns, cap beams, and diaphragms. Figure 2.12 shows the large diameter bars extended from the top of the columns through corrugated ducts and anchored in the CIP diaphragms placed at the top of the bent cap. Four assemblies were tested consisting of one scaled CIP specimen and three 40 percent scaled precast specimen of the proposed connection. In one of the precast specimens, the bars were fully bonded while the other two specimens used two different debonding methods. Debonding is a procedure of restraining high strain concentration at the joint locations by sleeving the bar along a specified distance from the joint face, primarily to preclude premature bar fracture at the joints. The specimens were tested at a constant axial loading and cyclic lateral displacement. All the four specimens exhibited adequate ductility and the precast specimens indicated results similar to the CIP specimen.

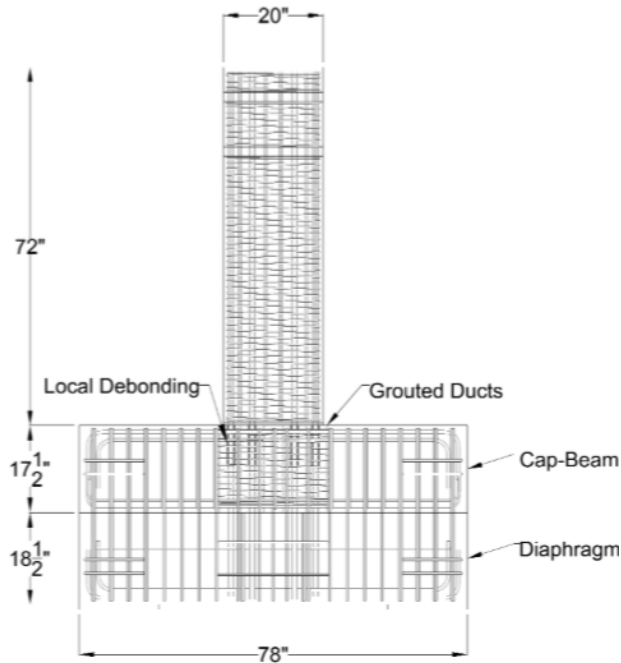


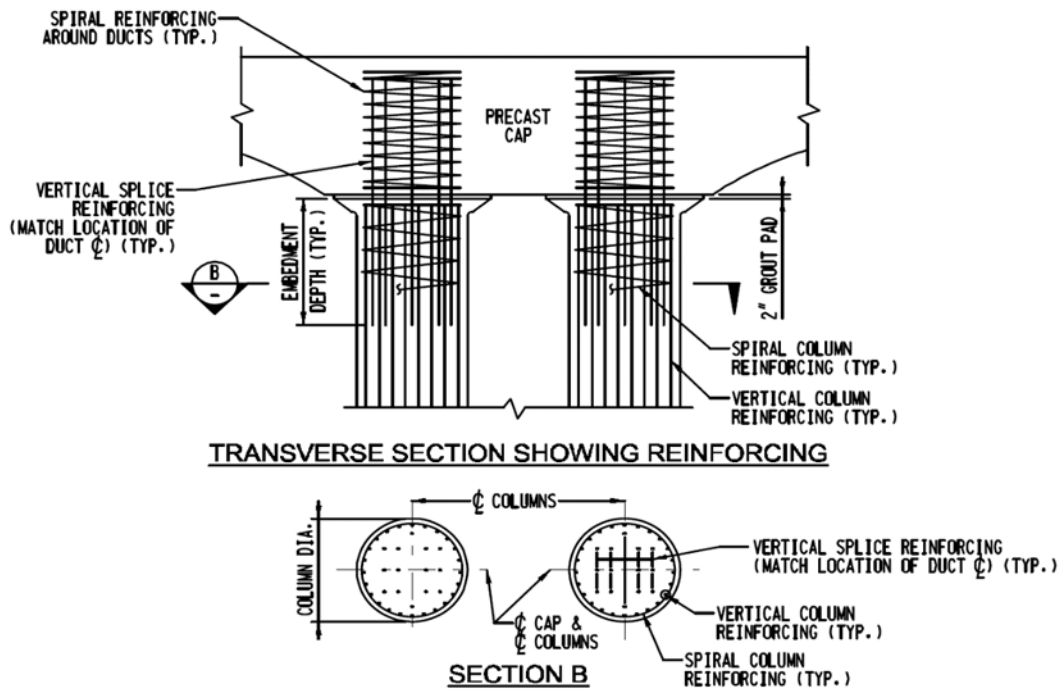
**Figure 2.12. Scaled (40 Percent) Specimen Connection Tested by Pang et al. (2008).**

Using the concepts developed in the research and testing results described above, Khaleghi et al. (2012) developed a bridge bent cap system supporting ABC in high seismic regions as a part of a Highway for Life project supported by FHWA. The system consisted of a CIP spread footing, precast column, first stage precast bent cap, and a second stage CIP bent cap. For bent cap to column connection, 6-#18 diameter bars extending from column were projected into 8.5-in. corrugated pipes embedded in the first stage precast cap beam. The second stage CIP cap beam was constructed integrally with the girders placed at the cap top in consistence with WSDOT's standard practice. Both the column-to-cap beam and column-to-footing connections were individually tested under cyclic loading and then implemented in a demonstration bridge project executed by WSDOT to ensure the constructability of the bent system on a bridge project.

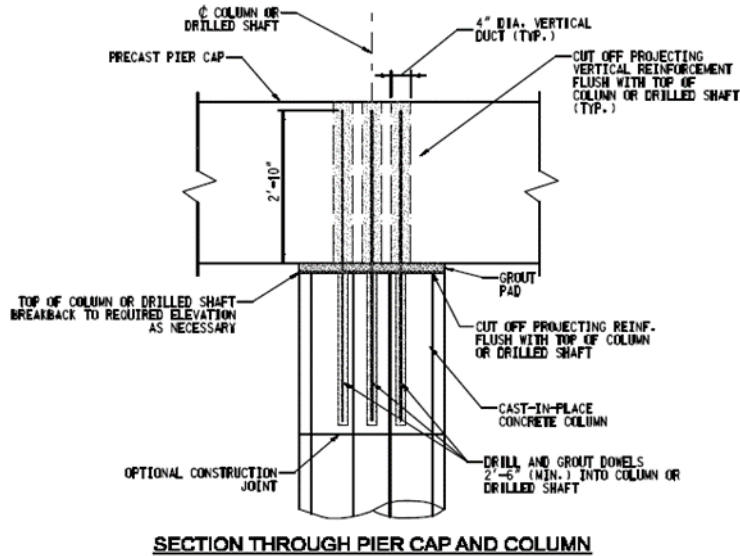
#### **2.7.2.2.2. Field Implementation**

Figure 2.13 and Figure 2.14 present examples of two field implementations where grouted vertical ducts have been used in Texas. Several other projects have also been implemented in other states. Early use of this connection by TxDOT between precast bent caps and CIP columns was in the Lake Belton project. Column reinforcement was extended through the corrugated ducts to near the

top of the bent cap, with spiral reinforcement confining the full height of the group of bars. Similar configuration in the connections can be seen in Lake Hubbard project by TxDOT.



**Figure 2.13. Lake Belton Project- TxDOT (Culmo 2009).**



**Figure 2.14. Lake Hubbard Project TxDOT (Culmo 2009).**

Project 20-68A performed under NCHRP presented a Scan Team report, which intended to collect and disseminate information pertaining to practices involving ABC connections with some



particular focus given to areas experiencing extreme loading events. Connections in ABC columns that were in practice included socket connections (embedded column ends), grouted couplers and grouted ducts. A grouted vertical duct connection used in Washington State is shown in Figure 2.15. In Figure 2.16, a precast pretensioned bent cap is built with vertical ducts to create a connection (Miller et al. 2014).



**Figure 2.15. Grouted Vertical Duct Connection in Washington State (Project 20-68A).**



**Figure 2.16. Pretensioned Precast Cap (Miller et al. 2014).**

The bent cap system developed by Khaleghi et al. (2012) using #18 diameter bars in 8.5-in. duct for the connection between precast bent cap and columns was implemented in a Washington bridge project in the replacement of the I-5 Grand Mound to Maytown Interchange (Stanton et al. 2012).

Construction of the system proved to be easy and the only difficulty was the grouting of the column segments. However, this is an additional feature of the system and project specific, not typical of the bent column system.

#### **2.7.2.2.3. Discussion**

As discussed earlier in this section, although the grouted vertical duct connection has been used in several projects in and outside Texas and provides good performance in the field, TxDOT is interested in the implementation of a grout-less connection. However, increasing the duct size from 4-in. to 8.5-in. would enable the grout to be replaced with high strength concrete. This would also provide a solution to the tight tolerance available in connections with smaller ducts. The large corrugated pipes (four times the bar size) provides sufficient room for comfortable alignment of the bars.

#### *2.7.2.3. Pocket Connection*

##### **2.7.2.3.1. Description**

The grouted vertical duct connection used by TxDOT as standard connection type consists of a number of corrugated ducts present in the precast bent cap to which reinforcing bars embedded in the column are inserted. Similar to this concept is a pocket connection. In this type of connection, one large corrugated metal pipe creates a pocket in the precast bent cap centered about the position of column. Longitudinal column reinforcement is projected from the top of the column. During placement of the precast bent cap, the reinforcing bars run through the large pocket to the top of the bent cap. The pocket is then filled with CIP concrete.

##### **2.7.2.3.2. Previous Research**

In the research study reported in the NCHRP Report 681, Restrepo et al. (2011) examined this connection to test its suitability in high seismic regions. Figure 2.17 shows examples of their test specimen. The test specimen was 42 percent scaled and consisted of a bent cap, a column, and a footing. An 18-in. nominal diameter corrugated metal pipe was used to create the pocket to house column reinforcement. The pipe is present between the top and bottom longitudinal reinforcement in the cap, hence drums made of cardboard were used above and below the pipe to make the pocket continuous along the depth of cap beam. Two types of pocket connections were tested and

examined: cap pocket full ductility (CPFD) intended for use in high seismic regions and cap pocket limited ductility (CPLD) for low to moderate seismic regions. The CPFD specimen was designed based on seismic design category (SDC) D design, which required significant joint reinforcement. The CPLD specimen was based on SDC B design, which did not require any joint reinforcement other than the steel pipe. All dimensions and pipe size remained same, thus the CPLD differed from CPFD in terms of lack of joint confining reinforcement and reduction of cap longitudinal reinforcement. CPFD had additional hoops at both the ends of the pipe and construction stirrups in the joint. After placement of the cap beam on the column, the pocket and bedding layer between the bent cap and the column were filled with concrete. Concrete compressive strength was intended to be achieved at least 0.5 ksi greater than the concrete in the bent cap.

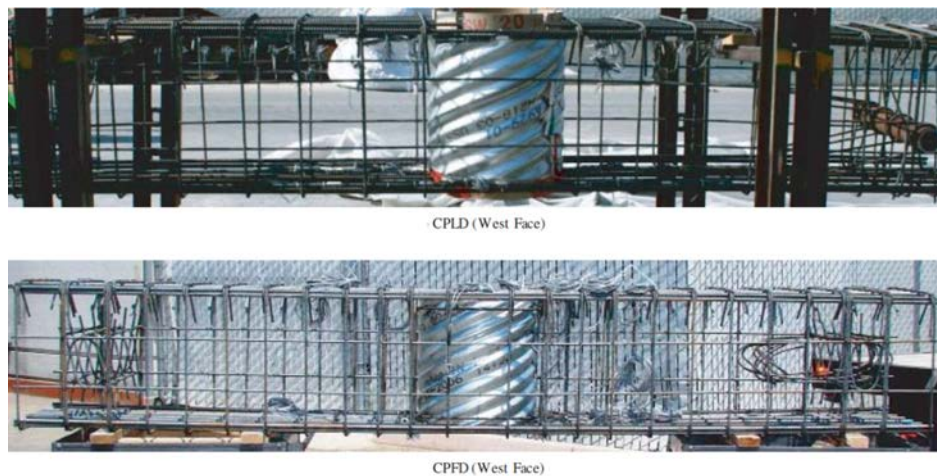


**Figure 2.17. Reinforcement in CPLD (Top) and CPFD (Below) (Restrepo et al. 2011)**

Testing of the specimen was done in an inverted position. Force controlled loading was applied until an expected first yield beyond which displacement controlled loading was applied. Test results indicated plastic hinging of column, adequate ductility, and “stable hysteretic behavior without appreciable strength degradation.” The limited ductility specimen (CPLD) showed more joint shear cracking and deformation in comparison to the full ductility specimen (CPFD) due to the intentionally reduced joint and flexural reinforcement. This proved that SDC B joint design should have at least minimum joint shear reinforcement. Both the specimens were able to emulate CIP connections. Failure occurred by buckling followed by low cyclic fatigue of the longitudinal reinforcement.

### 2.7.2.3.3. Field Implementation

Figure 2.18 presents a field implementation that is a similar arrangement of the pocket connection between precast concrete caps and steel pipe piles in Iowa DOT in their Boone County IBRC project. Concrete was filled in the interior of a steel pipe pile and #8 hooked bars were embedded. These bars were continued from the column top and projected into the pocket created in the cap by a 21-in. corrugated metal pipe. Voids were filled with low shrinkage concrete.

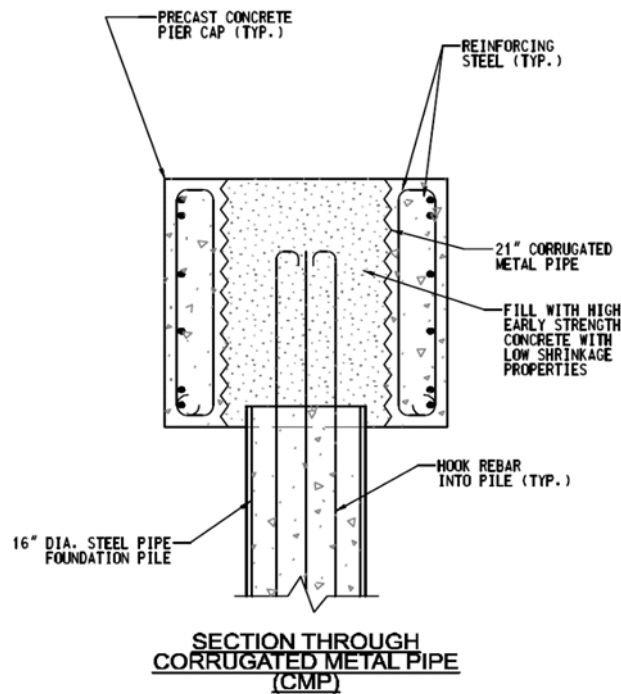


Figure 2.18. Boone County IBRC Project Iowa DOT (Culmo 2009).

### 2.7.2.3.4. Discussion

The primary advantage of a pocket connection is the use of normal weight CIP concrete rather than grout. Absence of grouting operations may result in improved economy and also mitigate durability concerns associated with formation of air voids during grouting operations. Large tolerances can be achieved for this class of connection as a large pocket can accept moderate misalignment of column reinforcement. This provides constructional advantage over grouted vertical duct connections that require the individual ducts to be precisely at the correct alignment with the projecting column reinforcement. The pocket connection showed favorable results during the inelastic cyclic loading tests representing high seismic regions performed by Restrepo et al.

(2011). The results of their research show that the pocket connections can be transferred with confidence to a low seismic region such as Texas.

#### 2.7.2.4. *Bolted Connection*

##### **2.7.2.4.1. Description**

A bolted connection is similar to a grouted vertical duct connection. Column longitudinal and spiral reinforcement are terminated at the top of the column. Threaded bars or post-tensioning bars are embedded in sleeves or holes built in the column. The bars extend above the top of the column and provide connection to the bent cap. The precast bent cap is built with individual vertical steel ducts that align with the extended bars. The difference from a grouted vertical duct connection is that the bars are anchored at the top of the cap with nuts in a bolted connection. The duct and bedding layer between the column and bent cap is grouted. Tobolski et al. (2006) mentioned that this connection is advantageous over the grouted vertical duct connection because it provides stability during construction before grouting, and anchoring provides secondary support in case of grout bond failure. Another variation of bolted connection was reported in which strands instead of reinforcing bars are projected from the top of the column and then the strands are post-tensioned at the cap top. This has been used in precast segmental columns.

##### **2.7.2.4.2. Previous Research**

In the three phase experimental program by Matsumoto et al. (2001) under project 0-1748, a full-scale beam column specimen with a bolted connection was tested in Phase 2. Different combinations of loading and eccentricity were applied for vertical (gravity) and horizontal (wind) loads. Similar to grouted vertical duct, no cracking occurred in the grout surface as flexural cracks were restrained by ducts. Results on spiral reinforcement and grout strength were the same as grouted vertical duct connections. Adequate bonding was achieved along the length of the bar, thus anchorage of the bars at the cap top provided redundancy. In comparison to a bolted connection, grouted vertical duct connections had a stiffer response in the test. Bolted connections were found to be an acceptable connection type for use in precast bent caps.

#### **2.7.2.4.3. Field Implementation**

Figure 2.19 shows an implementation of bolted connection in the Bridge over BNSF railroad project by Wyoming DOT, as reported in the synthesis report by Culmo (2009). The threaded rods were anchored at the top and bottom by anchor plates placed at cap top and CIP column, respectively.

Similar configuration of connection was implemented in the Pierce Street elevated bridge project by TxDOT as reported in Matsumoto et al. (2001). High strength high alloy (Dywidag<sup>TM</sup>) threaded bars were grouted in holes drilled in the columns. The bars were extended to corrugated ducts present in the bent cap. The bedding layer between the bent cap and the column, and the corrugated ducts were grouted. The bars were anchored at the cap top.

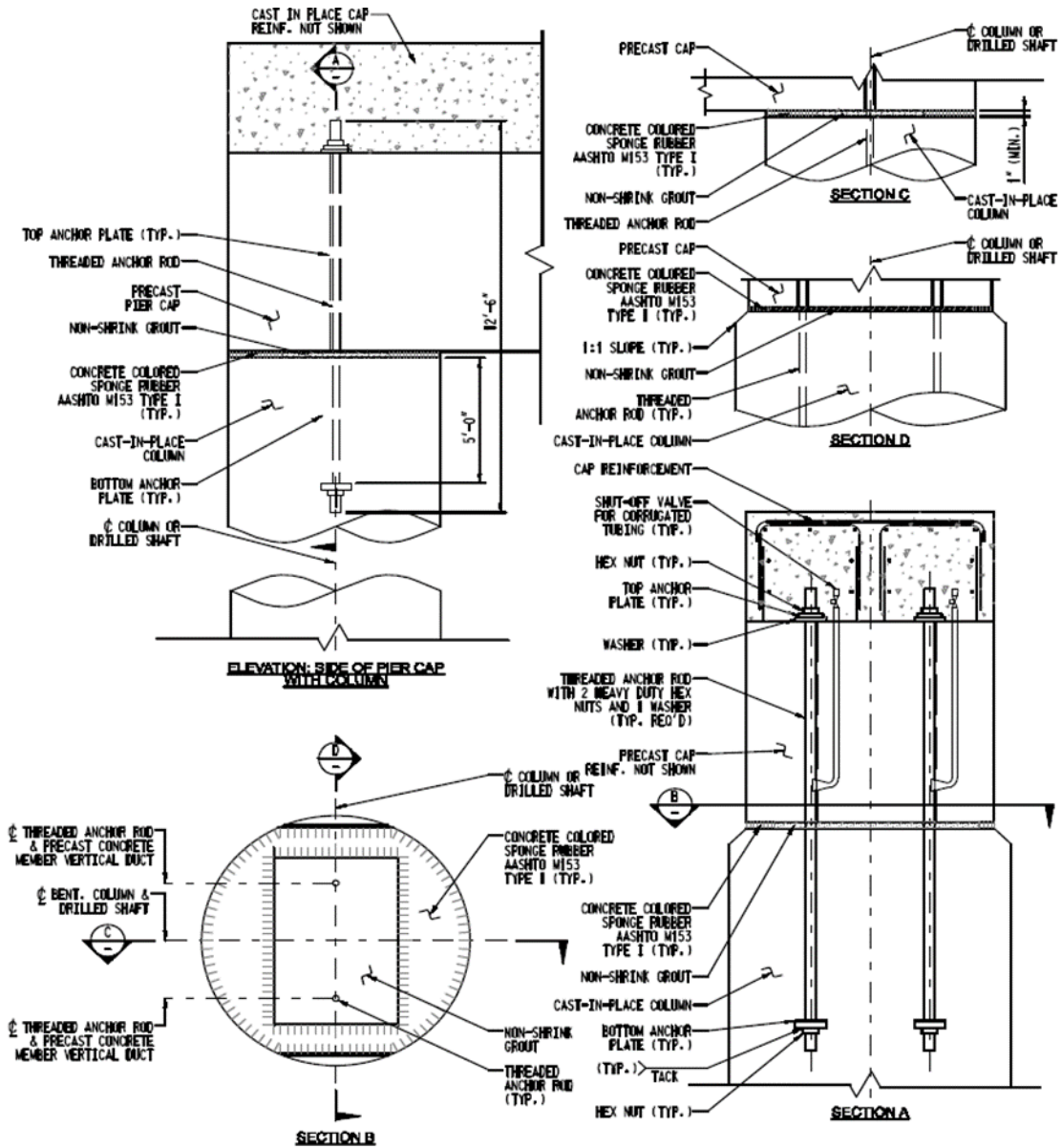


Figure 2.19. Bridge over BNSF Railway Project, Wyoming DOT (Culmo 2009).

#### 2.7.2.4.4. Discussion

A bolted connection is a suitable connection type and has been already implemented successfully by TxDOT at the Pierce Street elevated project. Another attractive feature of this connection type is that it is essentially a dry connection as it uses only minimal grout. Such grout strictly forms only a leveling pad to seat the cap beam. There seems little compelling reason to grout the bolts (extended bars) as they are well anchored at each end. Accordingly, this connection really looks somewhat like the new generation of jointed connections described later herein.

### 2.7.2.5. *Grouted Sleeve Coupler Connection*

#### **2.7.2.5.1. Description**

In this connection, a grouted sleeve coupler is embedded in a precast member (such as a bent cap). Reinforcing bars from an adjacent member (such as a column) are extended and inserted into the sleeve. The connection is then grouted.

Features of this connection were reviewed in TxDOT project 0-1748 by Matsumoto et al. (2001). This connection has been successfully used in the past in the building industry. But in the bridge industry, the minimal horizontal tolerance allowed in the connection causes concern during construction. Matsumoto et al. (2001) mentioned how templates were used in the construction of the Edison Bridge in Florida to avoid constraints of tight tolerance in the alignment of reinforcing bars projecting from the columns into the sleeve built in the precast bent cap. Also noted in the report was the disadvantage of limited availability of proprietors offering mechanical sleeve couplers. Grouting needs to be done separately for the connection and bedding layer between the bent cap and the column.

#### **2.7.2.5.2. Previous Research**

Although research has not been conducted particularly for bent cap-to-column connections with grouted sleeve couplers, studies have been done to evaluate the seismic behavior of this connection between columns and footings. Haber et al. (2014) conducted five experimental tests to evaluate the behavior of grouted sleeve coupler connections between precast columns and CIP footings. Four new connections were developed, each used mechanical couplers but varied in parameters such as the use of two different types of couplers, location of couplers in plastic hinge zone, and presence or absence of a pedestal above the footing. The four connections were each used in four precast columns. The connection between the precast column and CIP footing was tested under cyclic loading. A conventional CIP specimen was also similarly tested. The connection confirmed similarity in behavior to the traditional monolithic connection up to 6 percent drift. Ductility capacity of the connection was adequate for use in moderate to high seismic regions. Results also indicated that the presence of a coupler in the plastic hinge region can impact the plastic hinge mechanism.



### **2.7.2.5.3. Field Implementation**

WisDOT has implemented grouted sleeve coupler as a standard connection between precast columns and precast bent caps/CIP footings. The couplers are placed at the top and bottom ends of the column to create a connection with the bent cap and the column, respectively.

Figure 2.4 shows grouted sleeve coupler connection between I-shaped precast columns and an U-shaped precast bent cap in the Edison Bridge in Florida, as reported by Culmo (2009). The limitation of tight tolerance involved in this connection was resolved by using oversized splicers. However, to provide cover to the couplers the reinforcing bars were moved toward the center of the members. The Florida DOT commented that “quality control on bar and splicer locations” were critical.

Another application of this connection is in a standard detail that was under development by Utah DOT at the time of the report by Culmo (2009). For the cap to column connection, grouted couplers are placed in the bent cap, as seen in Figure 2.20.

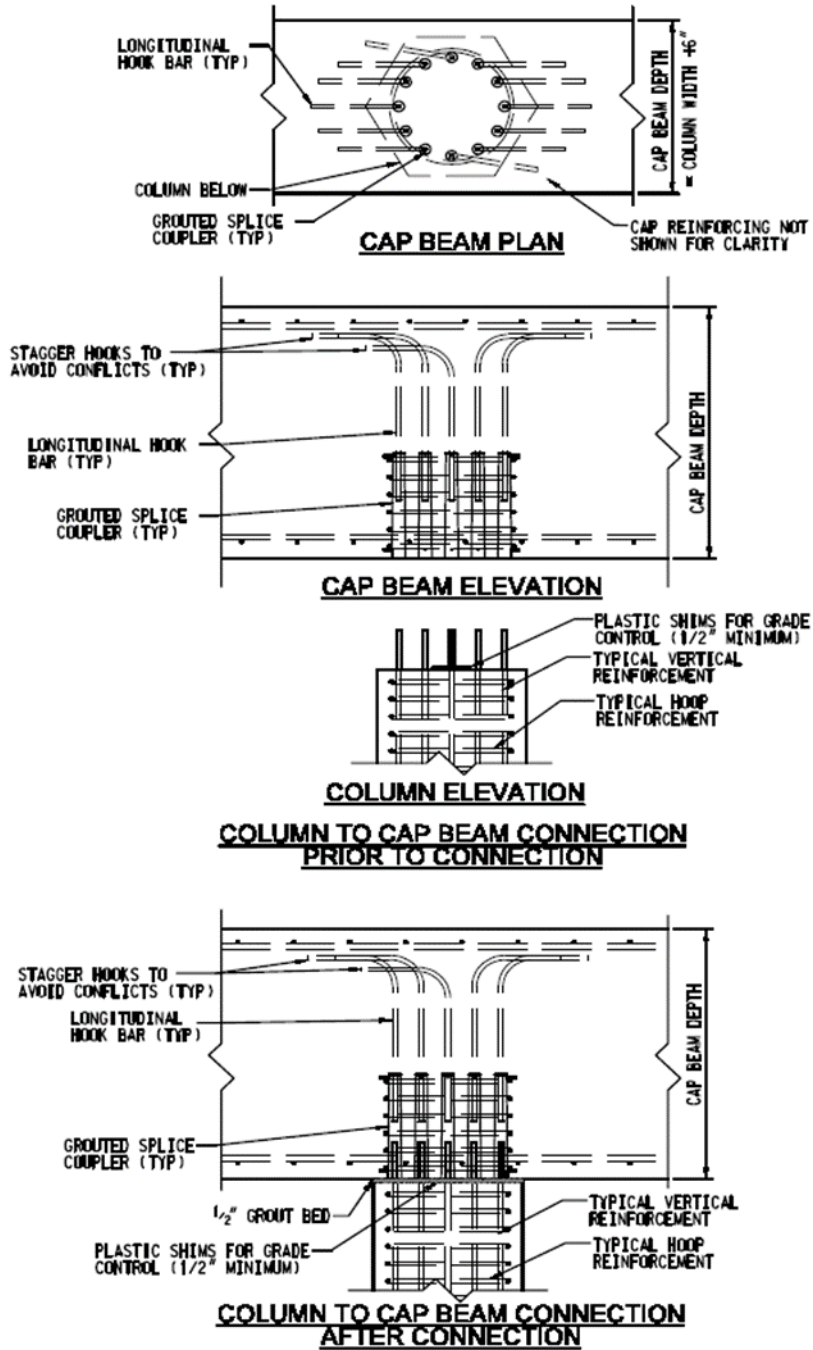


Figure 2.20. Utah DOT (Culmo 2009).

The Scan Team report under NCHRP Project 20-68A by Kapur et al. (2012) also reported on projects with implementation of this connection type. Apart from Florida DOT discussed above, Utah has used this connection between column and pile shaft. A noticeable feature in this connection is placement of couplers in the plastic hinge region of the columns. This was based on

some other codes, which unlike AASHTO, allowed placing of couplers in plastic hinge locations in high seismic regions.

#### 2.7.2.6. *Socket Connection*

##### **2.7.2.6.1. Description**

In a socket connection, one member is embedded to a certain length into an adjacent member. In a precast bent cap system, this connection is made between the precast piles and the precast bent cap. The connection is then grouted. The difference from a pocket connection is that there is no reinforcement projecting from the embedded member to make a connection. Marsh et al. (2011) in the NCHRP 698 report mentions that the embedded member is anchored by the bond formed with grout and by the prying action. Bond resistance can be increased by roughening the connecting surfaces of both members.

##### **2.7.2.6.2. Previous Research**

Research has been performed to evaluate the seismic performance of a precast socket connection. Ziehl et al. (2011) conducted research on connections between PSC piles and precast concrete bent caps. The study focused on testing two full-scale single pile bent cap specimens, which included one interior (T-joint) and one exterior (knee joint) specimen. A pocket was created in the bent cap with a combination of a 3-ft diameter corrugated pipe and cardboard, centered about the location of the pile. The precast piles were embedded 26-in. into the bottom of pocket in the bent cap. The pocket was then filled with low shrinkage concrete. Testing was done under displacement control with varying step sizes up to 8-in. corresponding to a 5 percent drift. An axial load representing dead load and a compressive load perpendicular to the pile was applied on both specimens. Finite element modeling was also performed. Test results showed that plastic hinging was formed at the pile just below the bent cap. Ductility capacities of both the specimens were greater than the desired ductility, moment capacity exceeded desired value, cracks in the bent cap were small, and stresses at the joint were below allowable limits.

In the bridge bent system developed by Khaleghi et al. (2012) discussed earlier, a socket connection was used between the footing and column. A socket connection was developed by placing the precast column and footing reinforcement in the excavation and then casting the

footing concrete around the column. Although the same concept of embedment of the column into the adjacent member has been used, this detail is not directly applicable in a precast bent cap to column connection.

### 2.7.2.6.3. Field Implementation

The synthesis report by Culmo (2009) indicates the use of this connection by the state DOTs, as shown in Figure 2.21 and Figure 2.22. All the connections were between precast bent caps and precast piles. In the South Carolina DOT, large sized pocket connections were built in the precast bent caps. A smaller hole was built between the top of large pocket and cap top and was meant for grouting from the top. The connection in Louisiana has a drift pin hole in the precast pile to make it a pinned connection allowing the transfer of axial and lateral forces.

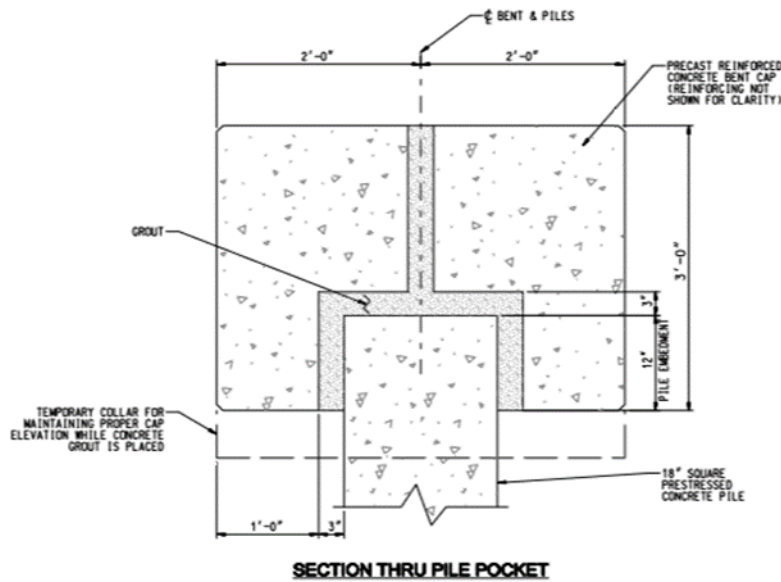


Figure 2.21. South Carolina DOT (Culmo 2009).

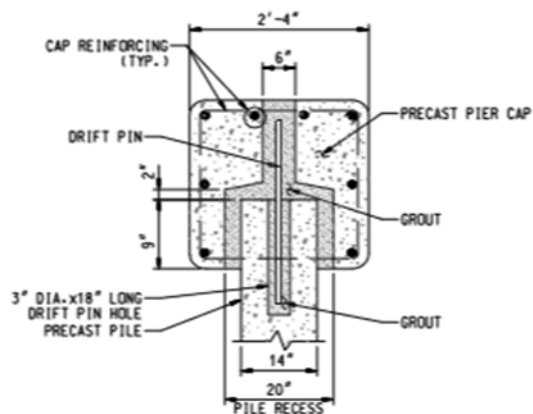


Figure 2.22. Louisiana DOT (Culmo 2009).

#### **2.7.2.6.4. Discussion**

This connection type is an easily constructible connection between precast bent caps and precast piles. Its applicability in seismic regions has been confirmed from the research discussed above. There might be a requirement of increasing the width of bent cap to accommodate a large pocket. The use of non-shrink concrete is a viable option for a grout-less connection.

#### **2.7.2.7. Partially Prestressed (Hybrid) Connection**

##### **2.7.2.7.1. Description**

This connection is different from the connections described so far. As discussed earlier, those connections were emulative connection, and are so named as they intend to perform or emulate a CIP connection. The partially prestressed (hybrid) connections use both mild steel reinforcement and unbonded post-tensioning. Their design intent is particularly for seismic regions where large inelastic cyclic loading may be expected. Mild steel allows dissipation of energy, while unbonded post-tensioning strands combine both beam and column together and enables controlled rocking at the joint interface. Even if deformation is caused during seismic activity, since the strands remain elastic, the structure is re-centered back to original position. This ensures minimal residual damage in this connection.

##### **2.7.2.7.2. Previous Research**

Research and use of hybrid connections in building industry has been performed before the bridge industry. Stone et al. (1995) performed tests on precast moment resisting hybrid connections used in buildings in high seismic regions as Phase IV testing of an experimental program. The objective of the program was to establish guidelines for such connections. Phase IV was conducted in two phases. Phase IV-A tested three specimens with variation in the locations of mild steel and post-tensioning strands. The best result was yielded when the strands were placed at mid depth of the beam, with the condition that the strands be stressed less than that in conventional procedure. The test results were implemented in Phase IV-B testing, which aimed at evaluating the seismic performance of the connection and compare with a CIP connection. The test specimens varied in types and amount of mild steel. Precast hybrid connection was found to yield comparable results with a CIP connection, showed minimal residual drift was present, and exhibited a large lateral

drift capacity. Cheok et al. (1998) analytically investigated precast moment resisting hybrid connections using a non-linear analysis computer program. Similar results were achieved that demonstrated that precast hybrid connections performed equivalent to or better than monolithic connections.

Restrepo et al. (2011) in NCHRP Report 681 classified and examined three types of hybrid connections for precast bent cap systems intended to be used in seismic regions. Tobolski (2010) described the three types of partially prestressed (hybrid) connection investigated by Restrepo et al. (2011). The first type of hybrid connection referred in that paper was conventional hybrid connections. These connections are similar to the grouted vertical duct connection in the way the reinforcement is projected from the column to individual corrugated ducts present in the bent cap. Reinforcement was debonded at the column ends to prevent premature bar fracture, as can be seen in Figure 2.23. In addition, a single post tensioning duct with strands was located at the center. Spiral reinforcement was provided along the full height of the column. The second type of hybrid connection mentioned in the paper was concrete filled pipe hybrid connections, as shown in Figure 2.24, and it differed from the conventional type as it consisted of an outer steel pipe filled with concrete. Column reinforcement was provided to a certain length from the ends of the column for dissipation of energy instead of continuous reinforcement in its full height as used in the conventional type. Configuration of duct, debonding of reinforcement, and shear reinforcement was the same as the conventional type. The third type referred to as dual steel shell hybrid connection shown in Figure 2.25 was developed as a lighter alternative of the concrete filled pipe, in which an additional inner steel pipe was present inside the outer steel shell to form a void interior.

Tests were conducted on 42 percent scaled specimens for each of the above three connections. All the specimens displaced excellent ductility, exhibited negligible damage, and residual drift in comparison to a CIP specimen.

#### **2.7.2.7.3. Field Implementation**

Researchers are currently not aware of any implementation of this connection between precast bent caps and columns in any bridge projects.

#### 2.7.2.7.4. Discussion

The hybrid connection is expected to be promising for seismic regions with a performance equal to or better than a conventional monolithic connection. Texas is in a non-seismic region and the current TxDOT standard drawings do not implement precast columns. Considering these factors, hybrid connections may not be in the focus of this research study.

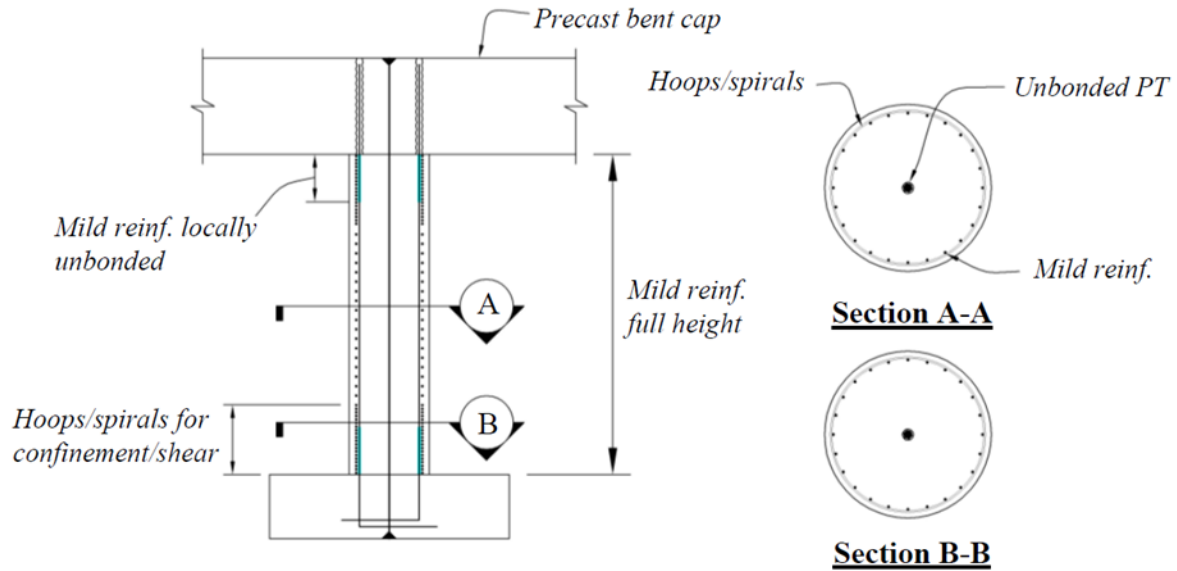


Figure 2.23. Conventional Hybrid Connection (Tobolski 2010).

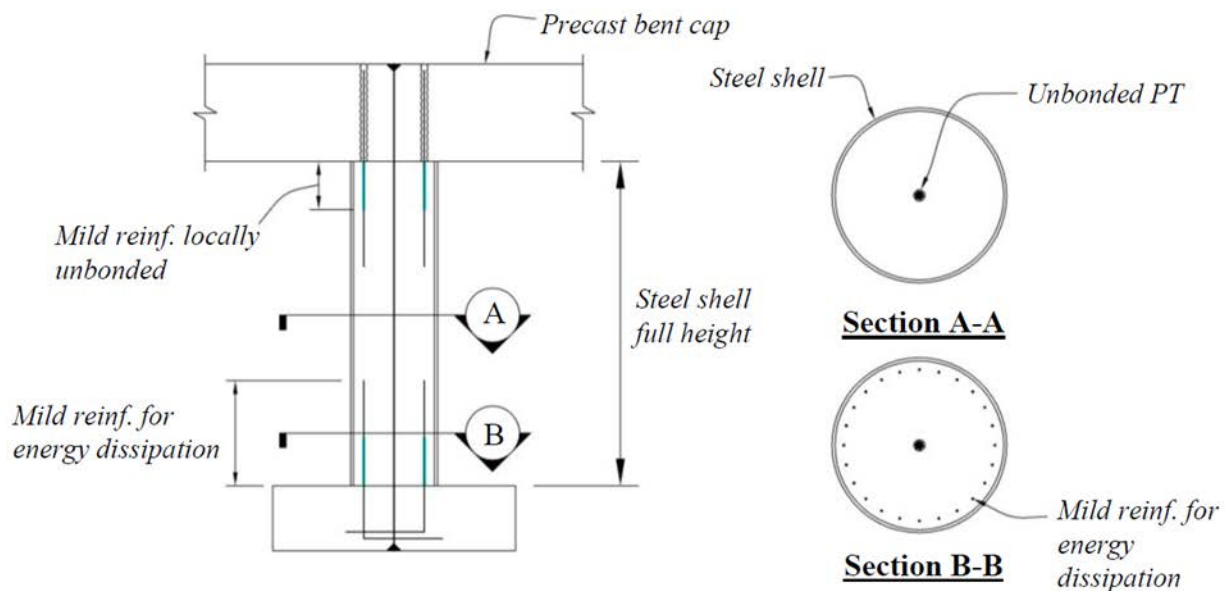
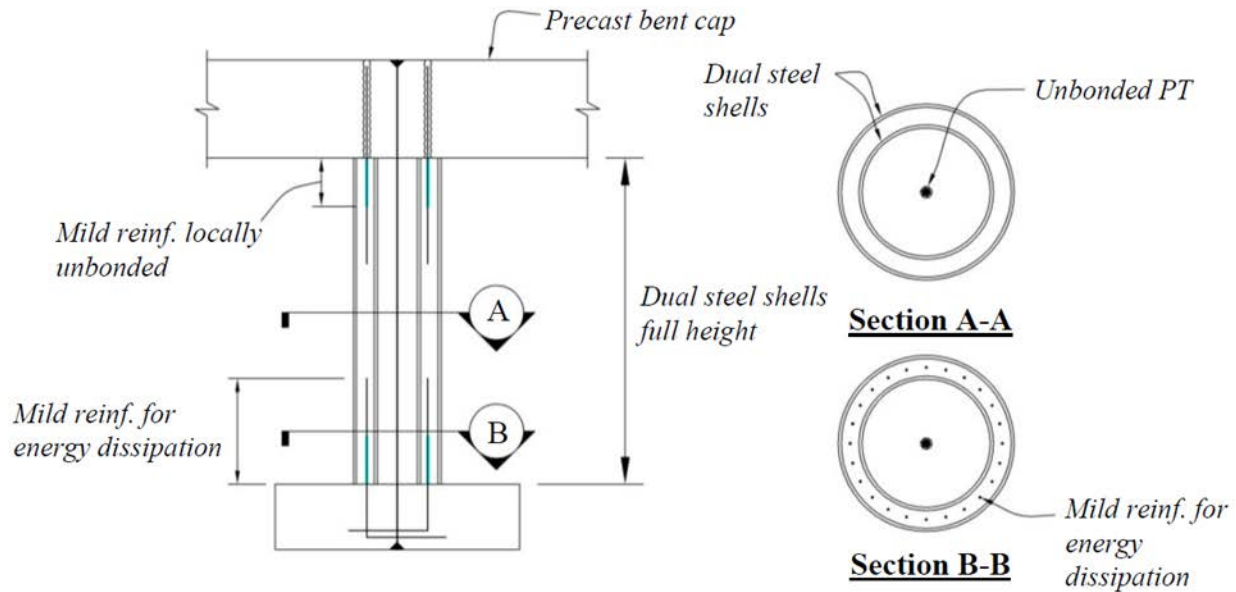


Figure 2.24. Concrete Filled Pipe Hybrid Connection (Tobolski 2010).



**Figure 2.25. Dual Steel Shell Hybrid Connection (Tobolski 2010).**

2.7.2.8. *Damage Avoidance Design*

**2.7.2.8.1. Description**

The concept of DAD is functionally different than the above mentioned partially prestressed (hybrid) connections. The column reinforcement is anchored to and within armor plates terminated at the column top. A similar plate is in the cap beam. Under lateral load, the column rocks from head-to-toe. The concrete remains in the elastic range due to the armoring, thereby avoiding damage by design. Post-tension strands are used to provide a moment connection. In DAD, a steel interface is provided at the joint region to prevent damage in concrete due to rocking. Mander and Cheng (1997) proposed this design philosophy named DAD for connections between column-to-bent cap/footing, particularly for moderate to high seismic zones. The objective of DAD is to maintain post-earthquake serviceability along with life safety in subsequent large earthquakes. While conventional systems are designed for plastic hinging at columns, DAD involves special detailing of the connection enabling rocking of the column at the joints. The special detailing at the joints allows inelastic energy to dissipate at large lateral loads and minimal strength degradation up to several cycles of loading. Although energy dissipation occurs at column ends in plastic hinge zones in conventional column designs in a bridge, in most cases the inelastic deformation after a major earthquake is such that either the member needs retrofitting or the whole



bridge needs to be replaced or rebuilt. In contrast, DAD requires no post-earthquake serviceability maintenance.

#### 2.7.2.8.2. Previous Research

The design methodology developed by Mander and Cheng (1997) involves curtailing of the column reinforcement at the column top enabling the column to rock at the column-bent cap interface to avoid damage. A steel-steel rocking interface is provided at the joints in the column ends, as shown in Figure 2.26, providing resistance against damage induced by stress concentration at the rocking toe. In addition to this, detailing of the columns at the ends results in no permanent deformation. Post-tensioning strands may be provided in the column to increase lateral restraint and prevent overturning of the column in large earthquakes. Testing was conducted on a full-scaled precast concrete rocking column under seismic loading to validate the proposed model. Results were in agreement with the predicted performance and hence validated the design philosophy.

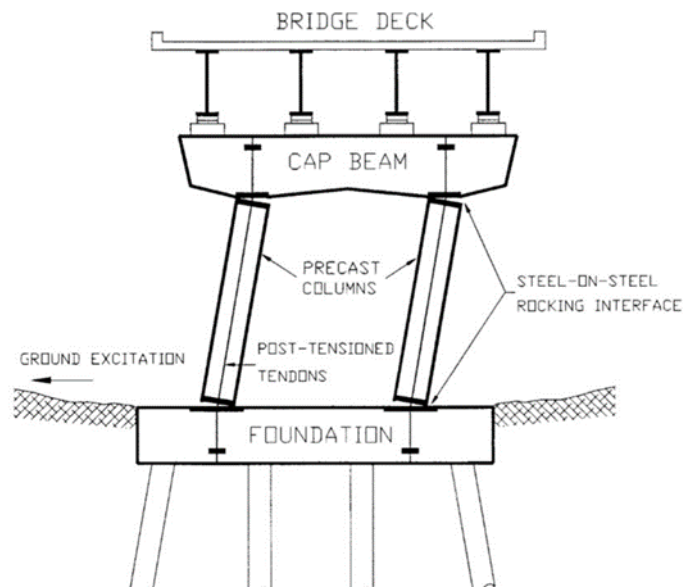


**Figure 2.26. Design Based on DAD (Mander and Cheng 1997).**

Li et al. (2008) assessed the performance of an 80 percent scaled precast prestressed beam to column connection of a frame designed in accordance to the DAD philosophy. Tests were done in two orthogonal directions under unidirectional and bidirectional loadings. The beam ends were reinforced with steel angles to prevent concrete damage due to rocking. Results showed good

performance of the specimen up to 4 percent drift with no damage or cracking in the column and minor flexural cracking in the precast bent cap.

#### **2.7.2.8.3. Field Implementation**

Although several buildings have now been constructed in New Zealand using the elements of DAD, researchers are not aware of any implementation of this connection between precast bent cap and column for a bridge project.

#### **2.7.2.8.4. Discussion**

Although DAD is a promising concept in high seismic zones, it can be also implemented in non-seismic regions such as Texas to protect the bridge columns and the structure against vehicular crashing.

#### *2.7.2.9. Pretensioned Rocking Bridge Bent*

##### **2.7.2.9.1. Description**

Following some of the DAD concepts of Mander and Cheng (1997), Stanton et al. (2014) recently developed a similar concept that dissipates seismic energy by controlled rocking at the joints between the column and the bent cap/footing. The column ends are detailed so that the column can rock as a rigid body at the cracks produced near the ends. The column ends are also reinforced with a steel toe or shoe to prevent damage to the concrete due to rocking, as seen in Figure 2.27. Pretensioning strands present in the center of the column are unbonded in the middle and bonded at ends and are so designed for the system to return to original position after ground motion stops. The reinforcing bars are debonded at the ends to prevent premature bar fracture.

##### **2.7.2.9.2. Previous Research**

Stanton et al. (2014) performed cyclic tests on cap-column and column-footing connections. Connection types included large diameter bar connections and socket connections between the column to bent caps and columns to footings, respectively. An octagonal column was used and reduced in section at the interface with the bent cap. The reduction in section allowed convenient placement of the bent cap during construction without the need for temporary support mechanisms. Results showed that at drift ratios up to 6 percent the column returned to its original position at

unloading and lateral load resistance continued even at drift ratios of 10.4 percent after two cycles of deformation. Spalling and buckling were not visible. Thus it was observed that cyclic performance of the subassemblies was better than the conventional RC connection.

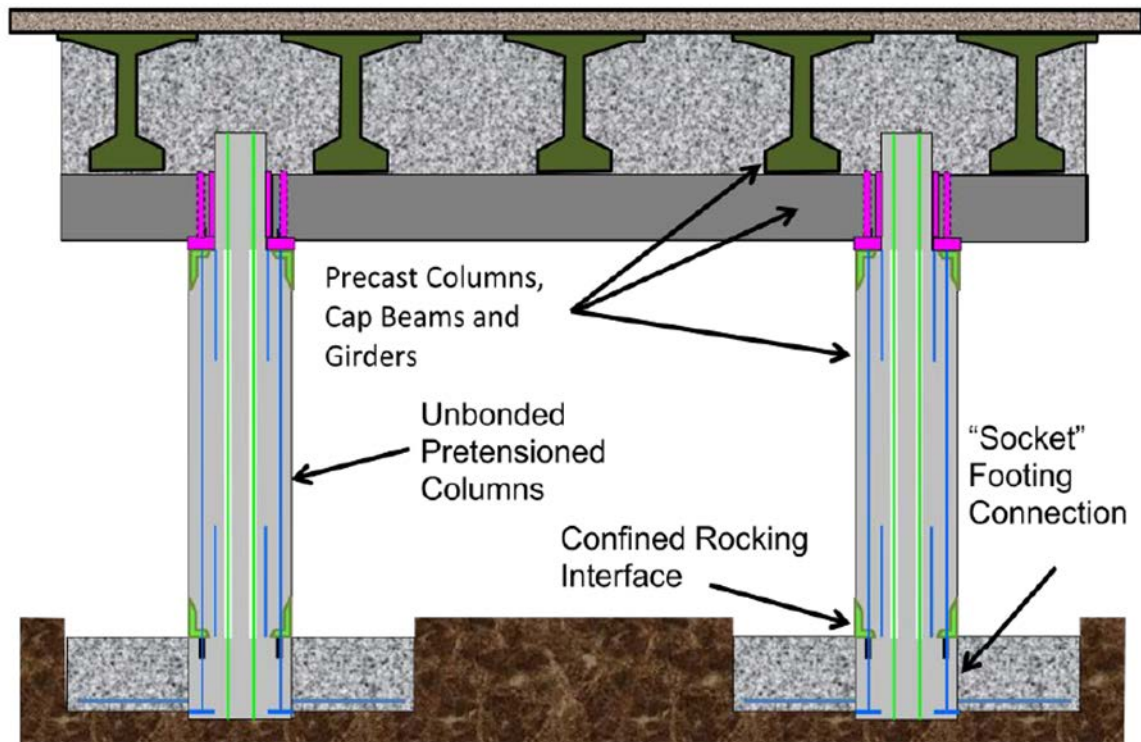


**Figure 2.27. Precast, Pretensioned Rocking Column (Stanton et al. 2014).**

### **2.7.2.9.3. Field Implementation**

Researchers are currently not aware of any implementation of this connection between precast bent caps and columns in any bridge projects.

### **2.7.2.9.4. Discussion**

Unlike emulative connections where inelastic energy is dissipated by a plastic hinge mechanism at the column ends, the jointed connections dissipate the seismic energy either by controlled rocking at the column ends or by mild reinforcement in case of hybrid connections. Appropriate detailing of the joints avoids damage in the joint interfaces. These connections showed high drift capacity and reduced damage. However, the pretensioned rocking bridge bent connection is not damage-free as the reinforcing bars can still be damaged through yielding, leaving the owner in a quandary of how repairs could be implemented, if at all.

### **3. DESIGN CONSIDERATIONS**

#### **3.1. INTRODUCTION**

To develop designs for precast, pretensioned concrete bent caps, it is first necessary to identify potential design challenges and opportunities for improvements in design efficiency. This chapter is devoted to a preliminary investigation of design challenges.

To establish a starting point for the design of pretensioned bent caps, Section 3.2 provides an overview of TxDOT reinforced concrete (RC) bent cap designs, including connection details for a precast option. This is followed by a summary of the design objectives for pretensioned bent caps in Section 3.3.

Section 3.4 presents flexural design considerations, including a proposed design procedure and investigation of the impact of strand configuration and the use of reduced weight cross-sections. To evaluate the flexural design, the proposed design procedure is applied to a suite of TxDOT standard bridge designs. Section 3.5 provides an overview of the characteristics of these bridges, and Section 3.6 discusses the performance of these pretensioned designs.

Section 3.7 provides a discussion of and recommendations for the reinforcement needed in the end region to reduce the potential for damage due to bursting forces within the transfer zone. Section 3.8 provides a discussion of the challenges associated with shear design of the pretensioned bent caps. Recommendations for the adoption of pocket connections, including the necessary geometry and pocket thickness, are presented in Section 3.9.

Section 3.10 provides a summary of design challenges, design recommendations, and need for future work.

#### **3.2. TXDOT REINFORCED CONCRETE BENT CAPS**

The motivation for investigating the design of pretensioned bent caps is to offer an alternative to precast RC designs, providing another option in TxDOT's current library of standard bridge designs. In offering a pretensioned alternative, it is desired to provide improved constructability and performance under service and ultimate loads. As such, a summary of RC bent cap design requirements and standard practice are presented here.

Unless higher strength materials are needed for special cases, Class C concrete with a compressive strength of 3.6 ksi and Grade 60 reinforcing steel are use. Bent cap width is based on the size of the columns, with the cap width at least 3-in. wider than the column on each side. For I-girder bridges with Tx-62 girders, a 42-in. diameter column and a 48-in. cap width is used. For other I-girder bridges, a 36-in. diameter column and a 42-in. bent cap is used. The depth of the cap is required to be in 3-in. increments, but not less than the width of the cap; the width of the cap is typically used for aesthetics.

Analysis of multicolumn caps is done as simply supported beams on knife-edge supports at the center of columns or piles with moments taken at the center of the column expect in the instance of bent caps widths of 4-ft or larger, in which case the moment at the face of the support is used for design (TxDOT 2015a). TxDOT uses in-house bent cap analysis program CAP18 establish demands for dead, service, and ultimate loading. Loading on the bent cap considered for design consists of dead and vehicular live load with impact.

Both Strength I and Service I limit state load combinations are considered for design. Under the Service I load combination, the tensile stress in the steel reinforcement is limited to  $0.6f_y$ . Historically, an additional serviceability limit of 22 ksi under service dead load was considered; however, this provision was removed following in the 2015 update to the design guidelines.

Detailing specifications indicate a preference for the use of #11 bars for flexural reinforcement, although smaller bars can be used to satisfy development length characteristics; mixing of bars sizes is prohibited. Longitudinal skin steel is required along the sides of the cap; typically, this is provided as #5 bars.

Design for shear reinforcement in the spans between columns requires use of the AASHTO LRFD General Procedure; the use of the simplified methods is prohibited. An alternative design approach, the strut-and-tie procedure is only required for deep components. Shear reinforcement is typically provided by #5 stirrups, although up to #6 stirrups are allowed. The spacing ranges between 4-in. and 12-in. spacing, with the amount of spacing changes minimized. Shear reinforcement in the overhang is not specifically designed; instead, stirrups at a spacing of 6-in. are specified.

Monolithic connections for CIP bent caps consist of an extension of the column longitudinal reinforcement into the cap. An alternative connection detail is provided to allow construction of precast RC bent caps; details of this connection are discussed in Section 3.9.1.

### **3.3. DESIGN OBJECTIVES FOR PRETENSIONED BENT CAPS**

The primary design objective for precast, pretensioned bent caps is to provide equivalent or superior performance to RC designs. To achieve this, additional limits on stresses in the bent cap are introduced by this research. Under dead loads, the tension stress is limited to zero to allow cracks to close under the removal of live loads. At service, the stresses are limited to the AASHTO LRFD tension and compression stress limits of  $0.19\sqrt{f'_c}$  and  $0.45f'_c$ , respectively.

Provisions for compressive strength requirements for PSC bent caps are not explicitly stated in AASHTO LRFD and TxDOT standards. The TxDOT Design Manual specifies the use of class H concrete for pretensioned concrete beams with a minimum  $f'_{ci} = 4$  ksi and  $f'_c = 5$  ksi, and a maximum  $f'_{ci} = 6$  ksi and  $f'_c = 8.5$  ksi (TxDOT 2015b). This provision has been adopted for the design of PSC bent caps and is in conformity with the requirement in AASHTO LRFD that specifies the use of a minimum specified compressive strength of 4 ksi for PSC members and decks. Due to common use of 0.6-in. diameter strands in the TxDOT PSC I-girder standard designs, 0.6-in. diameter low relaxation strands with a specified tensile strength of  $f_{pu} = 270$  ksi are used in this study.

Prestressing losses of 20 percent are assumed for pretensioned members and is used in the design (Garber et al. 2013). Design of the cap to resist the bursting and spalling stresses at the ends of prestressed members is considered, with reinforcement designed to prevent cracking under these stresses.

### **3.4. FLEXURAL DESIGN**

The design approach for RC bent caps selects flexural reinforcement to provide sufficient strength. Skin reinforcement is not considered to contribute to the strength of the specimen. The design is then checked for stresses in the reinforcement at dead and service loads, resulting in an increase in reinforcement in some cases. The dead load stress is intended to limit the observed cracking under dead load.

In establishing a flexural design procedure for pretensioned bent caps, it is desired to provide equivalent or superior performance to RC bent caps. To improve the performance, it is necessary to limit the extent of cracking in the bent cap. In exploring potential design procedures, a number of approaches were considered. These approaches generally focused on achieving target stress levels under dead, service, and/or ultimate loads. The proposed design procedure, presented in detail in Section 3.4.1, was found to be simple while achieving the design objectives of providing strength and limiting the cracking in the bent cap. An alternative approach, presented in Section 3.4.2, serves as a useful approach when a pretensioned design is developed as an alternative to an existing design for a RC bent cap.

The proposed design procedure was developed for solid, square cross-sections with strands located primarily at the top and bottom of the section. To provide flexibility in construction, two modifications are considered. The first considers a rearrangement of the strands to better accommodate the cap-to-column connection and to allow the use of interior voids. The impact of strand configuration on the strength and serviceability of bent caps is presented in Section 3.4.3. The second modification is the use of reduced weight cross-sections to allow larger caps that might otherwise be restricted by shipping/construction lifting capabilities. The impact of interior voids on the strength and serviceability of bent caps is presented in Section 3.4.4.

### **3.4.1. Proposed Design Procedure**

The proposed design procedure for pretensioned bent caps is based on a philosophy of achieving zero tension under dead loads. This is done to allow any cracks formed under application of the ultimate loads to close under the full removal of live loads. The steps in the design procedure are detailed below, with in-depth discussion presented in the subsequent paragraphs:

- Step 0: Determine minimum number of strands.
- Step 1: Calculate number of strands for zero tension under dead load.
- Step 2: Determine required minimum concrete compressive strength.
- Step 3: Check ultimate strength capacity.
- Step 4: Check deflections.

3.4.1.1. *Step 0: Determine Minimum Number of Strands*

To preclude a brittle failure of the section, it is necessary to check that the flexural resistance is greater than the cracking moment.

AASHTO LRFD Section 5.7.3.3.2 specifies that the amount of prestressed tensile reinforcement shall be adequate to develop a factored flexural resistance,  $M_r$ , which is at least equal to the lesser of a) 1.33 times the ultimate moment and b) cracking moment. The cracking moment is given by:

$$M_{cr} = (f_t A + F) S_x \quad (3-1)$$

in which  $M_{cr}$  = cracking moment;  $f_t = 0.24\sqrt{f'_c}$  (AASHTO LRFD 5.4.2.6);  $A$  = area of cross-section;  $F$  = prestressing force; and  $S_x$  = section modulus (for a solid rectangle  $S_x = BD^2/6$  where  $B$  = width and  $D$  = overall depth).

The number of strands for which Equation (3-1) equals the nominal moment capacity is determined and increased by a factor of 1.33 to evaluate the minimum number of strands.

3.4.1.2. *Step 1: Calculate Number of Strands for Zero Tension under Dead Load*

The first step in design is to select the number of strands to achieve zero tension under dead load. The flexural stresses under dead load should remain compressive at the extreme tension fiber (see Figure 3.1):

$$-\frac{F}{A} + \frac{M_{DL}}{S_x} < 0 \quad (3-2)$$

and within the normal service limits at the extreme compression fiber:

$$-\frac{F}{A} - \frac{M_{DL}}{S_x} > -0.45f'_c \quad (3-3)$$

in which  $F$  = prestress force after losses;  $M_{DL}$  = dead load moment;  $f'_c$  = specified compression strength of the concrete.

From Equation (3-2) and Equation (3-3), it follows that the required prestressing force is:



$$F \geq 6 \frac{M_{DL}}{D} \quad (3-4)$$

with an upper bound value determined by the limits on compressive stresses:

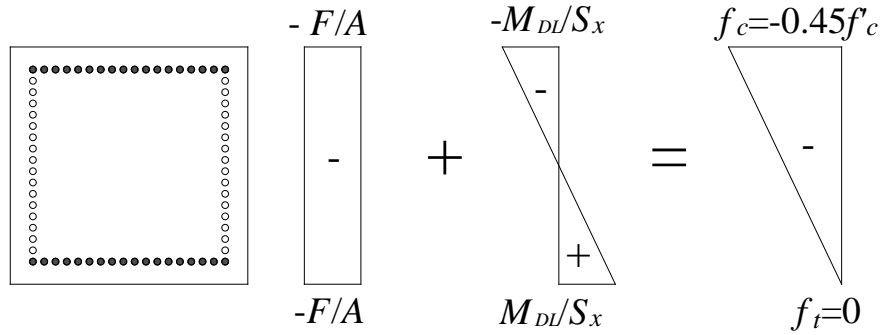


**Figure 3.1. Stresses Under Dead Load: No Tension.**

$$F \leq 0.45 f'_c A - 6 \frac{M_{DL}}{D} \quad (3-5)$$

In Equation (3-5), only a provisional value for  $f'_c$  (6 - 8.5 ksi) needs to be selected at this stage of the design. The concrete compressive strength should be sufficiently strong to prevent time dependent losses. Excessive concrete strength results in a higher cracking moment and thus greater minimum reinforcement to prevent a brittle failure.

The number of strands is calculated as:

$$n = \frac{F}{T_{strand}} \quad (3-6)$$

where  $T_{strand}$  = prestressing force per strand and is calculated as:

$$T_{strand} = f_{pbt} A_{ps} (1 - \Delta f_{pT}) \quad (3-7)$$

in which  $f_{pbt} = 0.75f_{pu}$  = stress limit in low relaxation strand immediately prior to transfer;  $f_{pu}$  = specified tensile strength of prestressing strand = 270 ksi (AASHTO LRFD Table 5.4.4.1-1);  $A_{ps}$  = area of each strand = 0.217 in<sup>2</sup> for 0.6-in. diameter strand; and  $\Delta f_{pT}$  = prestress loss in pretensioned members = 20 percent.

The number of strands from Equation (3-6) is rounded up to the nearest multiple of 2 or 4 for symmetric arrangement of strands in the bent cap.

3.4.1.3. *Step 2: Determine Required Minimum Concrete Compressive Strength*

To ensure that the bent cap does not crack at service loads, a minimum concrete compressive strength should be provided such that the service stresses are less than or equal to the service stress limits specified in AASHTO LRFD.

The tensile and compressive stresses are calculated from the service moments (see Figure 3.2):

$$f_t = -\frac{F}{A} + \frac{M_{DL+LL+IM}}{S_x} \quad (3-8)$$

$$f_c = -\frac{F}{A} - \frac{M_{DL+LL+IM}}{S_x} \quad (3-9)$$

in which  $M_{DL+LL+IM}$  = moment due to dead load and live load with impact;  $f_t$  = tension stress; and  $f_c$  = compression stress.

The design concrete compressive strength must be selected such that the AASHTO tension (Table 5.9.4.2.2-1) and compressive (Table 5.9.4.2.1-1) service stress limits are met:

$$f_t \leq 0.19\sqrt{f_c'} \quad (3-10)$$

$$f_c \geq -0.45f_c' \quad (3-11)$$

If the calculated value of  $f_c$  is less than 6 ksi, a minimum design concrete compressive strength of 6 ksi is recommended.

√

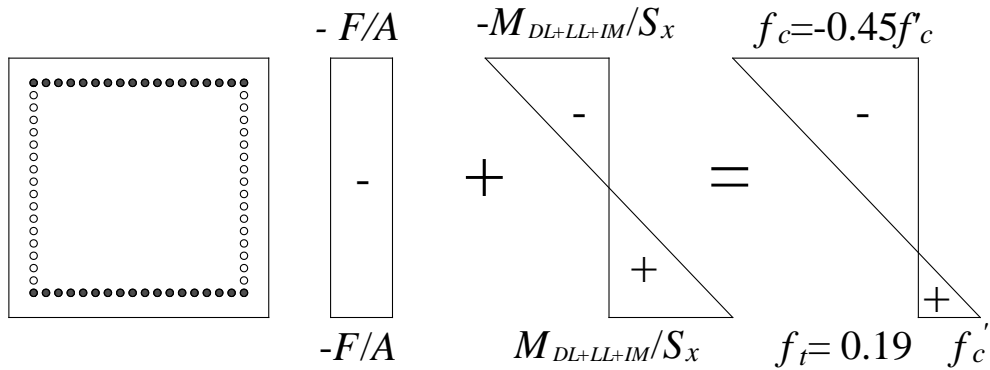


**Figure 3.2. Stresses under Service Load and Establish Minimum Concrete Strength.**

3.4.1.4. *Step 3: Check Ultimate Strength Capacity*

The bent cap should have at least the nominal strength capacity such that it does not fail under ultimate loads. The ultimate flexural moment capacity ( $M_n$ ) is calculated per AASHTO LRFD 5.7.3.2 (see Figure 3.3) and evaluated against the demands:

$$\phi M_n \geq M_u \quad (3-12)$$

in which  $M_u$  = flexural demand under ultimate loads;  $\phi = 1.0$  for tension-controlled PSC sections (AASHTO LRFD 5.5.4.2.1). If  $\phi M_n < M_u$ , the prestressing force should be increased such that Equation (3-12) is satisfied.

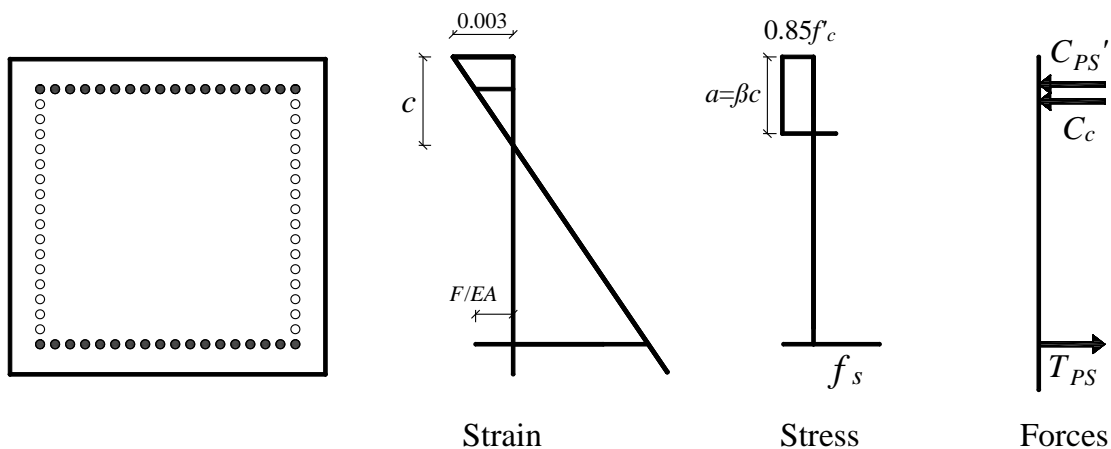


**Figure 3.3. Ultimate Strength Capacity.**

3.4.1.5. *Step 4: Check Deflections*

To ensure that the deflection of the bent cap does not affect serviceability, the deflection should be checked to be within the specified limit.

The deflection,  $\Delta$ , under vehicular loading should be less than the limit specified in AASHTO LRFD 2.5.2.6.2, specifically:

$$\Delta < Span / 800 \quad (3-13)$$

### 3.4.2. Alternate Design Approach

An alternate design approach is to replace Step 1 of the proposed design procedure with another method of selecting the number of strands. The proposed alternative calculates the number of strands needed to provide an equivalent reinforcement capacity. This approach would allow the use of existing designs, thereby preventing the need to start the design from the beginning. Standard TxDOT practice is followed for the RC solution to determine the amount of reinforcing steel. The equivalent reinforcement capacity is provided as the prestressed solution:

$$A_{ps} 0.75 f_{pu} = A_s f_y \quad (3-14)$$

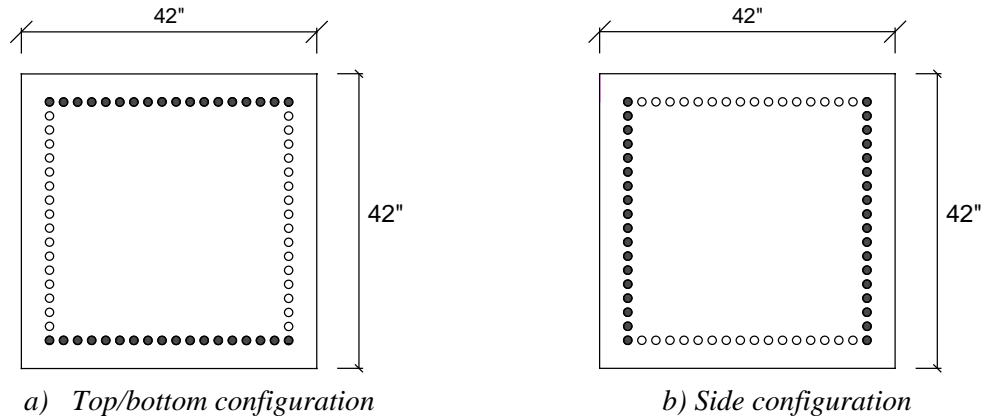
The number of strands is determined by:

$$n = \frac{A_{ps}}{A_{strand}} \quad (3-15)$$

in which  $A_{strand}$  is the area of each strand. Equation (3-15) is the alternative to (3-6) in the design procedure; all other steps remain unchanged.

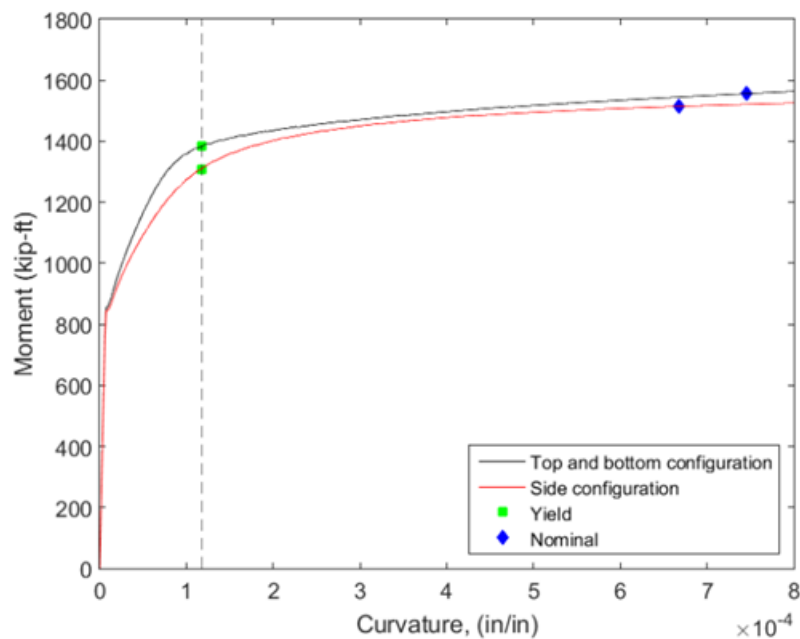
### 3.4.3. Effect of Strand Configuration

The design procedure proposed in Section 3.4.1 was developed for solid square cross sections with strands located primarily at the top and bottom of the section, as shown in Figure 3.4(a). For bent caps constructed with voids to reduce section weight and with large openings for the cap to column connection, this top/bottom configuration can be problematic. To accommodate the openings, the strands can be relocated to the sides of the section, as shown in Figure 3.4(b). A brief analysis of the impact of the strand configuration is presented here; the strand layouts shown are for illustrative purposes only and should not be considered a recommendation for implementation in a pretensioned cap design.



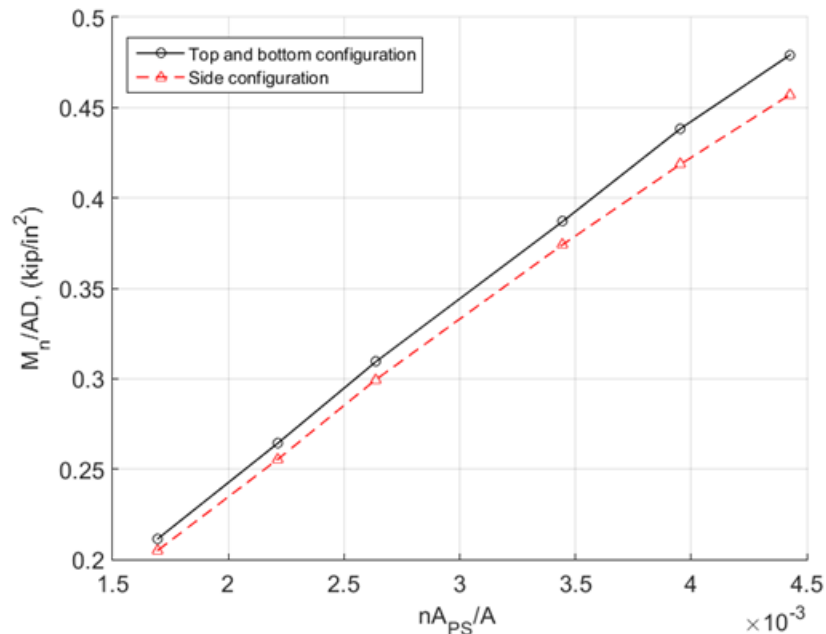
**Figure 3.4. General Strand Layouts.**

Figure 3.5 shows the full moment-curvature response of a 42-in. bent cap with 18 strands obtained by fiber-section analysis (OpenSees Version 2.4.6). Three critical points are indicated: 1) cracking, 2) yield  $f_{py}$ , and 3) nominal strength. Both configurations have the same behavior prior to cracking. After cracking occurs, the stiffness is greater for the top/bottom configuration. At yield, the curvature is the same in both the configurations, with a higher moment in the top/bottom configuration. At the nominal strength, the top/bottom configuration has slightly larger moment and curvature. This is due to a lower number of strands in tension than the side configuration, resulting in a smaller concrete compression stress block and thus higher curvature.



**Figure 3.5. Moment Curvature Response of 42-in. Square Bent Cap with Top and Side Strand Configuration.**

The most important effect of the configuration of strands is the nominal strength, particularly the sensitivity to the number of strands. Figure 3.6 illustrates the impact of the amount of prestressing on the moment strength for the 42-in. and 48-in. square bent caps for a concrete compressive strength of 8.5 ksi. To eliminate the impact of the cross-section dimensions, the nominal strength is normalized by  $AD$  and the area of prestressing is normalized by  $A$ . The solid black line represents the top and bottom configuration, and the dashed red line represents the side configuration. The range of variation in strength between the two configurations increases with the increase in the area of prestressing, but the strength of the side configuration is not more than 5 percent less than the strength of the top/bottom configuration.



**Figure 3.6. Nominal Strength vs Area of Prestressing.**

#### 3.4.4. Reduced Weight Section

The large size of the bent caps is not a weight issue when CIP. However, the weight of long pretensioned bent caps may be prohibitive for shipping and placement. To reduce the weight of the bent cap, permanent interior voids may be used in the span regions; the overhang and connections to columns must remain solid. Cross-sections with permanent voids, such as box-girders, are an attractive option as the section uses significantly less material than a solid section. The top, bottom, and sides provide the necessary space for prestressing strands. The two sides and any associated shear reinforcement can provide significant shear resistance.

To assess the impact of a permanent interior void, a 42-in. square section with 18 strands in a side configuration is considered. The moment curvature response of a solid section is compared to that of section with a 30-in. square void in the center; this void is considered to be the largest practical void and thus will offer a worst case scenario evaluation of permanent void sections. The differences in the section behavior is most apparent prior to yield, shown in Figure 3.7, although the differences are minor. The section with an interior void has a lower initial stiffness, a larger cracking moment, and a nearly identical nominal strength.

If the proposed design procedure is applied to a section with an interior void, the number of strands is lower than in a solid section with the same exterior dimensions and design demand. The interior void section has higher minimum concrete design strength, and higher stresses under service and ultimate loads.

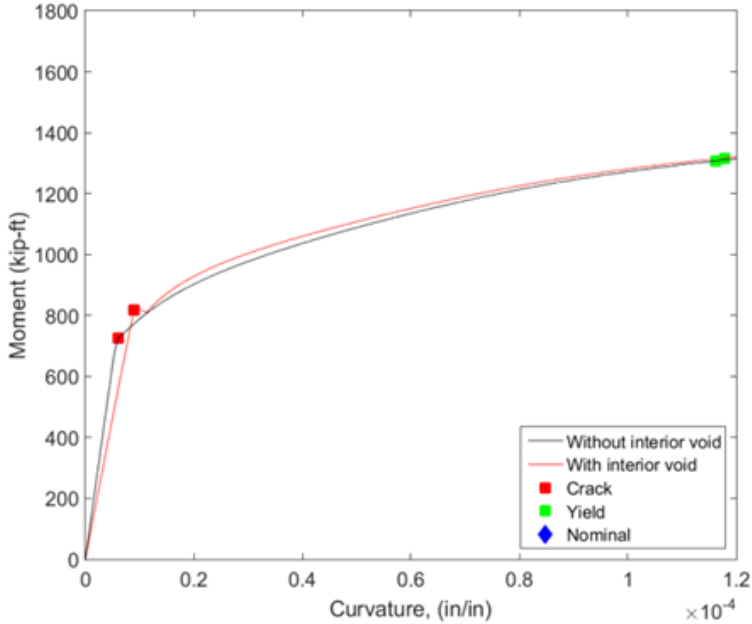


**Figure 3.7. Moment Curvature up to Yield for Bent Cap with 18 Strands, Side Configuration.**

**3.5. OVERVIEW OF TXDOT STANDARD BRIDGE INVENTORY**

To evaluate the application of the proposed design procedures, the TxDOT standard bent designs are used as a demonstration bridge inventory. Non-skewed I-girder bridge results are presented here and are representative of results for a large suite of standard bents for skewed I-girder, box

beams, and x-beams bridges. Results for the full suite of bridges are presented by Barooah (2016). Section 3.5.1 discusses the bridge characteristics. Section 3.5.2 summarizes the sources of loads and method of analysis. Section 3.5.3 overviews the demands for the bridge inventory.

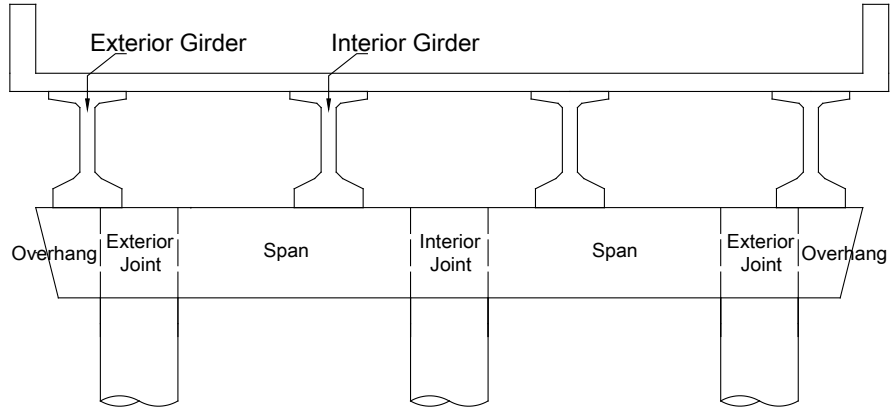
### **3.5.1. Bridge Characteristics**

The roadway widths of the TxDOT bridges are 24-ft, 28-ft, 30-ft, 32-ft, 38-ft, 40-ft, and 44-ft. In this report, three span lengths are considered for each bridge width: minimum, intermediate, and maximum span length. For Tx-28 to Tx-54 girders, the minimum, intermediate, and maximum span lengths considered are 40ft, 80-ft, and 120-ft, respectively. For Tx-62 girders, the minimum, intermediate, and maximum span lengths considered are 60-ft, 95-ft, and 130-ft, respectively.

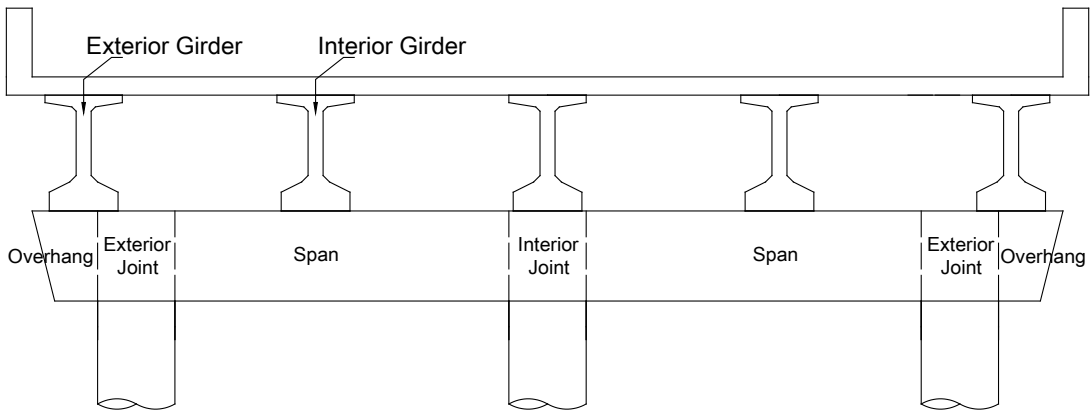
The non-skewed I-girder bridges consist of three unique bent configurations shown in Figure 3.8. Figure 3.8(a) shows the three column, four girder configuration (24-ft, 28-ft, 30-ft, and 32-ft bridge widths). Figure 3.8(b) shows the three column, five girder configuration (38-ft and 40-ft bridge widths). Figure 3.8(c) shows the four column, six girder configuration (44-ft bridge width). The column spacing for the bridges varies from 8-ft to 12-ft, except for the 38-ft and 40-ft width bridges in which the column spacing is 15-ft and 16-ft, respectively. The girder spacing for the bridges varies from 6.67-ft to 9.33-ft. The exterior girders in all non-skewed bridges are located 2-ft from the edge of the bent cap and 2-ft from the center of the exterior column.

The column dimensions in the standard TxDOT bridge inventory are based on the girder sizes. For girder sizes of Tx-28 to Tx-54 the columns are 36-in. diameter, while for Tx-62 girder the columns are 42-in. diameter. TxDOT design requirements specify that the width of the bent cap be 6-in. greater than the column dimension. For girder sizes of Tx-28 to Tx-54 the bent cap is 42-in. wide. For Tx-62 girder the bent cap is 48-in. wide. A square shape is preserved for aesthetics.

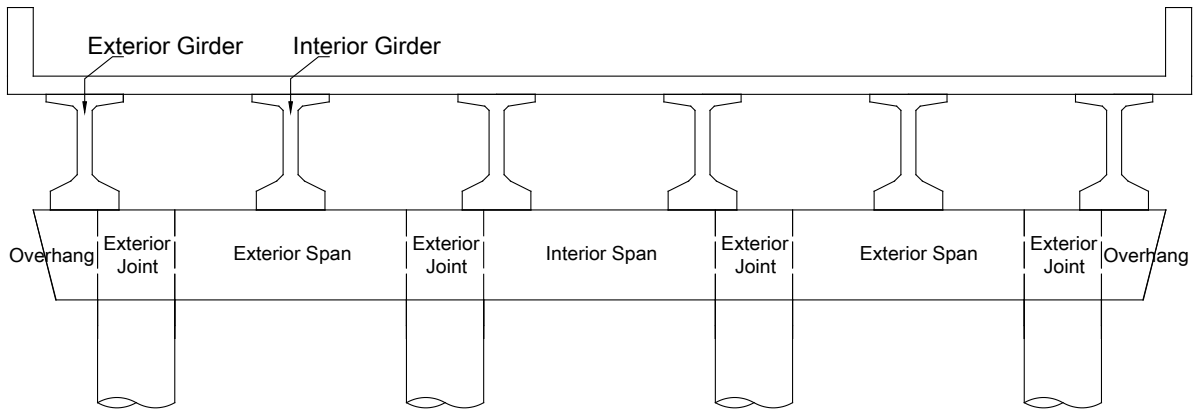




(a) 3 column, 4 girder



(b) 3 column, 5 girder



(c) 4 column, 6 girder

**Figure 3.8. Bent Configurations in Bridge Inventory.**

### **3.5.2. Loads and Analysis**

Sources of loads on the bent cap used for structural design are the permanent dead load and the transient vehicular live load. The dead loads consist of loads from structural and non-structural attachments (DC) such as self-weight of all bridge elements (e.g., slab, wearing coat [overlay], railing, girder and bent cap, and wearing surfaces and utilities [DW]). An 8.5-in. thick slab was used for this research study. The vehicular live load is the combination of the design truck or tandem, and the design lane load, calculated with the AASHTO LRFD HL-93 design live load. The maximum live load reaction at an interior bent cap is always governed by design truck. The dynamic load allowance factor specified in AASHTO LRFD Table 3.6.2.1-1 is applied to the truck load to account for wheel load impact from moving vehicles. Multiple presence factors specified in AASHTO LRFD Table 3.6.1.1.2.1 are used for single or multiple lanes.

Flexural and shear demands were determined using the TxDOT bent cap analysis program CAP18 (Version 6.2.2). The CAP18 program considers the bent cap as a continuous beam placed on knife-edge supports (Matlock and Ingram 1996). The program analyzes dead and live loads that conform to AASHTO standard specifications. CAP18 has the unique feature of a movable load that runs across the width of the deck. The program determines the largest demands at the bent cap control points (such as column and girder positions) due to the movable load. This feature enables CAP18 to achieve conservative demands for the movable load.

The live load is a movable load to enable the program to determine the maximum demands. The live load model is stepped across the deck slab in 0.5-ft increments. The live load consists of a combination of concentrated load ( $P$ ) and a uniform load ( $w$ ) defined on a 10-ft design lane width. This load is used in combination with the dead loads to generate the service and ultimate shear and moment envelopes.

### **3.5.3. Summary of Demands**

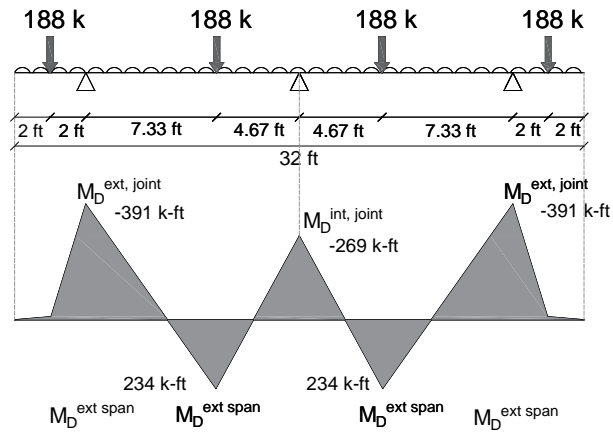
The demands for the full bridge inventory were determined using CAP18. Sample results are provided for each configuration in Figure 3.9. Figure 3.9(a), (b), and (c) shows the bending moment diagrams under dead load for the 42-in. bent caps of 32-ft, 40-ft, and 44-ft, respectively. For comparison, demands were also evaluated using frame analysis of the bent caps. CAP18 provided more conservative maximum demands.

For the bents evaluated, two scenarios were observed for the location of maximum moment demands: a) maximum moment at the column, and b) maximum moment in the span. For most bridges, the maximum moment occurs at the exterior columns. The maximum moment occurs at the interior columns for dead loads on bridges with short spans and larger column. The maximum moment occurs in the span for bridges with longer spans and larger column spacing, although not always for all load combinations. Table 3.1 summarizes the bridges and load combinations for which the maximum demand occurs in the span

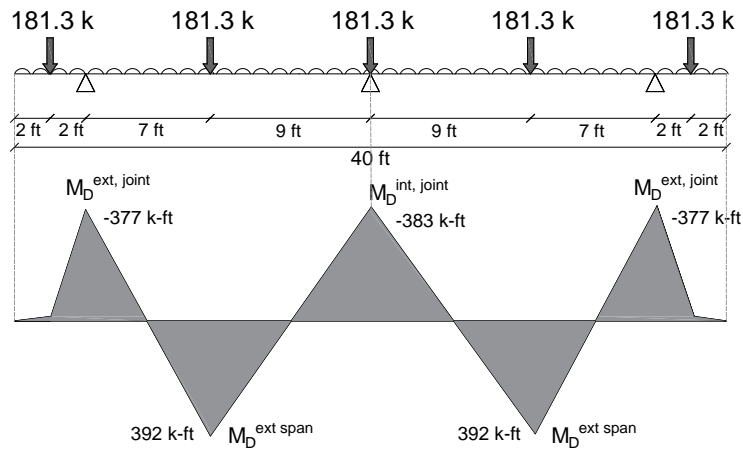
Table 3.2 provides a summary of the maximum moment demands in the 42-in. and 48-in. bent caps. The first three rows provide the largest values for dead, service, and ultimate loads; these may be at different locations for each load combination. To facilitate a generalized evaluation of the demands between different size caps, the fourth row presents dead load moments normalized by  $AD$  in which  $A$  is the area of cross-section and  $D$  is the depth of the bent cap. The moments at service and ultimate states are expressed as ratios to the dead load moments in the fifth and sixth rows of the table. Although the demands are larger for the 48-in. bent caps, the normalized values are actually lower for these larger bents, indicating the potential for a more favorable design and performance.

For the bents evaluated, two scenarios were observed for the location of maximum shear demands: a) maximum shear at the exterior columns, and b) maximum shear at the interior column. For most bridges, the maximum shear occurs in the exterior columns. Maximum shear occurs at the interior columns for bridges of 44-ft roadway width.

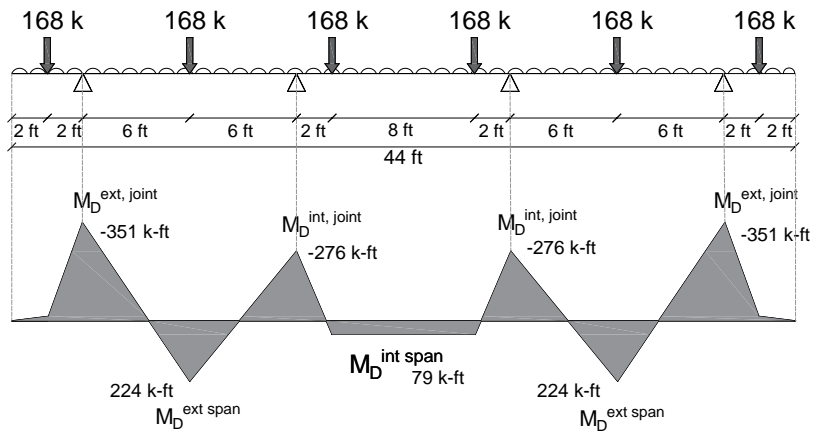
Table 3.3 provides a summary of maximum shear demands in the 42-in. and 48-in. bent caps. The first three rows provide the largest values for dead, service, and ultimate loads. To facilitate a generalized evaluation of the demands between different size caps, the fourth row presents the dead load shear forces normalized by the area of cross-section of the bent cap. The shear at service and ultimate are expressed as ratios to the dead load shear.



(a) 32-ft bent cap



(b) 40-ft bent cap



(c) 44-ft bent cap

Note: Moments are drawn on tension side.

**Figure 3.9. Bending Moment Diagram under Dead Load for 80-ft Span Length.**

**Table 3.1. Scenarios at Which Span Moment Controls Design or Evaluation of Bent Cap.**

Width (ft)	DL	DL + LL	1.25 DL + 1.75 LL
38		✓	✓
40	✓*	✓	✓

\*Intermediate to maximum spans

**Table 3.2. Summary of Maximum Moment Demands in 42-in. and 48-in. Bent Cap.**

	42-in. bent cap			48-in. bent cap		
	Minimum	Intermediate	Maximum	Minimum	Intermediate	Maximum
$M_{DL}$ (k-ft)	173–217	331–392	489–579	268–327	413–487	559–656
$M_{DL+LL+IM}$ (k-ft)	310–486	516–760	713–1021	431–647	613–885	791–1,118
$M_U$ (k-ft)	457–746	737–1,133	1,003–1,499	621–972	866–1,306	1,105–1,631
$M_{DL} / AD$ (k/in <sup>2</sup> )	0.028–0.035	0.054–0.063	0.079–0.094	0.029–0.035	0.045–0.053	0.061–0.071
$M_{DL+LL+IM} / M_{DL}$	1.8–2.3	1.6–1.9	1.5–1.8	1.6–2.0	1.5–1.8	1.4–1.7
$M_U / M_{DL}$	2.6–3.5	2.2–2.9	2.0–2.6	2.3–3.0	2.1–2.7	2.0–2.5

**Table 3.3. Summary of Maximum Shear Demands in 42-in. and 48-in. Bent Cap.**

	42-in. bent cap			48-in. bent cap		
	Minimum	Intermediate	Maximum	Minimum	Intermediate	Maximum
$V_{DL}$ (kips)	86–101	165–195	244–289	133–155	205–241	278–327
$V_{DL+LL+IM}$ (kips)	154–184	257–307	355–424	214–255	305–362	394–468
$V_U$ (kips)	227–272	367–439	500–598	309–368	431–513	551–655
$V_{DL} / A$ (k/in <sup>2</sup> )	0.048–0.057	0.093–0.110	0.138–0.164	0.075–0.088	0.116–0.137	0.158–0.185
$V_{DL+LL+IM} / V_{DL}$	1.80–1.84	1.56–1.60	1.45 – 1.49	1.61 – 1.65	1.48–1.52	1.41–1.45
$V_U / V_{DL}$	2.65–2.73	2.23–2.30	2.05 – 2.11	2.32 – 2.39	2.10–2.16	1.98–2.04

### **3.6. FLEXURAL DESIGN FOR STANDARD BRIDGE INVENTORY**

The design procedure recommended in Section 3.4.1 is based on the philosophy of zero tensile stresses under dead load to allow closure of cracks following removal of live load. In this section, the design procedure is evaluated for the bridge inventory summarized in Section 3.5.

Section 3.6.1 discusses the selection of strands for standard bridge inventory. Section 3.6.2 discusses the minimum concrete design strength for these designs. The stresses at service and ultimate loads are evaluated in Section 3.6.3. The strength of the sections is assessed in Section 3.6.4. Finally, Section 3.6.5 presents a comparison between performance of the RC and PSC bent caps.

#### **3.6.1. Number of Strands**

The minimum number of strands, calculated by Step 0 of the proposed design procedure, is sensitive to the design strength of the concrete. For a design strength of 6 ksi, the minimum number of strands is 14 for a 42-in. square and 18 for a 48-in. square. If a higher strength were actually used, the minimum number of strands would increase. For concrete with a compressive strength of 8.5 ksi, the minimum number of strands increases to 16 and 20 for 42-in. and 48-in. square sections, respectively. In evaluating the designs for the bridge inventory in this study, the minimum strands associated with 6 ksi concrete strength are used. However, use of numbers for 8.5 ksi concrete strength would be prudent in practice. Figure 3.10 shows the configuration of the minimum strands for the two bent cap sizes.

After establishing the minimum number of strands in step 0, the number of strands required to achieve the design objective of zero flexural tensile stresses under dead load are calculated using the method established in Step 1. The calculated number of strands ranges from 10 to 30 for 42-in. sections and from 12 to 28 for 48-in. sections. Bridges with the short span lengths are governed by the minimum number of strands.

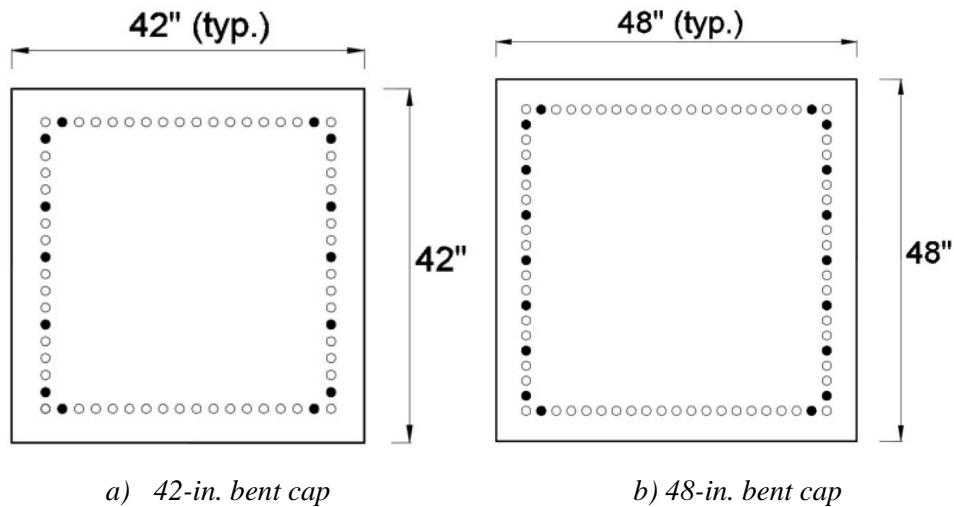


**Figure 3.10. Minimum Strands Configuration.**

### 3.6.2. Minimum Concrete Strength

The minimum design concrete strength is determined from Step 2 of the design procedure. For the bridge inventory evaluated, the highest minimum concrete strength calculated was 5.2 ksi, which occurred for the 42-in. square, 40-ft bent cap with maximum span length. However, a concrete strength of 6 ksi is used as the design strength in evaluating the designs. For most bridge widths and span lengths, the minimum design concrete strength is governed by the compression limit. Minimum design concrete strength is governed by the tension limit for bridges with longer spans and larger column spacing such as the 38-ft and 40-ft roadway widths.

### 3.6.3. Service and Ultimate Stresses

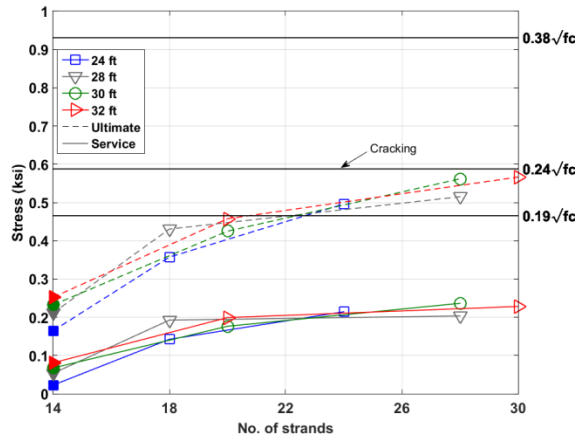
The performance of pretensioned bent cap design can be best evaluated by assessing the stresses at service and ultimate loads. Figure 3.11 and Figure 3.12 show the tension stresses at service and ultimate versus the number of strands for the 42-in. and 48-in. bent cap, respectively. For clarity, each bent configuration is shown on a different subfigure. The tension stresses are calculated at the location of the maximum moments at service and ultimate; this may be a different location than the dead load moment used to select the number of strands. The solid markers indicate designs for which the minimum number of strands governs. The solid lines represent the service stresses and the dashed lines represent the ultimate stresses. The horizontal limits of  $0.19\sqrt{f'_c}$  (ksi) and  $0.24\sqrt{f'_c}$  (ksi) are the AASHTO service stress limit for tension and the cracking stress,

respectively. The horizontal limit of  $0.38\sqrt{f'_c}$  (ksi) is the stress limit beyond which the bent cap is assumed to behave as a cracked member (ACI 318-14 Section 24.5.2). If the stresses are  $0.24\sqrt{f'_c}$  (ksi) to  $0.38\sqrt{f'_c}$  (ksi), the bent cap is assumed to be in transition between a cracked and uncracked member.

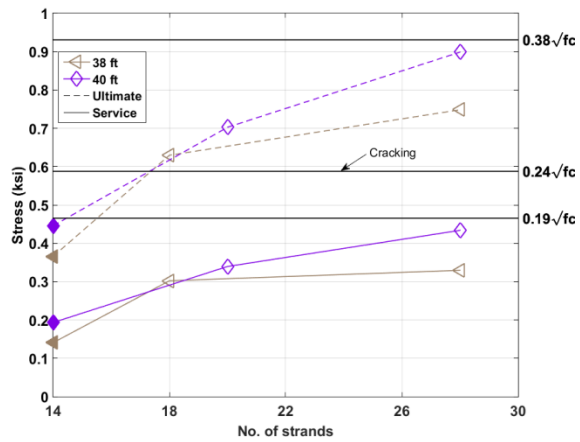
At service loads, the AASHTO stress limits enforce the expectation that stresses will be less than the cracking demands of  $0.24\sqrt{f'_c}$  (ksi). The tensile service stress at the location of maximum service moment (exterior joint or span) for each of the designs are shown by solid lines in Figure 3.11 and Figure 3.12. For bridges with the minimum span lengths, the design is controlled by the minimum number of strands (indicated by solid markers in the figures). In these bent caps, the service stresses are 67 percent below the expected cracking stress. As the span length increases, the number of strands in the design increases. The increase in strands is accompanied by a minor increase in the service stresses, but these stresses still remain well below the expected cracking stress. The highest service stress is 0.43 ksi in the 42-in., 40-ft bent cap. This stress is 26 percent lower than the expected cracking stress.

At service loads, the tensile stresses are well below the cracking stress, thus providing a margin of over strength to prevent cracking under demands exceeding the expected service loads. For most of the bridges considered in this study, the over strength is sufficiently large to prevent cracking even under ultimate loads. The tensile ultimate stresses at the location of the maximum ultimate moment for each of the designs are shown by dotted lines in Figure 3.11 and Figure 3.12. In these bent caps, the ultimate stresses are 24 percent below the expected cracking stress. The increase in strands is accompanied by an increase in the ultimate stresses. For the intermediate and maximum spans of Configuration 2, the ultimate stresses exceed the expected cracking stress. The highest ultimate stress is 0.90 ksi in the 42-in., 40-ft bent cap. This stress is 53 percent higher than the expected cracking stress.

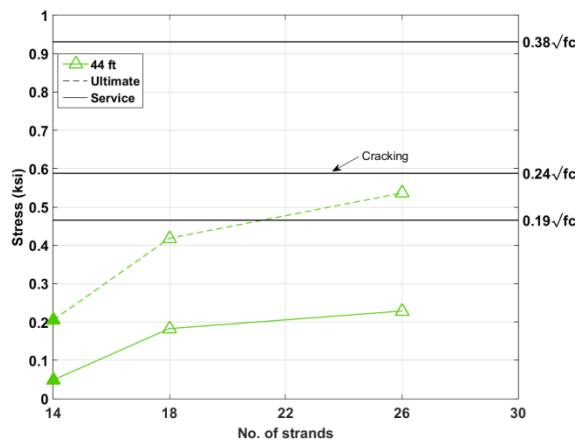




(a) Configuration 1: 3 column, 4 girder



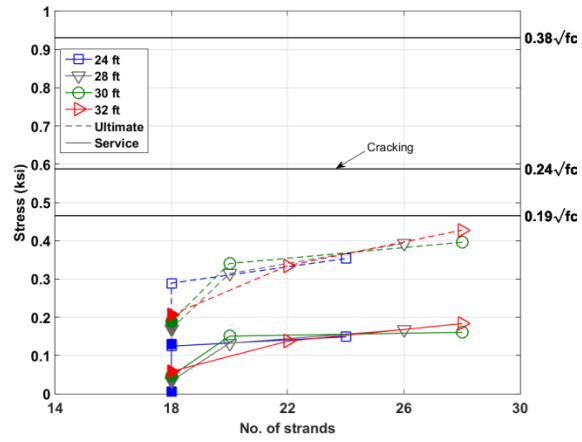
(b) Configuration 2: 3 column, 5 girder



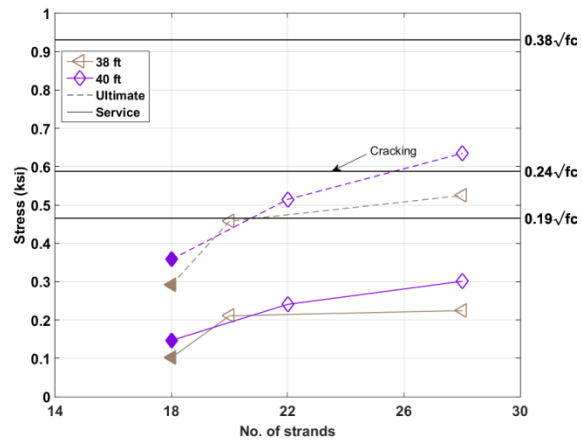
(c) Configuration 3: 4 column, 6 girder

Note: Solid markers indicate minimum strands control design.

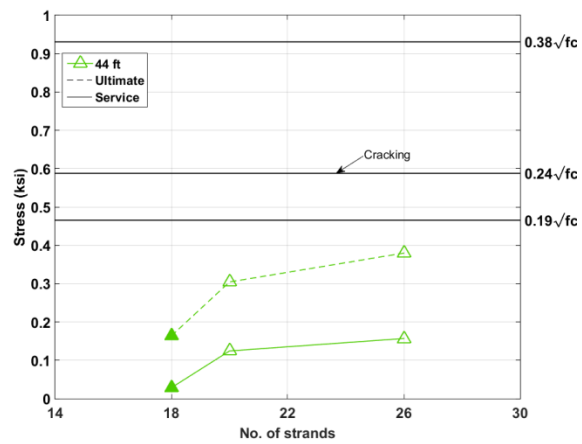
**Figure 3.11. Maximum Tensile Stress vs. Number of Strands for 42-in. Bent Cap.**



(a) Configuration 1: 3 column, 4 girder



(b) Configuration 2: 3 column, 5 girder



(c) Configuration 3: 4 column, 6 girder

Note: Solid markers indicate minimum strands control design.

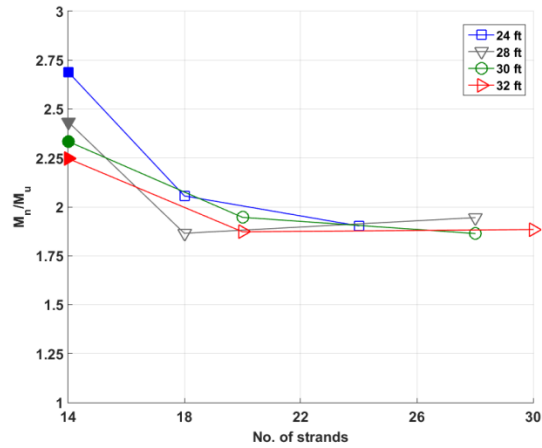
**Figure 3.12. Maximum Tensile Stress vs. Number of Strands for 48-in. Bent Cap.**

#### **3.6.4. Factor of Safety**

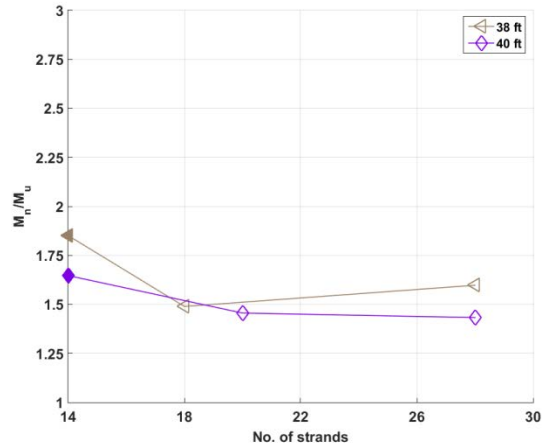
Step 3 of the design procedure requires the designer to check that the number of strands (Step 1) and concrete strength (Step 2) are sufficient to provide the necessary strength. For designs in the bridge inventory used in this study, the original design provided sufficient strength and no adjustments were needed. The overstrength, or factor of safety, provided by the designs is presented here as a ratio of the nominal capacity to the ultimate moment demand. This ratio is shown in Figure 3.13 and Figure 3.14 for the 42-in. and 48-in. bent caps, respectively. Solid markers indicate designs that are controlled by the minimum number of strands.

The factor of safety is essentially the same for both bent cap sizes. Bent configuration 1 (Figure 3.13[a] and Figure 3.14[a]) and Configuration 3 (Figure 3.13[c] and Figure 3.14[c]) have factors of safety between 1.8 and 2.1 for designs controlled by the number of strands for zero tension under dead load; the factor of safety is as large as 2.92 when the minimum number of strands governs the design. For bent Configuration 2 (Figure 3.13[b] and Figure 3.14[b]), the overstrength is not as large, with factors of safety between 1.4 and 1.8 for designs controlled by the number of strands for zero tension under dead load. The factor of safety increases to as large as 2.1 when the minimum number of strands governs the design.

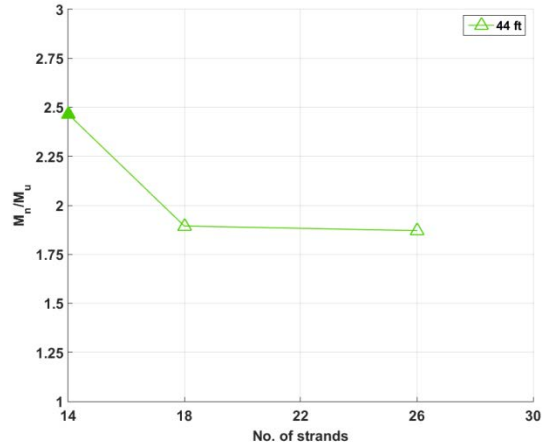
The lower overstrength for Configuration 2 is consistent with the increased tensile stresses and likelihood for cracking in these bents. While the overstrength and limited cracking under ultimate demands may be interpreted as an overdesign, it is important to assess this for the original objective in developing the design procedure—zero tension under dead load. This ensures that if overloading resulting in cracking were to occur, the cracks would close under full removal of live load, thus preventing exposure of the steel to environment effects that may reduce the service life of the bent cap.



(a) Configuration 1: 3 column, 4 girder



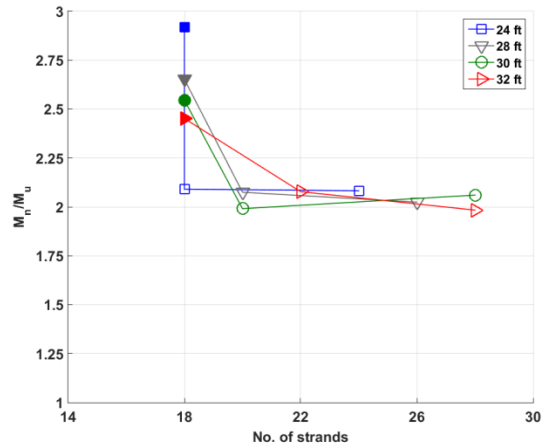
(b) Configuration 2: 3 column, 5 girder



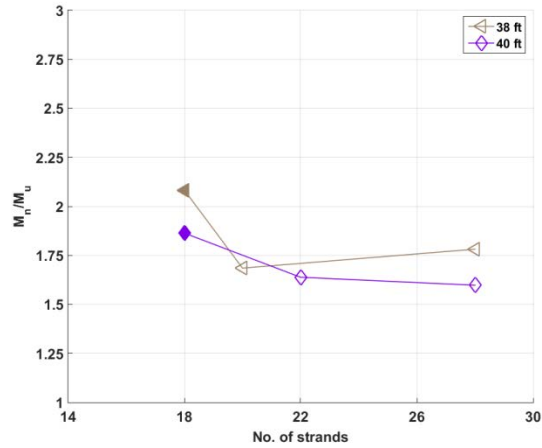
(c) Configuration 3: 4 column, 6 girder

Note: Solid markers indicate minimum strands control design.

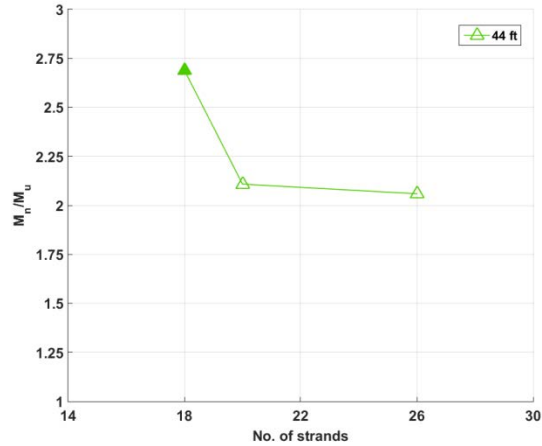
**Figure 3.13. Factor of Safety vs. Number of Strands for 42-in. Bent Cap.**



(a) Configuration 1: 3 column, 4 girder



(b) Configuration 2: 3 column, 5 girder



(c) Configuration 3: 4 column, 6 girder

Note: Solid markers indicate minimum strands control design.

**Figure 3.14. Factor of Safety vs. Number of Strands for 48-in. Bent Cap.**

### 3.6.5. Comparison to RC Designs

The objectives of the research study are met when the pretensioned precast concrete bent cap has an equivalent or higher performance than a RC bent cap. In lieu of a comparison of RC and PSC for all bridges, comparison of the 42-in. and 48-in. square, 40-ft bent caps with maximum span length were considered. These bridges have the largest stresses for 42-in. and 48-in. bent caps, respectively.

#### 3.6.5.1. Strength

The RC designs were adopted from the TxDOT standard drawing. For both bridges, the reinforcement consists of 6-#11 bars at the top, and 4-#11 bars at the bottom for the full length of the cap, with an additional 6-#11 bars at the bottom in the spans (does not continue through over the column). Skin reinforcement is provided as 5-#5 bars on each side face of the bent cap. The PSC designs both requires 28 strands, which are symmetrically placed at the top and bottom faces of the bent cap. Table 3.4 shows a comparison of the factor of safety of the RC and PSC bent caps.

**Table 3.4. Comparison of Strength between RC and PSC for the 40-ft Bent Cap.**

	Reinforced concrete		Prestressed concrete	
	42-in.	48-in.	42-in.	48-in.
Moment capacity (k-ft)	2,496	2,929	2,292	2,747
Ultimate moment (k-ft)	1,499	1,631	1,499	1,631
Factor of safety	1.67	1.80	1.53	1.68

#### 3.6.5.2. Expected Regions of Cracking

The cracking moment for a RC bent cap can be estimated from AASHTO LRFD equation 5.7.3.6.2.-2:

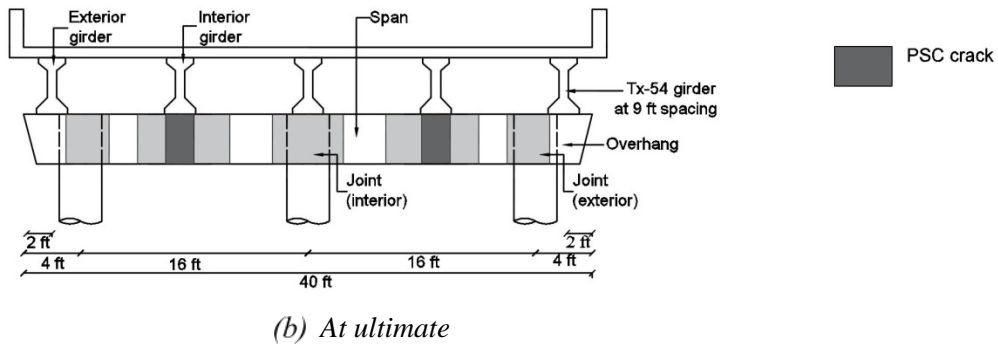
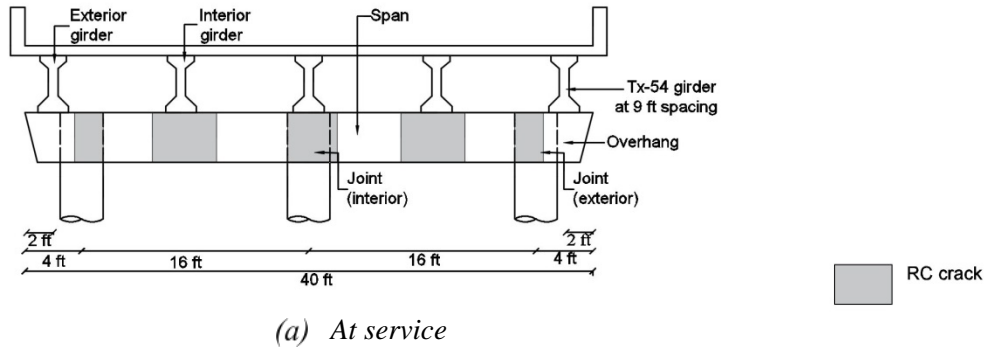
$$M_{cr} = f_r \frac{I_g}{y_t} \quad (3-16)$$

in which,  $f_r$  = modulus of rupture of concrete (ksi);  $I_g$  = gross moment of inertia; and  $y_t$  = distance from the neutral axis to the extreme tension fiber (in.). For the PSC bent cap, the cracking strength is determined from Equation (3-1) in Section 3.4.1.

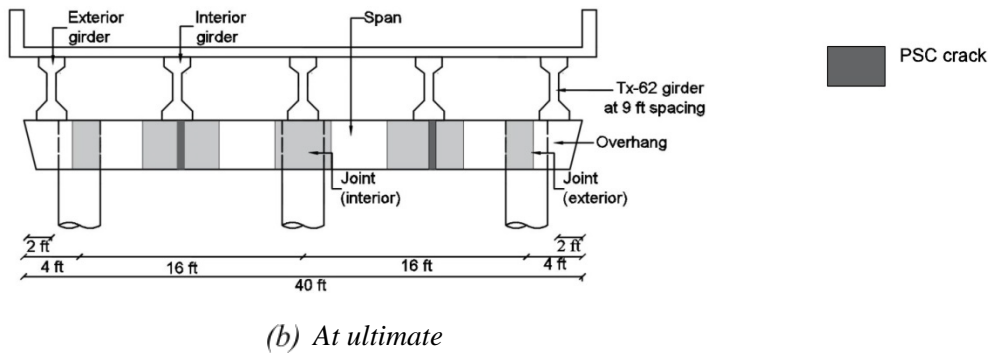
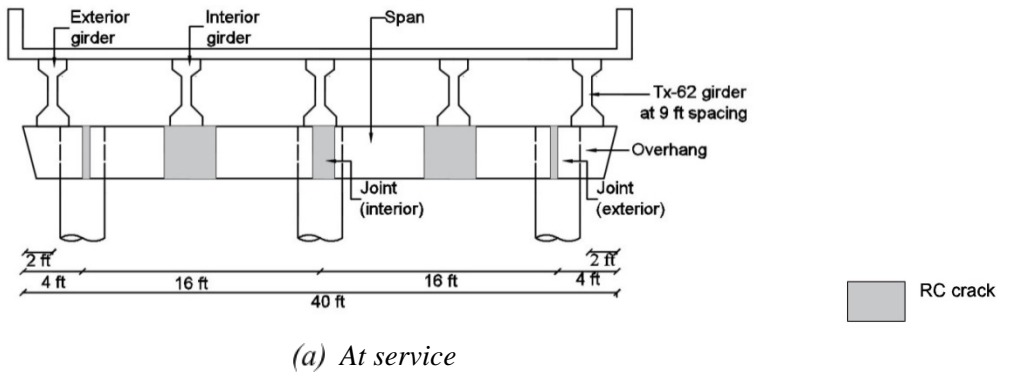
For RC designs with 3.6 ksi concrete compressive strength,  $M_{cr}$  is 469 k-ft and 700 k-ft, respectively. For PSC bent caps with 28 strands,  $M_{cr}$  is 1179 k-ft and 1560 k-ft, respectively. The bent caps will undergo cracking in the regions where the flexural demand is greater than the cracking moment.

Figure 3.15(a) and Figure 3.16(a) show the regions of cracking of the bent cap at service for the 42-in. and 48-in. bent caps, respectively. At service, the prestressed caps are uncracked, while the RC caps are cracked at the regions of maximum positive (at girder in span) and negative moments (above the columns).

Figure 3.15(b) and Figure 3.16(b) show the regions of cracking of the bent cap at ultimate for the 42-in. and 48-in. bent caps, respectively. The extent of cracking in the RC cap spreads. The prestressed cap now has cracking, but only where the maximum positive moment demands are located (at the girder locations in the span). The bridges shown in Figure 3.15 and Figure 3.16 have the highest demands at service and ultimate and are the worst cases of cracking in the bridge inventory. For bent Configuration 1 and 3, the prestressed designs are not expected to crack at ultimate; companion RC designs would be expected to have some regions of cracking under service loads. The intermediate and maximum span lengths of Configuration 2 undergo cracking in the span at ultimate.



**Figure 3.15. Cracking of 40-ft, 42-in. Bent Cap (Maximum Span).**



**Figure 3.16. Cracking of 40-ft, 48-in. Bent Cap (Maximum Span).**



### 3.7. SHEAR DESIGN FOR STANDARD BRIDGE INVENTORY

#### 3.7.1. Application of AASHTO Provisions to Bridge Inventory

In this section, the AASHTO shear design provisions are applied to the bridge inventory summarized in Section 3.5. Sectional shear design was conducted using shear and moment demands from CAP18 and section properties determined in the flexural design. Overhang and connection regions were not considered here since the assumptions of beam theory are not valid in these regions. Shear critical sections used for design were those where significant shear or moment demands are expected (near the column face and the interior girder locations).

Shear design was conducted in accordance with AASHTO LRFD 5.8.3 – Section Design Method. Two methods were used to obtain  $\theta$  and  $\beta$ : (1) iterative method using tables in AASHTO LRFD Appendix B5; (2) simplified method using equations in AASHTO LRFD 5.8.3.4.2. The method from Appendix B5 is more accurate, but the solution may require iteration, making it hard to calculate by hand. The method from AASHTO LRFD 5.8.3.4.2 is simple to calculate by hand, but is less accurate and can be excessively conservative in some cases (Hawkins et al. 2005; TxDOT 2010). By comparing shear design results of the two methods, it can be seen which method is more appropriate for shear design of PSC bent caps with consideration for both accuracy and practicality.

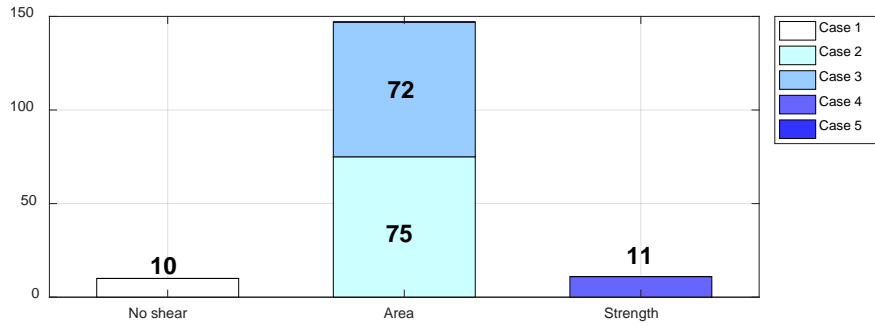
For consistency of design and in keeping with standard TxDOT practice, single #5 stirrups are used for transverse reinforcement. Consequently, only the spacing of the reinforcement must be specified to finalize the design for shear, with the spacing a function of the need to provide adequate strength, provide minimum reinforcement, and satisfy maximum spacing requirements (note that the TxDOT practice of limiting the spacing to a maximum of 12-in. is not considered here). The resulting designs can be grouped into five categories:

- Case 1:  $V_u < 0.5\phi V_c$  – Shear demand is less than one-half the factored concrete shear strength so that no shear reinforcement is required in accordance with 5.8.2.4.
- Case 2:  $0.5\phi V_c \leq V_u < \phi V_c$  – Factored concrete shear strength is less than the shear demand but shear reinforcement must be provided and satisfy the minimum area of AASHTRO LRFD 5.8.2.5.

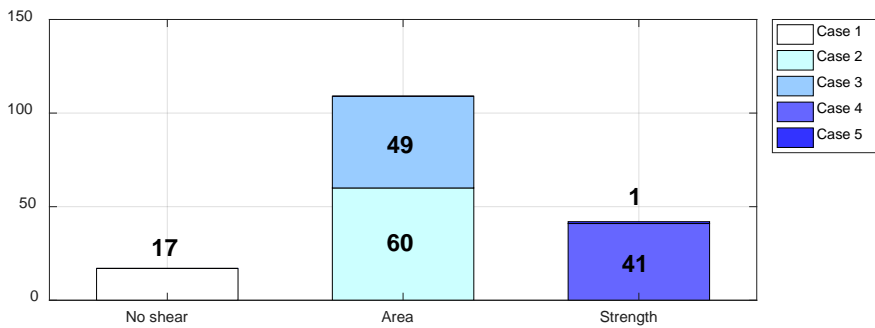
- Case 3:  $\phi V_c \leq V_u$  and  $s_{area} < s$  – Shear demand exceeds the factored concrete shear strength, thus shear reinforcement is required to provide strength; however, the minimum area of steel requirement controls over the strength requirement ( $s_{area} < s_{strength}$ ).
- Case 4:  $\phi V_c < V_u$  and  $4\text{-in.} \leq s \leq s_{area}$  – Shear demands exceed the factored concrete shear strength, thus shear reinforcement is required. Required spacing controls over the minimum area of steel requirement, with the spacing greater than 6-in.
- Case 5:  $\phi V_c < V_u$  and  $s \leq 4\text{-in.}$  – Shear demands exceed the factored concrete shear strength, thus shear reinforcement is required. Excessively tight spacing is required to satisfy the shear strength requirement and double stirrups should be used.

Figure 3.17 through Figure 3.19 summarize the results for all bridge designs considered. The smallest spacing in the bent cap is used to categorize each design based on the five cases described above. The following observations are made:

1. Area requirement controls the shear design in the majority of the bent caps. This is due in part to the minimum area requirement of AASHTO 5.8.2.5-1 in which the required spacing for a fixed stirrup size decreases as the width of the section increases and as the concrete strength increases. For pretensioned bent caps, the large width and higher concrete strengths result in the minimum reinforcement controlling over the strength requirements to a larger extent than is seen in RC bent caps or pretensioned girders.
2. AASHTO 5.8.3.4 provides larger concrete strengths,  $V_c$ , for low shear stress demands and smaller concrete strengths for higher shear stress demands. The shear stress demands for the bent caps considered are at the lower limits of the Appendix B5 tables and that expanded tables may be appropriate.
3. Small shear spacing primarily occurred when the girders were in close proximity to the column. Conventional beam theory cannot be applied in this region and another approach would be appropriate to ensure that the crack angle used is physically admissible.

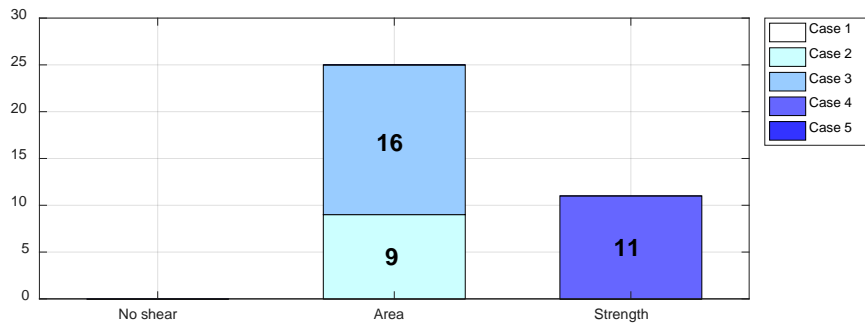


(a) AASHTO Appendix B5.

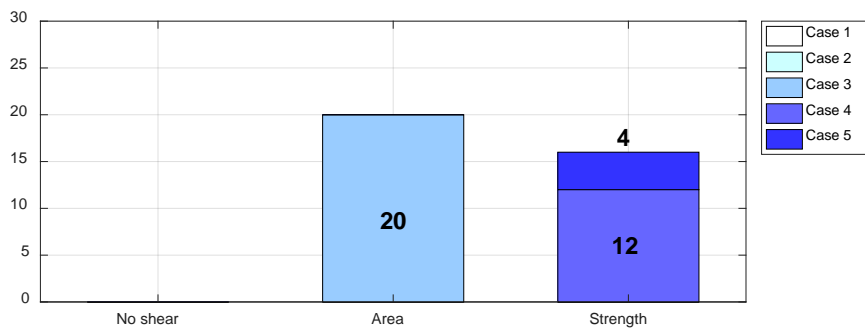


(b) AASHTO 5.8.3.4

**Figure 3.17. Bent Caps with I-Girder (BIG Type).**

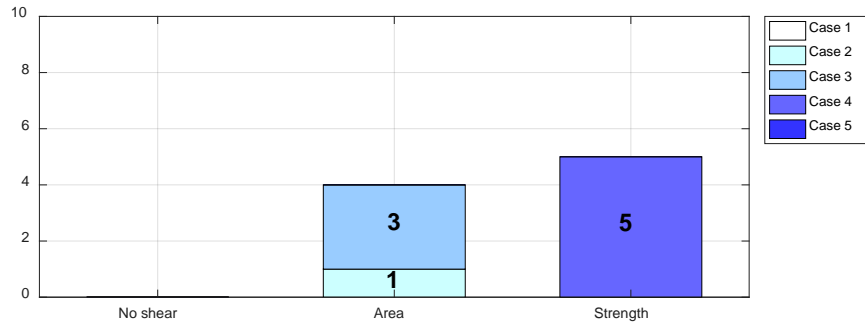


(c) AASHTO Appendix B5.

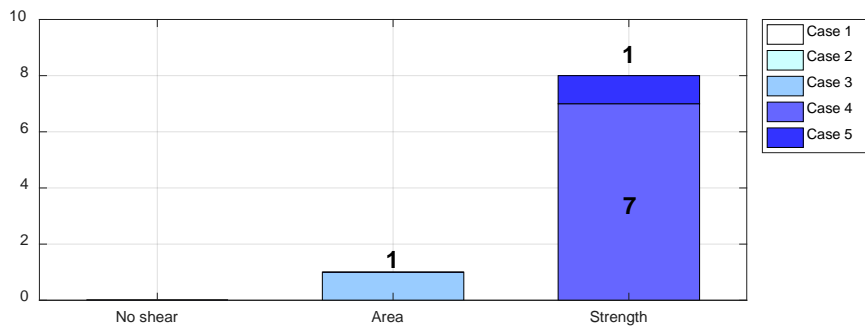


(d) AASHTO 5.8.3.4

**Figure 3.18. Bent Caps with X-Beam (BxB Type).**



(a) AASHTO Appendix B5.



(b) AASHTO 5.8.3.4

**Figure 3.19. Bent Caps with Box-Beam (BxB Type).**

### 3.7.2. Deficiency of Application of AASHTO Shear Provisions for Pretensioned Bent Caps

Bent caps are different from the girders for which AASHTO shear provisions were developed. Differences include: (1) relatively short clear spans between columns; and (2) the short distance between the concentrated loads and support faces.

The shear provisions in AASHTO and TxDOT that use the recently established sectional method have their roots in the MCFT that dates back to the inaugural 1994 LRFD Design Specifications (AASHTO 1994). The intent at that time was to use a more rational shear design approach for narrow webbed PSC girders based on strain compatibility considerations. Little is known on applicability for wide members such as bent caps. Moreover, the MCFT and its simplified successor, the AASHTO Section Method, break down in disturbed regions. For bent caps, the short clear spans between columns and the close proximity of girders to columns results in the majority of the bent cap length being classified as a disturbed region.

The diagonal (shear) crack angle is an important factor in concrete structures since it influences member's post-cracking behavior (Kim and Mander 2005) and is closely associated with the shear strength provided by the concrete and the shear. There have been extensive studies to reveal the relation between diagonal angle and shear strength in concrete members (Collins and Mitchell 1986; Collins and Mitchell 1991; Collins et al. 1996). The studies have shown that shear span-depth ratio ( $a/d$ ; where  $a$  is the shear span and  $d$  is the depth of the member) is the major variable affecting the shear strength and diagonal crack behavior of concrete members. While the use of diagonal crack angle in accordance with the AASHTO provisions might be appropriate for regular beams with shear span-depth ratio ( $a/d$ ) greater than 2.5, it may be inappropriate for deep beams with shear span-depth ratio less than 2.5 since deep beams have different behavior and shear failure mechanism (Kani 1964; Cook and Mitchell 1988; Zararis and Papadakis 2001; Choi et al. 2007).

Current TxDOT practice implements the AASHTO provisions for RC bent caps; however, maintaining this for use with pretensioning will result in a flatter crack angle that may be physically inadmissible. Figure 3.20 illustrates this for a standard I-girder bridge.

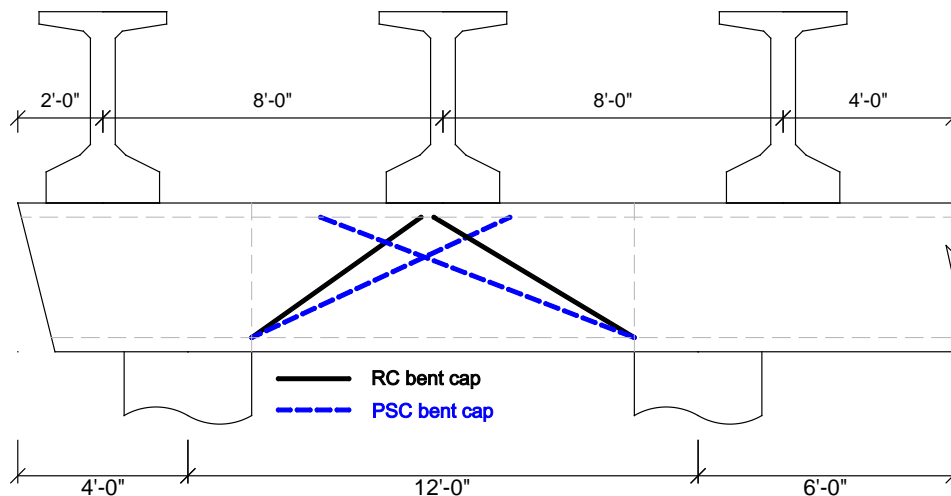


**Figure 3.20. Crack Angle for RC and PSC Bent Cap Designs Following the AASHTO Sectional Design Method for Shear Design.**

### 3.8. END REGION DETAILING

Pretensioned concrete members have been observed to have high tensile stresses in the end regions during prestress transfer actions. In a pretensioned bent cap, these bursting stresses may lead to tensile splitting cracks, and thereby affect the serviceability of the bent cap. Section 3.8.1 discusses

the background to the phenomenon of splitting, spalling, and bursting stresses. Section 3.8.2 discusses the provisions in AASHTO LRFD Bridge Design Specifications for handling these issues and other recommendations arising from recent research investigations. Section 3.8.3 presents proposed end region detailing.

### 3.8.1. Stresses in End Regions of PSC Beams

On release of a strand, the full prestressing force develops through bond over a transfer length. At this transfer length where the steel stress reduces from a high tensile force to zero at transfer, the strand dilates and a high localized circumferential hoop tension stress forms in the concrete around each strand. Radial cracks form transversely to these circumferential tensions (see Figure 3.21[a]). Figure 3.21(b) shows how these radial cracks propagate when the strand is close to the edge or another strand, resulting in spalling of the concrete. The method of mitigating this end splitting effect and the potential for spalling is to provide transverse hoop steel to bridge cracks, as shown in Figure 3.21(c).

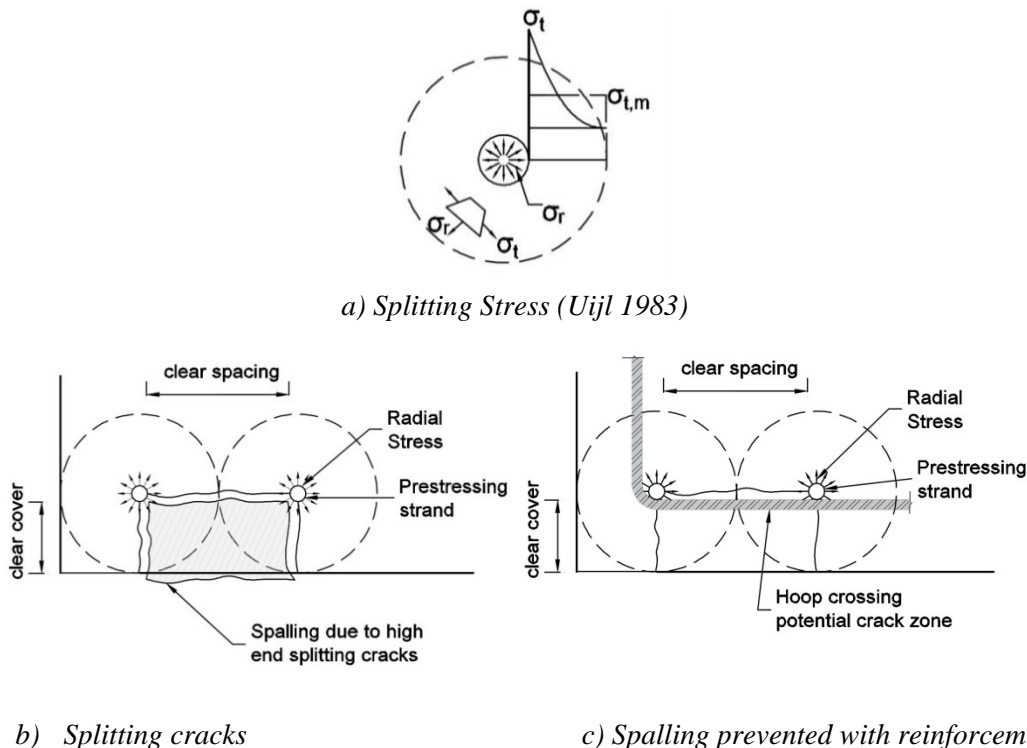


**Figure 3.21. Local Effects of Applied Prestressing Forces (adapted from Uijl 1983).**

In addition to the local effects of prestressing discussed above, global effects of applied prestress occur. When prestress is applied, the high end-stress concentrations eventually disperse, in

accordance with St. Venant's principle, over about one-member depth to provide a uniform distribution of prestress. Figure 3.22 to Figure 3.24 show this effect for two cases, one where the prestress is applied near the member edges, the other at the member center. Figure 3.22 shows the stress trajectories for elastic behavior. Note that for more than one member depth from the ends, the stresses are uniform. Figure 3.23 shows the stresses transverse to the longitudinal axis of the member. The location of the highest transverse tension stresses is where the transverse reinforcement should be provided. To assess the quantity of reinforcement necessary, a strut and tie model can be used as shown in Figure 3.24. For the case where there is an upper and lower layer of strands, a tension force denoted by the tie AB near the end of the member is equal to  $F/4$ , where  $F$  is the overall applied prestress at transfer. In contrast, for the case where there is a concentrated prestress force ( $F$ ) applied at the center of the member, the strut and tie model shows bursting forces that must be restrained approximately  $D/2$  away from the force application. The strut and tie model shows that the force denoted by the tie AB is equal to  $F/2$ .

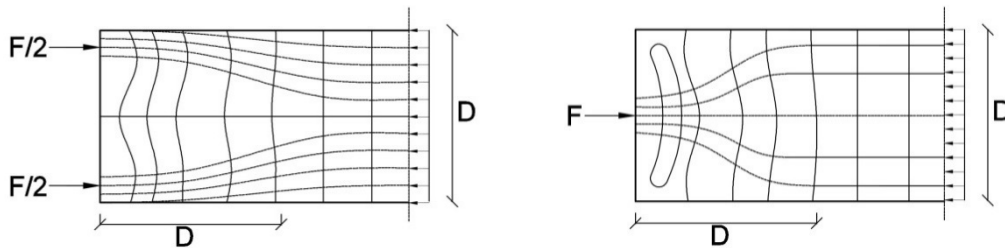


**Figure 3.22. Stress Trajectories due to Applied Prestress.**

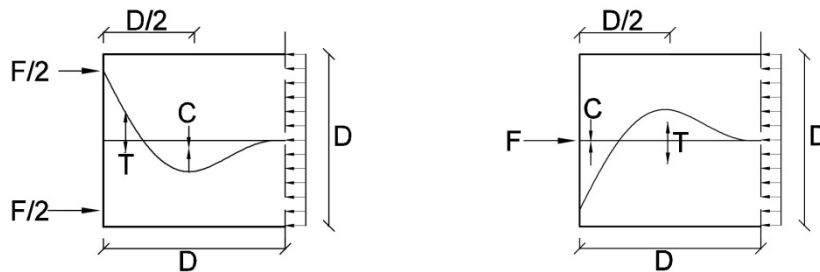


**Figure 3.23. Transverse Stresses due to Applied Prestress.**

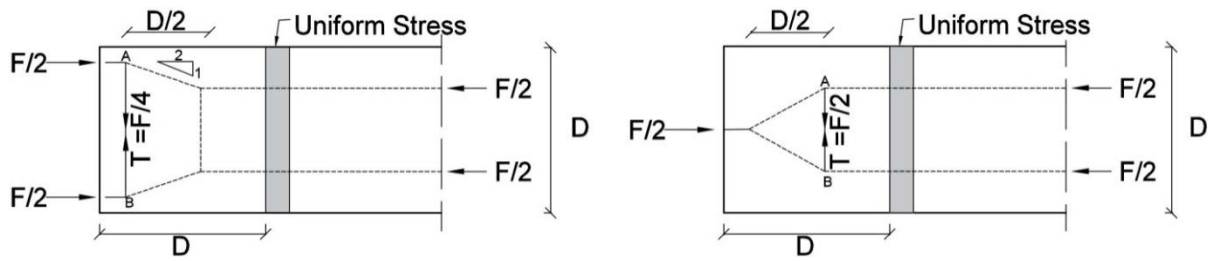


**Figure 3.24. Strut and Tie Model to Assess Reinforcement Requirement.**

### 3.8.2. AASHTO and Research Recommendations

AASHTO LRFD 5.10.10.1 specifies splitting resistance provided by end zone reinforcement in pretensioned beams as 4 percent of the prestressing force and placed within a distance of  $D/4$  from the member end, where  $D$  is the member depth.

$$A_s = 0.04 \frac{P_i}{f_s} \quad (3-17)$$

The stress in the reinforcement should not exceed 20 ksi for crack control. The reinforcement should be placed as close to the member end as practicable.

Experimental tests have shown that end zone reinforcement is more effective in controlling cracks if the reinforcement is concentrated at the member end and reduced gradually along the length of the member. Tuan et al. (2004) recommended that 50 percent of the end zone reinforcement be placed within  $D/8$  from the member end and the remaining 50 percent to be placed within  $D/8$  to  $D/2$  from the member end. Splitting reinforcement should not be needed to be provided beyond  $D/2$  from member end.

In TxDOT project 0-5831-3, Avendaño et al. (2013) conducted several experimental tests to evaluate end region detailing of box beams and the stresses at the ends during prestress transfer. The bursting force in the region  $D/4$  from the beam end did not exceed 4 percent of the prestressing force. However, the bursting force beyond  $D/4$  from the beam end to approximately the transfer length of the beam exceeded 50 percent of the bursting force in the first  $D/4$  of the beam. This result is in accordance with O'Callaghan and Bayrak (2008) who found from their experimental tests on pretensioned I-beams that bursting stresses occur up to a distance of the transfer length from member ends. In their report, O'Callaghan and Bayrak mentioned that the AASHTO provision of reinforcement within  $D/4$  from the member end is in reality meant to handle spalling



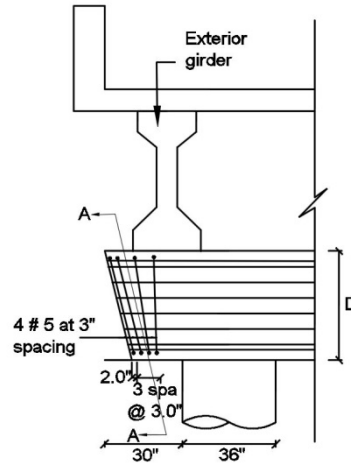
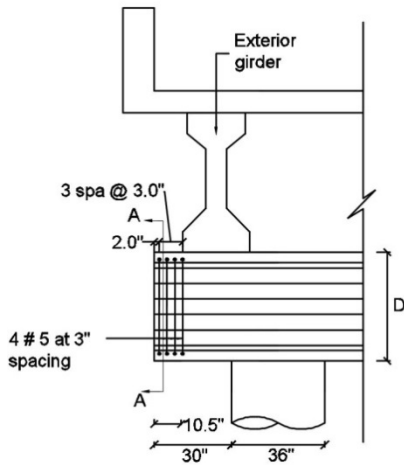
stresses that occur near the beam end. Bursting stresses reach a maximum value before the end of the transfer length and decreases rapidly to nearly zero some distance beyond the transfer length. The authors in both reports recommended that bursting reinforcement be placed immediately after spalling reinforcement, from  $D/4$  to the transfer length.

### **3.8.3. Application to Pretensioned Bent Caps**

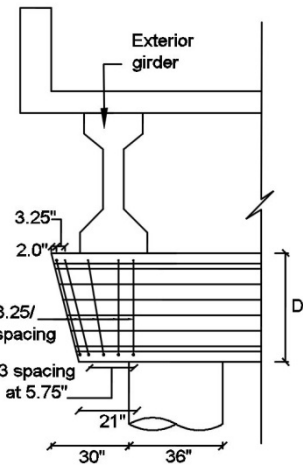
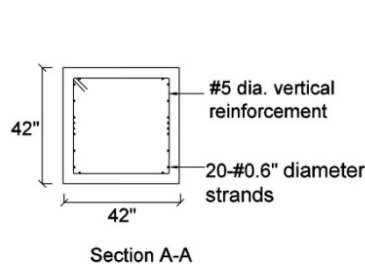
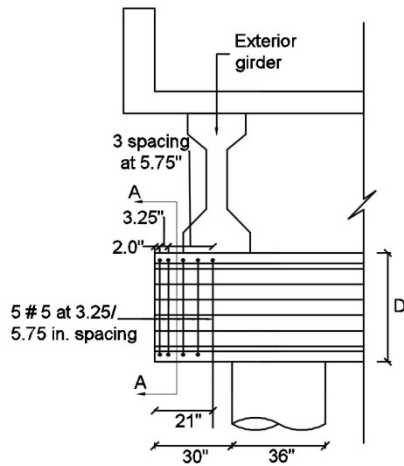
The provisions on end zone reinforcement discussed above are applied to the 32-ft roadway bridge of 80-ft span and 42-in. square bent cap with and without battered ends. Girders of size Tx-54 have been considered, and the exterior girders are placed at 2-ft from the edge of the bent cap. The exterior column face is 2.5-ft from the edge of the bent cap. Considering a precast pocket connection of 21-in. diameter at the joint, 37.5-in. space is available from the member end for detailing the end regions.

From Step 1 of the design procedure, the number of strands calculated as 20 strands. The initial prestressing force ( $P_i$ ) is then determined from the number of strands as 879 k. From Equation (3-17), the area of steel is calculated as 1.76-in.<sup>2</sup>. Figure 3.25(a) shows the steel provided within 10.5-in. ( $D/4$ ) from member end. It is determined that 4-#5 hoops @ 3-in. centers be provided, with the first stirrup placed 2-in. from the member end. Figure 3.25(b) shows the end zone reinforcement provided as recommended by Tuan et al. (2004), with 50 percent of 1.76-in.<sup>2</sup> placed within 5.25-in. ( $D/8$ ) and the remaining 50 percent placed from 5.25-in. to 21-in. ( $D/8$  to  $D/2$ ). Figure 3.25(c) shows the application of the recommendations from O'Callaghan and Bayrak (2008), in which the area of steel of 1.76-in.<sup>2</sup> has been placed within 10.5-in. ( $D/4$ ) from member end, and an additional steel area of 1.76-in.<sup>2</sup> placed from 10.5-in. to 36-in. from member end ( $D/4$  to transfer length). In the battered ends, two stirrups are provided parallel to the battered end, followed by a transition stirrup and then the remaining are placed as vertical stirrups.

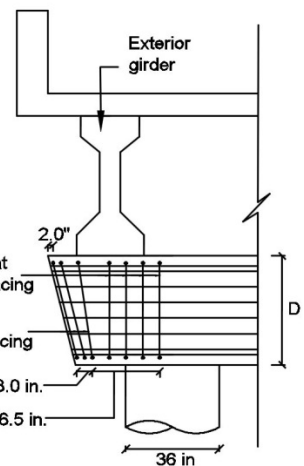
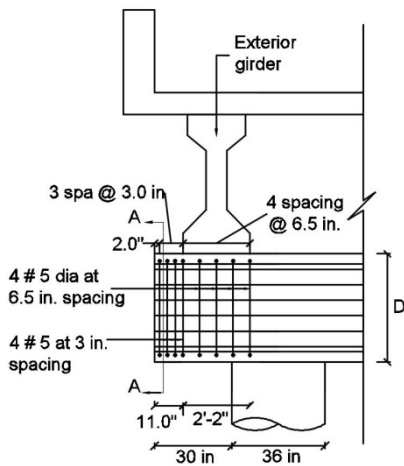
It is considered prudent that the more conservative recommendations of O'Callaghan and Bayrak (2008) be used for bent cap design. These recommendations are in keeping with the STM shown in Figure 3.24. The end region reinforcement provided up to the transfer length includes the region of high shear at the exterior girder location that may result in high stresses in the reinforcement. These stresses should be checked not to exceed 20 ksi. To prevent this, additional transverse reinforcement may be required.



(a) AASHTO LRFD (2014)



(b) Tuan et al. (2004)



(c) O'Callaghan and Bayrak (2008)

Figure 3.25. Application of End Region Detailing Provisions.

### **3.9. POCKET CONNECTIONS**

The use of precast bent caps eliminates the monolithic connection found in CIP bent caps. Connections for precast members must be designed to provide the same performance of monolithic connections, including the transfer of critical forces, elastic or inelastic behavior, joint shear resistance, and stability and ductility of the structure. At the same time, precast connections must consider constructability of the structure, including ease of construction, labor skills required, time, and cost.

TxDOT currently uses a grouted vertical duct for precast RC bent caps and early adoption of pretensioned bent caps. The research leading to the use of this connection went on to inspire an alternative connection called a pocket connection. Section 3.9.1 discusses these connections and the associated research. This research investigates the use of a pocket connection for pretensioned bent caps. Section 3.9.2 discusses the preliminary design of pocket connections, which is inspired largely by geometry and constructability. Section 3.9.3 overviews the demands that connection must resist. Section 3.9.4 evaluates the moment capacity of the connection. The connection resistance to joint shear is primarily a function of the geometry and thickness of the pipe forming the pocket. Section 3.9.5 discusses the impact of the pipe thickness on the shear resistance and the stress concentrations introduced by prestressing. The flexural strength of the connection provides a potential weakness in the structure subjected to crash loads; Section 3.9.6 presents an assessment of this impact.

#### **3.9.1. Discussion of Current Practice and Previous Research**

TxDOT provides a standard connection detail for precast RC bent caps, intended to be used with standard multicolumn interior bent designs. The connection, known as a grouted vertical duct connection, is based on TxDOT research projects 0-1748 and 0-4176. In this connection, the column bars are terminated at the top of the column. Dowel bars are embedded into the core of the column and extended into 4-in. diameter galvanized steel ducts precast in the bent cap. To provide confinement and shear strength, transverse reinforcement is provided around the group of ducts, extending the length of the dowel bars. After placement of the bent cap, the ducts are filled with grout.

The specific details of the precast connection vary based on the size of the columns in the standard bent, with differences primarily being the size and number of dowel bars. For bents with 36-in. and 42-in. columns (the sizes considered in this research), the connection uses 4 and 6-#11 bars, respectively. The dowels are located where they maximize the spacing while providing adequate cover and clearance from other reinforcement in the column and bent cap.

Construction of bridges using the grouted vertical duct connection has identified a number of challenges that may be better addressed with an alternative connection. This includes 1) tight horizontal tolerance for alignment of bars with the corrugated ducts, 2) minimal room for accidental misalignment of the column for the bent cap, and 3) challenges in grouting the connection. Grouting operations involved in the precast connection requires special care and attention to ensure a successful mix. Improper grouting may lead to segregation of water from the grout. The migration of water to the surface of the grout is known as bleeding, which may result in voids created in the grout. These voids further lead to reduced strength of the grout and act as channels for ingress of unwanted materials into the grout, possibly resulting in corrosion of the reinforcement.

An alternative to a grouted vertical duct connection is a pocket connection. The pocket connection was introduced by Restrepo et al. (2011) for connection of precast, RC bent caps to circular columns in seismic regions. The pocket connection investigated by Restrepo et al. extended all bars from the column and in a single large duct, referred to as a pocket, formed by a corrugated steel pipe. A variation of this is the use of dowel bars similar to those in a grouted vertical duct. The size of the pocket allows for the use of concrete instead of grout, making it an attractive alternative to the grouted vertical duct connection. The pocket connection also allows large construction tolerance, thus providing room for accidental misalignment of column with respect to the bent cap.

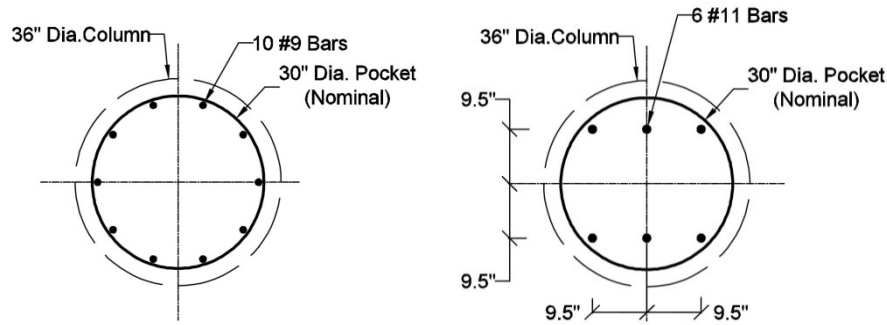
Restrepo et al. (2011) experimentally investigated the performance of pocket connections and found the performance to be satisfactory. The connections tested were intended for use in seismic regions and were subjected to cyclic loading. The damage was concentrated primarily in the top of the column, as desired. The use in seismic regions motivated a focus on the confinement and

shear resistance provided by the corrugated pipe connection and the need for supplemental joint reinforcement.

While the results of this previous research demonstrate the potential for successful use of the pocket connection in precast, pretensioned bent caps, there are some key differences that must be considered. The primary difference is the use of a pretensioned, rather than a RC, bent cap. This is a major consideration in determining the size and thickness of the pocket, which can introduce vulnerability in the form of stress concentrations where the width of the original cross-section is reduced by the temporary void. Another difference is the size of the connections investigated. Restrepo et al. tested scaled specimens, using an 18-in. diameter pocket in 25-in. square cap beam; this is significantly smaller than the 42-in. square and 48-in. square bent caps considered in this study. Additionally, challenges encountered during the previous pocket connection research should be taken into account in developing recommendations for TxDOT. These include challenges in construction due to interference of the column and cap reinforcing bars.

### **3.9.2. Alternative Connections**

Two preliminary options for a pocket connection in TxDOT standard bents are the extension of column longitudinal reinforcement into the cap (method used by Restrepo et al. [2011]) and the use of the same dowel bars used in grouted vertical duct connections. Figure 3.26 shows these two options for a 36-in. diameter column. For both, a minimum pocket diameter of 30-in. is required to fully enclose all bars, leaving a minimum clear distance from the edge of the bars to the pocket wall of 0.125-in. and 0.667-in., respectively. This provides little room to accommodate construction tolerances and raises concerns about the development of bond of the bars. A larger diameter pocket is impractical as it would require a pocket the same diameter as the column.

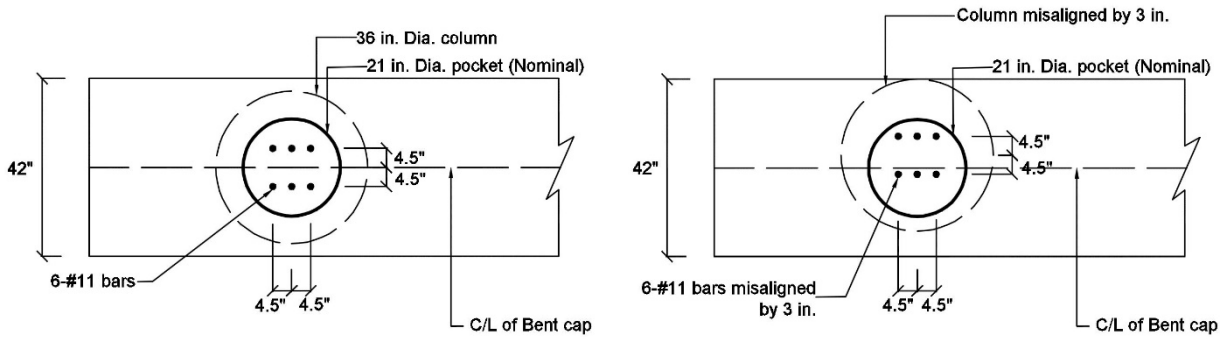


a) Extension of column bars.      b) Dowel bars for grouted vertical duct connection.

**Figure 3.26. Preliminary Options for Pocket Connection for 36-in. Diameter Connection around Standard TxDOT Bar Configuration.**

To improve the ease of construction from these two preliminary options, the use of dowel bars with alternative spacing and pocket sizes is considered. The geometry of the connection is controlled by the ability of the connection to accommodate accidental column misalignment. The maximum misalignment considered is 3-in. in the longitudinal direction of the bridge. An additional objective is to use the pocket size that causes the least disturbance to the cross-section, thereby minimizing stress concentrations due to pretensioning.

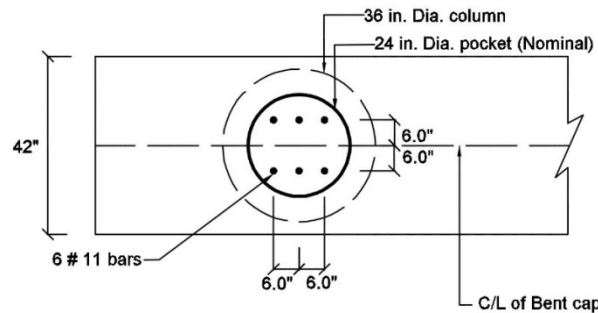
The smallest pocket can be accommodated by minimizing the spacing between the dowel bars. AASHTO LRFD 5.10.3.1.1 requires a clear distance between parallel bars of not less than 1.5 times the nominal diameter of the bars. In this study, a clear spacing of 2.0 times the nominal diameter of bars has been considered as the minimum spacing. Assuming the use of 6-#11 dowel bars in a 36-in. diameter column for consistency with TxDOT grouted vertical duct connections, a center-to-center spacing of 4.5-in. is used. Considering this spacing, available sizes of corrugated pipes, and potential column misalignment, a 21-in. diameter pocket is required for this dowel bar configuration. Figure 3.27 shows the recommended pocket configuration with and without column misalignment. Figure 3.28 shows the maximum dowel spacing for larger pocket diameters. Potential pocket configurations can be developed for 42-in. diameter columns through a similar process, although the increased number of dowels must be taken into consideration.



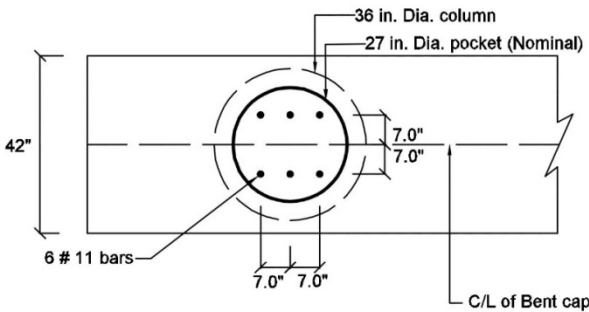
a) Without misalignment

b) With misalignment

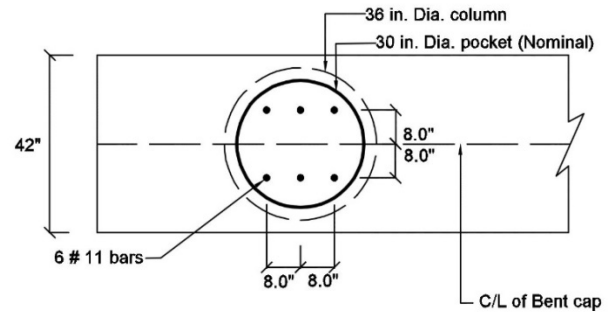
**Figure 3.27. Geometry of 21-in. Diameter Pocket Connection with 6-#11 Dowel Bars.**



(a) 4-in. diameter



(b) 27-in. diameter



(c) 30-in. diameter

**Figure 3.28. Example Pocket Connections to Handle Misalignment of Column.**

### 3.9.3. Connection Demands

The pocket connection configurations presented in Section 3.9.2 are based on geometry and constructability, but must be capable of providing transfer of forces from the cap to the column. This section provides a brief summary of the demands that must be transferred. Sections 3.9.4 and 3.9.5.1 provide an evaluation of the capacity of connection in resisting these demands.

The connection must be capable of transferring forces resulting from the dead and transient vehicular live loads used in designing the bent caps, as well as wind loads that may introduce overturning forces into the bent. Section 3.5.2 describes the dead load and vehicular live load with impact. The column moment is maximum when the live load is applied only at one exterior lane. To further maximize the possible exterior column moments, the live load is considered from the exterior girder only, with a multiple presence factor of 1.2 for one loaded lane (AASHTO LRFD Table 3.6.1.1.2-1). Wind loads acting on the superstructure, bent cap, and live loads are calculated according to the provision of Section 3.8 in AASHTO LRFD. The dead, live, and wind loads are combined in accordance with the load factors in AASHTO LRFD 2014 Table 3.4.1-1.

A 32-ft wide bridge with an average span of 80-ft is used to provide an example of the demands a connection; analysis of the full standard bridge inventory considered for flexural design of the bent caps is not considered. SAP2000 (SAP2000 v.17.1.0) frame models were used to calculate demands from the gravity (dead and line) loads and the lateral (wind) loads. Joint demands due to dead, live, and wind loads were determined from the bent was modeled as a frame using SAP2000 (SAP2000 v17.1.0). The columns were assumed to have a height of 13.75-ft with fixed supports. A concrete strength of 3.6 ksi and 6 ksi were used for the column and bent cap, respectively. The modulus of elasticity of concrete was calculated using AASHTO LRFD 5.4.2.4-1. Table 3.5 provides a summary of demands joint moment and column axial force for the load combinations considered. The maximum moment, 178 k-ft, occurs with the Strength V load combination; the associated axial load is 582 kips.

**Table 3.5. Joint Moment and Column Axial Forces in 32-ft Roadway, 80-ft Span.**

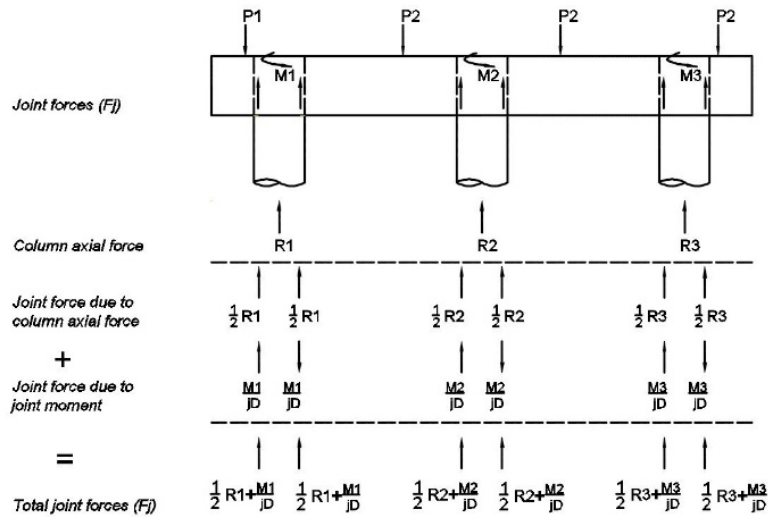
	Strength I		Strength III		Strength V	
	Max.	Min.	Max.	Min.	Max.	Min.
Moment (k-ft)	161	147	166	151	<b><u>178</u></b>	165
Column axial forces (kips)	649	532	318	202	<b><u>582</u></b>	465

The joint shear is calculated from the joint moments and column axial forces. Figure 3.29(a) shows the loads and internal reactions acting on the bent, resulting in the largest joint shear demands. The largest demand occurs at an external column when a full live load reaction acts on the external

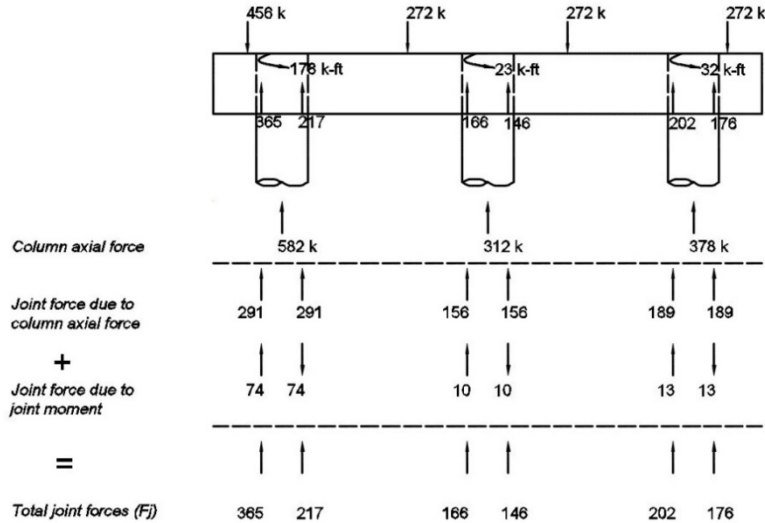


girder adjacent to the joint and only dead load is applied at the other girders. The column axial forces in each column are shown as  $R_1$ ,  $R_2$ , and  $R_3$ , and joint moments are shown as  $M_1$ ,  $M_2$ , and  $M_3$ . The joint forces are calculated as the sum of the compression forces in the joint due to column axial force and the compression-tension couple with a moment arm of 0.8 times diameter of the column formed by the joint moment. Figure 3.29(b) shows the joint forces for the prototype bridge. Figure 3.29(c) shows the resulting shear force diagram for the bent. The maximum joint shear in the prototype bridge is 91 kips.

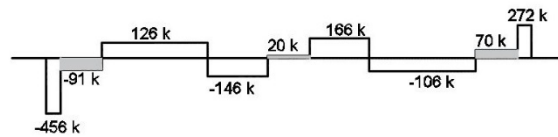
Rigorous analysis will show that when sidesway is not present, the joint shear demands are small and similar to the shears encountered in adjacent beams. If sidesway occurs, which is a possibility under crash loads, joint opening (or closing) will occur. If there is substantial reinforcing steel from the column into the joint, an end couple of forces is formed (equivalent to the end moment within the column). This force couple introduces a high shear force within the bent-column joint region. The inherent shear strength of the concrete within the joint has limitations on the magnitude of shear force that can be transferred and without adequate transverse reinforcement in the joint, diagonal cracking may occur. Under these circumstances, it is likely that a substantial amount of joint shear reinforcement will be necessary to inhibit concrete cracking.



(a) Joint forces



(b) Joint forces in prototype bent



(c) Shear force diagram for prototype bent

**Figure 3.29. Evaluation of Joint Forces and Shear Force Diagram.**

### 3.9.4. Moment Capacity of the Pocket Connection

The moment capacity of the pocket connection can be calculated similar to the calculation of the flexural capacity of a column. Figure 3.30 shows the geometry, strains, stresses and internal forces used for calculating the strength of the connection.

The axial load ( $N$ ) in the joint is assumed to result only from dead loads. To ensure conservative results, the dead load is calculated using the minimum load factors corresponding to the load combination, for which the joint demand is the highest.

For simplicity of calculation, the resultant tension force in the dowels is assumed to act at the column centroid. All bars are assumed to yield, providing a tension force:

$$T = f_y A_s \quad (3-18)$$

Equilibrium of the section internal forces provides the resultant force of the concrete compression block

$$C_c = N + T \quad (3-19)$$

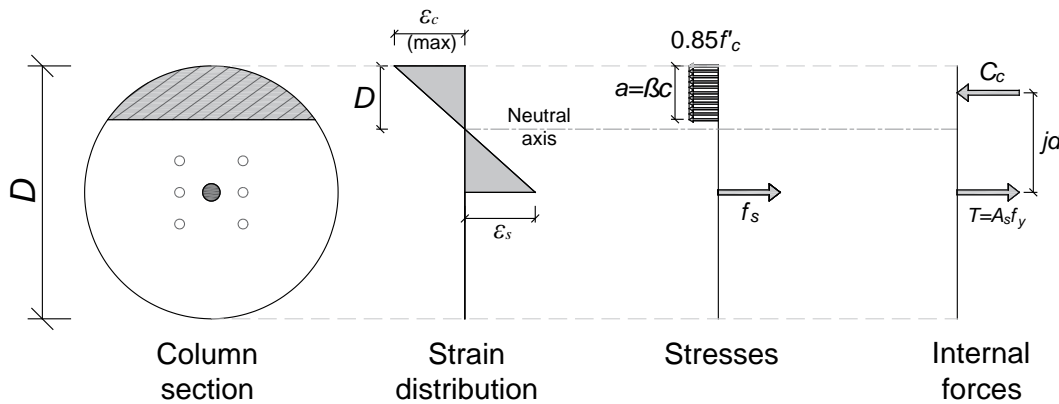


**Figure 3.30. Calculation of Moment Capacity.**

Dutta and Mander (2001) provide an equation for the compression force  $C_c$ :

$$\frac{C_{cc}}{f'_c A_g} = 1.32 \alpha_c \left( \beta_c \frac{c''}{D''} \right)^{1.38} K \frac{A_{cc}}{A_g} \quad (3-20)$$

in which  $C_{cc}$  = concrete compression force considering core dimensions of joint;  $f'_c$  = unconfined compressive strength of concrete;  $A_g$  = gross cross-sectional area of column;  $\alpha_c, \beta_c$  = stress block factors for core concrete;  $c''$  = neutral axis depth measured from centerline of transverse steel;  $D''$  = overall depth of section measured from centerline of transverse steel;  $K$  = confinement coefficient; and  $A_{cc}$  = area of core concrete.

Assuming that the connection does not provide any confinement,  $K = 1$  and  $A_{cc} / A_g = 1$ . For  $f'_c \leq 4$  ksi,  $\beta_c = 0.85$  and  $\alpha_c$  is assumed as 0.85. From Equation (3-20):

$$C_{cc} = 1.122 f'_c A_g \left( \frac{a}{D} \right)^{1.38} \quad (3-21)$$

The depth of compression block ( $a$ ) is given by:

$$a = 0.92 \left( \frac{C_c}{f'_c A_g} \right)^{0.725} D \quad (3-22)$$

The lever arm between tension and compression forces is computed as:

$$jd = \frac{D}{2} - 0.6a \quad (3-23)$$

The moment in the joint is given by:

$$M_j = C_c jd \quad (3-24)$$

If the provided capacity is less than the demands, the total area of steel provided by the dowel bars must be increased to provide the necessary capacity. A 21-in. diameter pocket with 6-#11 dowel bars has a capacity of 718 k-ft, well above the 178 k-ft demand in the prototype bridge.

### 3.9.5. Pipe Thickness

Section 3.9.4 demonstrated the dowel bars in pocket connection recommended in Section 3.9.2 provide sufficient strength to allow for transfer of moments demands from the bent cap to the column. Another critical characteristic of the pocket connection is the diameter and thickness of the corrugated pipe used to form the pocket. These pipe characteristics are important for providing resistance to shear demands and to reduce stress concentrations that may arise from prestressing; these issues are discussed in Sections 3.9.5.1 and 3.9.5.2, respectively.

#### 3.9.5.1. Joint Shear

The joint should be provided with transverse reinforcement to ensure it is not a weak link in the structure. Minimum shear reinforcement can be provided in the form of stirrups, hoops, spirals, or

the corrugated pipe used to form the pocket connection. In the current study on pocket connections, the corrugated pipe is used to satisfy the requirement of transverse reinforcement.

A preliminary selection of the thickness is based on providing equivalent shear strength to the spiral reinforcement in the columns:

$$t_{pocket} = \frac{A_b}{s} \quad (3-25)$$

in which  $t_{pocket}$  = thickness of the corrugated pipe (in.);  $A_b$  = area of the spirals (in.<sup>2</sup>); and  $s$  = spiral spacing (in.).

The reinforcement ratio of the corrugated pipe is determined by:

$$\rho_t = \frac{4t_{pocket}}{d_{pocket}} \quad (3-26)$$

in which  $\rho_t$  = reinforcement ratio of the corrugated pipe;  $d_{pocket}$  = diameter of the pocket (in.).

The shear strength provided by the corrugated pipe is given by:

$$V_s = \frac{1}{2} \frac{\pi}{4} \rho_t d_{pocket}^2 f_{yp} \quad (3-27)$$

in which  $f_{yp}$  = nominal yield stress of the corrugated pipe (ksi).

The shear strength contribution from the concrete is computed as:

$$V_c = 2 \sqrt{\frac{f'_{c\_pocket}}{1000}} A_v \quad (3-28)$$

in which  $f'_{c\_pocket}$  = specified compressive strength of pocket fill (ksi);  $A_g$  = gross area of the column;  $A_v$  = shear area =  $0.8A_g = 0.8 \frac{\pi}{4} D_{col}^2$  (in.<sup>2</sup>);  $D_{col}$  = diameter of the column.

The total shear strength  $V_r$  is the sum of the contributions from the steel and the concrete:

$$V_r = V_s + V_c \quad (3-29)$$

For the prototype bridge, the joint is assumed to have transverse reinforcement from continuation of the #3 spiral at 6-in. spacing present in the column. The thickness of the corrugated pipe calculated from Equation (3-24) is 0.0183-in. The minimum pipe thickness available in the market, 16 gage, has a thickness of 0.064-in. and a yield stress 33 ksi. A 21-in. pipe, along with a pocket filled with concrete the same strength as a RC cap (3.6 ksi), provides a strength of 167 kips. This is greater than the joint shear force of 91 kips in the prototype bridge.

The joint demand increases for larger width bridges and longer spans. In addition to the corrugated pipe, hoops or spirals may be required to be provided such that shear strength is greater than the joint shear demand.

### 3.9.5.2. *Prestressing Impact on Pocket Connection*

In a prestressed bent cap with concentric prestressing, compressive stresses equal to  $F/A$  are developed. Prior to filling the pocket with concrete, the corrugated pipe is empty, leading to a discontinuity in the stress flow. This discontinuity leads to a local increase in the stress around the pipe. If this stress intensity exceeds the cracking stress, the bent cap will crack in those areas. Ideally, the corrugated pipe should be sufficiently thick to avoid any stress concentrations by ensuring uniform stress in the bent cap, as shown in Figure 3.31(a). To achieve this ideal stress, the pipe thickness should provide equivalent stiffness as the displaced concrete.

From Figure 3.31(b), the stress per unit length in the pocket due to prestressing that must be resisted by the corrugated pipe is:

$$2 f_{st} t_{pocket} = \sigma_{ps} d_{pocket} \quad (3-30)$$

in which  $f_{st}$  = allowable stress of the corrugated pipe (ksi) =  $0.6 \times$  nominal yield stress of the pipe;  $t_{pocket}$  = thickness of the corrugated pipe (in.);  $\sigma_{ps}$  = compressive stress due to initial prestressing (ksi) =  $F_i/BD$ ;  $F_i$  = initial prestressing force (k);  $B$  = width of bent cap (in.);  $D$  = depth of bent cap (in.); and  $d_{pocket}$  = diameter of the pocket.

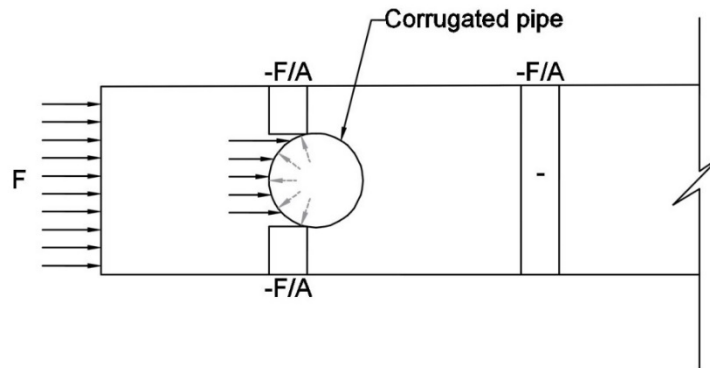
From Equation (3-30), the required thickness of the pocket to maintain uniform stress is:

$$t_{pocket} = \frac{F_i d_{pocket}}{2 f_{st} B D} \quad (3-31)$$

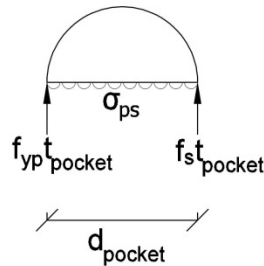
This can be simplified for design by specifying the pocket diameter  $d_{pocket}$  as a factor  $\lambda$  of the width of the bent cap  $B$ :

$$t_{pocket} = \frac{F_i \lambda}{2 f_{st} D} \quad (3-32)$$

For a bent cap with 16 strands, the initial prestressing stress is 703 kips. An allowable stress of 33 ksi for the pipe is assumed. For a 21-in. diameter pocket ( $\lambda=0.5$ ), a thickness of 0.21-in. (5 gage) is required to force a uniform stress condition. This thickness is not readily available in the market, thus it is not practical to achieve a uniform stress at the pocket. Instead, the thickness available pipe should be used to minimize stress concentrations at the edge of the pocket. In addition to providing the thickest pipe possible, stress concentrations are minimized by limiting the diameter of the pocket.



(a) Stresses in pretensioned bent cap



(b) Stresses acting on pipe

**Figure 3.31. Corrugated Pipe Thickness Required to Minimize Stress Concentrations.**

### 3.9.6. Connection Performance under Collision Loads

While TxDOT standard bridges do not take into consideration collision loads, the proposed pocket connect has the potential for use in many other bridges. As such, it is worth examining the strength of the connection for such demands.

In assessing collision loads, the potential plastic failure mechanisms of a bent are considered. A failure mechanism is determined by identifying the locations of possible plastic hinges that will result in a collapse of the structure. The applied loads needed to produce each failure mechanism is calculated; the lowest applied load is considered to be the true collapse load of the structure. For a bent to have the necessary strength to resist a collision load, the collapse load must exceed the relevant component of the 600-kip design force is considered to be acting on the exterior column at 5-ft above ground in a direction of  $15^\circ$  to the edge of the roadway. This force can be resolved into two components: a 580-kip force,  $F_x$ , acting in the transverse direction and a 155 k force,  $F_y$ , acting in the longitudinal direction of the bridge.

Failure mechanisms for a typical bent are established based on the assumption of strong beam-weak column design, meaning the bent cap is sufficiently strong to prevent the formation of hinges in the bent cap. Additionally, the joint is assumed to be weaker than the column. If the joint is stronger than the column, a hinge will form at the top of the column. If the joint is weaker than the column, the hinge will form in the joint. Figure 3.32 shows the failure mechanisms considered for a bent assuming a joint weaker than the column. Mechanism 1 is a global mechanism in which all of the columns sway due to the lateral load. Mechanism 2 is a local mechanism affecting the column in which the collision occurs. Mechanism 3 is a combination of Mechanisms 1 and 2, in which the column under collision has a local mechanism while the other columns have a global mechanism. Mechanisms 1, 2, and 3 are in the transverse direction. Mechanism 4 is the local mechanism in the longitudinal direction of the bridge. Mechanisms 1, 2, and 3 are in the transverse direction. Mechanism 4 is the local mechanism in the longitudinal direction of the bridge. Mechanism 2 will govern when  $2h < H$ , in which  $h$  = distance of 5-ft from the ground where the collision load is applied;  $H$ = height of column.

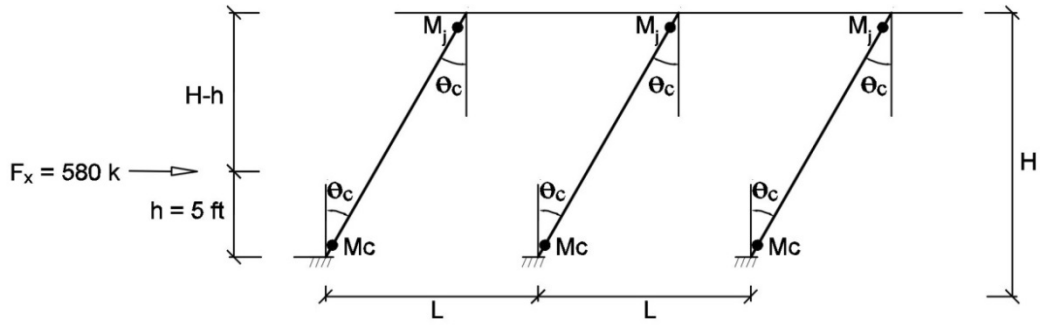
The recommended pocket connection (21-in. diameter with 6-#11 dowel bars) has a moment capacity of 718 k-ft, lower than the 727 k-ft moment capacity of the 36-in. diameter column



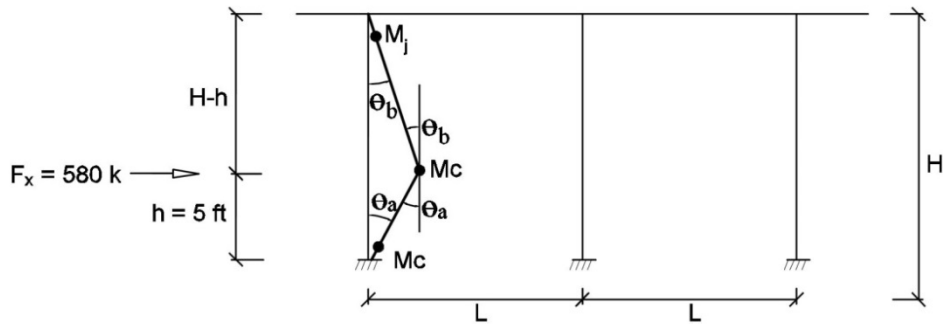
reinforced with 9-#11 bars. To assess this impact of the weak connection on the collapse load of the structure, the 32-ft wide, 80-ft average span prototype bridge is again considered. The use of the pocket connection results in a collapse load of 497 kips, a reduction of only 1 kip compared to the same structure with a stronger joint.

This collapse force is less than the 580-kip load that must be resisted if designing for collision loads. This is inconsequential for the bridges considered in this research study, which do not require design for collision loads. However, the use of a pocket connection does not introduce a weak link in the bent that would otherwise not be present. Additionally, this evaluation can be extrapolated to demonstrate the potential to use a pocket connection on individually designed structures for which collision loads must be considered. If the prototype bridges were required to resist collision loads, adequate capacity could be provided by increasing the column longitudinal reinforcement from 10-#9 bars to 14-#9 bars without modification to the connection; a smaller increase in the amount of column reinforcement may be attained when accompanied by an increase in the connection reinforcement.

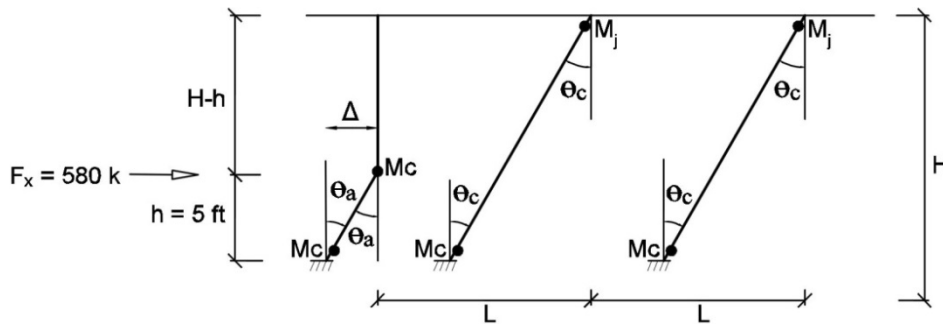
In bridges designed for collision loads, the designer must consider both the strength of the column and the pocket connection in assessing the capacity of the structure. The optimal design should balance the increase in column and connection reinforcement with the design demands and constructability issues (e.g., congestion and construction tolerances).



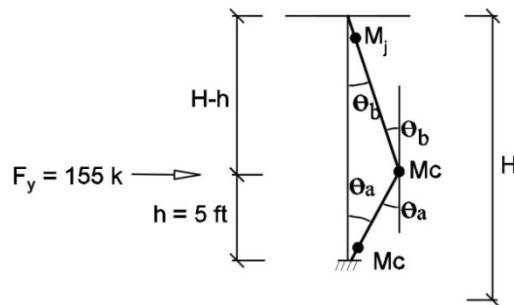
(a) Mechanism 1: Sidesway (transverse direction)



(b) Mechanism 2: Local column (transverse direction)



(c) Mechanism 3: Mixed column and sidesway (transverse direction)



(d) Mechanism 4: Local column (longitudinal direction)

**Figure 3.32. Failure Mechanism Due to Vehicle Collision Load.**

### 3.10. SUMMARY

This chapter explored design considerations for precast, pretensioned concrete bent caps for use in standard TxDOT bridge bents. Key findings, recommendations, and need for future work are summarized here.

For the flexural design of pretensioned bent caps, key results include:

1. A design procedure was proposed based on the objective of achieving zero tensile stresses under dead load only. This allows, under removal of live loads, the closure of cracks that may have formed under ultimate demands.
2. Application of the proposed design procedure to TxDOT standard bents for non-skewed I-girder bridges indicated success in achieving the design objectives. In most cases, the bents are expected to remain uncracked, even under ultimate demands. In bridges with larger column spacing and intermediate to long spans, cracking is expected at ultimate demands, but only immediately below the girder located near mid-span. Similar conclusions would be found for the larger spans in skewed bridges.
3. Relocation of strands from a top/bottom configuration to a side configuration has a minimal impact on the strength of the pretensioned section, with a decrease not more than 5 percent.
4. The addition of interior voids to reduce bent cap weight for shipping and construction has a minimal impact on the flexural response of a pretensioned section when compared to a solid cross-section with the same number of strands. The section with interior voids has a lower initial stiffness, a larger cracking moment, and a nearly identical nominal
5. Design of void sections using the proposed design procedure results in a lower number of strands, a higher minimum design strength, and higher stresses under service and ultimate loads. In sections requiring reduced weight sections, demands are expected to be higher due to larger span lengths and the higher stresses may result in a larger cracked region. For these sections, a design approach based on limiting service and ultimate stresses, rather than zero tension under dead load may be more appropriate.

Beyond flexural design, shear design, detailing of end regions, and connection of precast cap to column connections were considered. Key results include:

1. Investigation of the shear design for pretensioned bent caps is complicated by the nature of the disturbed regions in the bent cap, and the fact that the AASHTO sectional design provisions procedure was developed for narrow webbed concrete girders and has not been demonstrated to be valid for deep and wide sections such as those considered in this study.
2. Application of the AASHTO provisions to the TxDOT standards bents for non-skewed I-girder bridges led to the minimum reinforcement requirements controlling for many designs. Evaluation of design values indicates that, for pretensioned bent caps, the crack angle given by AASHTO is often physically inadmissible, indicating that application of these methods for pretensioned bent caps may be inappropriate.
3. Transverse reinforcement is required at the ends of the bent caps for resistance of bursting stresses. Application of recommendations from recent studies of prestressed girders indicates the need for this reinforcement to extend the full length of the overhang and into the exterior joint. This transverse reinforcement may also serve as shear reinforcement for the shear demands introduced by the girder located in the overhang region.
4. The use of a pocket connection was explored as an alternative to the grouted vertical duct connection currently used by TxDOT. The optimal pocket diameter should take into account geometry of the column and cap, potential for column misalignment, and the impact of the void on the stresses introduced by prestressing. The stresses from prestressing are also important for specifying the thickness of the pipe.
5. A 21-in. diameter pocket connection is recommended for a 42-in. wide pretensioned bent cap. This was shown to provide adequate strength in both shear and flexure for a prototype bridge.



## **4. EXPERIMENTAL TEST PROGRAM: OVERVIEW**

The experimental test program sought to test full-scale subassemblages of a standard TxDOT I-girder bridge bent cap to show the benefits of prestressed bent caps in comparison to RC bent caps. Pretensioned bent caps investigated the influence of shear reinforcement, amount of prestressing, and the use of interior voids to reduce the bent cap weight. The objectives were to validate the proposed design procedure, assess performance at service and ultimate demands, and establish failure modes.

The experimental test program consisted of six full-scale subassemblages, tested in two phases. The phases were distinguished by the specimen geometry and the amount of prestressing. Phase 1 tested one RC bent cap as a reference test and three 16 strand pretensioned bent caps. The pretensioned bent caps included an equivalent strength design to the RC design, a variation in the shear reinforcement spacing, and use of an interior void. Phase 2 consisted of two longer specimens, both with 28 strands and interior voids. The Phase 2 specimens investigated the impact of void detailing.

This chapter presents an overview of the experimental test program. Section 4.1 presents an overview of the experimental test program. Section 4.2 contains the design of specimens including flexure, shear, end region detailing, and the pocket connection. Section 4.3 discusses the test matrix and geometry of both the RC and pretensioned bent cap specimens. Section 4.4 contains the construction of the test specimens. Section 4.5 discusses the experimental setup in the Texas A&M High Bay Structural and Materials Testing Laboratory (SMTL). The instrumentation plan is summarized in Section 4.6. Section 4.7 presents results from the material properties tests conducted for the concrete and steel used in the fabrication of the specimens. Calculated expected strengths are given in Section 4.8.

### **4.1. OVERVIEW**

The experimental test program investigated the performance of full-scale precast bent caps under realistic loading conditions. Bents for standard I-girder bridges in Texas have three or four columns, creating an indeterminate structure with negative moments near columns and positive moments near the center of spans. Although design demands are established from beams on knife-edge supports, the column stiffness influences the demands in an actual bent and the

beam-column connection must provide sufficient strength for transfer of moment from the beam to the column. Figure 4.1 shows the shear and moment diagrams for a three column bridge with four girders. To study the performance of bent caps, the experimental test setup must accurately simulate these demands.

Previous experimental studies of reinforced bent caps (both CIP and precast) have used a subassembly that consists of a single column with the bent cap cantilevered from both sides. In some test programs (Bracci et al. 2001; Young et al. 2001), one overhang was modified to represent the reinforcement characteristics of the span. In others (Matsumoto et al. 2001), a horizontal actuator was used to simulate wind loads and introduce additional moment into the connection. A major shortcoming in all of these is that the demands were limited to negative moment demands and the shear-moment demand ratios do not accurately reflect those in bents. Other tests (Matsumoto et al. 2001) have tested large-scale or full-scale bents to assess the performance of connections, but did not test the bent cap to failure.

The test setup in this study is intended to address the shortcomings of previous research while testing full-scale components to capacity. To accomplish this, the test specimens were designed as a subassembly of a full bent consisting of the bent from the overhang to the second inflection point in the first span and the column from the bent to the inflection point. This region, indicated by a blue dashed oval in Figure 4.1, allows for experimental evaluation of the performance under both positive negative moment demands and the transfer of forces from the bent cap to the column. Figure 4.2 shows a schematic of the subassembly and the shear and moment demands produced by the loads.

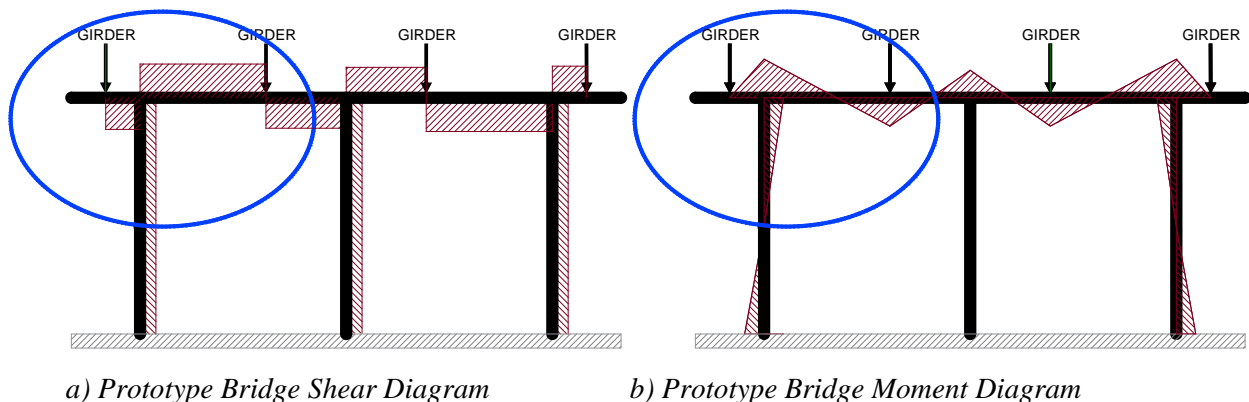


**Figure 4.1. Prototype Bridge Shear and Moment Diagrams.**

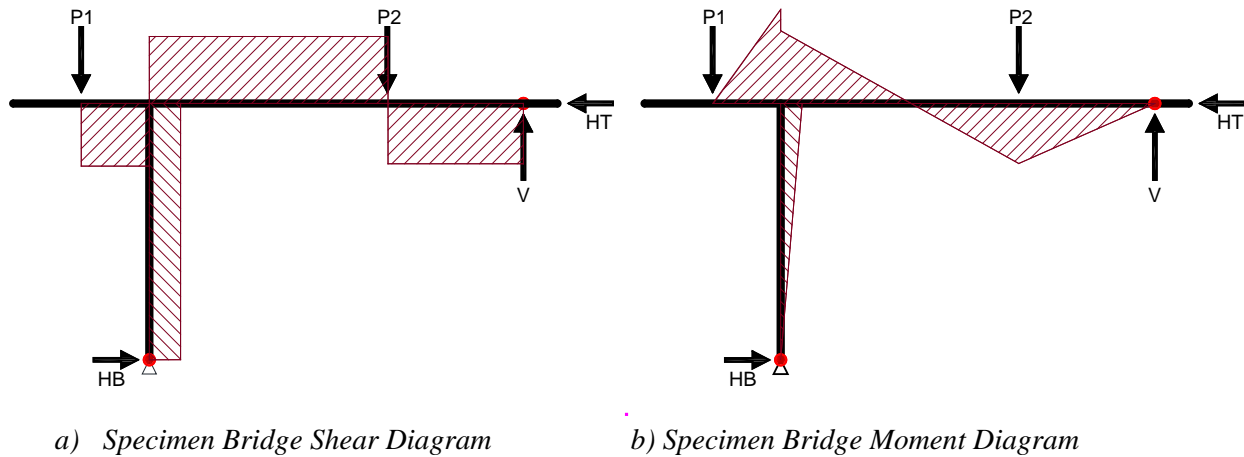


**Figure 4.2. Specimen Shear and Moment Diagrams.**

Loads are introduced to the bent cap via two actuators (P1 and P2) simulating girder demands. A pin at the base of the column provides the necessary shear and axial reactions at the base of the column. At the right side of the specimen (referred to as the “square end”), a vertical actuator (V) and horizontal actuator (HT) are controlled with specified forces and/or displacements to achieve the desired outcome (realistic bent demands or maximize positive or negative moment to fail specimen). To realistically simulate the behavior of a bridge bent, the HT actuator should be locked to produce zero displacement and the V actuator should be specified to generate the shear at the inflection point. Vertical displacement is present but is very small at this inflection point. Thus, an alternative approach for the square end is to set both the HT and V actuators to have zero displacement. This will alter the demands only slightly and will produce realistic demands while simplifying controls and enhancing safety. Although this creates an indeterminate structure, the forces recorded by the actuators ensure that all demands in the structure are accurately known.

The subassembly size and component strengths were controlled by limitations of the Texas A&M High Bay SMTL: 1) overhead crane capacity of 20 tons, 2) 3-ft grid for anchoring reaction towers and connection plates, 3) clearance below header beams supporting P1 and P2 actuators, 3) 600-kip capacity for the vertical actuators (P1, P2, and V), and 4) 110-kip capacity of the horizontal actuators (HT and HB). The desired prototype bridge was a standard, non-skewed I-girder bridge with girders up to Tx54. Such a bridge has 3-ft diameter columns, a 42-in. square bent cap, and an overhang with a battered end extending 4-ft from the center of the exterior column, and the first girder located 2-ft from the column centerline.



Given these constraints, the subassembly geometry shown in Figure 4.3(a) was selected for Phase 1. The bent cap was 16-ft long, with girder loads (P1 and P2) acting 2-ft and 7-ft from the column centerline. The inflection point shear (V) was located 4-ft from the interior girder (P2). An additional 1-ft was included in the length of the bent cap to allow for the development of prestressing. In Phase 2, the use of interior voids permitted longer bent caps, shown in Figure 4.3(b). The exterior girder load (P1) and the inflection point shear (V) were moved 3-ft farther from the column centerline. The distance from the end of the bent cap and the inflection point shear (V) remained the same for both phases. For both phases, a subassembly column height of 8-ft from the base to the center of the bent cap was selected by balancing the needs of demands and clearance and can be considered a reasonable inflection point in standard bridge bent heights.

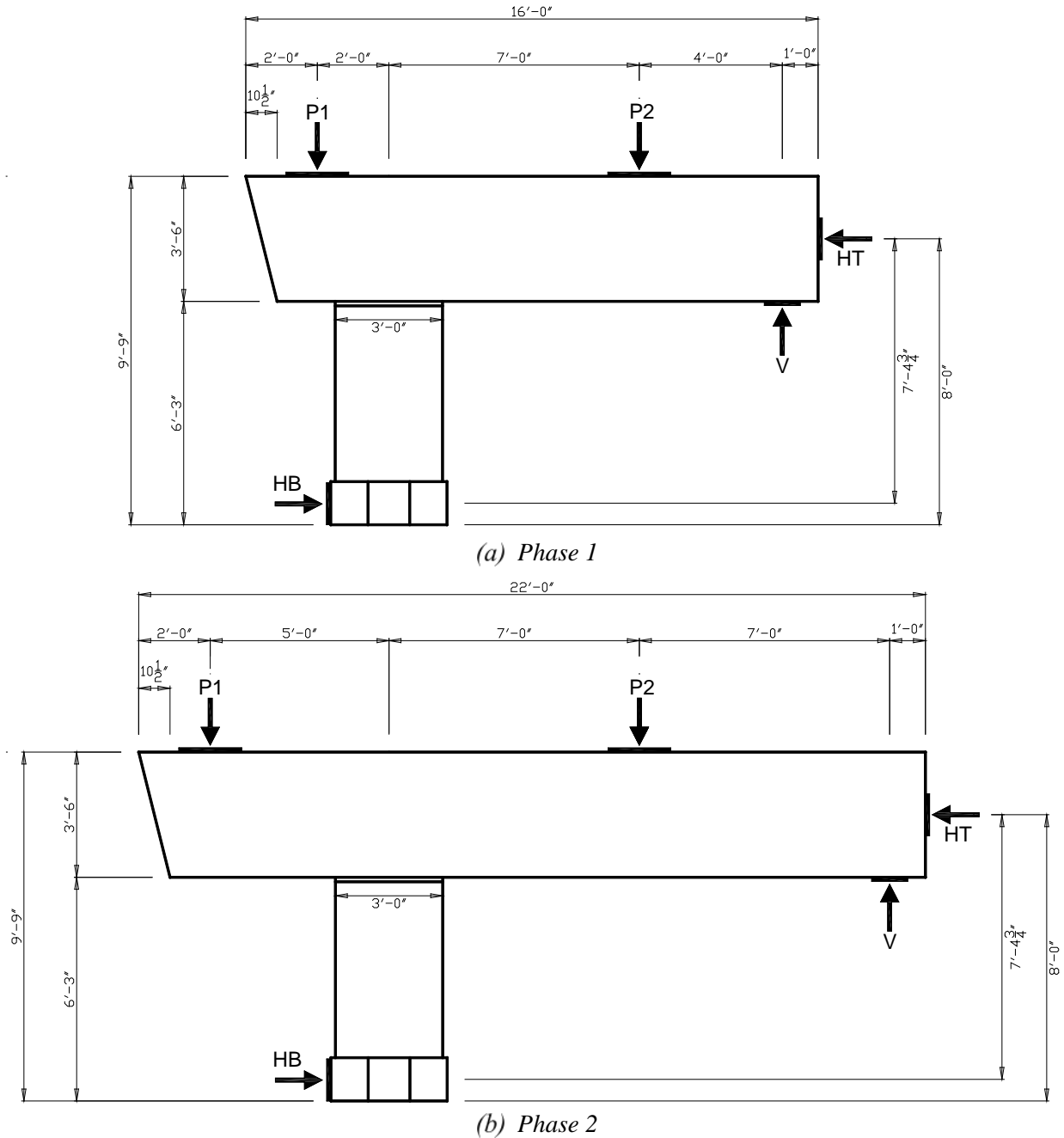


**Figure 4.3. Elevation View of Test Specimens.**

For Phase 1, subassembly geometry does not correlate perfectly with a standard I-girder bridge bent that could be used as a prototype, but does closely resemble BIG-32 (32-ft wide) and BIG-40 (40-ft wide) bents. Thus, these two bridges are used as prototypes for designing the specimens and establishing, dead, service, and ultimate load demands. For Phase 2, the geometry is similar to a modified BIG-32 with a column removed to optimize the design. Table 4.1 summarizes the

characteristics of these prototype bents. The following section discusses design of the test specimens.

**Table 4.1. Prototype Bridges Phases 1 and 2.**

<b>Bent Cap Property</b>	<b>Phase 1</b>		<b>Phase 2</b>
	<b>BIG-32</b>	<b>BIG-40</b>	<b>Modified BIG-32</b>
Length (ft)	32	40	32
Height (in.)	42	42	42
Width (in.)	42	42	42
Girder Types	Tx28 - Tx54	Tx28 - Tx54	Tx28 - Tx54
Number of Girders	4	5	5
Girder Spacing (ft)	9.33	9	7
Column Diameter (ft)	3	3	3
Number of Columns	3	3	2
Column Spacing (ft)	12	16	18
Overhang (ft)	4	4	7

## **4.2. DESIGN**

Design of the Phase 1 and Phase 2 test specimens did not follow a traditional design procedure that would be used for design of bridge bents. Instead, it was necessary to ensure that the expected capacity of the specimen could be reached. To this end, selection of the flexural reinforcement was the first step in design and is described in Section 4.2.1. From the selected flexural reinforcement, the demands for a prototype bridge were identified such that the proposed design objective (zero tension stresses under dead load) could be evaluated. Section 4.2.2 summarizes the prototype bridge that was identified to result in the flexural design used. Section 4.2.3 presents shear design for the bent cap. Detailing of the end regions and connections are presented in Section 4.2.4.

### **4.2.1. Flexural Design**

#### *4.2.1.1. Phase 1*

The flexural design of the specimens was governed by the maximum demands of the test setup (1,500 k-ft). An additional consideration was ensuring the nominal strength exceeded cracking strength. A 42-in. square section with 6 ksi concrete and 16 strands has a moment capacity of 1,379 kip-ft. To avoid interference between flexural reinforcement and the pocket connection, a

side configuration of strands was used. Side reinforcement is uniformly distributed to control cracks effectively.

To allow comparison of the overall performance of pretensioned bent caps to RC bent caps, a RC prototype was designed to have the same steel configuration and similar strength to the pretensioned prototype, leading to the use of 16-#8 bars. Figure 4.4 shows the RC cross-section. The layout of the bars was identical to the strand layout for the pretensioned section; this deviates slightly from the cover used in standard TxDOT designs.

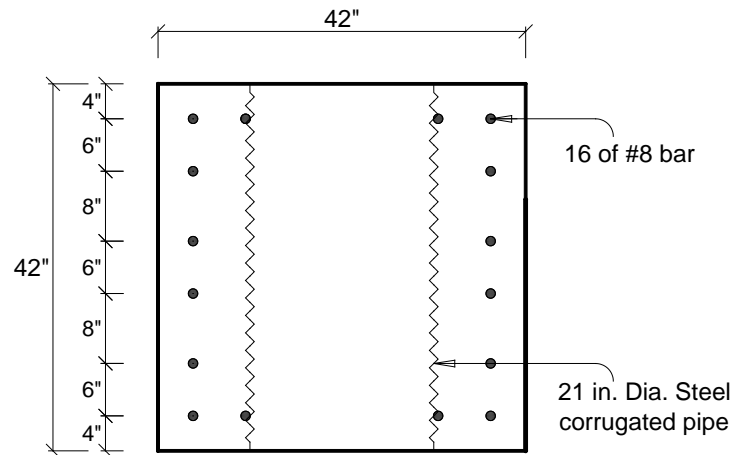


**Figure 4.4. RC Bent Cap Cross-Section.**

#### 4.2.1.2. Phase 2

The modified geometry of Phase 2 specimens allowed for increased demand that in turn permitted an increase in flexural capacity. Flexural design of Phase 2 specimens had the following design objectives:

1. Use the maximum number of strands possible to investigate the effect of larger prestressing force, while ensuring the test setup had capacity to fail the specimen.
2. Have greater strength in negative bending than in positive bending while minimizing eccentricity. This was motivated by initial cracking in this region in Phase 1 tests and greater negative moment capacity in the Phase 2 setup (3,000 k-ft in negative moment region and 2,015 k-ft in positive moment region).
3. Distribute side strands evenly so that they can act as not only flexural reinforcement but also skin reinforcement.

The selected design was 28 strands with a 2.57-in. eccentricity. Figure 4.5 compares the strand layout from Phase 1 and Phase 2. The cracking moment strength is calculated using modulus of rupture for normal-weight concrete given in AASHTO 5.4.2.6, and the flexural capacity is computed by fiber Section analysis using OpenSees considering concrete compressive strength ranging from 6 ksi to 8 ksi. The analyzed moment capacities are summarized in Table 4.2 along with maximum achievable positive and negative moment demands with the test setups in Phases 1 and 2.

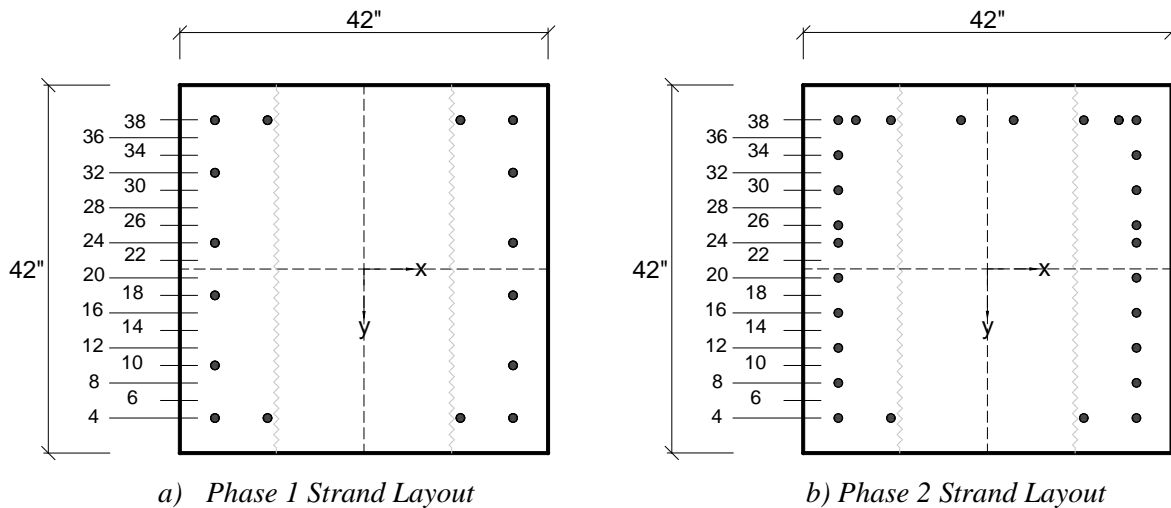


**Figure 4.5. Strand Layout.**

**Table 4.2. Summary of Flexural Strength and Lab Capacity.**

	<b>Region</b>	$M_{cr}$ (k-ft)	$M_n$ (k-ft)	$M_{test\_max}$ (k-ft)
<b>Phase 1</b>	Positive	926–1,019	1,380–1,437	1,745
	Negative			1,800
<b>Phase 2</b>	Positive	1,081–1,160	1,893–1,992	2,400
	Negative	1,397–1,489	2,511–2,629	3,600

*Note: Compressive strengths ranging 6–8 ksi were used for the calculation;  $M_{test\_max}$  is the maximum achievable moment*

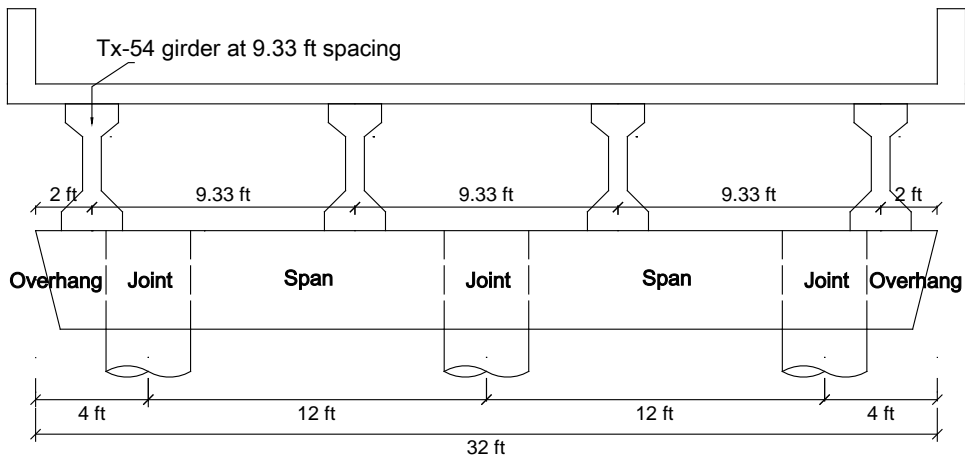
## 4.2.2. Prototype Selection

### 4.2.2.1. Phase 1

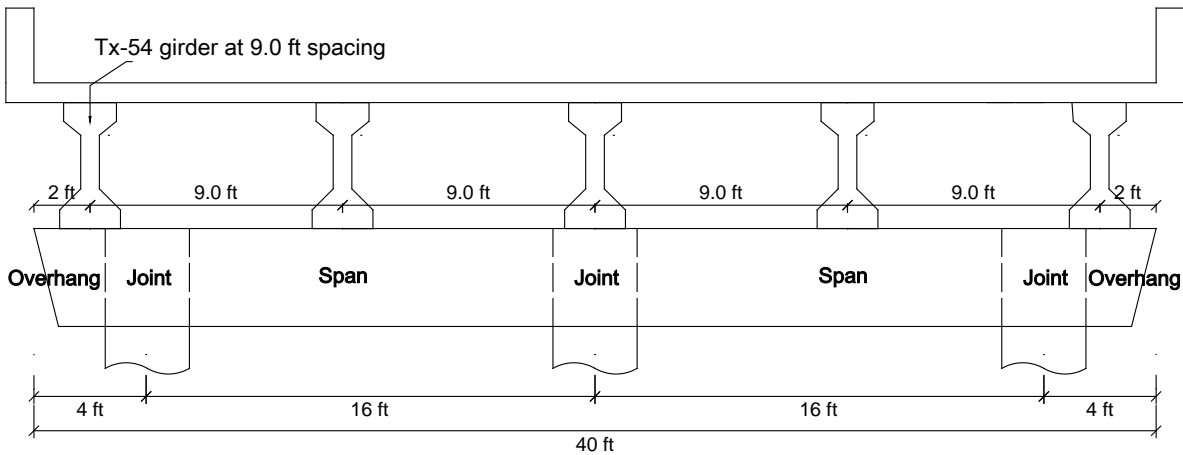
Having established a flexural design, it was necessary to identify prototype bridge(s) that would result in the selected design. For the prestressing force from 16 strands, the zero tension moment

is 328 k-ft. This established the selection criterion for the prototype bridge; the pretensioned bent cap should have a maximum flexural demand under dead load of 328 k-ft.

From a preliminary study of the bent configuration in the TxDOT bridge inventory with I-girders, the 32-ft and 40-ft roadway width bridges were observed to be a close representation of the specimen that could be built in the laboratory. An iterative analysis of the bridge with different span lengths was done in CAP18 (CAP18 Version 6.2.2) to find the span length producing these demands. The maximum dead load moment for a 66-ft span is very close to the required moment for both prototypes. Figure 4.6 shows the configuration. Maximum ultimate demands of both 32-ft and 40-ft roadway width bridges are  $-767.7$  k-ft and  $1,003$  k-ft, respectively, and do not exceed the moment capacity of the specimens.



(a) BIG-32 interior bent in TxDOT standard

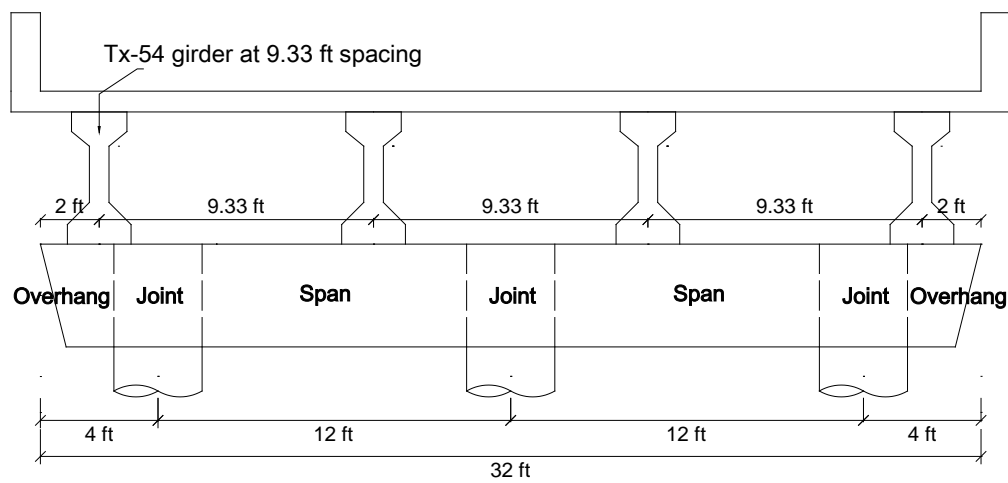


(b) BIG-40 interior bent in TxDOT standard

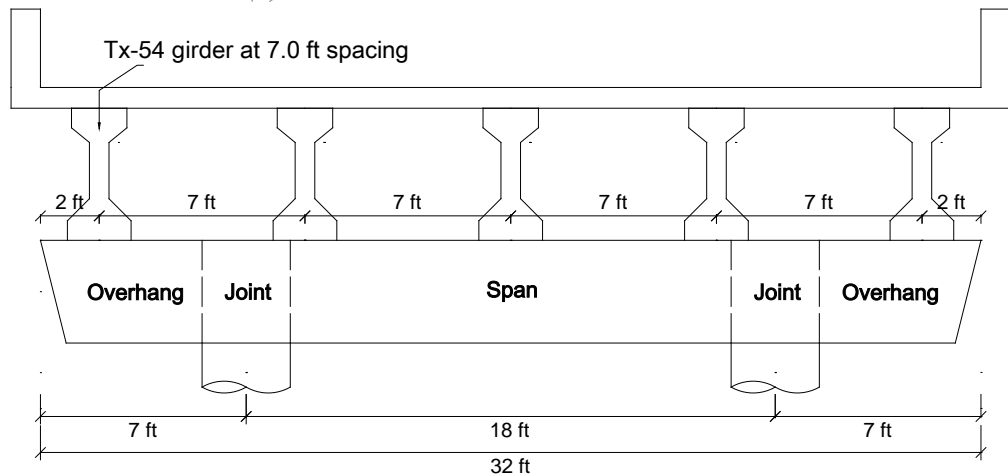
**Figure 4.6. Phase 1 Prototype Bridge Configuration.**

4.2.2.2. Phase 2

Since the specimen geometry changed in Phase 2, identifying a new prototype bridge that can represent the specimen was necessary. To do that, a feasible bridge geometry that has an equivalent moment and shear demand to the specimen in Phase 2 was found. After considering several alternatives, the new prototype bent cap was modified from a 32-ft bent (BIG-32 in TxDOT inventory). In the modified BIG-32 bent cap, the number of columns supporting the bent cap was reduced from three to two while the overhang length increased from 4-ft to 7-ft, and four Tx-54 girders at 9.33-ft spacing was replaced by five Tx-54 girders at 7-ft spacing. Figure 4.7 compares the standard and optimized geometry. Moment and shear demands for the prototype and the specimen under equivalent loading on all girders are compared in Figure 4.8. On the specimen, the girder nearest the column was considered to act over the column and not included in loading.

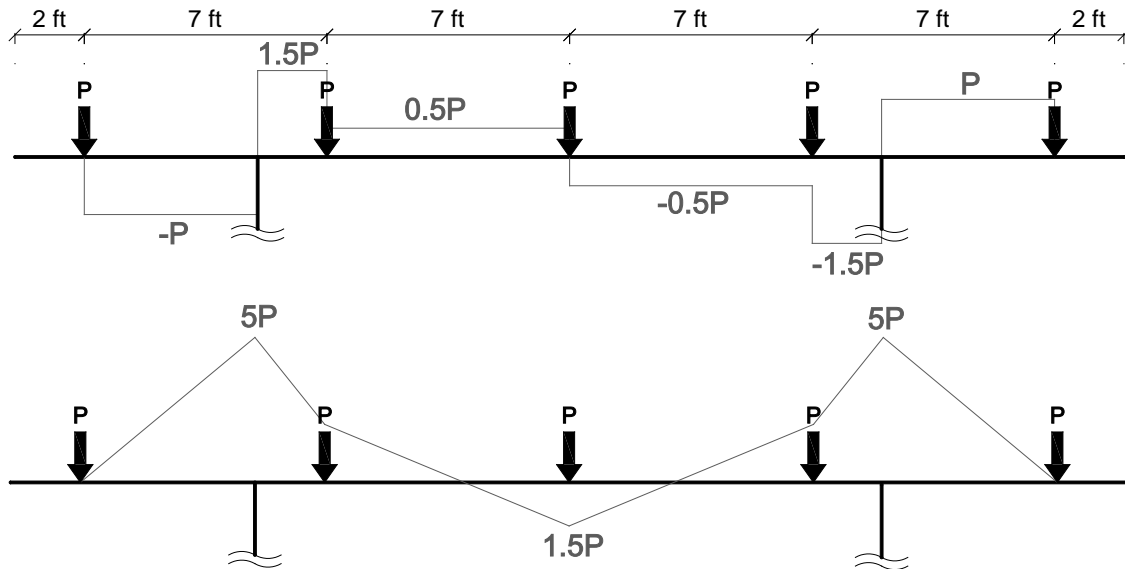


(a) BIG-32 interior bent in TxDOT standard

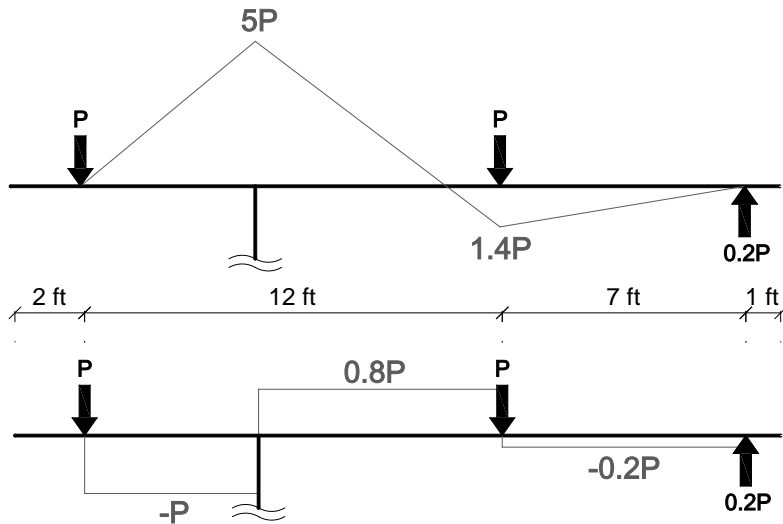


(b) Modified BIG-32 bent

**Figure 4.7. Phase 2 Prototype Bent Cap Schematic.**



(a) Prototype Shear force and Bending Moment Diagram



(b) Specimen Shear Force and Bending Moment Diagram

**Figure 4.8. Phase 2 Prototype and Specimen Demands.**

Since the prototype and specimen had almost equivalent moment demands in the overhang (negative moment region) and the span (positive moment region), the prototype would be a close representation of the specimen; however, shear demands were not exactly the same. This shear demand difference between the prototype and specimen is explained in Section 4.2.3.2.

The design philosophy of zero tension stress under dead load was also applied in Phase 2. Unlike the bent cap section in Phase 1, which had a concentric strand layout, the section in Phase 2 had an eccentric strand layout. Positive and negative moment regions both needed to be taken into



consideration to find dead load moment generating zero stress. The strand layout selected had zero tensile stress of 584 k-ft and  $-785$  k-ft for positive and negative regions, respectively. Although a required dead load moment was smaller in the positive moment region, negative moment region governed the design because the specimen test setup and prototype generate a greater negative moment than positive moment. Therefore, the selection criterion for the prototype bridge was established based on the dead load moment for zero tension in negative moment region.

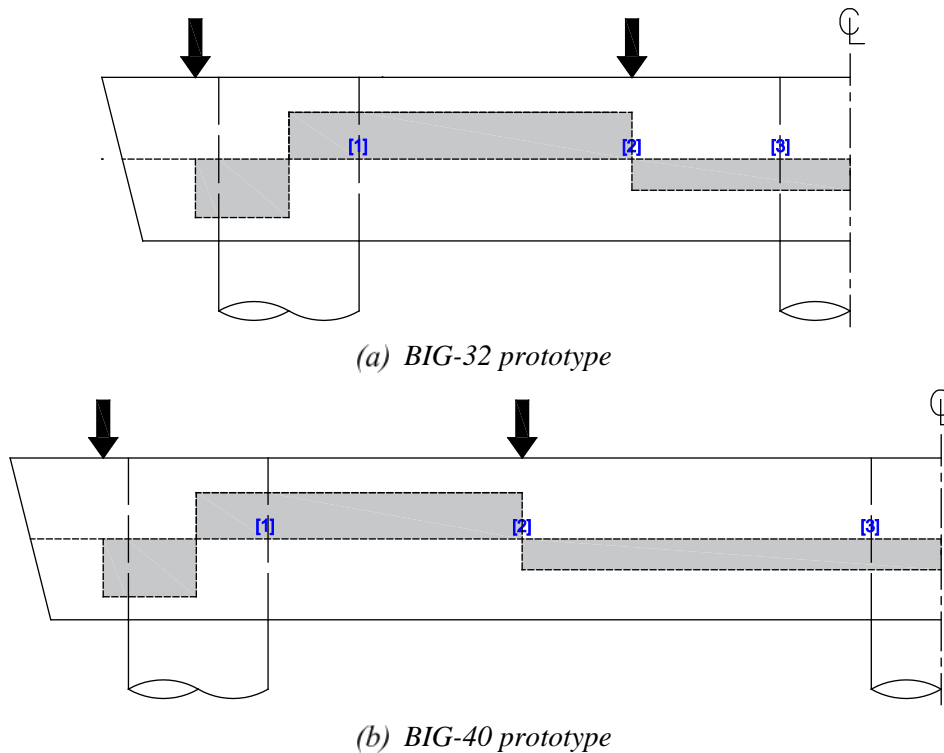
CAP18 was used to find the prototype span length, which generates a required moment ( $-785$  k-ft) under dead load. Several cases with different span lengths were analyzed iteratively, and the dead load moment for an 80-ft span girder was found to generate demands nearly equivalent to the targeted dead load moment. Thus, an 80-ft span was adapted as the prototype in Phase 2. Ultimate moment demand under factored load was 1,900 k-ft in this prototype, and it was less than the capacity of the setup (3,600 k-ft).

### **4.2.3. Shear Design**

#### *4.2.3.1. Phase 1*

Shear design of the specimens was in accordance with AASHTO LRFD Bridge Design Specification (AASHTO 2014), the general procedure of sectional design, in Appendix B5. According to AASHTO LRFD, the sectional design method is appropriate for the design of components where the assumptions of beam theory are valid. For this reason, shear design is conducted only in the spans between columns. Transverse reinforcement in the overhang is discussed in Section 4.2.4.

AASHTO LRFD shear design requires both moment and shear demands ( $M_u$  and  $V_u$ ) to evaluate shear strength of the section. Demands from both prototype bridges were considered. Three points where shear and moment demands are significantly higher than other locations were selected as critical locations including interior face of the exterior column, interior girder location, and the interior column face in both prototypes, as shown in Figure 4.9. Concrete compressive strengths of 3.6 ksi and 6 ksi were used for RC and PSC bent caps, respectively. Two legs of #5 reinforcing steel bar were used as a transverse reinforcement.



*Note: Magnitude of shear demand is symmetric about the centerline; Critical section locations are numbered;*

**Figure 4.9. Shear Force Diagram and Three Shear Critical Section Locations in BIG-32 and BIG-40 Prototypes in Phase 1.**

TxDOT uses a spreadsheet for designing shear based on the general procedure for shear design with tables in AASHTO LRFD provisions. The spreadsheet was used to design shear for both RC and PSC bent caps. Table 4.3 summarizes the results. The table provides moment and shear demands ( $M_u$  and  $V_u$ ), longitudinal tensile strain at mid-depth of the member ( $\epsilon$ ), angle of inclination of diagonal compressive stresses ( $\theta$ ), factor indicating ability of diagonally cracked concrete to transmit tension and shear ( $\beta$ ), shear strengths provided by concrete and steel ( $V_c$  and  $V_s$ ), factored shear strength ( $\phi V_n$ ), and required spacing ( $s_{req'd}$ ) at each critical section.

**Table 4.3. Summary of Demands and Shear Design Results for RC and PSC Bent Caps Phase 1.**

		RC			PSC			
		Critical 1 <sup>[1]</sup>	Critical 2 <sup>[2]</sup>	Critical 3 <sup>[3]</sup>	Critical 1 <sup>[1]</sup>	Critical 2 <sup>[2]</sup>	Critical 3 <sup>[3]</sup>	
32-ft prototype	Demands	$M_u$ (k-ft)	587	467	542	587	467	542
		$V_u$ (kips)	123	253	261	123	253	261
	AASHTO Shear Design	$\epsilon$	$8.4 \times 10^{-4}$	$1.0 \times 10^{-3}$	$1.0 \times 10^{-3}$	$2.7 \times 10^{-4}$	$9.9 \times 10^{-4}$	$1.0 \times 10^{-3}$
		$\theta$ (deg)	34.7	36.4	36.4	26.8	36.3	36.4
		$\beta$	2.33	2.23	2.23	2.9	2.24	2.23
		$V_c$ (kips)	189	181	181	287	220	219
		$V_s$ (kips)	144	135	135	185	128	127
		$\phi V_n$ (kips)	300	284	284	425	313	312
$s_{req'd}$ (in.)	14.8	14.8	14.8	24.0	11.4	11.4		
40-ft prototype	Demands	$M_u$ (k-ft)	461	902	673	461	902	673
		$V_u$ (kips)	225	215	195	225	215	195
	AASHTO Shear Design	$\epsilon$	$1.0 \times 10^{-3}$	$1.0 \times 10^{-3}$	$1.0 \times 10^{-3}$	$9.1 \times 10^{-4}$	$1.0 \times 10^{-3}$	$8.2 \times 10^{-4}$
		$\theta$ (deg)	36.4	36.4	36.4	35.5	36.4	34.5
		$\beta$	2.23	2.23	2.23	2.28	2.23	2.34
		$V_c$ (kips)	181	181	181	224	219	230
		$V_s$ (kips)	135	135	135	131	127	137
		$\phi V_n$ (kips)	284	284	284	320	312	330
$s_{req'd}$ (in.)	14.8	14.8	14.8	11.4	11.4	11.4		

<sup>[1]</sup> interior face of exterior column; <sup>[2]</sup> interior girder location; <sup>[3]</sup> interior column face

As shown in Table 4.3, 14.8-in. and 11.4-in. transverse reinforcement spacing were required for RC and PSC bent caps regardless of critical section considered for both prototype bridges. These required spacing values highlight a shortcoming of the AASHTO design procedures, which is that it does not reflect the fact that prestressing improves shear resistance (Collins et al. 1996; Runzell et al. 2007). The design spacing for the prototype bridges are governed by the requirements for minimum area of steel. AASHTO requirements for minimum area of steel are dependent on the concrete compressive strength. The design concrete strength is higher in pretensioned bent caps (6 ksi) than in RC bent caps (3.6 ksi), leading to the smaller spacing for the same area of steel.

For this reason, additional shear spacing is calculated considering shear strength requirement without satisfying requirement of maximum spacing limit and minimum area of steel, and compared with design values in Table 4.4. In the table, the first column ( $V_u > \phi V_c$ ) indicates if the

demand exceeds the capacity provided by the concrete, that is, is shear reinforcement needed to provide strength. The second value,  $s_{design}$ , is the spacing by design following the AASHTO provisions. The third value,  $s_{strength}$ , is the spacing that would be required to provide the necessary strength, ignoring any requirements on minimum area of steel or maximum spacing limits.

**Table 4.4. Key Values for Shear Spacing Selection.**

Prototype	RC Bent Cap			PSC Bent Cap		
	$V_u > \phi V_c$	$s_{design}$ (in.)	$s_{strength}$ (in.)	$V_u > \phi V_c$	$s_{design}$ (in.)	$s_{strength}$ (in.)
<b>BIG-32</b>	Yes	14.8	14.8	No	11.4	None
<b>BIG-40</b>	Yes	14.8	24.0	Yes	11.4	24.0

$s_{design}$  = spacing satisfying all minimum spacing requirement in AASHTO LRFD specification including minimum area of steel (AASHTO 5.8.2.5) and maximum spacing of transverse reinforcement (AASHTO 5.8.2.7).

$s_{strength}$  = required spacing to resist demands without considering minimum area of steel and maximum spacing of transverse reinforcement.

TxDOT uses a maximum spacing of 12-in., which would lead to a revision of the RC design. For simplicity, the transverse reinforcement was not varied along the spans rather the smallest required was used so that both RC and pretensioned prototype designs are considered to have a 12-in. spacing.

As an alternative to the design spacing, the spacing needed to only provide adequate strength for the section was considered. As shown in Table 4.4, when the minimum area requirements are ignored, the spacing of the transverse reinforcement for the pretensioned bent cap increases dramatically, requiring 24-in. for one prototype, while the other, theoretically, has sufficient strength from the concrete alone and does not require shear reinforcement. While a design with no transverse reinforcement or 24-in. spacing would not meet design requirements in a TxDOT bridge, they were considered in establishing the experimental test matrix (see Section 4.3).

A section with an interior void was considered as another alternative design. As mentioned earlier, the use of the interior void can bring many advantages by the reduction of the bent cap weight (Taylor et al. 1995; Ueda and Stitmannathum 1991). A 26-in. size void was regarded to be appropriate to ensure the cover thickness in both interior and exterior sides. Shear design results for a section with 26-in. void from the spreadsheet are summarized for both prototypes in Table 4.5. The table shows the result at critical section 2 only because section 1 and 3 are solid

section and have the same result in Table 4.4. Although required spacing was 9.0-in. and 11.3-in. for BIG-32 and BIG-40 prototypes, respectively, 12-in. spacing was used for voided to be consistent with other specimens.

**Table 4.5. Summary of Demands and Shear Design Results for a Section with 26-in. Square Void.**

		<b>BIG-32</b>	<b>BIG-40</b>
		Critical 2 <sup>[2]</sup>	Critical 2 <sup>[2]</sup>
Demands	$M_u$ (k-ft)	467	902
	$V_u$ (kips)	253	215
AASHTO Shear Design	$\epsilon$	$9.3 \times 10^{-3}$	$1.0 \times 10^{-3}$
	$\theta$ (deg)	36.3	36.4
	$\beta$	2.23	2.23
	$V_c$ (kips)	104	104
	$V_s$ (kips)	128	127
	$\phi V_n$ (kips)	209	208
	$s_{req'd}$ (in.)	9.0	11.3

#### 4.2.3.2. Phase 2

Although the Phase 2 prototype bridge and test setup generated almost equivalent moment demands in both the overhang and the span, shear demands were different. High shear demand was expected between the column and interior girder in the prototype compared to the specimen, resulting in a very tight shear reinforcement spacing in that region. Thus, shear design was based on the shear demand of the specimen rather than the prototype. The expected shear demand in the specimen was calculated using the girder demands at the ultimate limit state (ULS). Three critical sections in Phase 2 include 1) interior column face, 2) adjacent to column where the interior void starts, and 3) interior girder location as shown in Figure 4.10. Table 4.6 summarizes demands and shear design results at each critical section using the TxDOT spreadsheet.

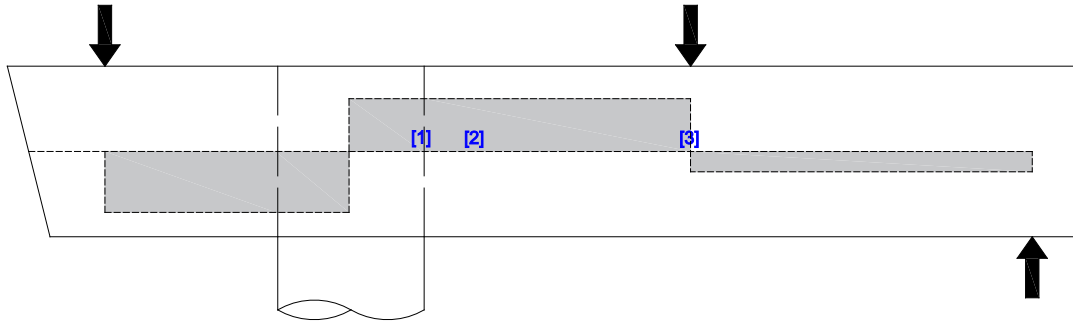


**Figure 4.10. Shear Force Diagram and Three Shear Critical Section Locations in Phase 2 Specimen.**

**Table 4.6. Summary of Demands and Shear Design Results for Phase 2 Specimen.**

		Critical 1 <sup>[1]</sup>	Critical 2 <sup>[2]</sup>	Critical 3 <sup>[3]</sup>
<b>Demands</b>	$M_u$ (k-ft)	1298	998	553
	$V_u$ (kips)	301	301	79
<b>AASHTO Shear Design</b>	$\epsilon$	$5.5 \times 10^{-4}$	$2.0 \times 10^{-4}$	$-1.1 \times 10^{-4}$
	$\theta$ (deg)	31.1	26.7	20.5
	$\beta$	2.56	2.73	4.83
	$V_c$ (kips)	251	102	181
	$V_s$ (kips)	155	186	251
	$\phi V_n$ (kips)	365	260	388
	$s_{req'd}$ (in.)	11.4	9.6	24.0

<sup>[1]</sup> interior face of exterior column; <sup>[2]</sup> adjacent to column where the interior void starts; <sup>[3]</sup> interior girder location

Required shear spacing for the sections considered were 11.4-in., 9.6-in., and 24.0-in. Phase 1 tests revealed that the amount of shear reinforcement did not affect the overall performance of the bent cap, so researchers concluded that less shear reinforcement than the design results would not cause significant shear capacity deterioration. Therefore, the same type of shear reinforcement (two legs of #5 mild reinforcing steel) and the same spacing (12-in.) were used for consistency with Phase 1.

#### 4.2.4. End Region

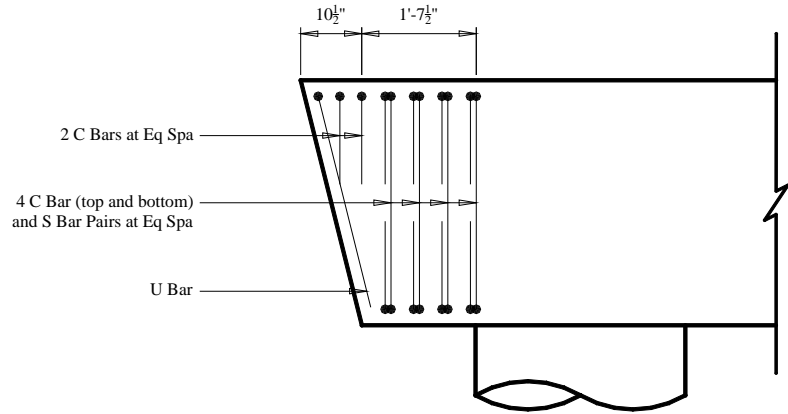
The end region detailing for the prestressed bent caps in both Phase 1 and Phase 2 took into consideration the spalling reinforcement from the AASHTO LRFD 5.10.10.1 and the recommendations by O'Callaghan and Bayrak (2008) to include bursting reinforcement immediately after spalling reinforcement from  $D/4$  to the transfer length. Individual C-bars

(#5 bars) were used at  $D/4$  for the spalling reinforcement. C-Bars and S-Bars pairs were used for the bursting reinforcement up to the transfer length.

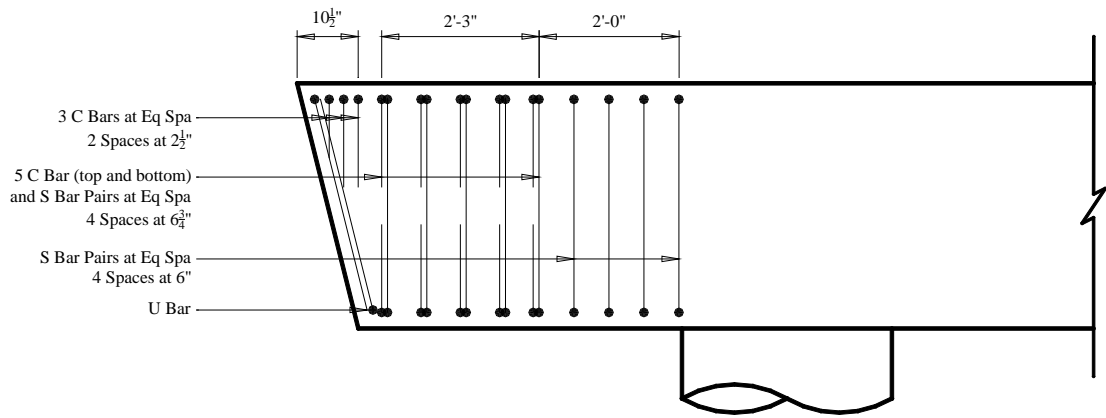
Figure 4.11 summarizes the end region detailing of the prestressed bent caps. For Phase 1, this consisted of one U-bar placed parallel to battered end face, two C-Bars for the spalling and shear reinforcement up to  $D/4$  with four pairs of S-Bars and C-Bars for bursting forces and shear reinforcement up to the transfer length of the prestressing steel (Figure 4.11[a]). The square end of the bent caps only exists for the experimental testing of the bent cap specimens. The end region detailing of the square ends was the same as the battered ends, except modified to account for the non-sloped face.

Two designs of end region detailing were considered for Phase 2. The first, shown in Figure 4.11(b), followed the same procedure as Phase 1. Due to the increased prestressing forces, an additional C-Bar was required for spalling and shear reinforcement up to  $D/4$  and an additional S-Bar and C-Bar pair was required for bursting forces up to the transfer length. The second, as shown in Figure 4.11(c), used detailing from standard drawings released by TxDOT during the completion of Phase 1 of the project, with modification for the longer overhang length used during Phase 2. The detailing for the area within the transfer length remained consistent with the reinforcement spacing shown in the TxDOT standards. Since the region from the transfer length to the face of the column is not incorporated in current TxDOT standards, S-Bar pairs were included in this region to satisfy shear design requirements.

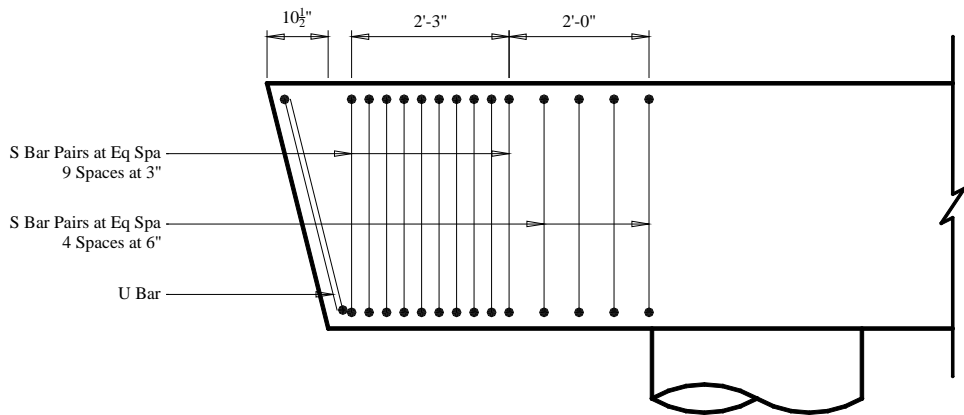
For the RC bent cap, similar layouts for the end region detailing were designed to have a viable comparison between the RC and PSC models and did not follow current TxDOT standards. The end region detailing for the RC specimen used S-Bars consisting of single pieces of rebar forming the closed hoop and did not incorporate any C-Bars (Figure 4.12).



(a) Phase 1 Design



(b) Phase 2 Design



(c) Phase 2 (TxDOT Standard)

**Figure 4.11. Pretensioned Specimens Battered End Detailing.**



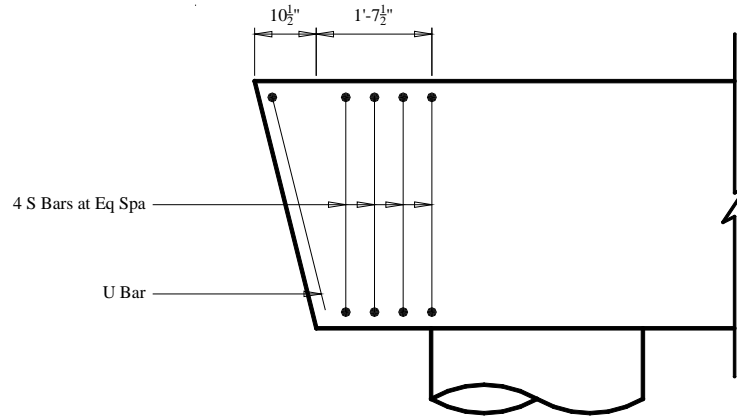


**Figure 4.12. RC Specimen End Region Detailing.**

#### **4.2.5. Column and Connection**

The design of the column longitudinal and spiral reinforcement was the same as current TxDOT design standards for PSC girder bridges. The column diameter was 3-ft with 10-#9 longitudinal reinforcing bars and #4 deformed spiral reinforcement.

To connect the precast bent caps to the columns, a pocket connection was designed to provide a connection that emulates monolithic connections. The connection replaces the 4-in. vertical ducts in current TxDOT standards with a single large pocket that encloses the dowel bars extending from the column. As in current the TxDOT detail, 6-#11 bars were used. The spacing of the bars was modified to improve the ease of construction. The size of the pocket was chosen to allow for a 3-in. misalignment, while minimizing disturbance of the cross-section, therefore minimizing the stress concentrations from prestensioning. Figure 4.13 shows the layout of the pocket and dowel bars. A single 21-in. nominal diameter corrugated pipe serves as a stay-in-place form. A 12 gage pipe was selected as it provided the largest thickness that would not require special orders from pipe manufactures. The steel pipe also provides resistance to compensate for the circumferential forces from the prestressing and acts as confining and shear reinforcement on the joint.

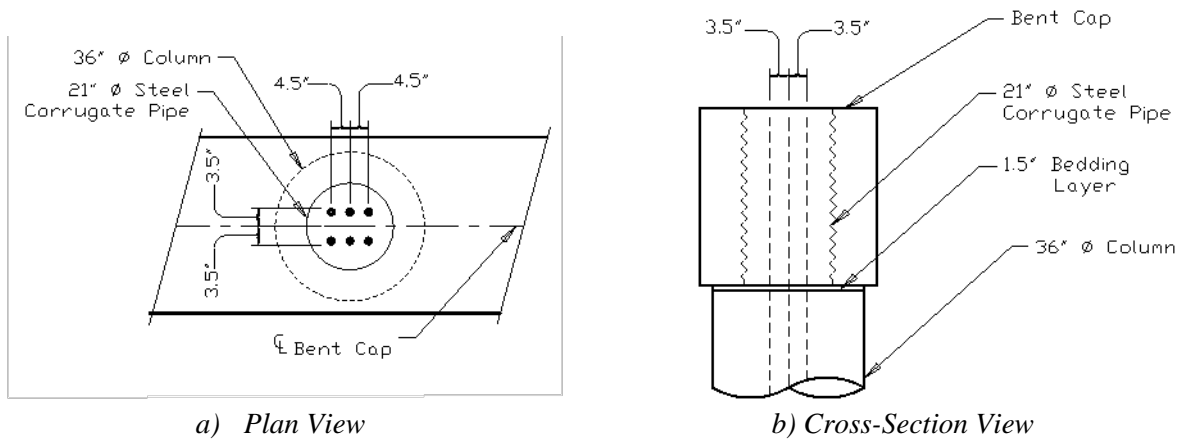


**Figure 4.13. Steel Corrugated Pipe Connection.**

### 4.3. TEST MATRIX

The design options of the bent cap specimens presented in Section 4.2 were used to establish the experimental test matrix. Phase 1 consisted of four specimens, and Phase 2 consisted of two specimens. The objective of the test matrix was to investigate a pretensioned design, an equivalent RC design, and four variations on the pretensioned design. The variations considered are less shear reinforcement, the use of an interior void to reduce weight, number of strands, and details of interior voids. Table 4.7 shows the names and characteristics of each test specimen. The naming of the specimens has the first set of characters showing the type of specimen (RCS = Reinforced Concrete Solid, PSS = Pretensioned Solid, PSV = Pretensioned Void). The second set of characters shows the number of reinforcement bars or strands. The third set of characters indicates the spacing of the span shear reinforcement in inches. The two specimens in Phase 2 have the same number of strands and shear spacing but different details, with names distinguished by A and B without using the third set of characters.

Phase 1 specimens investigated the performance of RC versus pretensioned concrete bent caps, the impact of different transverse reinforcement spacing, and the effects of incorporating an interior void. Phase 2 specimens examined the effects of a larger prestressing force on the performance of the bent caps, impact of varied interior void geometry, effects of differed pocket connection details, and the performance of longer overhangs, both solid and voided.

To study the effect of increased prestressing force, longer specimens were designed during Phase 2. The exterior girder load (P1) and the inflection point shear (V) were moved 3-ft farther

from the centerline of the column. The maximum allowable force limitations remained the same from Phase 1 to Phase 2, but the longer specimen length allowed for greater moment demands to be applied to the positive and negative moment regions of the specimens. Figure 4.14 shows the differences. Phase 1 specimens are represented by PSV-16-12 (Figure 4.14[a]).

PSV-16-12 contained a 7-ft long, 26-in. by 26-in. square interior void placed 2-in. from the interior face of the column. During Phase 2, the nominal size of the interior void remained the same with the cross-section and lengths varying between specimens. PSV-28A contained a 10-ft long, 26-in. by 26-in. square interior void placed 2-in. from the interior face of the column. PSV-28B contained an 8-ft 5-in. long, 26-in. by 26-in. interior void with 5-in. chamfers on all edges in the span region. The interior void was placed  $D/2$  (21-in.) from the interior face of the column. In the overhang, a 3-ft long, 26-in. by 26-in. square interior void was placed 2-in. from the exterior face of the column. Figure 4.15 shows the interior void cross-sections.

In addition to the varied designs summarized in Table 4.7, each specimen had different end region and connection detailing. Table 4.8 summarizes these differences. End region detailing followed design in Figure 4.11 as a baseline. Revisions were made to Phase 1 in collaboration with the precaster based on cracking observed in similar bent caps. Six additional C-Bars were placed vertically and horizontally at both the battered and square ends of PSV-16-12 and the square end of PSS-16-12 to prevent cracking from the releasing of the strands. To validate the effectiveness of additional C-Bars at end region of bent caps, no additional bars were provided in PSS-16-24.

Detailing modifications were also made for the pocket connection. In PSS-16-12 and PSV-16-12, two additional transverse reinforcement bars were provided 2-in. from each of the corrugate pipe faces. This addition was termed “detail A” in the test matrix. To allow comparison, no additional transverse reinforcement was placed in PSS-16-24. During Phase 2, no additional mild steel reinforcement was added at the precaster. To examine the effects on negative moment flexure cracking, two #5 mild steel hoops were placed around the top of the corrugated steel pipe in PSV-28B. In PSV-28A, single leg #3 P-Bar transverse reinforcement was added in the joint region, following the standard released by TxDOT (detail B). In PSV-28B, single leg #5 J-Bar transverse reinforcement was added in the joint region (detail C). For Phase 1 specimens, the corrugated steel pipe extended the full depth of the cap. During Phase 2, the lengths of the corrugated steel pipes

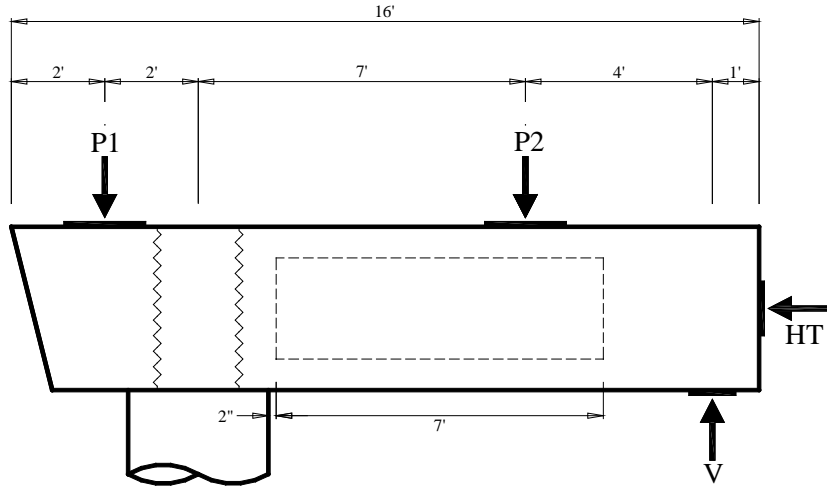
were varied to study the effects on the performance of the connection. In PSV-28A, the steel pipe was detailed to have 6-in. cover at both the top and the bottom of the cap. In PSV-28B, the steel pipe extended to the bottom of the cap, 2-3/4-in. cover was provided at the top of the cap.

**Table 4.7. Test Matrix Overview.**

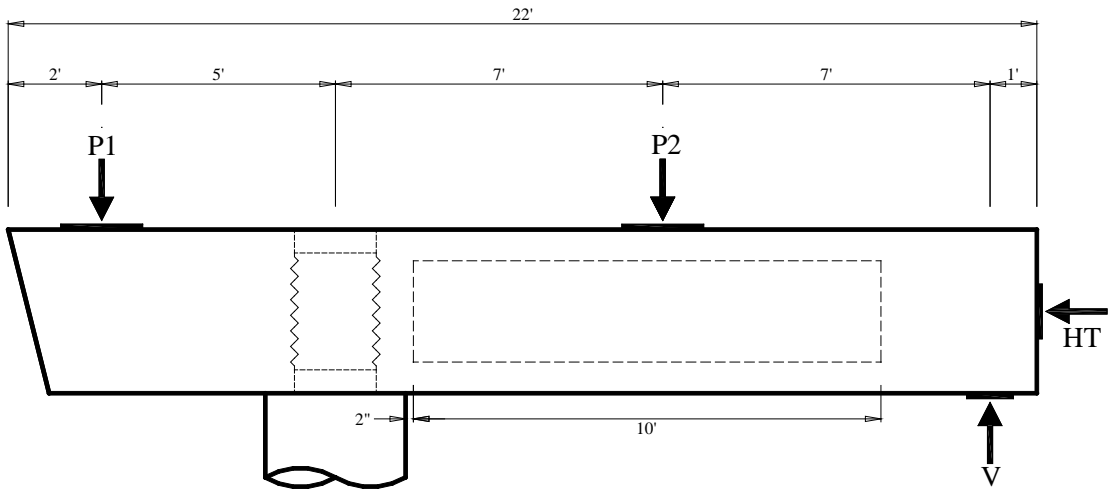
	<b>Specimen</b>	<b>Flexural Reinf.</b>	<b>Shear Spacing</b>	<b>Void</b>	<b>Overhang</b>	<b>Description</b>
<b>Phase 1</b>	RCS-16-12	16-#8 Bars	12 in.	N	Standard*	RC design
	PSS-16-12	16-0.6 in $\phi$	12 in.	N	Standard	Pretensioned design
	PSS-16-24	16-0.6 in $\phi$	24 in.	N	Standard	Reduced shear reinforcement
	PSV-16-12	16-0.6 in $\phi$	12 in.	Y	Standard	Interior void
<b>Phase 2</b>	PSV-28A	28-0.6 in $\phi$	12 in.	Y	Long**	Longer specimen with void
	PSV-28B	28-0.6 in $\phi$	12 in.	Y	Long w/ void	Longer specimen with two voids and modified void geometry

\* Current TxDOT overhang design (4-ft)

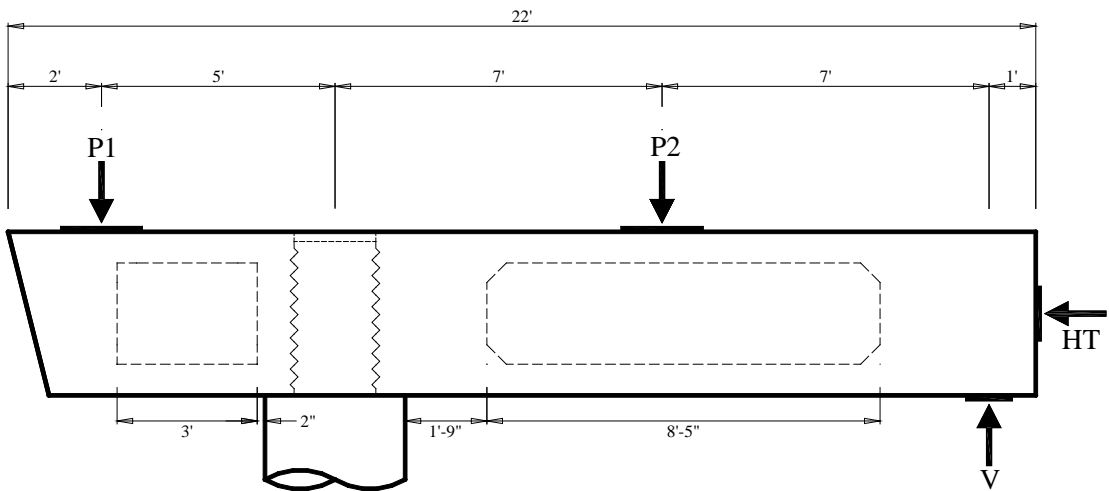
\*\* Longer overhang, discussed in Section 4.1 (7-ft)



(a) Phase 1 – PSV-16-12



(b) Phase 2 – PSV-28A



(c) Phase 2 – PSV-28B

**Figure 4.14. Specimen Geometry and Interior Void Placement.**

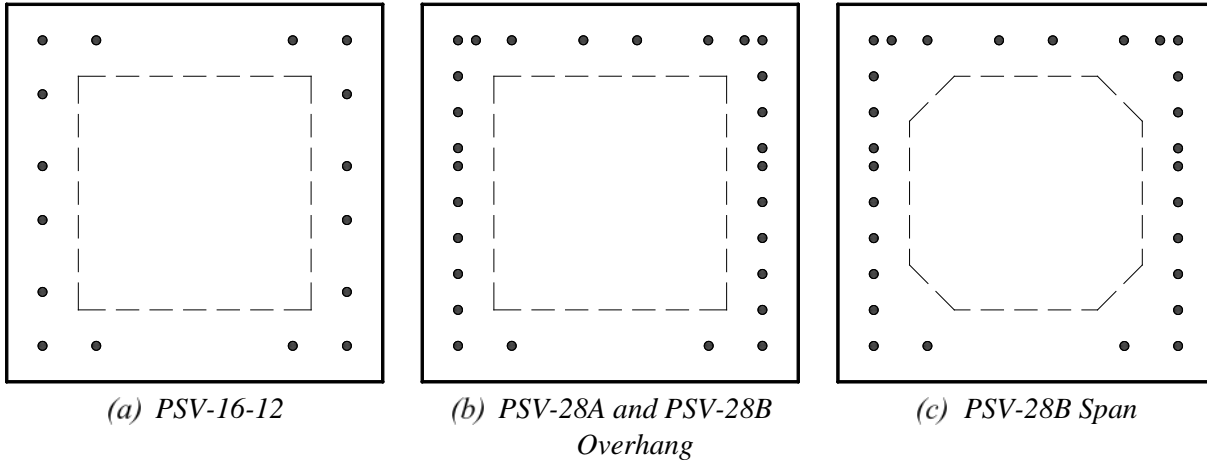


**Figure 4.15. Interior Void Cross-Sections.**

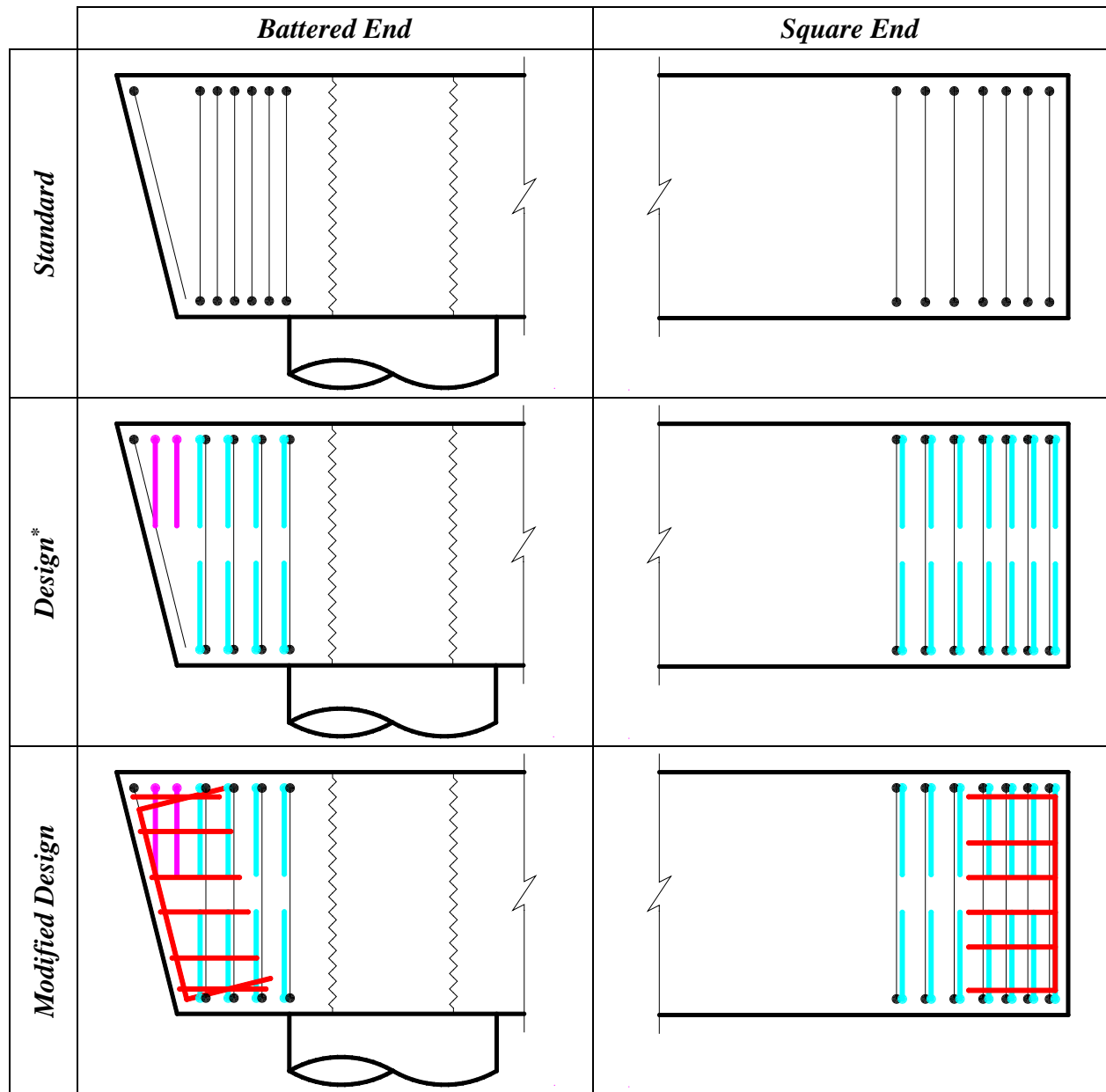
**Table 4.8. Pretensioned Specimens Pocket and End Region Detailing Matrix.**

Specimen	Battered End	Square End	Near Pocket	Corrugated Pipe Depth
PSS-16-12	Design*	Mod. Design**	Detail A	Full Depth
PSS-16-24	Design	Design	None	Full Depth
PSV-16-12	Mod. Design	Mod. Design	Detail A	Full Depth
PSV-28A	Standard	Standard	Detail B	6-in. cover (top and bottom)
PSV-28B	Design	Design	Detail C	2-3/4-in. cover (top only)

\* End region detailing as discussed in Section 4.2.4

\*\* Precaster modifications

See Figure 4.16 and Figure 4.17 for details



\* Shown for Phase 1. Phase 2 design similar, as discussed in Section 4.2.4.

*Magenta* = C-Bars

*Cyan* = C-Bar pairs

*Red* = B-Bars

**Figure 4.16 Pretensioned Specimens End Region Detailing Options.**

	<i>Cross-Section</i>	<i>Elevation</i>
<i>None</i>		
<i>Detail A</i>		
<i>Detail B</i>		
<i>Detail C</i>		

*Blue* = S-Bar pairs  
*Red* = P-Bar pairs  
*Magenta* = J-Bars  
*Cyan* = 30" Diam. #5 hoop

**Figure 4.17. Pretensioned Specimens Pocket Connection Detailing.**

#### 4.4. TEST SPECIMEN CONSTRUCTION

The support columns and the RCS-16-12 bent cap were constructed in the Texas A&M High Bay SMTL, while the pretensioned bent caps for both Phase 1 and Phase 2 were fabricated at Bexar Concrete Works in San Antonio, Texas, under the inspection and supervision of TxDOT and Texas A&M Transportation Institute (TTI) personnel. Appendix A provides a construction timeline for each specimen.



#### 4.4.1. RCS-16-12

A wooden formwork was constructed for RCS-16-12. Figure 4.18 shows completed formwork. Star flat head screws were used to ease formwork demolition. Additional braces along the walls of the bent cap were incorporated with cuts of lumber to secure the walls of the bent cap relative to each other.

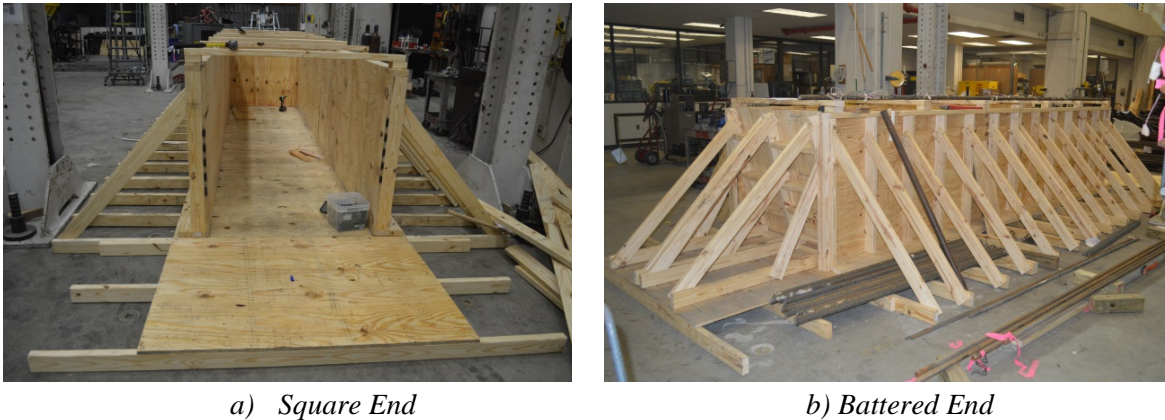


**Figure 4.18. RCS-16-12 Bent Cap Formwork.**

Figure 4.19 shows an overview of the construction of the bent cap. The overhead crane was used to lift the steel cage and install into the bent cap formwork. The corrugated steel pipe for the pocket connection was also installed using the overhead crane and fastened into its proper location with lumber. Once the steel cage and corrugated pipe were installed, the square end wall of the formwork was constructed to completely enclose and seal the bent cap formwork. Finally, two lifting hooks at equal distances from the center of gravity of the bent cap were installed for lifting the bent cap.

Concrete was provided by Martin Marietta Materials and poured inside the temperature controlled environment of the SMTL. A slump of 5.5-in. was recorded. Lifts using a hopper supported by the laboratory overhead crane were used to transport the concrete from the ready-mix truck to the bent cap formwork. The lever handle on the side of the shoot was used to regulate the flow rate of concrete into the formwork. The 42-in. height of the bent cap was cast in three 14-in. lifts. The concrete in each lift was consolidated with vibrations (15,000 rpm). The corrugated steel pipe comprising the pocket was held in position by compression with lumber and thin plywood. During placement of the first lift of concrete, a shift in the position of the corrugated steel pipe occurred from placing the concrete at a high rate into the battered end of the bent cap.

The pocket was reset to its original position by spreading the previously placed concrete around and away from the pipe, allowing the pipe to be easily moved. After all concrete lifts were placed, the bent cap top surface was finished with smooth trowels and floated. Filleted trowels were used approximately one hour after the last concrete lift to provide smooth round edges at the top surface of the bent cap. Once the concrete had set (~5 hours), the top surface of the bent cap was watered, covered with soaked towels, and covered again with a black plastic tarp for 4 days of moist curing.

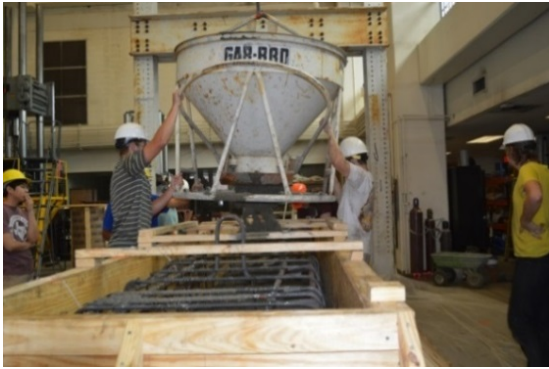
In efforts to protect the strain gauges during the casting of the bent cap, improper vibrating resulted in honeycombing in certain areas of the bent cap after releasing the formwork, as seen in Figure 4.20. According to the Chapter 2—Damage Assessment and Repair Types of the TxDOT Concrete Repair Manual (Freeby 2015), the honeycombing was determined to be minor with no effects to the structural integrity of the specimen. The average depths of the honeycombs were less than 7/8-in. The only two areas of largest honeycombs were 1-1/8-in. and 1-1/2-in. deep (depth of cover concrete 2-7/8-in.). No rebar was exposed. Repair guidelines were followed and the areas were cleaned and filled with cement grout. The surface of the specimen was finished with a diamond concrete surface grinder.



*(a) Steel Reinforcement Cage*



*(b) Pocket Pipe Placement*



*(c) Concrete Lifts*



*(d) Corrugated Steel Pipe Anchorage*



*(e) Corrugated Steel Pipe Anchorage*



*(f) Surface Finishing*



*(g) Finished Surface*



*(h) Impermeable Curing Tarp*

**Figure 4.19. Fabrication of RCS-16-12 Bent Cap.**



(a) *Span - Honeycombing*



(b) *Span - Repairs*



(c) *Battered End – Honeycombing*



(d) *Battered End - Repairs*

**Figure 4.20. RCS-16-12 Honeycombing and Honeycombing Repair.**

#### **4.4.2. Pretensioned Bent Caps**

The fabrication of Phase 1 and Phase 2 pretensioned bent caps (PSS-16-12, PSS-16-24, PSV-16-12, PSV-28A, and PSV-28B) occurred on prestressing line BB at Bexar Concrete Works. The specimens were positioned approximately at the middle along the length of the prestressing bed; Figure 4.21 shows the orientation of the prestressing line.

Prestressing strands were fed through the wooden square end formwork and metal battered end formwork. The polystyrene forming block for PSV-16-12 during Phase 1 was placed within the formwork before stressing the strands. In Phase 2, due to the geometry of the bent caps, details of the pocket connection, and size/location of the polystyrene voids, only 22 of the 28 strands were stressed at the start of fabrication. All prestressing strands were stressed to a force equivalent to  $0.75f_{pu}$  of the 0.6-in. diameter Grade 270 7-wire strands (44 kips). The six strands located at the top of the strand pattern (B-38, F-38, and H-38 in Figure 4.22[b]) were placed after pocket and interior void placement. After the initial strands were pulled through the header plates, the headers

were spread to the correct positions along the prestressing bed (Figure 4.23). The headers were secured with metal plates welded to the base of the prestressing bed to prevent any movement.

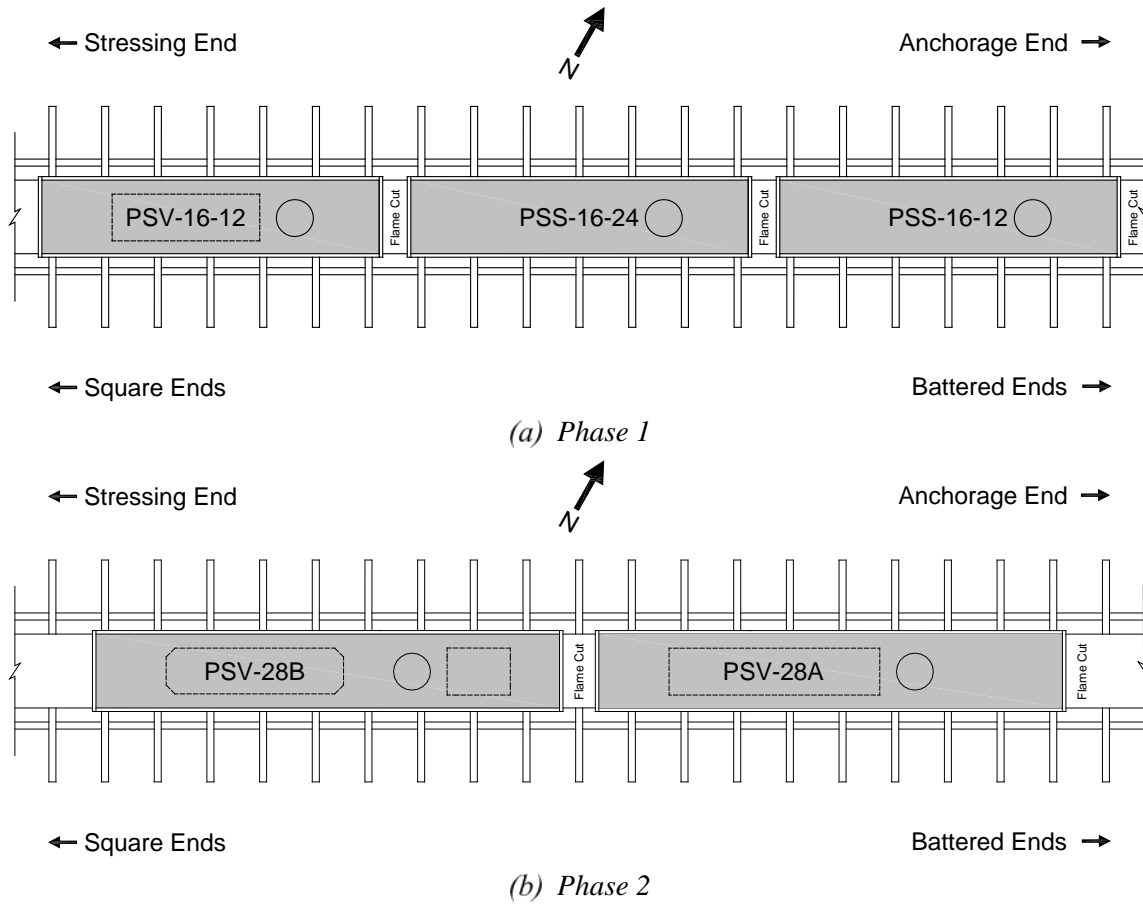


**Figure 4.21. Prestressing Bed Layout.**

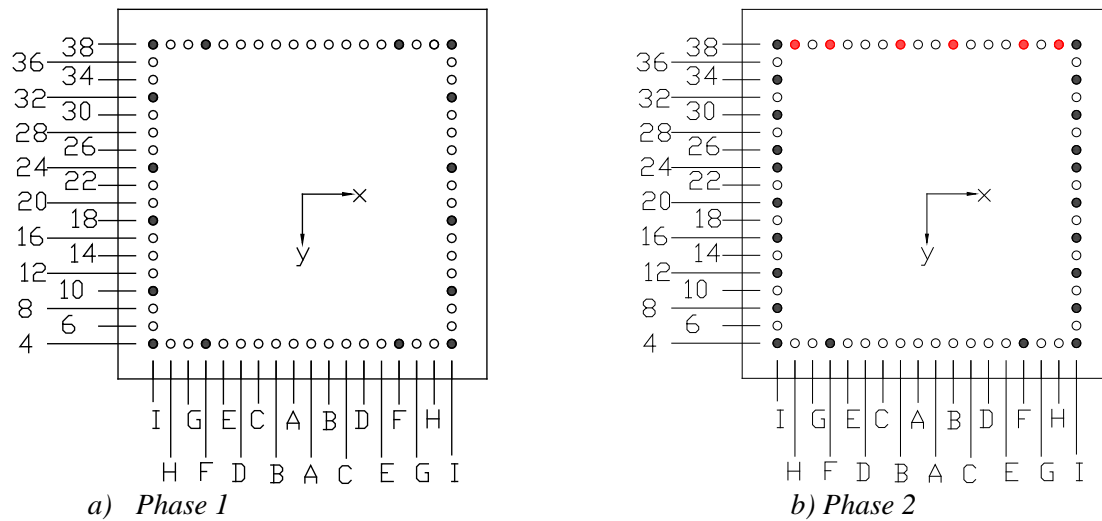


**Figure 4.22. Initial (Black) and Final (Red) Prestressing Strand Layout.**



a) *Prior to Spreading Headers*



b) *Prior to Stressing Initial Group of Strands*

**Figure 4.23. Placement of Initial Strands and End Formwork (Phase 2).**

Following the stressing of the initial strands, workers placed the interior components of the bent caps. The all-thread actuator load assemblies (Figure 4.24) were placed in the wooden formwork of the square ends of the specimens, as required for experimental testing and shown in the construction plans.

The corrugated steel pipes were installed into the formwork. Due to the differences in pocket connection details, different methods of securing the corrugated steel pipe were used. For Phase 1 specimens (PSS-16-12, PSS-16-24, and PSV-16-12), the corrugated steel pipe extended to both the bottom and top of the steel formwork. Welded metal tabs were used to prevent movement of the corrugated steel pipe during concrete placement (Figure 4.25[a]), and a protective layer of duct-tape was used to cover the top of the corrugated steel pipe to seal the pocket connection during concrete placement (Figure 4.25[b]). The corrugated steel pipe for specimen PSV-28A was secured on top of a 6-in. polystyrene forming plug using a threaded rod (Figure 4.25[c]). For specimen PSV-28B, the corrugated steel pipe extended to the bottom of the formwork and welded metal tabs were used to prevent movement of the corrugated steel pipe during concrete placement (Figure 4.25[d]). A polystyrene forming plug was placed at the top of each corrugated steel pipe in Phase 2 to seal the pocket connection during concrete placement.

The geometry, size, and quantity of the interior voids differed between PSV-16-12, PSV-28A, and PSV-28B. The interior voids were formed with polystyrene blocks. The longitudinal 5-in. chamfer on the polystyrene blocks for PSV-28B were precut at the time of manufacturing, while the transverse 5-in. chamfer was field cut after the block was cut to the appropriate length (Figure 4.26 and Figure 4.27). The polystyrene blocks were held in place with #3 rebar tied to the prestressing

strands. PVC drain pipes were installed at the bottom corners of the polystyrene blocks (Figure 4.28). Polystyrene blocks were restrained from floating during concrete placement with rectangular plywood held down with threaded rods secured to the transverse formwork bracing. Due to the geometry of interior void in specimen PSV-28B, adjustments were made to the hold down mechanism. Instead of a single piece of plywood held with two threaded rods, two pieces of plywood were held in place with individual threaded rods. These differences can be seen in Figure 4.29.

During Phase 2, after the interior void forming blocks and corrugated steel pipes were installed, the last six strands were fed through the formwork and the pocket connection (Figure 4.30). In both Phase 2 specimens, the strands were passed through the polystyrene plugs at the top of the corrugated steel pipes; holes were formed in the polystyrene using a heated piece of strand (Figure 4.30[a]). The prestressing strands were passed through holes in the corrugated steel pipe in specimen PSV-28B (Figure 4.30[b]).



(a) All-Thread Actuator Load Assembly  
(Typ. for both Phase 1 and Phase 2)



(b) Phase 2 Actuator Load Assembly Installed

**Figure 4.24. Square End Actuator Load Assembly.**



(a) Phase 1 Welded Metal Tabs Securing Corrugated Pipes (Typ.)



(b) Top of Phase 1 Corrugated Steel Pipes (Typ.)



(c) PSV-28A Corrugated Pipe Secured to Prestressing Bed



(d) PSV-28B Welded Metal Tabs Securing Corrugated Pipe



(e) PSV-28A Polystyrene Plug Secured with All-Thread Rod



(f) PSV-28B Top Polystyrene Plug

**Figure 4.25. Corrugated Steel Pipe Installation.**





(a) *PSV-28B Interior Void Polystyrene Forming Block (span) - Elevation*



(b) *PSV-28B Interior Void Polystyrene Forming Block (span) - Side*

**Figure 4.26. PSV-28B Polystyrene Forming Block.**



(a) *PSV-16-12*



(b) *PSV-28A*



(c) *PSV-28B (span)*



(d) *PSV-28B (overhang)*

**Figure 4.27. Polystyrene Forming Blocks Installed.**



(a) PSV-16-12



(b) PSV-28A



(c) PSV-28B

**Figure 4.28. PVC Drain Pipe Installation.**



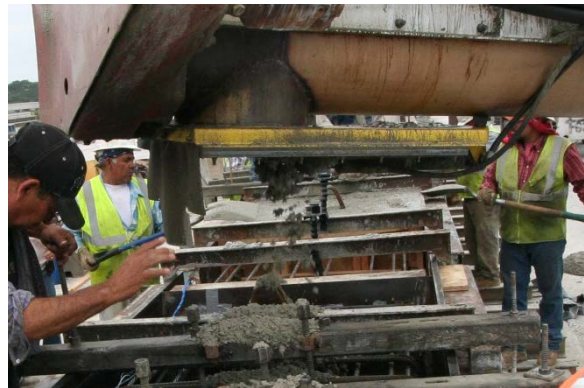
(a) PSV-16-12



(b) PSV-28A



(c) PSV-28B (span)



(d) PSV-28B (overhang)

**Figure 4.29. Interior Void Polystyrene Forming Block Anchorage.**



(a) Strands Placed Through PSV-28A Forming Plug



(b) Workers Feeding Strands Through PSV-28B Corrugated Steel Pipe

**Figure 4.30. Strands Through Pocket Connection (Phase 2).**

Mild steel reinforcement was placed after all strands had been stressed. Researchers provided transverse reinforcing bars gauged for monitoring during experimental testing. The two #5 mild steel hoops were placed around the top of the corrugated steel pipe in PSV-28B (Figure 4.32). The hoops were secured to the reinforcing cage using tie wire and #3 reinforcing bars where necessary

to maintain the correct position. Thermocouples were installed in all specimens, as seen in the thermocouple plans shown in Figure 4.33. Prior to placing concrete, TxDOT and TTI personnel inspected the reinforcement cages. Adjustments were made where necessary. The metal side formwork was placed to close the formwork and transverse bracing was attached along the length of both specimens.



*(a) PSV-28A Strain Gauged Mild Steel Reinforcement and Corrugated Steel Pipe*



*(b) PSV-28A Strain Gauged Mild Steel Reinforcement, Mild Steel Hoop, and Corrugated Steel Pipe*

**Figure 4.31. Strain Gauged Reinforcement.**



*(a) Elevation View*



*(b) Hoops at Top of Steel Pipe*

**Figure 4.32. PSV-28B Mild Steel Hoop Installation.**

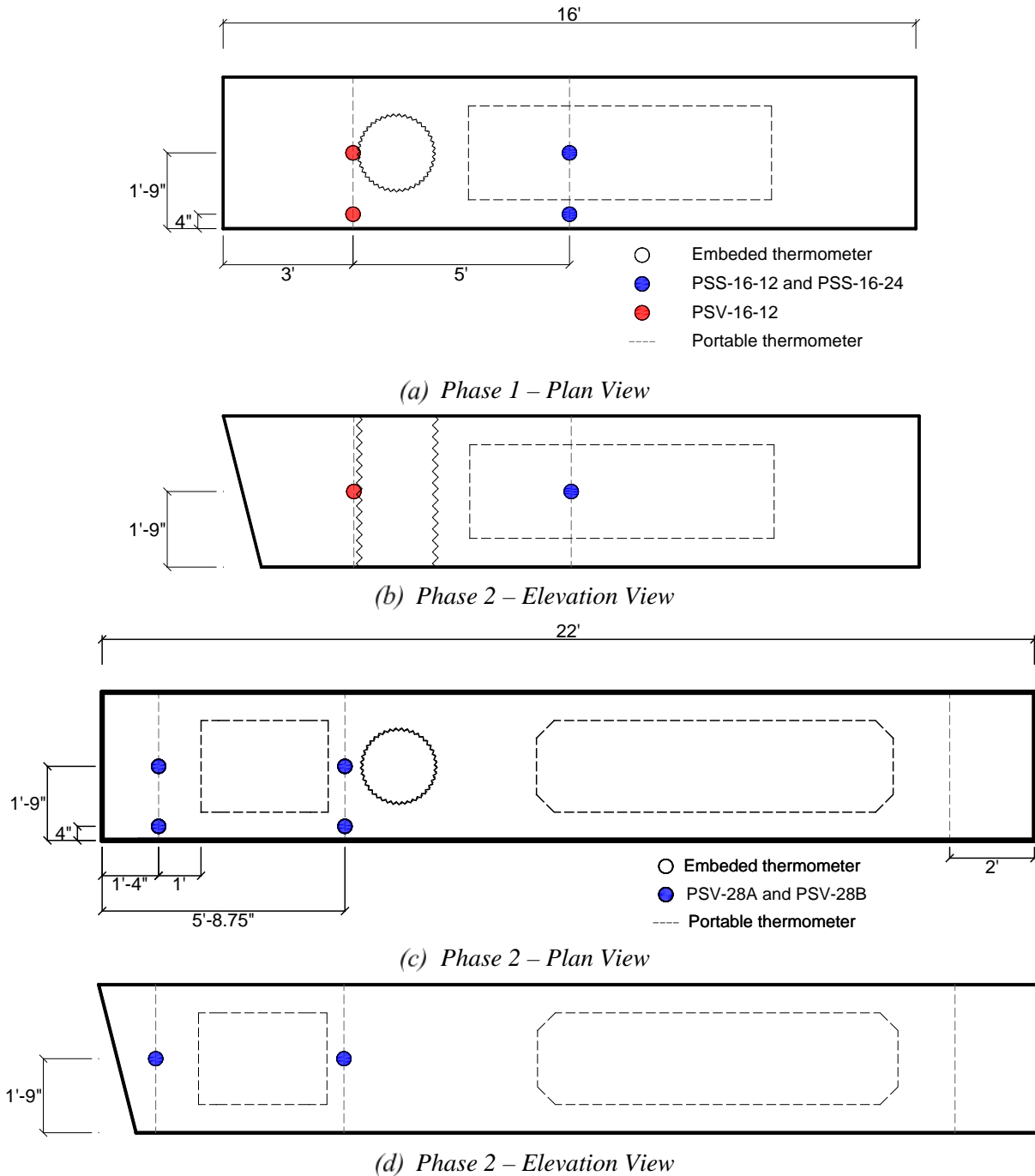


**Figure 4.33. Phase 1 and Phase 2 Thermal Couple Plans.**

Concrete was placed in 4 cubic yard batches from the onsite plant. Six batches were used to cast the Phase 1 specimens, and five batches were used to cast the Phase 2 specimens. These batches are referred to as batches A, B, C, D, E, and F (Phase 1) and batches J, K, L, M, and N (Phase 2). For each concrete batch, slump was recorded and test samples were made. For each batch, cylinders were made for 3, 28, 56, and test day compression, 28-day modulus of elasticity, and

28-day and test day indirect tensile tests. Each concrete batch had a slump ranging between 7 to 7-1/2-in. For Batch C (Phase 1) and Batch L (Phase 2), additional materials testing specimens were made for 7 and 14-day compression, and 28-day modulus of rupture tests. Figure 4.34 shows the approximate distribution of the concrete (by batch) in each of the specimens. The concrete was placed in approximately equal lifts, and workers used vibrators to consolidate the concrete (Figure 4.35). During placement of the concrete in PSS-16-24, the corrugated steel pipe moved out of position and was corrected to within 1/4-in. from the original position. Due to the interruption, the remainder of Batch D was discarded. During the placement of concrete near the square end of PSV-28B, the interior void forming block was shifted out of place. Workers adjusted the polystyrene block back to within 3/8-in. from the correct position and resumed the concrete placement (Figure 4.36). After completing the concrete placement, workers removed the threaded rods holding down interior void forming blocks, finished the surface with metal and wooden trowels, and installed a water irrigation system. The Phase 2 specimens were covered with black plastic to retain heat and moisture during the initial curing process (Figure 4.37).

Concrete compressive strength was tested each day. The morning of the third day after casting (for both Phase 1 and Phase 2), the concrete had reached or exceeded the specified compressive strength of 4 ksi. The black plastic covers were removed (Phase 2), and the formwork was removed from the specimens. The prestressing strands were released with the hydraulic jacks at the stressing end of the prestressing bed. Strands were cut using a flame torch at the anchorage end of the prestressing bed (Figure 4.38). Strands were released in the circular symmetric pattern shown in Figure 4.39. At the time of strand release, no initial cracking was noted for both Phase 1 and Phase 2. The specimens were lifted from the prestressing beds and moved to another location for the removal of the header plates. No cracking was noted on the end faces of the specimens after the removal of the header plates.

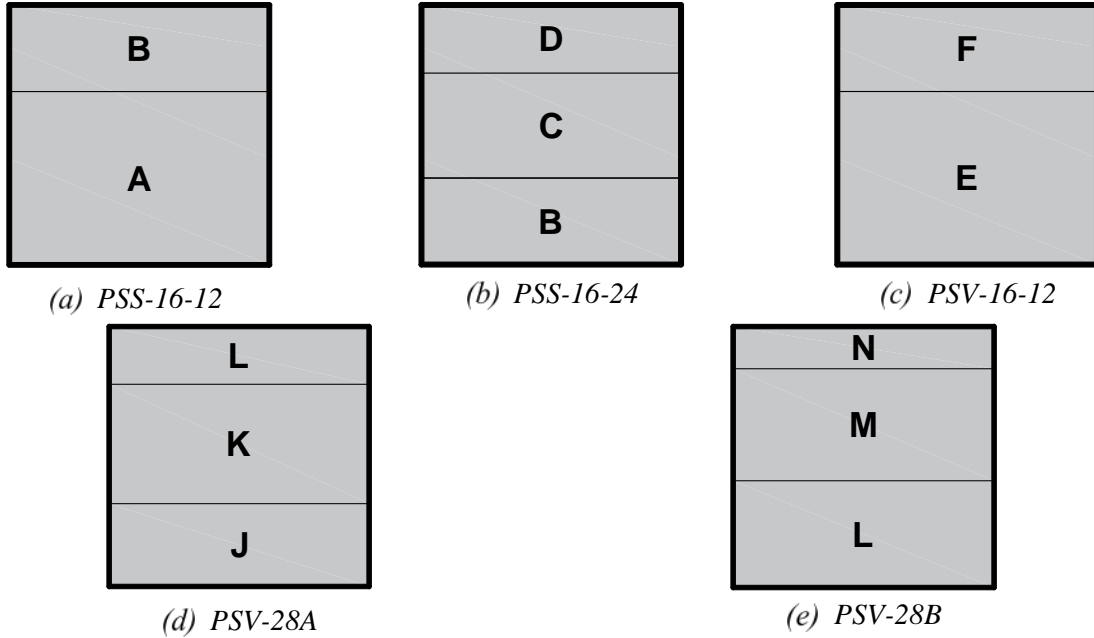


**Figure 4.34. Concrete Batch Distribution.**



(a) Concrete Placement



(b) Concrete Consolidation

**Figure 4.35. Concrete Placement and Consolidation.**



(a) Shifted Void



(b) Correcting the Shift

**Figure 4.36. PSV-28B Polystyrene Void Shifting.**



*(a) Trowel Finishing*



*(b) Irrigation System*



*(c) Removing All-Thread Rods Securing Polystyrene Voids*



*(d) Black Plastic Covering (Phase 2)*

**Figure 4.37. Concrete Finishing and Curing.**



*(a) Phase 1*



*(b) Phase 2*

**Figure 4.38. Torch Cutting Prestressing Strands.**



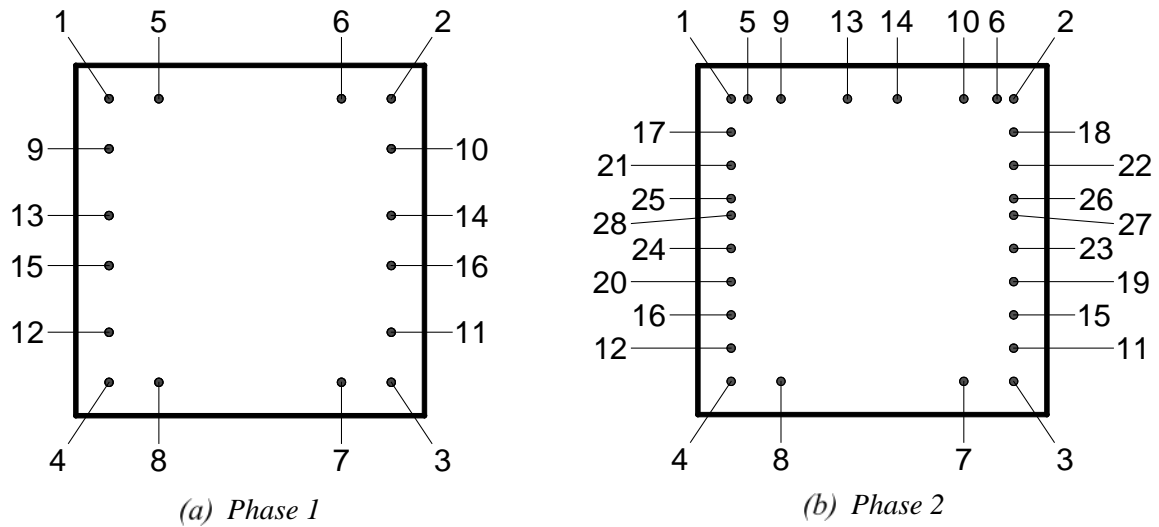
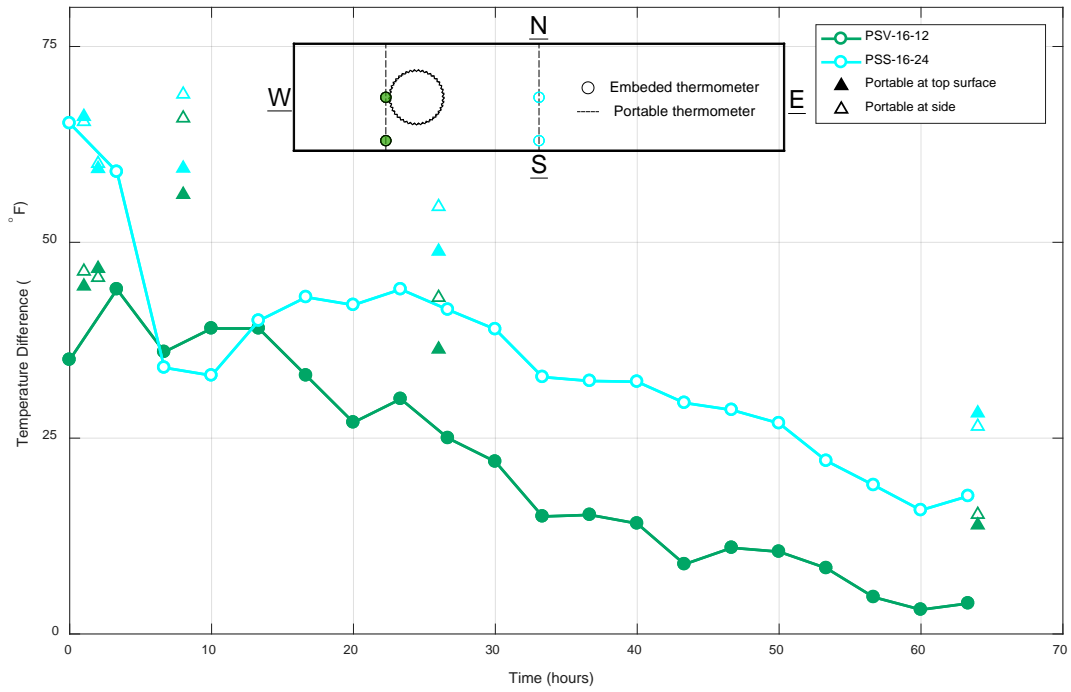
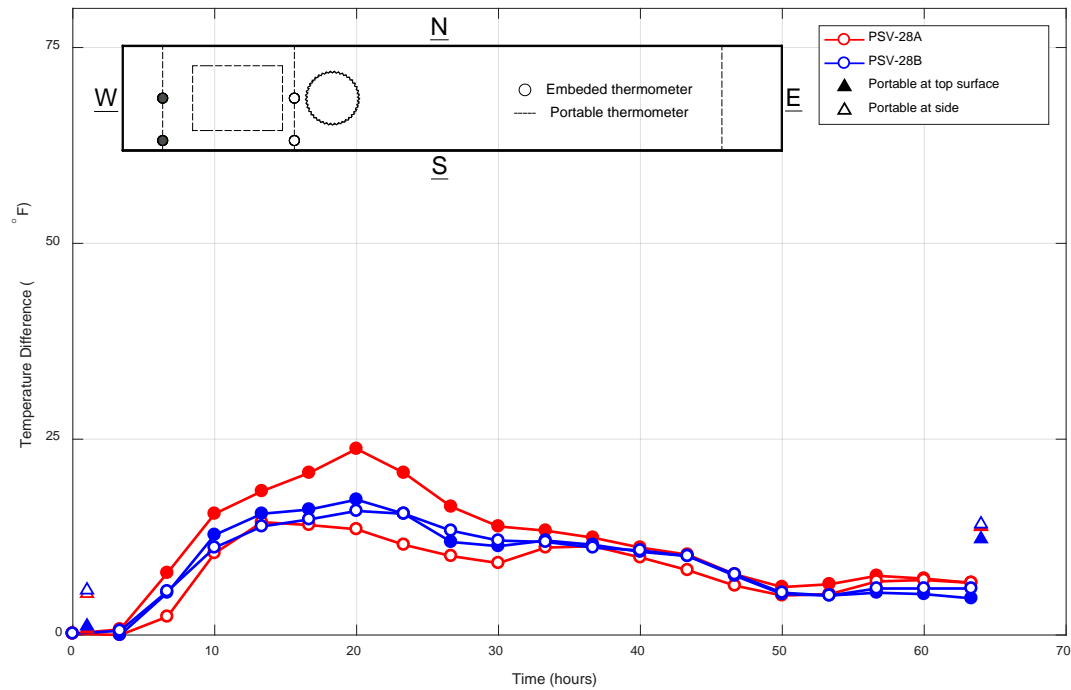


**Figure 4.39. Strand Release Pattern.**

During fabrication of Phase 1 specimens, the maximum ambient temperature reached 102°F and the maximum internal concrete temperature reached 160°F. During Phase 2, the maximum ambient temperature reached 92°F, and the maximum internal concrete temperature reached 138°F. Appendix C provides detailed thermocouple readings and measured surface temperatures. Temperature differences between the surface and the internal concrete were obtained using data measured by a portable thermometer and thermocouples, as shown in Figure 4.40.



(a) Phase 1

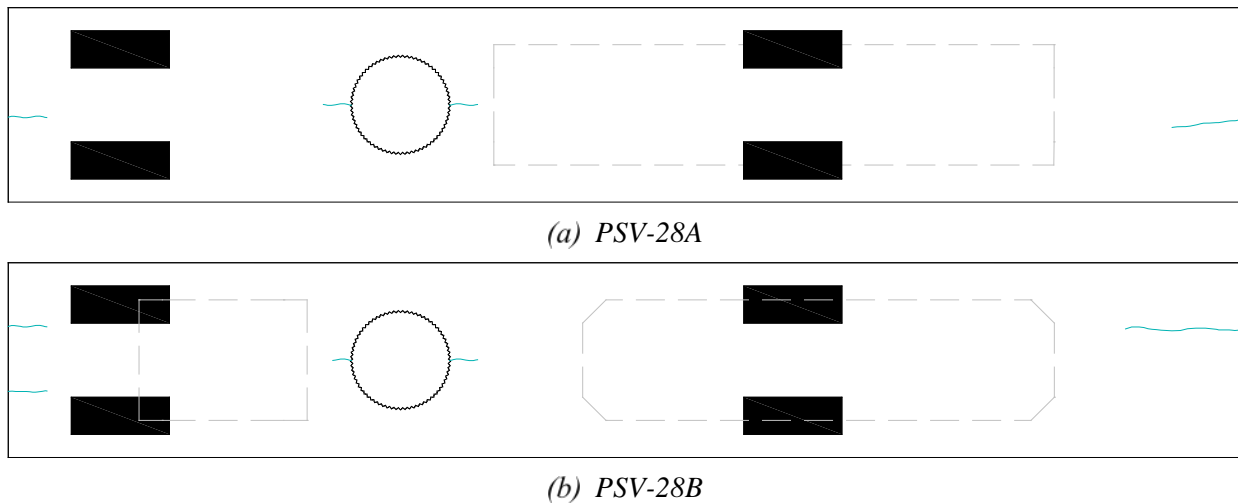


(b) Phase 2

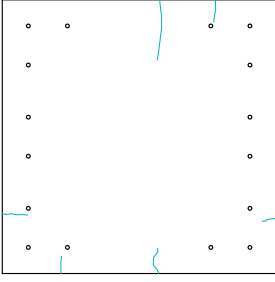
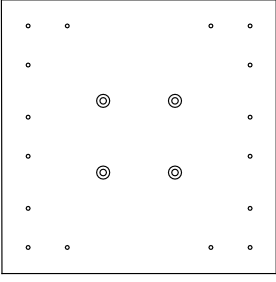
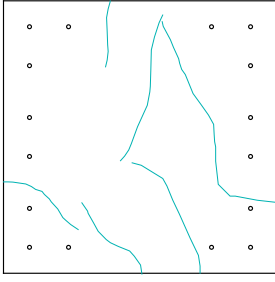
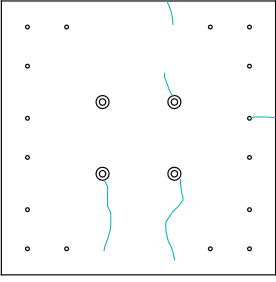
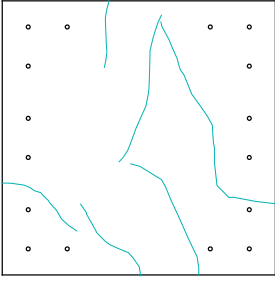
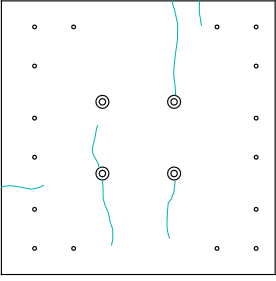
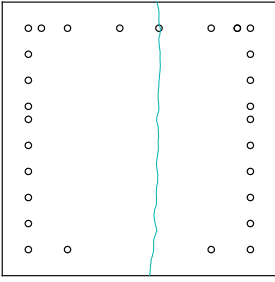
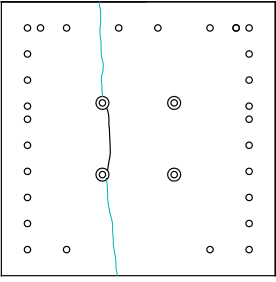
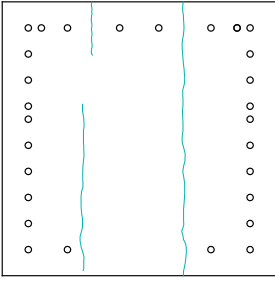
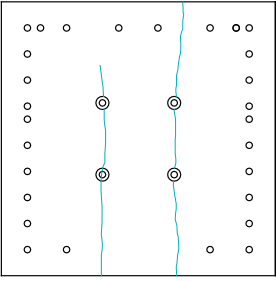
**Figure 4.40. Measured Temperature Difference.**

### 4.4.3. Pretesting Damage

As noted in Section 4.4.2, no cracks were observed immediately following the release of the prestressing strands during both Phase 1 and Phase 2. However, cracking was noted in the end regions of all pretensioned bent caps prior to testing. In Phase 1, no visible cracks were noted on delivery of the pretensioned specimens, but cracks appeared after several days in the temperature controlled lab and were monitored. In Phase 2, TxDOT representatives inspected the specimens prior to the delivery to the SMTL. Cracking was observed in the end regions and along the center line of the bent caps near the corrugated steel pipes on both PSV-28A and PSV-28B. The observations from Phase 1 and Phase 2 are noted in Figure 4.41 and Figure 4.42. In Phase 1, the pretesting cracks were hairline in width and had minimal extension prior to testing. In Phase 2, the pretesting cracks had a maximum width of 0.006-in. As cracks were not observed immediately after the initial prestressing strand release, it is hypothesized that the cause of the cracking is related to thermal shock of the bent cap components during the curing process and the associated drying shrinkage. To better understand the nature of the pretesting cracking, additional research is necessary.



**Figure 4.41. Phase 2 Pretesting Cracks (Top of Bent Cap).**

	<i>Battered End</i>	<i>Square End</i>
<i>PSS-16-12</i>		
<i>PSS-16-24</i>		
<i>PSV-16-12</i>		
<i>PSV-28A</i>		
<i>PSV-28B</i>		

**Figure 4.42. End Region Pretesting Cracks.**

#### 4.4.4. Support Columns

The RC columns were constructed in the Texas A&M University SMTL. The support columns consisted of three main parts: column base, columns, and protruding dowel bars. Construction of the columns began by threading the bottom 1-in. of the 10-#9 column longitudinal reinforcement bars into a 1-in. steel plate. The octagonal column bases were constructed to provide a flat contact surface for the connection of the bottom horizontal actuator to the column. The 14-1/2-in. high octagonal bases were constructed with  $2 \times 8$  lumber and secured to the 1-in. steel plate with all-thread rods (Figure 4.43 and Figure 4.44).

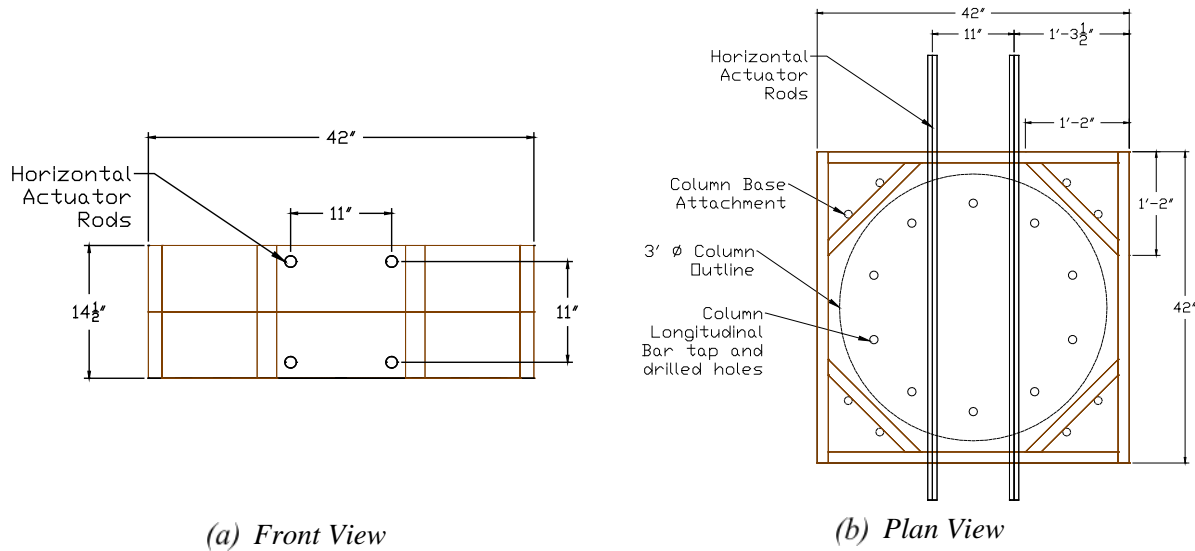
The #3 spiral reinforcement cage was installed around the 10-#9 longitudinal bars with a 6-in. pitch, incorporating an additional full loop of reinforcement at the top of the longitudinal reinforcement (Figure 4.45). The cage was tied at every longitudinal bar location. The column formwork was a 36-in. cardboard Sonotube. A  $2 \times 4$  lumber frame was fabricated to secure the Sonotube to the column base formwork.

The #11 dowel bars for the connection between the bent cap and the column extended 5-ft 6-in. into the column and 3-ft 2-3/4-in. into the bent cap. With this configuration, the dowel bars extended into the base portion of the support columns. Using lumber and additional reinforcement, the dowel bars were secured in the correct positions (Figure 4.46).

Once the column reinforcement cage and formwork were complete, the concrete was poured. The column bases were cast separately than the columns. The column Sonotube formwork was removed prior to casting the column bases. Concrete was placed in approximately equal lifts, and consolidated with vibrations. The top surface of the column bases that were to interface with the concrete of the columns was left rough and unfinished to allow for a better bond. The top surface of the column bases that were outside of the column area were finished with trowels to allow for a smooth contact surface for the column Sonotube formwork.

The main portion of the columns were cast a minimum of 24 hours after the casting of the column bases. The Sonotube formwork was reinstalled and secured to the octagonal column base formwork. Wiring for internal instrumentation was fed through the Sonotube. Concrete was placed in three approximately equal lifts using a hopper attached to the overhead crane. Concrete was

consolidated with vibrations. The top surfaces of the columns were left rough and unfinished to allow for a better bonding surface for the pocket connection.



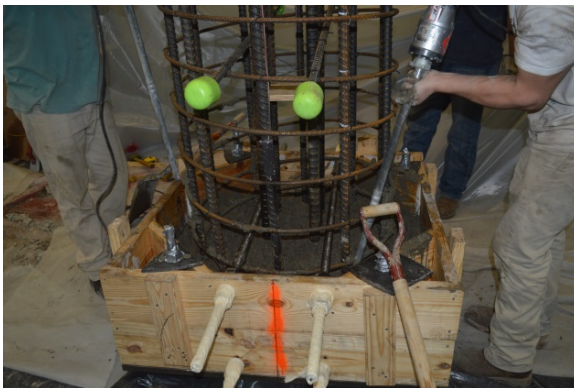
(a) Front View  
 (b) Plan View  
**Figure 4.43. Column Base Octagonal Formwork Plan.**



(a) Column Base Formwork Installation



(b) Column Base with Horizontal Actuator All-Thread Rods



(c) Consolidating Concrete



(d) Concrete Finish

**Figure 4.44. Column Base Construction.**



(a) Deformed Spiral

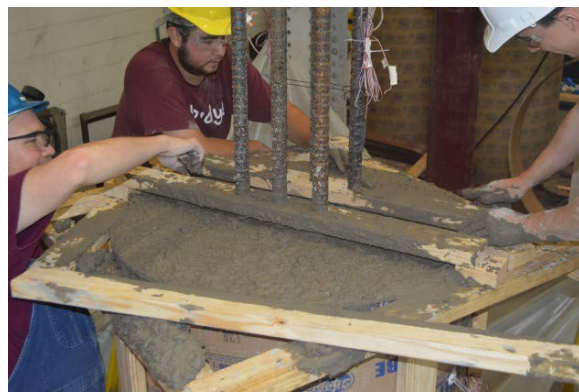


(b) Octagonal Base Formwork and Sonotube Attachment

**Figure 4.45. Column Reinforcement and Formwork.**



(a) Dowel Bars Alignment



(b) Rough Finish

**Figure 4.46. Column Construction.**

#### 4.4.5. Assembly of Specimens

Assembly of the specimen occurred in the experimental test setup location. Columns were placed first, followed by placement of the bent cap. The corrugated pocket connection in the bent cap fit over the dowel bars extending from the column. The pocket was then filled with concrete to complete the assembly. Details of the assembly are provided in the following paragraphs.

The installation of the bent cap onto the column took place by attaching the overhead crane to the lifting hooks. The ease of installment of the bent cap onto the column with the use of the larger single pocket connection allowed for a quick assembly of the specimen bridge in the laboratory

(Figure 4.47). Temporary shoring for the square end of the bent cap was provided by two angle iron headers attached to the reaction towers. Wood shims were used to obtain the correct height and level installation of the bent cap resting on the angle iron headers. The bent cap was supported on the columns by shims. Shims are inexpensive, readily available, and simple to install. The use of plastic shims instead of steel shims also prevents corrosion and reduces concerns of hard spots that could develop at the column-bent cap interface as the plastic is expected to creep and better transfer connection loads to the bedding layer. The plastic shim dimensions were 4-in.  $\times$  4-in.  $\times$  1-1/2-in., occupied less than 2 percent of the column area, and consisted of rigid high-density polyethylene (HDPE). The shims were placed 3-1/2-in. from the edge of the column along the centerline of the bent cap allowing the shims to sit at the outside edge of the pocket connection (Figure 4.48). The 1-1/2-in. thickness of the shims provided the necessary minimum thickness of the bedding layer according to TxDOT standards. The areas where the shims were installed on the column were prepared by grinding to provide a level surface on the rough finish left at the top of the column to ensure the shims could be placed level.



(a) *Placing Bent Cap on Column*



(b) *Bent Cap Position on Column*



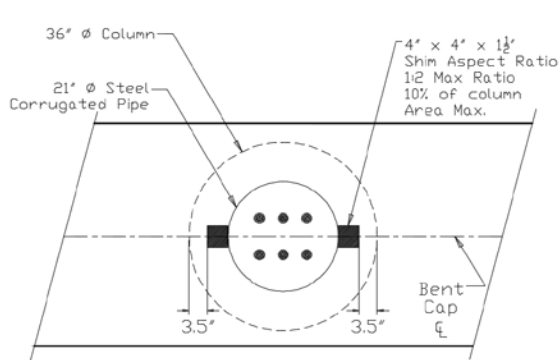
(c) *Bent Cap Positioned on Column*



(d) *Pocket Connection prior to Casting Concrete*

**Figure 4.47. Installation of Bent Cap onto Column.**





(a) Plans



(b) Placement

**Figure 4.48. HDPE Shim Installation.**

A sleeve made of sheet metal with a spring load chain and latch was constructed to provide the formwork for the bedding layer. The latch and the spring provided the necessary stiffness in the sleeve to remain in place during casting and vibration of the pocket concrete. For the first specimen (RCS-16-12), two 1/2-in. inner diameter clear tube vents were installed behind each of the two shims placed along the center line of the bent cap to allow any entrapped air to exit the interface between the edge of the column and the edge of the pocket during the casting of the bedding layer (Figure 4.49). For subsequent specimens, four small holes were drilled in the sheet metal sleeve to allow for air to escape the bedding layer and to allow for visual confirmation that concrete had consolidated behind the HDPE shims.

Prior to casting the bedding layer, the concrete at the top of the column inside the pocket connection was hydrated to ensure the bond of the bedding layer to the top of the column. The overhead crane and a side shoot on the concrete hopper were used to cast the concrete into the corrugated pipe connection (Figure 4.50).

The difficult access to the bedding layer from the top of the pocket connection made spreading and consolidating of the concrete challenging. In specimen RCS-16-12, two small areas of honeycombing were present in the bedding layer because of the constructability problems encountered while casting the pocket connection (Figure 4.51). The level of honeycombing in the bedding layer was determined to be minor and showed to have no negative effects on performance during testing. The honeycombing areas were cleaned and repaired using cement grout. Honeycombing was not an issue in subsequent specimens, as the slump of the fresh concrete was sufficient to allow for proper consolidation.



(a) Formwork



(b) Air Vents

**Figure 4.49. Bedding Layer Formwork and Air Vents.**



(a) Bottom View



(b) Top View

**Figure 4.50. Casting of the Bedding Layer.**



(a) Back Side



(b) Front Side

**Figure 4.51. Honeycombing in Bedding Layer (RCS-16-12).**

#### **4.5. EXPERIMENTAL TEST SETUP**

Figure 4.52 shows a 3D rendition of the experimental setup in the Texas A&M High Bay SMTL. The Phase 1 specimens had a bent cap length of 16-ft and a column height of 6.3-ft (8-ft to center of bent cap) (Figure 4.53). The Phase 2 specimens had a bent cap length of 22-ft and used the same column configuration (Figure 4.54). The column rested on a rocker foundation bolted to a 10-ft  $\times$  7-ft steel plate. Horizontal actuators (HT, HB) attached to horizontal load reaction frames provided stability. Two top vertical actuators (P1, P2) supported on 9-ft headers between the vertical reaction towers simulate the girder loads. The bottom vertical actuator acted as the shear at the bent cap inflection point and connected to the strong floor by a 4-ft  $\times$  4-ft steel plate. The following sections describe in detail the connection of the specimen, actuators, and support towers.

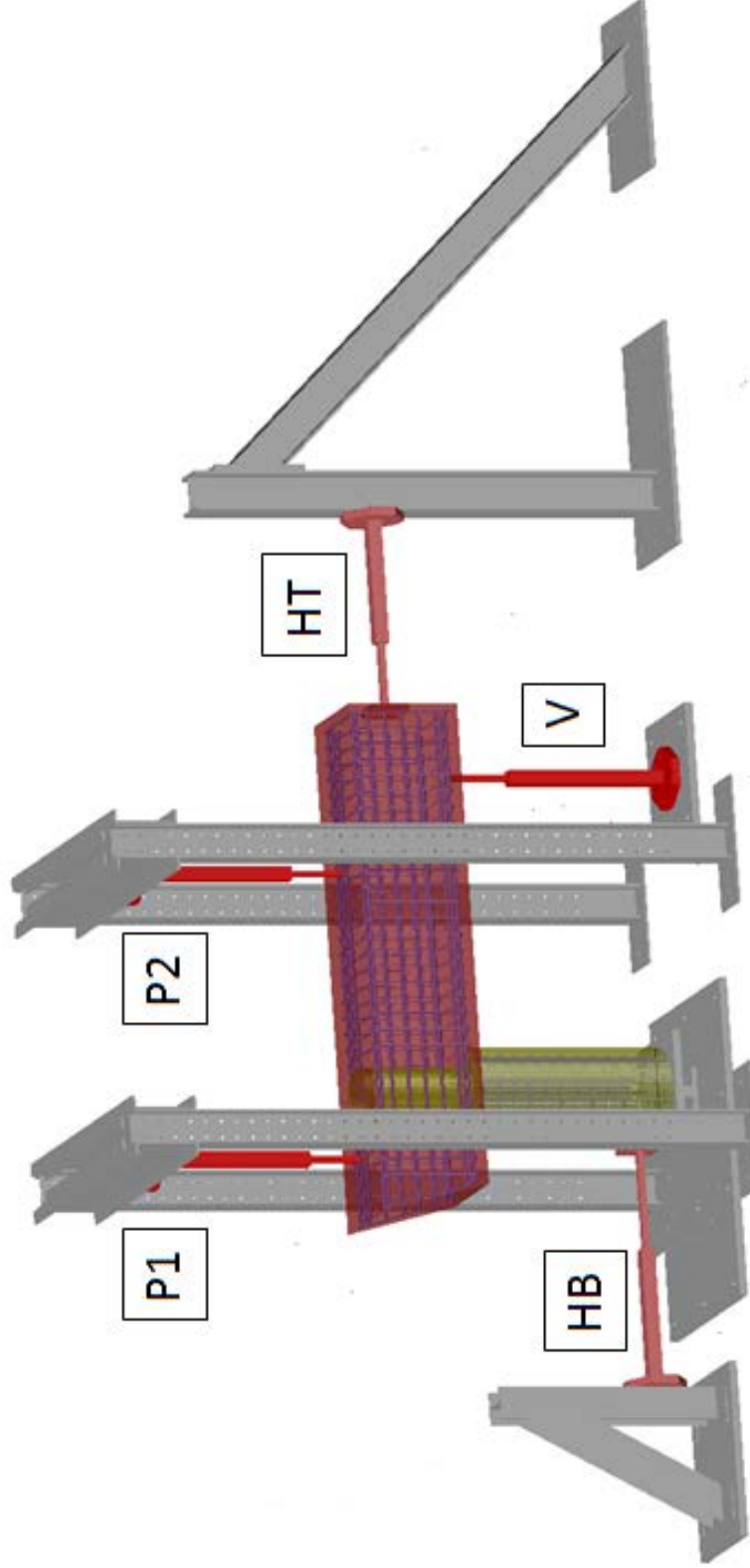
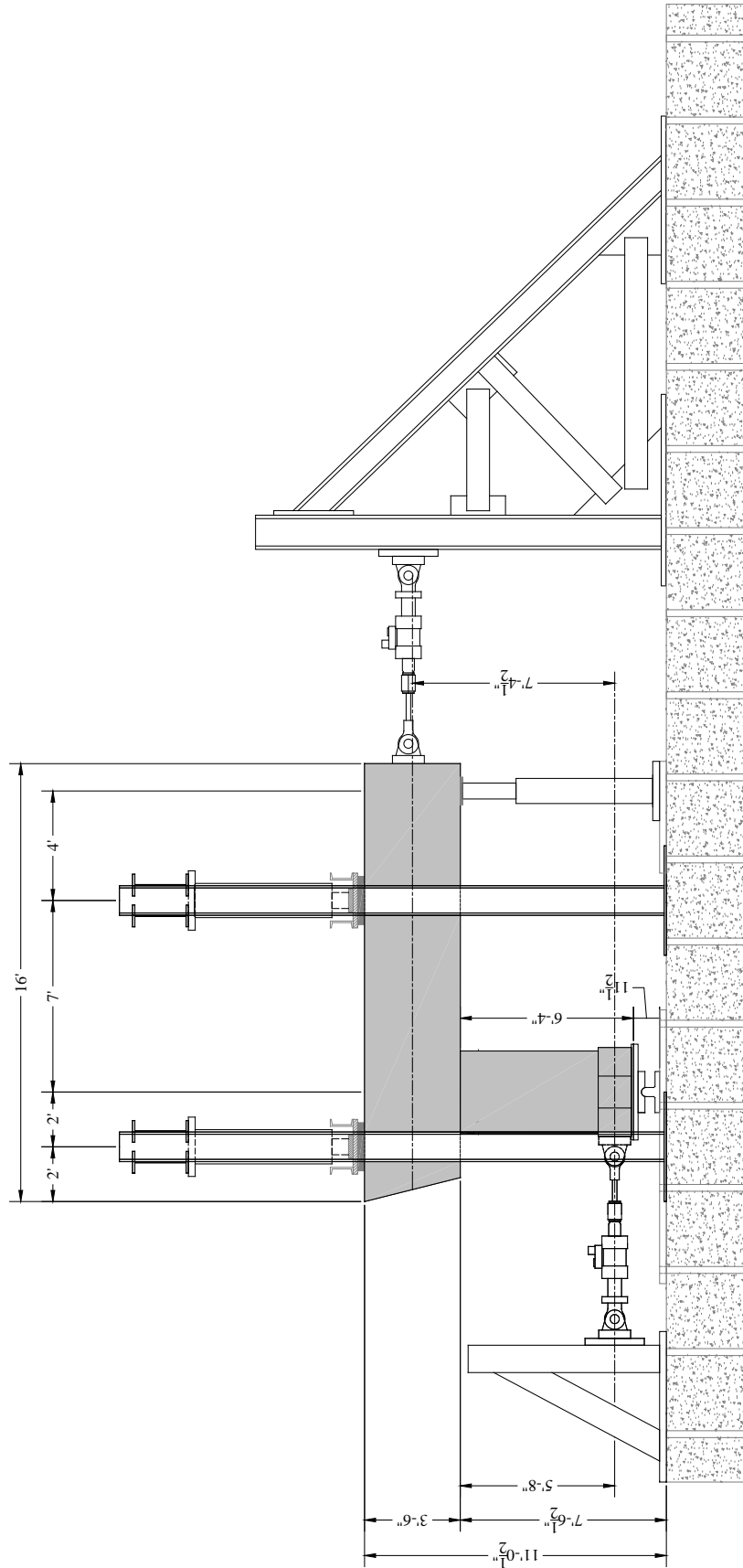
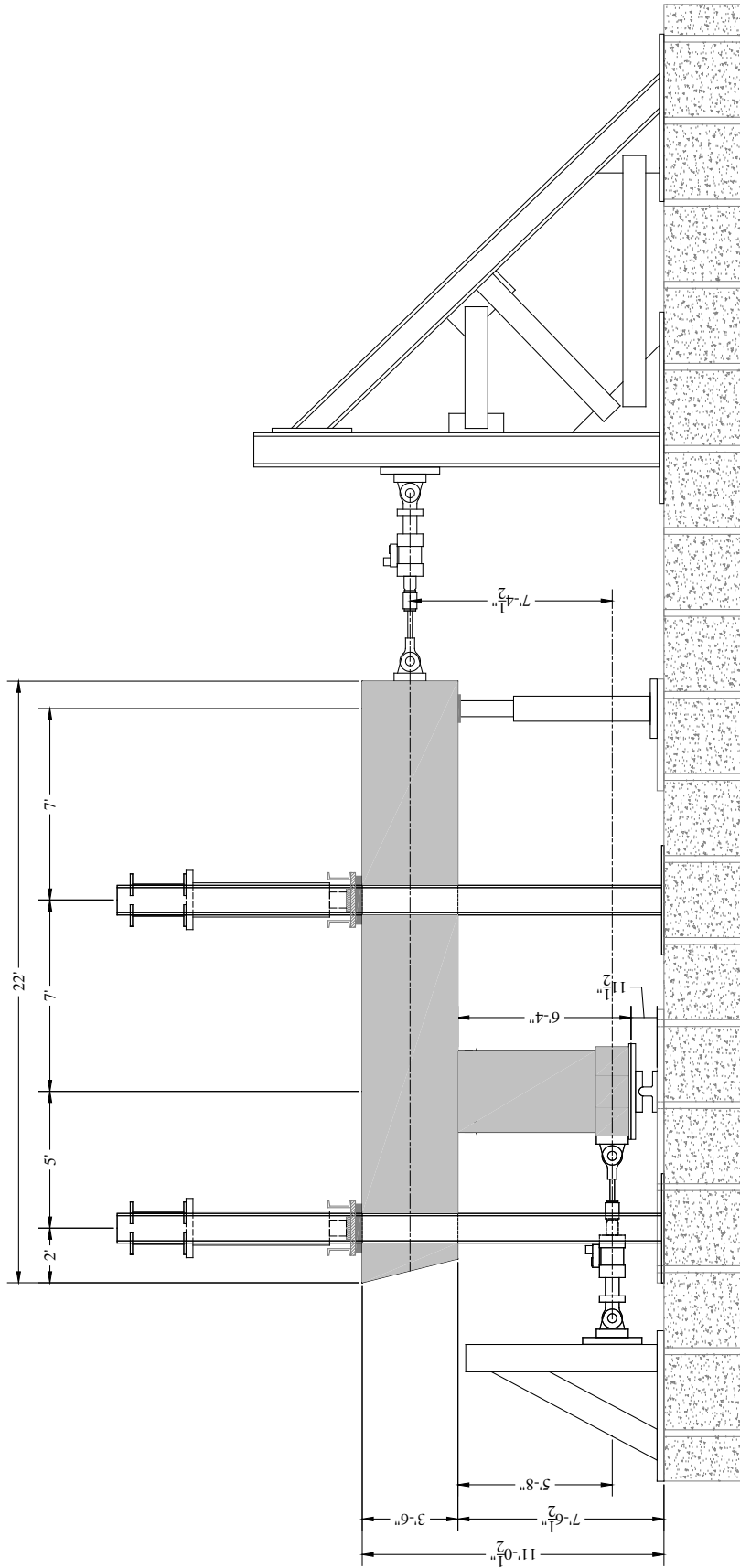


Figure 4.52. General Laboratory Experimental Setup – 3D Rendition.



**Figure 4.53. Phase 1 Experimental Test Setup.**



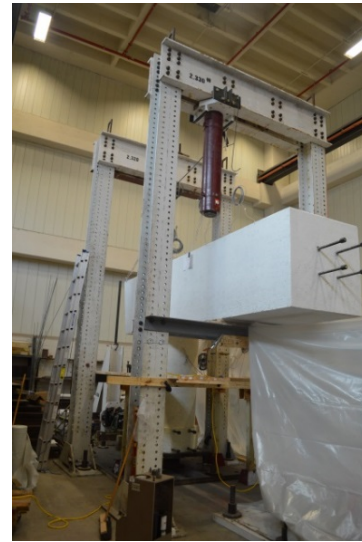
**Figure 4.54. Phase 2 Experimental Test Setup.**

#### 4.5.1. Connection Details – Installation of Reaction Towers to Strong Floor.

The laboratory floor has a 3-ft × 3-ft grid of 3-in. diameter holes. Each hole travels the thickness of the laboratory strong floor and allows the use of dywidags to secure reactions frames and towers. The vertical reaction towers (Figure 4.55), reaction plate, and horizontal reaction frames (Figure 4.56) for the specimens were attached to the laboratory strong floor by 2-1/2-in. dywidag threaded bars, with each tensioned to 3,000 psi. The specimen was aligned above a strong floor foundation wall to accommodate the large forces acting during testing.



(a) Vertical Reaction Towers



(b) Vertical Reaction Towers

**Figure 4.55. Vertical Reaction Towers.**



(a) Bottom Horizontal Actuator Reaction Frame



(b) Top Horizontal Actuator Reaction Frame

**Figure 4.56. Horizontal Reaction Frames.**

#### 4.5.2. Connection Details – 10-ft × 7-ft Base Plate

The TAMU SMTL had in its inventory a 10-ft × 7-ft × 3-in. plate that served as the base plate for the column to attach securely to the laboratory floor. The rocker foundation was attached to the base plate using 1-in. diameter tapped and drilled bolt connections. Additional 3-in. diameter holes for the dywidags were necessary for the base plate, as seen in Figure 4.57. The additional dywidag holes required the use of a magnetic drill press kit with a 3-in. diameter and 3-in. cutting depth titanium coated high speed Weldon 1-1/4-in. shank annular cutter. The rocker foundation plate was attached to the 10-ft by 7-ft plate in a similar fashion. The magnetic drill was used to drill 7/8-in. diameter holes and tapped for a 1-in. 8 UNC.

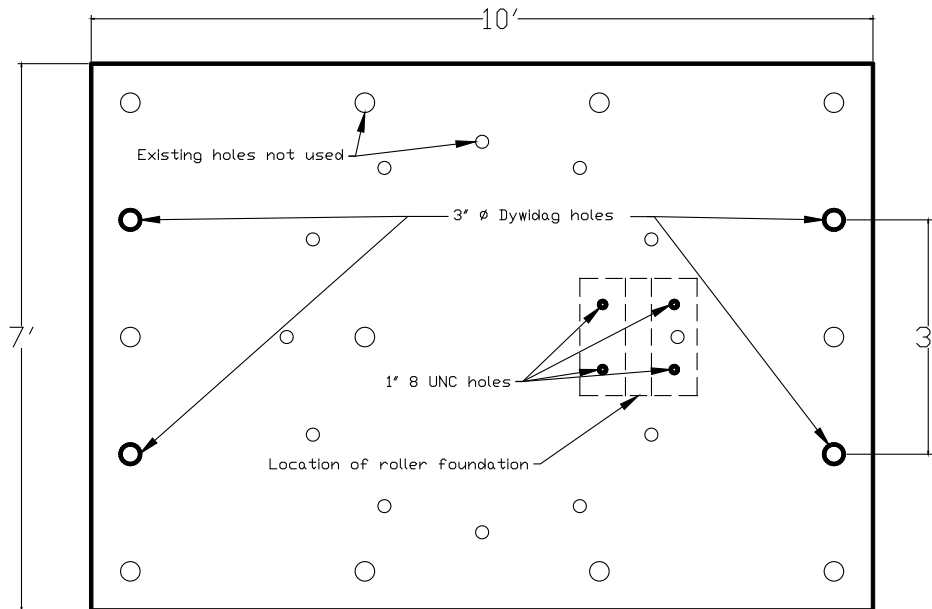


**Figure 4.57. 10-ft × 7-ft Base Plate.**

#### 4.5.3. Column Rocker Foundation

The pin foundation acted as a pin connection at the inflection point of the exterior column of the prototype bent. Brazos Industries Inc. was contracted to fabricate the rocker foundation consisting of a 4-in. diameter by 18-in. long rocker (Part D) welded to a 2-in. steel plate and three other separate steel plates (Parts A-C) manufactured with ASTM 572 Grade 60 steel (Figure 4.58). The column base was connected to the 10-ft × 7-ft base plate by threading the longitudinal column bars into the 1-in. plate (Part A) of the rocker foundation.



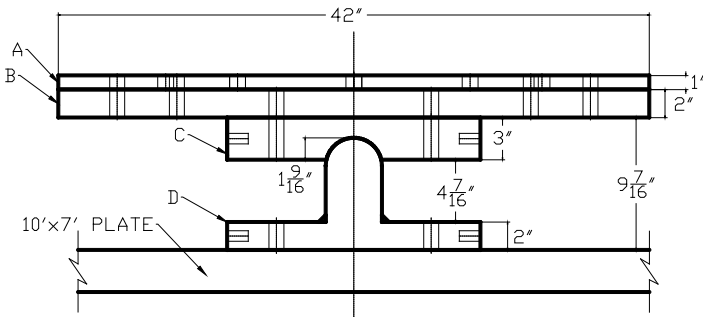


**Figure 4.58. Rocker Foundation (Pegs Removed prior to Testing).**

Part A consisted of a 42-in.  $\times$  42-in.  $\times$  1-in. steel plate and incorporated holes drilled and tapped for 1-in. 8 UNC matching the location of the column longitudinal bars, which were threaded into the 1-in. plate connecting the column base to the rocker foundation. Two 1-1/16-in. through-holes at each corner were also included in Part A for 1-in. bolts that would attach to Part B. Part A was designed to be disposed after each test with a total of six identical plates manufactured.

Part B had dimensions of 42-in  $\times$  42-in.  $\times$  2-in. with the 1-1/16-in. through holes at each corner to connect to Part A. Four additional holes were tapped and drilled near the center of Part B for 1-in. 8 UNC bolts to attach to Part C.

Part C consisted of an 18-in.  $\times$  18-in.  $\times$  3-in. steel plate that was machined to have a 4-in. diameter half circle void matching the top of the rocker of Part D. Part C also had four holes tapped and drilled for 1-in. 8 UNC bolts to attach to Part B.

Part D acted as the main component of the rocker foundation representing the pin at the moment inflection point at the exterior column of the prototype bridge and consisted of two pieces.



(a) Plate A - 1-in.



(b) Plate B - 2-in.



(c) Part C



(d) Part D

**Figure 4.59. Rocker Foundation Assembly.**

#### **4.5.4. Connection Details – Actuators**

The 110-kip actuators providing the horizontal stability for the specimens required the installation of rods cast into the specimens, as seen in Figure 4.60. The cleats of the 110-kip actuators had four 1-1/4-in. holes located 11-in. apart. Williams Form Engineering 150 ksi 1-in. all-thread rods were cast into the column base and the square end of the bent cap to provide the proper attachment of the 110-kip actuators to the specimen. The horizontal actuators were mounted to the horizontal reaction frames.

The two vertical actuators (P1 and P2) acting as the girder loads were attached to 9-ft headers at the top of the steel towers and the bottom actuator acting as the shear at the moment inflection of the prototype bridge was connected to a 3-in. thick base plate attached to the laboratory floor.

The bearing pads were purchased from a TxDOT approved manufacturer, Dynamic Rubber Inc. The dimensions and locations of the bearing pads followed the guidelines from TxDOT elastomeric bearing and girder end details (Figure 4.61).

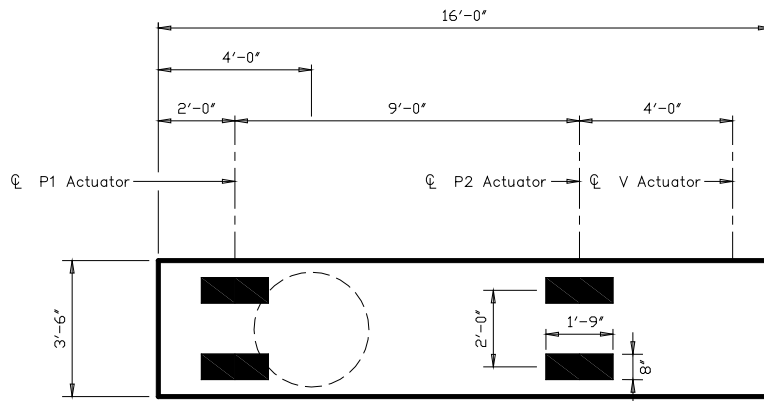


(a) HT Actuator Connection

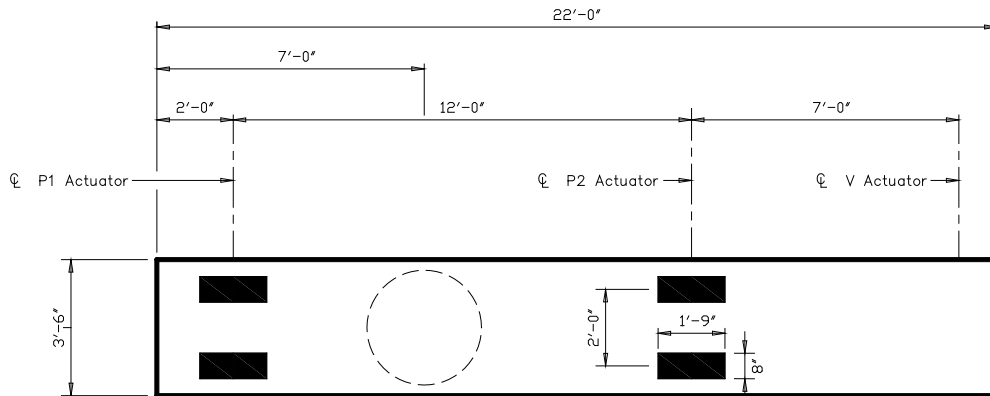


(b) HB Actuator Connection

**Figure 4.60. Horizontal Actuator Connections.**



(a) Phase 1

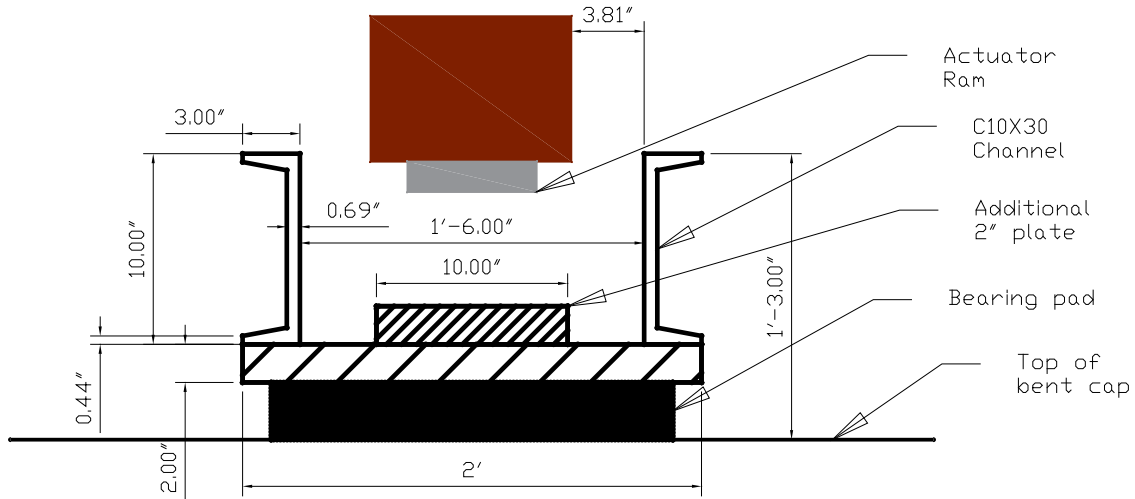


(b) Phase 2

**Figure 4.61. Elastomeric Bearing Pad Locations.**

Two actuator load assemblies were designed to evenly distribute the loads from the single actuator ram to the two bearing pads. The load assemblies consisted of two A-992 steel 10×30 C-channels welded to a 2-in. plate. An additional 2-in. plate was added to the assembly at the start of testing (Figure 4.62). The bottom vertical actuator (V) rested on a 3-in. thick base plate attached to the

laboratory floor. A 1-in. × 12-in. × 24-in. steel plate was secured to the bottom of the bent cap at the location of the V actuator to act as the bearing surface. Figure 4.63 shows the vertical actuators in their installed positions.



(a) Actuator Load Assembly Plan



(b) Installation



(c) Additional 2-in. Plate

**Figure 4.62. Top Actuator Load Assembly.**



(a) P1 and P2 Actuators



(b) V Actuator

**Figure 4.63. Vertical Actuator Connections.**

## 4.6. INSTRUMENTATION

One of major objectives of this experimental study was to obtain reliable data for the evaluation of the bent cap specimens with numerical analysis. To obtain the desired data, different types of instruments and their locations were carefully chosen. The instruments can be categorized into internal and external instrumentation. The internal instrumentation includes strain gauges while external instrument contains linear string potentiometers, linear variable differential transformers (LVDT), and the Optotrak motion capture system. The following sections explain the installation plan and description of each instrument. Appendix C provides detailed instrumentation plans.

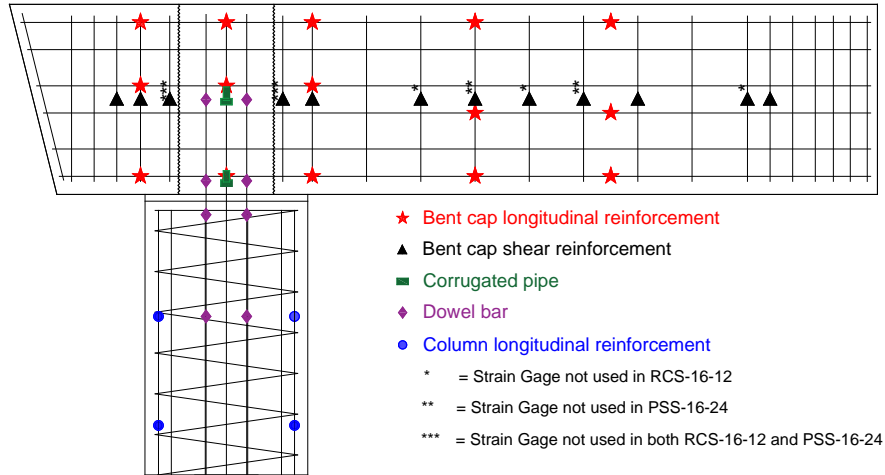
### 4.6.1. Strain Gauges

Strain gauges were used to measure the strain at critical locations. In RCS-16-12, a total of 38 strain gauges were attached to bent cap flexural reinforcement, shear reinforcement, column longitudinal bars, steel corrugated pipe, and dowel bars. Prestressed specimens in Phase 1 and Phase 2 had the same strain gauge layout, but without strain gauge on flexural reinforcement. Table 4.9 summarizes the number of strain gauges, and Figure 4.64 shows the locations.

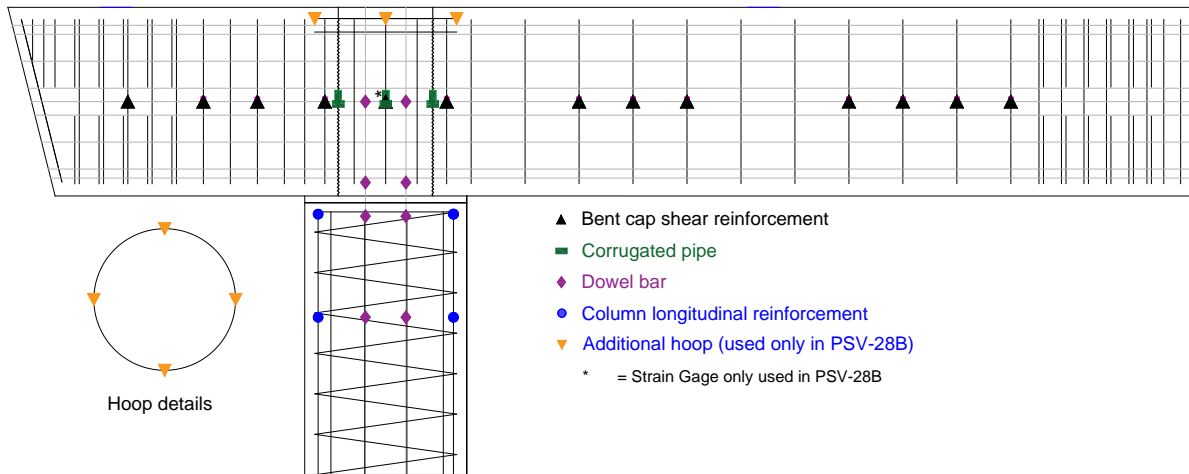
**Table 4.9. Summary of Strain Gauges.**

	Type	Bent cap		Column	Connection		Total
		Flexural	Transverse	Flexural	Dowel	Pipe	
Phase 1	RC	15	7	4	8	4	38
	PSC	-	7	4	8	4	23
Phase 2	PSV-28A	-	12	4	8	8	32
	PSV-28B	-	17 (4)*	4	8	8	37

\*(): strain gauges on the additional hoop



(a) Phase 1



(b) Phase 2

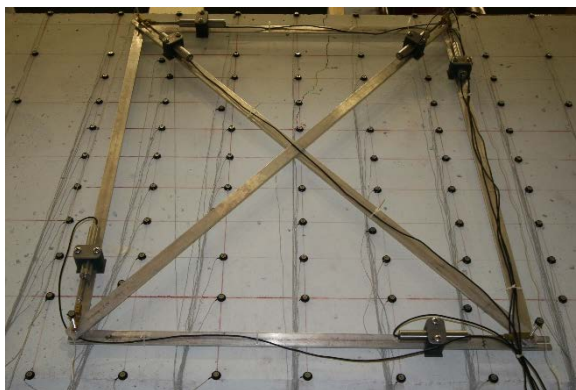
**Figure 4.64. Strain Gauge Layout.**

For the bent cap flexural reinforcement, strain gauges were attached at column faces, the center of the column, and at the P2 and V actuator locations. At these locations, gauges were placed on top, middle, and bottom bars to allow generation of strain profiles. For shear reinforcement, strain gauges are placed at the points where significant shear force and change are expected. Shear strain gauges were located at the vertical center of the hoop. Two strain gauges were evenly distributed for each of two column longitudinal bars. Eight strain gauges are installed in two dowel bars at mid-depth of the bent cap, bottom bent cap near joint, top column near joint, and middle of the column. In Phase 1, two horizontal and two vertical strain gauges are placed on corrugate pipe at

the bottom and mid-depth of the bent cap. In Phase 2, four horizontal and four vertical strain gauges were placed on the corrugated pipe at the mid-depth of the bent cap.

#### 4.6.2. Linear Variable Differential Transformers

During Phase 1, a total of six LVDTs were installed in horizontal, vertical, and diagonal directions in the joint region to measure relative vertical, horizontal, and diagonal displacement to monitor joint shear deformations (Figure 4.65[a]). In all tests two LVDTs were placed vertically under the bent cap adjacent to column to measure opening of the bedding layer. On PSV-28B, two LVDTs (Figure 4.65[b]) were placed vertically under the bent cap adjacent to the column in the location of the outer dowel bars to determine the strain in the dowel bars during loading. LVDTs within bent cap-column connection measured relative vertical, horizontal, and diagonal displacement to monitor joint shear deformations. Two vertical LVDTs under the bent cap adjacent to the column measured opening at the bedding layer. For PSV-28B, two additional LVDTs located at the locations of the dowel bars measured the displacement of the bent cap relative to the column at the location of the dowel bars to help determine the strain in the dowel bars during loading.



(a) Phase 1 Joint Region LVDTs



(b) Dowel Bar (PSV-28B only) and Bedding Layer LVDTs

**Figure 4.65. LVDT Locations.**

#### 4.6.3. Linear String Potentiometers

Twenty-eight linear string potentiometers were used to measure horizontal and vertical displacement of the specimens. In Phase 1, 13 were placed vertically along the centerline of the bottom of the bent cap, and 11 were placed horizontally on the bent cap and column. Four string potentiometers placed at corners were to check whether torsion occurred. From observations during experimental testing of Phase 1 specimens, string potentiometers to monitor torsion were

excluded from the instrumentation plan and added to the vertical string potentiometers for Phase 2. For Phase 2, 17 were placed vertically along the centerline of the bottom of the bent cap. For both Phase 1 and Phase 2, nine string potentiometers were placed horizontally on the bent cap and column to measure displacement. Two on the east end monitored displacement at the top horizontal actuator. Two string potentiometers at the column base were installed to check whether slip occurred at the column support.

#### **4.6.4. Optotrak Motion Capture System**

The Optotrak Certus motion capture system is able to measure the spatial position of up to 216 light emitting diode (LED) targets in three-dimensions. This system has the ability to track the displacement of the individual LED markers at an accuracy of 0.1 mm at a resolution of 0.01 mm. When used in conjunction with a strategic grid pattern, the relative displacements of the LED markers can be used to determine displacement profiles, strain fields, and measure crack widths. Figure 4.66 shows the general LED marker layout of Phase 1 and Phase 2. In Phase 2, the Optotrak motion capture system was focused on the negative moment region, due to restrictions on available measurement volume and obstructions from the experimental test setup. Detailed Optotrak layouts are provided in Appendix D. Both Phase 1 and Phase 2 used a two-camera system.



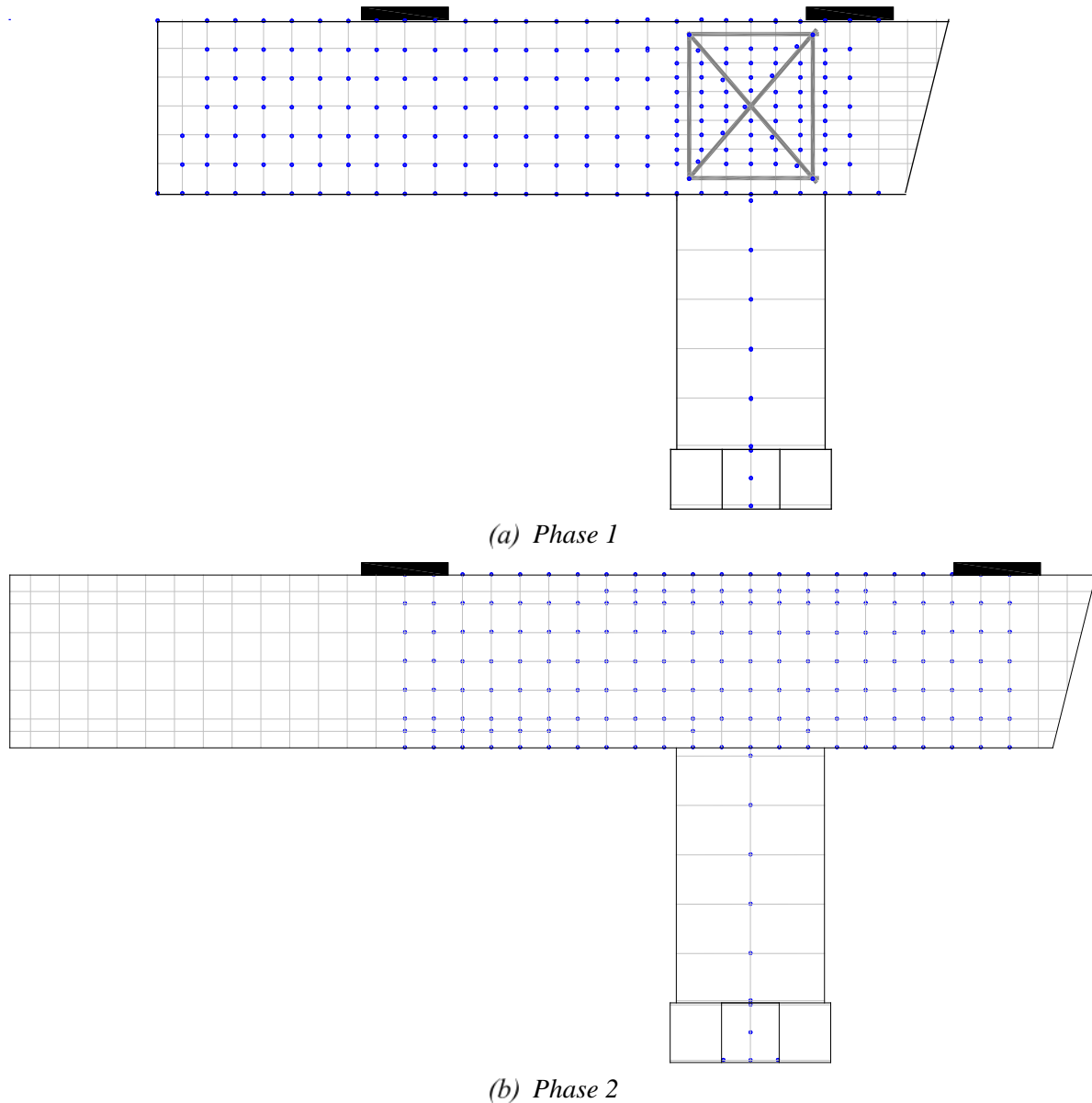


**Figure 4.66. Optotrak LED Marker Layout.**

## **4.7. MATERIAL PROPERTIES**

The following sections present the material properties results gathered for testing of samples collected for both concrete and steel.

### **4.7.1. Concrete Mix Designations**

Multiple concrete mixes were used to meet the specific needs of the experimental program. Separate mixes were used for bent caps (B), columns and bases (C), and pockets (P). All mixes

were TxDOT Class-C or Class-H or modifications of these. Table 4.10 summarizes each mix designation, the base concrete class, and any modifications.

Mix B-1 was TxDOT Class C modified to have a higher water-cement ratio (w/c) to achieve a 28-day compressive strength of less than or equal to 3.6 ksi. Concrete mix B-2 was a Class H concrete used for the pretensioned beams with a 28-day compressive strength less than or equal to 7.0 ksi. Table 4.11 shows the specifications of the standard Class C concrete mix design provided by Martin Marietta.

Mix design C-1 was the standard Class C concrete provided by Martin Marietta. Mix design C-2 used for PSS-16-12 had a 3/4-in. aggregate for the column base due to a miscommunication with the supplier. Mix C-3 was a high-strength concrete mix used in conjunction with an additional research project. Limited testing of mix C-3 was performed due to the column bases not being a focus of the research.

Mix design P-1 was specifically designed for the pocket connection using a lower aggregate size of 3/4-in. nominal diameter, lower paste content to reduce shrinkage compensating admixtures, and superplasticizer to increase the workability from the lower paste content. Mix design P-2 was a modification of mix design P-1 because of the problems encountered during the casting of the pocket connection for RCS-16-12. This mix contained 3/4-in. nominal diameter aggregate, shrinkage reducing admixture, used a standard paste content (because of the poor workability from the low paste content while casting the first pocket connection), and had no additional superplasticizer. Mix design P-3 was a modification of P-2 that did not use any shrinkage reducing admixture without changing any other parameters. This mix design was chosen to evaluate the effect of the shrinkage admixture on the performance of the pocket connection.

Table 4.12 provides the specifications for the P-1 mix design created to meet the research project needs.

**Table 4.10. Concrete Mix Designation.**

Concrete Mix ID	Specimen	Component	Concrete Class	Modifications
B-1	RCS-16-12	Bent Cap, Column, Base	C*	0.62 w/c ratio to delay 28-day strength
B-2	All Pretensioned	Bent Cap	H	Modified water/cement ratio to meet 4 ksi release strength
C-1	PSS-16-12 <sup>†</sup> , PSS-16-24, PSV-16-12, PSV-28A <sup>†</sup> , PSV-28B <sup>†</sup>	Column, Base <sup>†</sup>	C	-
C-2	PSS-16-12	Base	C*	3/4-in. nominal size aggregate
C-3	PSV-28A, PSV-28B	Base	N/A	10-ksi mix, Type A, F, and High Range water reducer, Class-C Fly Ash.
P-1	RCS-16-12	Pocket	C*	3/4-in. nominal size aggregate, lower paste, shrinkage admixture, additional superplasticizer
P-2	PSS-16-12	Pocket	C*	3/4-in. nominal size aggregate, shrinkage admixture
P-3	PSV-16-12, PSS-16-24, PSV-28A, PSV-28B	Pocket	C*	3/4-in. nominal size aggregate

\* *Modified Class C Concrete*

<sup>†</sup> *Column base not constructed with Mix C-1*

**Table 4.11. Standard Class C Concrete.**

Material	Description	Specific Gravity	Weight (unit/yd)
Cement	ASTM C150 - Type I/II Cement	3.15	358 lb
Alt. Binder	ASTM C618 - Class C Fly Ash	2.63	193 lb
Fine Agg.	ASTM C33 - Concrete Sand	2.63	1133 lb
Coarse Agg.	ASTM C33 - #57 Limestone	2.79	2070 lb
Water	ASTM C94 - 30 Gallons		250 lb
Air	ASTM C260 - MB-AE-90		3 oz
WR	ASTM C494 - PolyHeed 997		21 oz
		Totals:	4006 lb

*Specified Slump: 5.00" ± 1.50"*

*Designed Units Weight: 148.5 lb/cu.ft.*

*Specified Air: 4.50% ± 1.50%*

*Designed w/cm ratio: 0.45*

**Table 4.12. Modified Class C Concrete for Mix P-1.**

Material	Description	Specific Gravity	Weight (unit/yd)
Cement	ASTM C150 - Type I/II Cement	3.15	374 lb
Alt. Binder	ASTM C618 - Class C Fly Ash	2.63	161 lb
Fine Agg.	ASTM C33 - Concrete Sand	2.63	1333 lb
Coarse Agg.	ASTM C33 - #67 Limestone	2.79	1900 lb
Water	ASTM C94 - 29 Gallons		242 lb
Air	ASTM C260 - MB-AE-90		5 oz
WR	ASTM C494 - PolyHeed 997		22 oz
		Totals:	4010 lb

*Specified Slump: 5.00" ± 1.50"*

*Designed Units Weight: 148.5 lb/cu.ft.*

*Specified Air: 4.50% ± 1.50%*

*Designed w/cm ratio: 0.45*

#### **4.7.2. Concrete Material Properties**

To obtain measured material properties, each concrete batch was sampled to perform the following material properties tests: slump, compressive strength, modulus of elasticity, indirect tensile strength, and modulus of rupture. The fresh concrete was sampled following ASTM C172/C172M standards. Molded cylinder and beam specimens were sampled following ASTM C31/C31M standards.

Slump tests were performed on every batch of concrete following ASTM C143/C143M standards to determine the consistency and flowability of the concrete. The slump tests were performed to ensure compliance with TxDOT specifications for hydraulic cement concrete and to ensure that the fresh concrete would easily consolidate within the tight confines of the steel reinforcing cage and pocket connection. Table 4.13 shows results of the slumps tests.

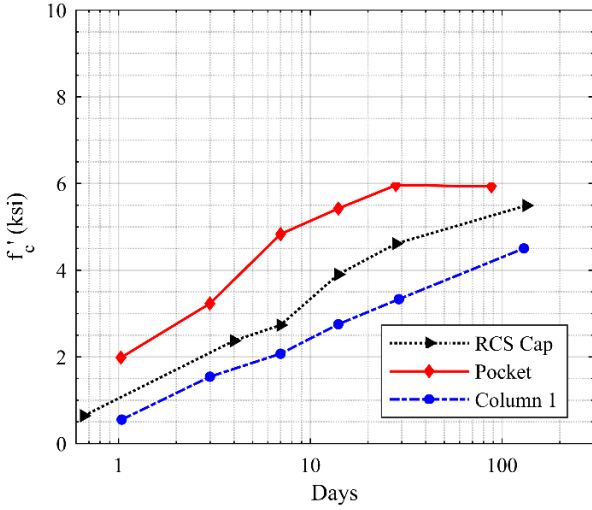
Concrete compressive tests were performed for every batch according to the sampling plan following ASTM C39/C39M standards. During Phase 1, the results of three 6-in. × 12-in. cylinder specimens were averaged, and during Phase 2, the results of three 4-in. × 8-in. cylinder specimens were averaged to indicate the representative compressive strength ( $f'_c$ ). Table 4.13 shows results of the concrete strength tests. Deviation from the target testing dates are noted where applicable in Table 4.13. Figure 4.67 shows plots comparing the concrete compressive strength ( $f'_c$ ) versus age.

Modulus of elasticity ( $E_c$ ), indirect tensile ( $f_{ct}$ ), and modulus of rupture ( $f_r$ ) tests were conducted in conjunction with the 28-day compressive strength tests. These tests were performed following ASTM C469/C469M, ASTM C496/C496M, and ASTM C78/C78M standards, respectively. Additional indirect tensile tests were conducted on, or close to, the date of experimental testing for each specimen. Table 4.14 summarizes the results of the modulus of elasticity, indirect tensile, and modulus of rupture for each batch of concrete. Figure 4.68 shows stress-strain curves for concrete batches used in the fabrication of the RC bent cap and the pretensioned bent caps. During Phase 1, only tested for Batch C was tested for 28-day  $E_c$ ,  $f_r$ , and  $f_{ct}$ . During Phase 2, all batches (J-N) were tested for 28-day  $E_c$ ,  $f_r$ , and  $f_{ct}$ .

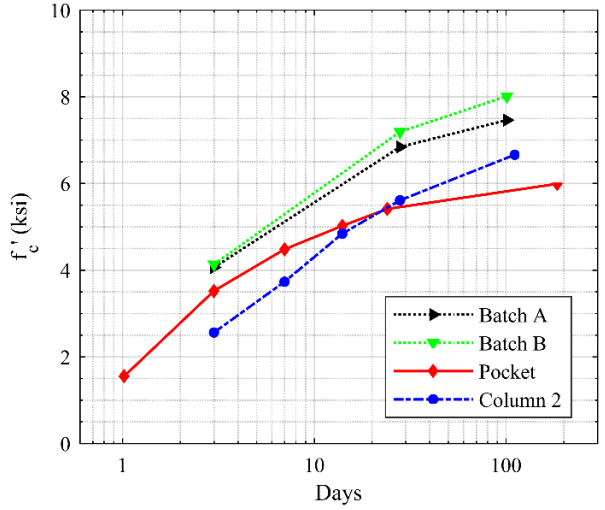
**Table 4.13. Concrete Compressive Strength Results.**

Specimen	Component	Mix ID	Slump (in.)	$f'_c$ (ksi)					
				1 Day	3 Day	7 Day	14 Day	28 Day	Test Day
RCS-16-12	Column 1	C-1	6.25	0.55	1.54	2.07	2.75	**3.33	4.49
	Pocket	P-1	4.50	1.98	3.23	4.83	5.42	5.96	5.93
	Cap	B-1	5.50	0.64	*2.37	2.73	3.90	4.61	5.59
PSS-16-12	Column 2	C-1	7.00	-	2.56	3.73	4.84	5.61	6.66
	Pocket	P-2	5.50	1.55	3.52	4.48	5.02	-	5.41
	Batch A	B-2	7.00	-	4.06	-	-	6.84	7.46
	Batch B	B-2	7.00	-	4.13	-	-	7.19	8.01
PSS-16-24	Column 4	C-1	8.00	1.04	-	3.33	4.48	**5.37	6.34
	Pocket	P-3	6.50	1.82	-	5.30	5.68	6.61	6.61
	Batch B	B-2	7.00	-	4.13	-	-	7.19	-
	Batch C	B-2	7.00	-	4.82	5.85	6.51	7.65	-
	Batch D	B-2	7.00	-	4.60	-	-	7.55	-
PSV-16-12	Column 3	C-1	8.00	1.04	-	3.33	4.48	**5.37	5.92
	Pocket	P-3	5.50	0.91	2.48	-	3.78	**4.79	4.72
	Batch E	B-2	7.00	-	3.85	-	-	7.90	8.82
	Batch F	B-2	7.00	-	4.04	-	-	7.65	8.38
PSV-28A	Column 5	C-1	-	0.77	-	4.28	5.27	5.81	7.01
	Pocket	P-3	8.00	-	*3.86	4.52	5.18	5.56	-
	Batch J	B-2	7.00	-	-	5.64	-	6.91	8.28
	Batch K	B-2	7.50	-	-	5.37	-	6.94	8.03
	Batch L	B-2	7.50	-	4.24	4.70	5.45	6.32	7.19
PSV-28B	Column 6	C-1	-	0.77	-	4.28	5.27	5.81	7.37
	Pocket	P-3	8.50	1.67	*5.12	5.83	†6.96	7.29	6.96
	Batch L	B-2	7.50	-	4.24	4.70	5.45	6.32	7.85
	Batch M	B-2	7.25	-	-	4.54	-	6.25	7.50
	Batch N	B-2	-	-	-	4.92	-	6.44	8.01

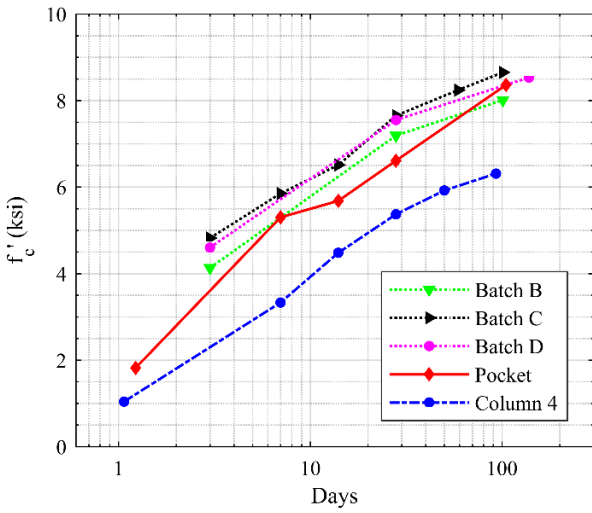
\*4 day, †15 day, \*\*29 day



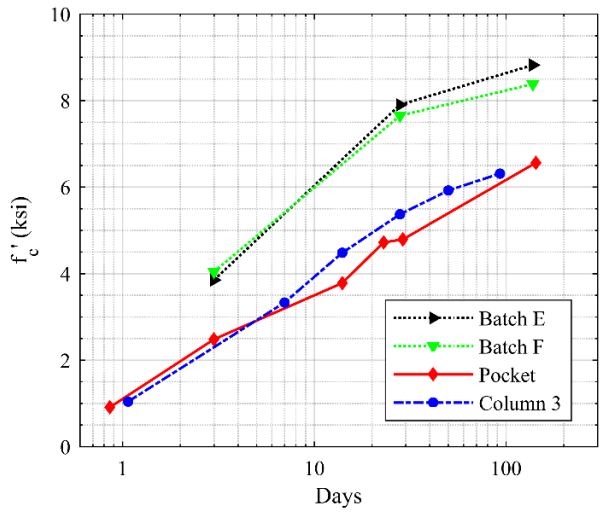
(a) RCS-16-12



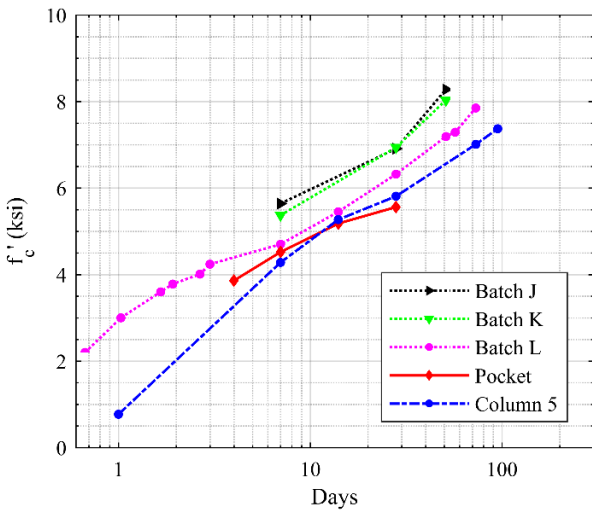
(b) PSS-16-12



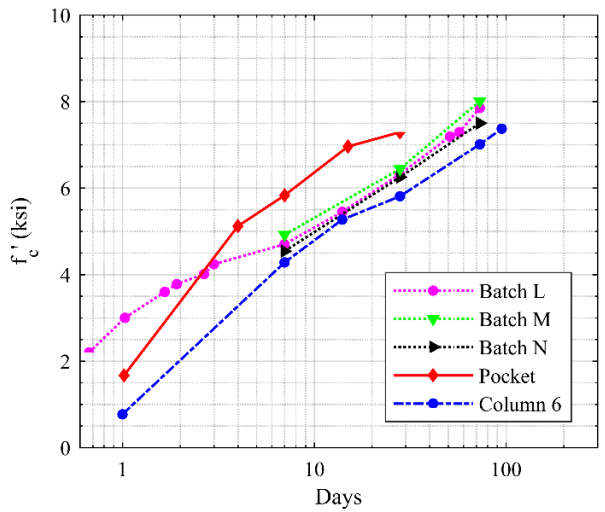
(c) PSS-16-24



(d) PSV-16-12



(e) PSV-28A



(f) PSV-28B

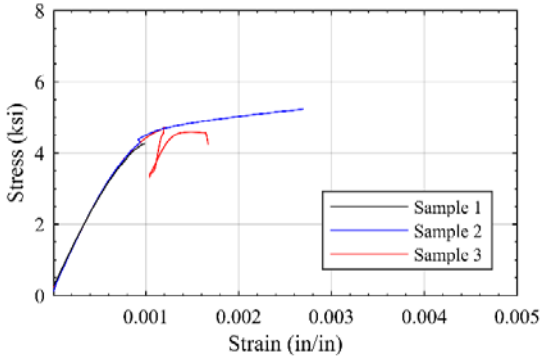
Figure 4.67. Concrete Compressive Strength vs. Age.

**Table 4.14. Modulus of Elasticity, Indirect Tensile, and Modulus of Rupture Results.**

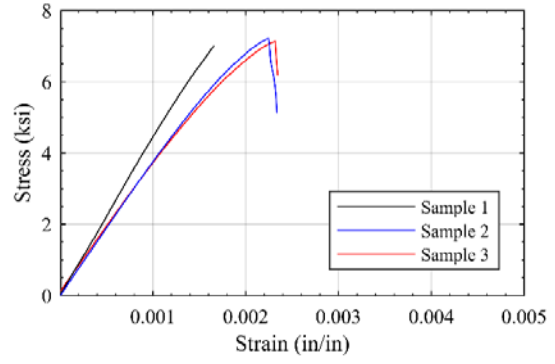
Specimen	Component	$E_c$ (ksi)		$f_{ct}$ (ksi)		$f_r$ (ksi)	
		28 Day	Test Day	28 Day	Test Day	28 Day	Test Day
RCS-16-12	Column 1	**4927	5574	**0.68	0.64	**0.59	0.74
	Pocket	-	6024	-	0.83	-	0.89
	Cap	5402	6195	0.67	0.73	0.67	0.79
PSS-16-12	Column 2	5447	6340	0.77	0.77	0.93	0.92
	Pocket	-	5840	-	0.79	-	0.85
	Batch A	-	4920	-	0.95	-	-
	Batch B	-	3914	-	0.87	-	-
PSS-16-24	Column 4	**5447	-	**0.93	-	**0.77	-
	Pocket	5610	5610	0.78	0.78	0.96	0.96
	Batch B	-	-	-	-	-	-
	Batch C	3976	-	0.83	-	0.85	-
	Batch D	-	-	-	-	-	-
PSV-16-12	Column 3	-	5333	**0.72	0.72	**0.84	0.92
	Pocket	**5027	4696	**0.71	0.63	**0.74	0.77
	Batch E	-	-	-	0.91	-	-
	Batch F	-	-	-	0.90	-	-
PSV-28A	Column 5	5290	-	0.75	0.91	0.86	-
	Pocket	5447	-	0.78	0.78	0.88	-
	Batch J	4066	-	-	0.97	-	-
	Batch K	3837	-	-	0.90	-	-
	Batch L	3764	-	0.79	0.86	0.86	-
PSV-28B	Column 6	5290	-	0.75	-	0.86	-
	Pocket	5848	-	0.93	0.81	0.87	-
	Batch L	3764	-	0.79	0.89	0.86	-
	Batch M	3941	-	-	0.87	-	-
	Batch N	3988	-	-	0.89	-	-

\*\*29 day

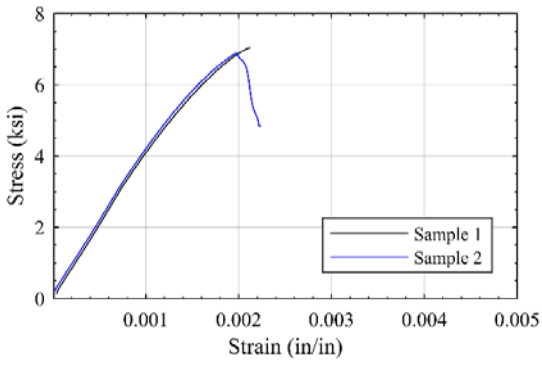




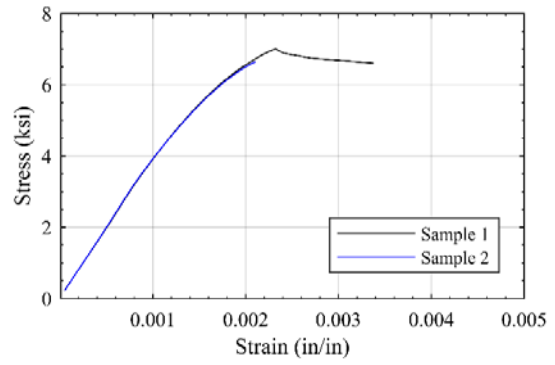
(a) RCS-16-12 Bent Cap



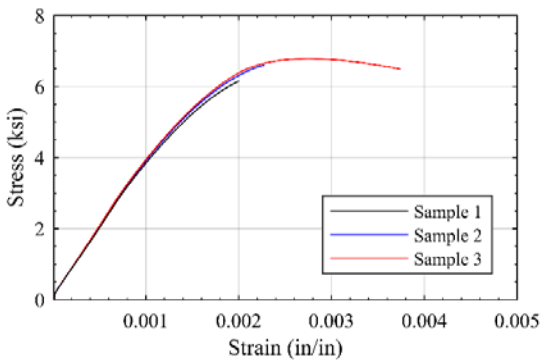
(b) Batch C



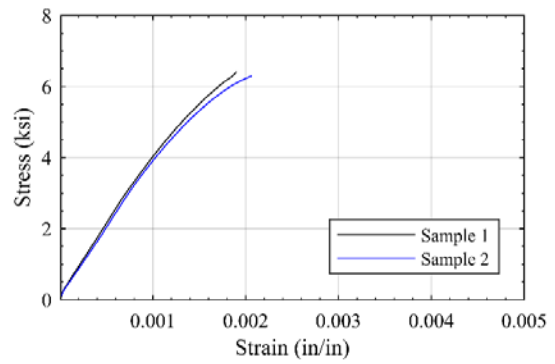
(c) Batch J



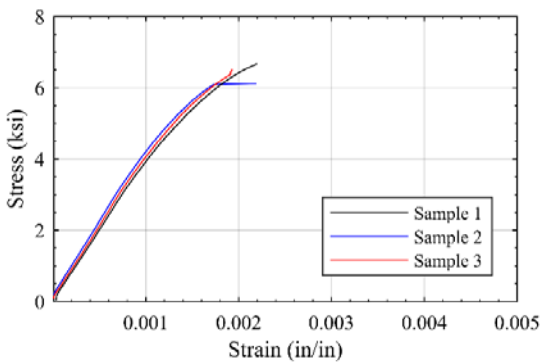
(d) Batch K



(e) Batch L



(f) Batch M



(g) Batch N

**Figure 4.68. 28-Day Bent Cap Concrete Stress-Strain Curves.**

### 4.7.3. Steel Material Properties

Tensile testing of reinforcing bar specimens was conducted to determine yield strength ( $f_y$ ), ultimate strength ( $f_u$ ), modulus of elasticity ( $E_s$ ), and yield strain ( $\epsilon_y$ ) of the mild steel reinforcement used in the construction of the columns and pretensioned bent caps. Rebar specimens were sent to Applied Technical Services for testing. Tensile tests were conducted on samples of #5 transverse reinforcing bars (Phase 1 and Phase 2), #8 longitudinal reinforcing bars (RCS-16-12), and #11 dowel bars. Three specimens from each rebar type were tested, and the results for each parameter were averaged to determine the material properties of the steel. Table 4.15 summarizes the results.

**Table 4.15. Steel Tensile Test Results.**

Rebar	$f_y$ (ksi)	$f_u$ (ksi)	$E_s$ (ksi)	$\epsilon_y$ (in./in.)
#5 (Phase 1)	64	103	28,480	0.00225
#5 (Phase 2)	65	105	29,273	0.00222
#8	66	107	29,497	0.00225
#11	68	106	28,147	0.00240

## 4.8. EXPECTED STRENGTHS

Before conducting the experimental test, expected strengths of the specimens were calculated to assist in development of the load protocols and result analysis. Measured test days material properties from Section 4.7 were used where possible. Both flexure and shear-flexure strengths were considered.

### 4.8.1. Flexural Strength

Flexural moment strength includes zero tension, cracking, yield, and nominal moment capacities. For all calculations, the prestressing force is computed as:

$$F = nT_{strand} \quad (4-1)$$

where  $n$  = number of strands;  $T_{strand}$  = prestressing force per strand, and is calculated by:

$$T_{strand} = f_{pbt} A_{ps} (1 - \Delta f_{pT}) \quad (4-2)$$

in which  $f_{pbt}$  = stress limit in low relaxation strand immediately prior to transfer ( $= 0.75f_{pu}$ );  $f_{pu}$  = specified tensile strength of prestressing strand ( $= 270$  ksi, AASHTO LRFD Table 5.4.4.1-1);  $A_{ps}$  = area of each strand ( $= 0.217$  in.<sup>2</sup> for 0.6-in. diameter strand);  $\Delta f_{pT}$  = prestress loss in pretensioned members (20 percent).

The cracking moment is calculated by:

$$M_{cr} = \frac{I_g}{y_t} \left( f_r + \frac{F}{A} \right) \quad (4-3)$$

in which  $f_r$  = modulus of rupture of concrete ( $= 0.24\sqrt{f'_c}$  in accordance with AASHTO LRFD 5.4.2.6 for design unless material test is conducted);  $I_g$  = gross moment of inertia;  $y_t$  = distance from the neutral axis to the extreme tension fiber (in.); and  $A$  = area of gross section.

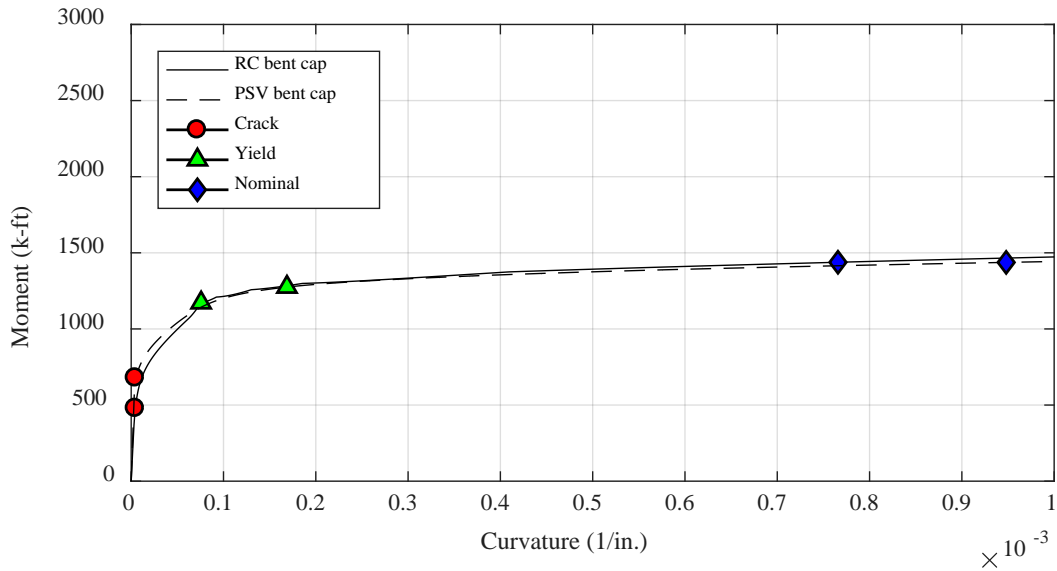
Yield strength ( $M_y$ ) and nominal strength ( $M_n$ ) are computed by fiber section analysis using OpenSees (Version 2.4.6). In the analysis, concrete model with linear tension softening (Yassin 1994) is used for concrete, and bilinear steel model and Guiffre-Menegotto-Pinto model with isotropic strain hardening (Filippou et al. 1983) are used for reinforcing bar and strand, respectively. Yield is defined as the point where the strain at the level of the extreme tension layer of steel is equal to the yield strain ( $\epsilon_y = 0.00207$  for mild steel and  $\epsilon_{py} = 0.012$  for prestressed strand). Nominal is defined as the point where the extreme compression fiber reaches a strain of 0.003.

Flexural moment capacities for positive and negative regions account for the concrete strengths of the different batches. For voided specimens (PSV-16-12, PSV-28A, and PSV-28B), negative and positive moment regions were considered as solid and void sections, respectively. Although different concrete batches were used in the pocket connection, that section is assumed to be solid for simplicity. Cracking ( $M_{cr}$ ), yield ( $M_y$ ), and nominal ( $M_n$ ) moment strengths of all specimens were calculated and summarized in Table 4.16 without considering a reduction factor. In the calculation, material properties in the test day were used for concrete compressive strength ( $f'_c$ ), and  $0.126\sqrt{f'_c}$  (ksi) was used for the concrete tensile strength ( $f'_t$ ) (ACI 2014; Mehta and Monteiro 2004).

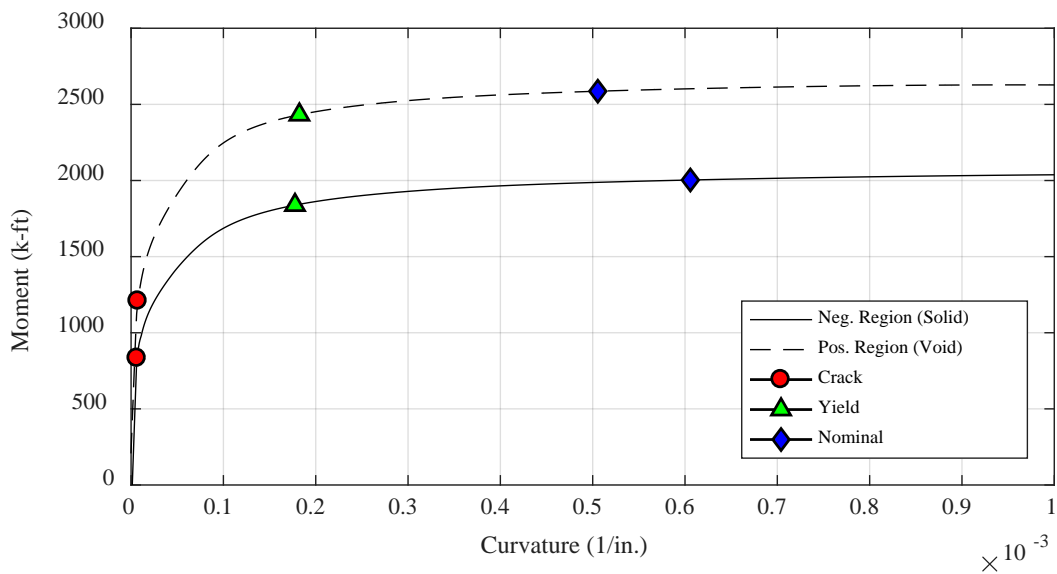
**Table 4.16. Summary of Expected Moment Strengths.**

<b>Specimen</b>	<b>Region</b>	$f'_c$ <b>(ksi)</b>	$f'_t$ <b>(ksi)</b>	$M_{cr}$ <b>(k-ft)</b>	$M_y$ <b>(k-ft)</b>	$M_n$ <b>(k-ft)</b>
RCS-16-12	Both	5.49	0.30	317	1,066	1,421
PSS-16-12	Positive	7.46	0.35	684	1,270	1,427
	Negative	8.01	0.36	697	1,275	1,437
PSS-16-24	Positive	8.27	0.36	703	1,278	1,444
	Negative	8.34	0.37	704	1,279	1,446
PSV-16-12	Positive	8.82	0.37	784	1,282	1,457
	Negative	8.38	0.38	705	1,276	1,446
PSV-28A	Positive	8.28	0.34	891	1,857	2,021
	Negative	7.19	0.36	1,148	2,432	2,587
PSV-28B	Positive	7.85	0.36	882	1,848	2,004
	Negative	8.01	0.35	1,168	2,453	2,630

Figure 4.69 shows full moment curvature responses obtained using OpenSees for Phases 1 and 2 bent caps. On account of negligible differences among PSC bent caps in Phase 1, a moment curvature response of PSS-16-12 specimen was selected as a representative of PSC bent caps and shown in the figure along with the response of RCS-16-12 specimen (Figure 4.69[a]). Similarly, the PSV-28A represented Phase 2 specimens, and both negative (solid) and positive moment (void) capacities are provided in Figure 4.69(b).



(a) Phase 1 specimens (PSS-16-12 represents PSC bent caps)



(b) Phase 2 specimens (PSV-28A is shown)

**Figure 4.69. Full Moment-Curvature Response for Phases 1 and 2.**

#### 4.8.2. Shear Strength

Expected cracking and nominal shear strengths for all specimens were presented in this section. The cracking shear was calculated by analyzing the principle planes and stresses using Mohr's Circle. It is based on the assumption that shear cracking occurs when the principal tensile stresses exceed the tensile strength of the concrete at the centroidal axis of the cross-section (ACI 1965). Cracking shear strength was considered for sections with and without the interior void. The

calculation of cracking shear can be conservative since the considered axis is assumed to be subjected to pure shear force without considering the effect of flexural moment (Kani 1966; 1967). The shear cracking is calculated by:

$$V_{cr} = \frac{I_g b_v}{Q} \sqrt{f_t^2 + f_t \left( \frac{nT}{A} \right)} \quad (4-4)$$

in which  $I_g$  = moment of inertia of the gross concrete section about the centroidal axis, neglecting the reinforcement (in.<sup>4</sup>);  $b_v$  = width of web adjusted for the presence of ducts (in.) or width of the interface (in.);  $Q$  = first moment of area (in.<sup>3</sup>);  $f_t$  = tensile strength of concrete (ksi);  $n$  = number of strands provided from the flexural design;  $T$  = prestressing force per strand after loss (kip); and  $A$  = area of cross section (in.<sup>2</sup>).

Nominal shear strengths were calculated for all specimens in accordance to LRFD sectional design method using tables in Appendix B5 of AASHTO LRFD (2014). The AASHTO LRFD design method, derived from MCFT (Vecchio and Collins 1986; 1988; Bentz et al. 2006), takes the interaction of shear and flexure into account.

In calculation of both cracking and nominal shear strengths, test day material properties were used for the compressive strength of concrete, and  $0.126\sqrt{f'_c}$  was regarded as the tensile strength of concrete. Test data of bending moment, shear force, and horizontal forces applied to the specimen were taken into account in the calculation. For PSC bent caps that consisted of different concrete batches, a concrete batch used in middle concrete layer was used in the calculation. Table 4.17 summarizes the cracking and nominal shear strengths.

**Table 4.17. Expected Cracking and Nominal Shear Strengths Using Actual Material Properties for All Specimens.**

Specimen	$f'_c$ (ksi)	$f_t$ (ksi)	$V_{cr}$ (kips)		$V_n$ (kips)		
			Solid	Void	Critical 1	Critical 2	Critical 3
RCS-16-12	5.49	0.30	352	–	378	359	359
PSS-16-12	7.46	0.35	565	–	513	378	371
PSS-16-24	8.22	0.36	586	–	436	324	320
PSV-16-12	8.60	0.37	596	289	538	231	390
PSV-28A	8.03	0.36	664	331	432	303	447
PSV-28B	7.50	0.35	648	324	442	499	413

In the table, nominal shear strengths were calculated at the three shear critical points. For Phase 1, critical sections are 1) interior face of exterior column, 2) interior girder location, and 3) face of interior column. PSV-16-12 specimen has a significantly less shear strength at critical section 2 due to the void in the span. Phase 2 critical sections are 1) interior face of exterior column, 2) adjacent to column where an interior void starts, and 3) interior girder location. PSV-28A has an interior void in Critical 2 section, but PSV-28B has a solid section, resulting in the different nominal shear strength in that region.

## 5. EXPERIMENTAL TEST PROGRAM: RESULTS

This chapter summarizes results from the experimental test program. Section 5.1 discusses the load patterns, and the visual observation and overview of the test are presented in Section 5.2. Section 5.2 summarizes crack damage by each phase, and test results were compared by design variables (see test matrix in Table 4.7) in Section 5.3. Finally, Section 5.5 has general findings.

In discussing results of tests, regions of the bent cap are referred to by the regions shown in Figure 5.1. Positive and negative moment regions are a function of demands. Overhang, joint, span, and square end are used to describe location of the observed damage.

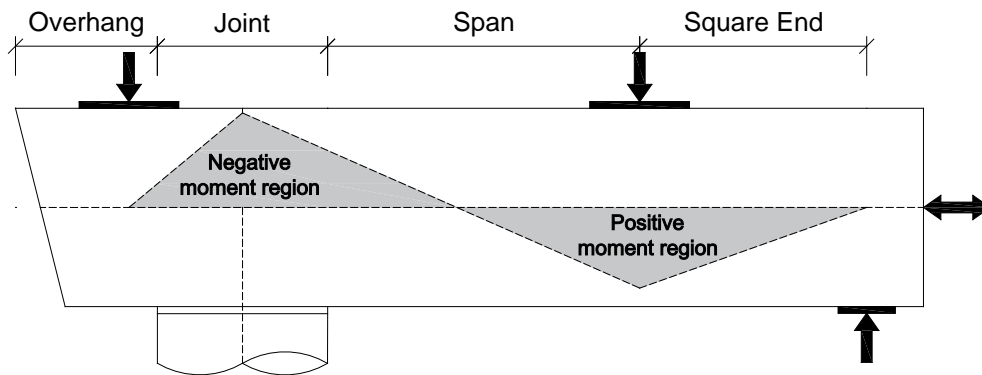


Figure 5.1. Moment Region Location.

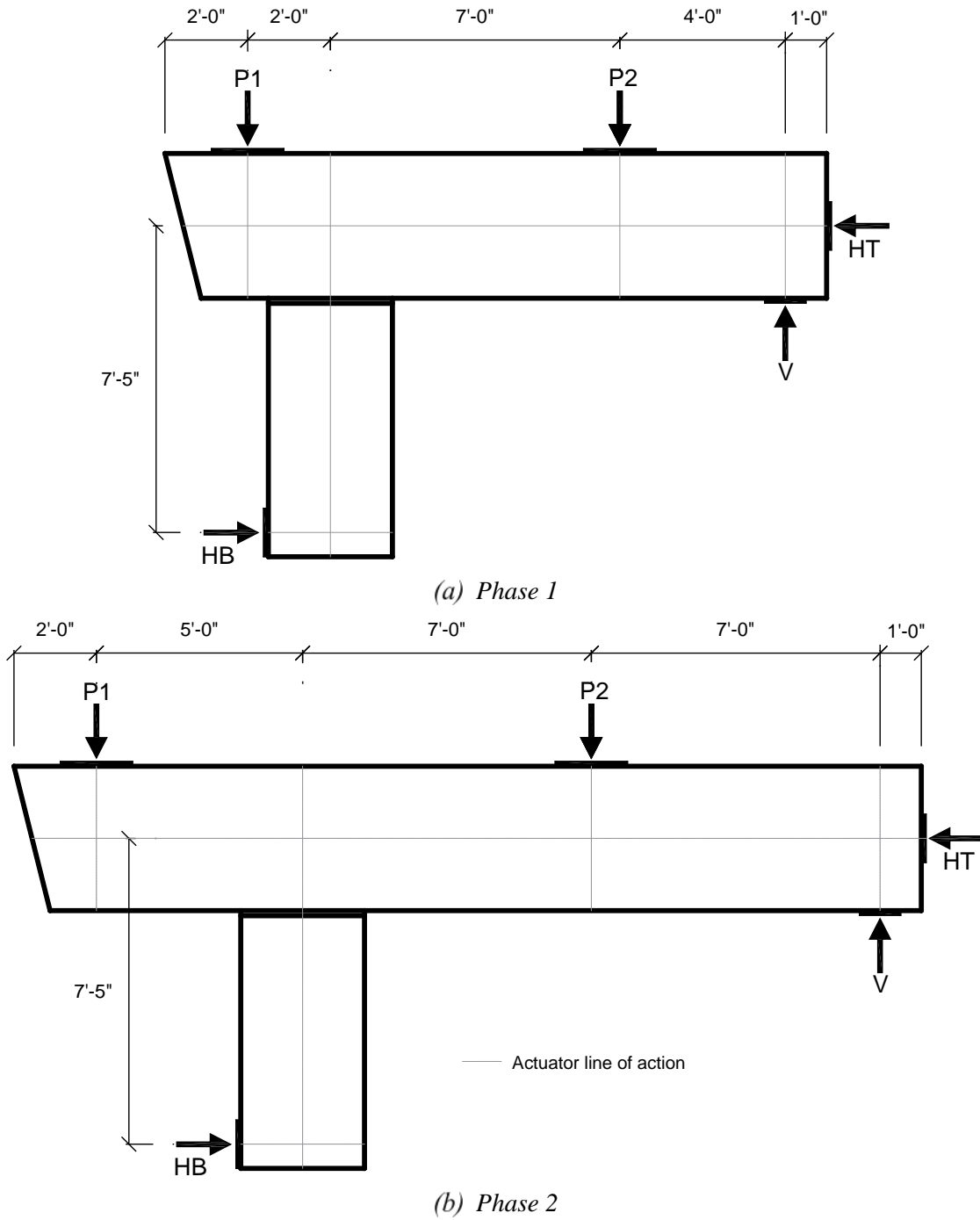
### 5.1. SPECIMEN LOADING

Figure 5.2 shows the forces applied to the specimens in Phases 1 and 2, respectively. Although Phases 1 and 2 had different geometries, all actuators were controlled the same. Two vertical actuators, P1 and P2, simulate girder loads. A third vertical actuator, V, simulates shear at the inflection point. The upper horizontal actuator, HT, at the square end provided an axial load in the bent cap. The lower horizontal actuator, HB, was slaved to HT to provide equilibrium of horizontal forces on the specimen.

All specimens were tested under multiple load patterns. The main pattern (Pattern A) generated shear and moment demands characteristic of multicolumn bridge bent caps. Patterns B and E were selected to generate the largest moment demands permitted by the experimental test setup. Joint opening and closing were conducted to test the bent cap–column connection performance in Patterns C and D, respectively. Finally, Pattern F was used to fail the specimens by using large axial forces in the bent caps. Figure 5.3 shows the moment diagrams for each load pattern. To



achieve each load pattern, P1, P2, V, and HT actuators were controlled through a mix of force and displacement control settings. Table 5.1 summarizes the actuator controls for each load pattern. The following paragraphs provide additional details.



**Figure 5.2. Schematic Drawing of Specimen with Actuator Forces.**

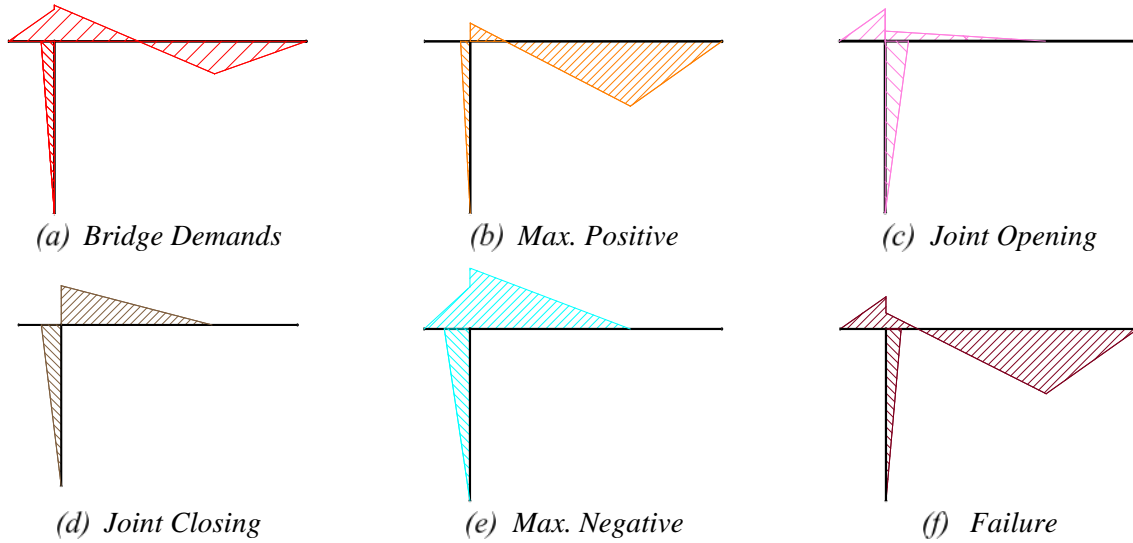


**Figure 5.3. Load Pattern Moment Diagrams.**

**Table 5.1. Actuator Control Pattern.**

Load Pattern	Description	P1 (kips)	P2 (kips)	V (kips)	HT (HB) (kips)
A	Bridge Demands	160* (160 <sup>†</sup> )	160* (160 <sup>†</sup> )	0.48P2* (0.21P2 <sup>†</sup> )	$\Delta = 0$
		270* (262 <sup>†</sup> )	270* (262 <sup>†</sup> )		
		400* (380 <sup>†</sup> )	400* (380 <sup>†</sup> )		
		Max. Capacity	Max. Capacity		
B	Max. Positive Moment	0	Max. Capacity	0.64P2* (0.48P2 <sup>†</sup> )	$\Delta = 0$
C	Joint Opening	$\Delta = 0$	0	0	100 (Tension)
D	Joint Closing	0	$\Delta = 0$	0	100 (Compression)
E	Max. Negative Moment	Max. Capacity	$\Delta = 0$	0	100 (Compression)
F	Failure	Max. Capacity	Max. Capacity	Max. Capacity	105 (Tension)

\*Actuator forces for Phase 1 test setup; <sup>†</sup>Actuator forces for Phase 2 test setup;  $\Delta$ : Displacement Control governed by zero change in displacement; P1, P2, and V compression only.

Pattern A generated shear and moment demands characteristic of multicolumn bent caps. To generate the demands seen in Figure 5.3(a), P1 and P2 increased simultaneously to simulate girder demands. Although the simultaneous loads in both actuators differed from AASHTO LRFD specifications, which have different live load factors for exterior and interior girders, this loading was in accordance with TxDOT design practice. To generate the desired shear demands at the span, V was set to be a factor  $\alpha$  of P2. The HT actuator was set to zero displacement. For the prototype discussed in Section 4.2.2,  $\alpha$  was set to 0.48 and 0.21 for Phase 1 and 2, respectively. In Pattern A, P1 and P2 forces of 160 kips generated dead load  $P_D$  for both phases. Live load,  $P_L$ , was 110 kips and 102 kips, respectively. Service limit state (SLS) demands were the sum of dead and live loads. The ULS demands were based on  $1.25P_D + 1.75P_L$  in accordance with AASHTO LRFD 3.4.1. In both phases, calculated ULS values were rounded up slightly for simplicity, resulting in girder loads of 400 kips and 380 kips for Phases 1 and 2, respectively. The maximum capacities of the actuators corresponded to 140 percent and 150 percent ULS in Phases 1 and 2, respectively.

Pattern B generated the maximum positive demands in the span of the bent cap that were achievable with the current test setup. Creating the demands represented in Figure 5.3(b) required locking HT in displacement control, completely removing P1 and increasing P2 to its maximum capacity while V was set to force control at  $0.64P_2$  and  $0.48P_2$  for Phases 1 and 2, respectively.

Patterns C and D provided demands testing the connection between the bent cap and column by opening and closing the joint at the interior face of the column. To achieve the demands seen in Figure 5.3(c), P1 was locked in displacement control to allow a reaction at the overhang while HT was increased to its maximum tensile capacity. The P2 and V loads were not used. The loads that generated the demands seen in Figure 5.3(d) were the reverse of Pattern C; P2 was locked in displacement control and HT was increased to its maximum capacity in compression. The P1 and V loads were not used.

Pattern E generated the maximum negative moment demands achievable with the current test setup. Creating the demands represented in Figure 5.3(e) required lowering P2 to make contact with the specimen acting as a break and increasing P1 to its maximum capacity while setting HT to its maximum compression capacity with V completely removed from the specimen.

Pattern F was the final load pattern and created the necessary demands to study the different failure mechanisms between the reinforced and pretensioned concrete bent cap specimens. To cause failure in each specimen, actuators P1, P2, HT (tension) were set to force control at their respective maximum load capacities while V was set to displacement control acting as a reaction. Control of V was changed to force control near the final stages of Pattern F to increase the force provided by P2.

Pattern A was applied first, with loads applied incrementally from dead to 140 percent ULS demands. The order of the subsequent load patterns varied, and in some instances, patterns were repeated. Appendix E contains the details of pattern application on each specimen.

In general, Phase 1 specimens were loaded in order of Bridge Demands up to 140 percent ULS (Pattern A) → Maximum Positive Moment Demands (Pattern B) → Joint Opening (Pattern C) → Joint Closing (Pattern D) → Maximum Negative Moment Demands (Pattern E) → Failure (Pattern F). Creep tests were done for a few hours and unloading to dead load or SLS was conducted to check the closure of cracks while applying Bridge Demands (Pattern A).

Phase 2 specimens were loaded by the order of Bridge demands up to ULS (Pattern A) → Joint Opening (Pattern C) → Joint Closing (Pattern D) → Bridge demands up to 150 percent ULS (Pattern A) → Maximum Positive Moment Demands (Pattern B) → Maximum Negative Moment Demands (Pattern E). In Phase 2 tests, Pattern A was applied up to only ULS to avoid severe damage in the overhang regions before conducting joint performance tests (Patterns C and D). For this reason, 150 percent ULS was applied after the joint performance tests. Unloading to dead load or ULS was also conducted during application of Bridge Demands, but creep test was not conducted in Phase 2.

## **5.2. OVERVIEW OF EXPERIMENTAL RESULTS**

During the experimental testing, it was possible to closely observe the specimens for the appearance of cracks. All longitudinal and transverse reinforcement and the corrugated pipe were drawn in pencil on the front face of each specimen prior to the test. The maximum width of each crack was measured using a crack comparator and documented. Figure 5.4 and Figure 5.5 show the extent of cracking and damage seen at the failure load patterns on the back face and on the most severely damaged region for all specimens, respectively.

All PSC bent cap specimens (PSS-16-12, PSS-16-24, PSV-16-12, PSV-28A, and PSV-28B) displayed remarkably improved flexural cracking control capacity in both positive and negative moment regions by delaying the onset of the cracking and also limiting crack widths compared to RC bent cap specimen (RCS-16-12). Only hairline or 0.004-in. wide cracks formed in the PSC bent caps under design loads. All voided specimens (PSV-16-12, PSV-28A, and PSV-28B) displayed shear cracks along the interior void in the span before design loads. Flexure-shear failures were observed in all solid specimens showing severe crack damage along the compression strut at span region in RC bent cap (RCS-16-12) and at the square end region in PSC bent caps (PSS-16-12 and PSS-16-24). Failure of voided specimens (PSV-16-12, PSV-28A, and PSV-28B) involved crushing of concrete in the compression zone under P2 in PSV-16-12 or at the column in PSV-28A and PSV-28B. Crack maps of Phase 1 specimens and of all voided specimens by each load stage are drawn in Figure 5.6 and Figure 5.7, respectively.



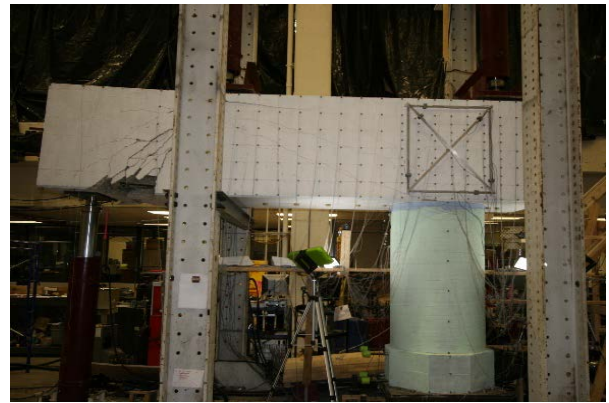
(a) RCS-16-12



(b) PSS-16-12



(c) PSS-16-24



(d) PSV-16-12



(e) PSV-28A



(f) PSV-28B

**Figure 5.4. Visual Observation at Failure (Back Face).**



(a) RCS-16-12



(b) PSS-16-12



(c) PSS-16-24



(d) PSV-16-12

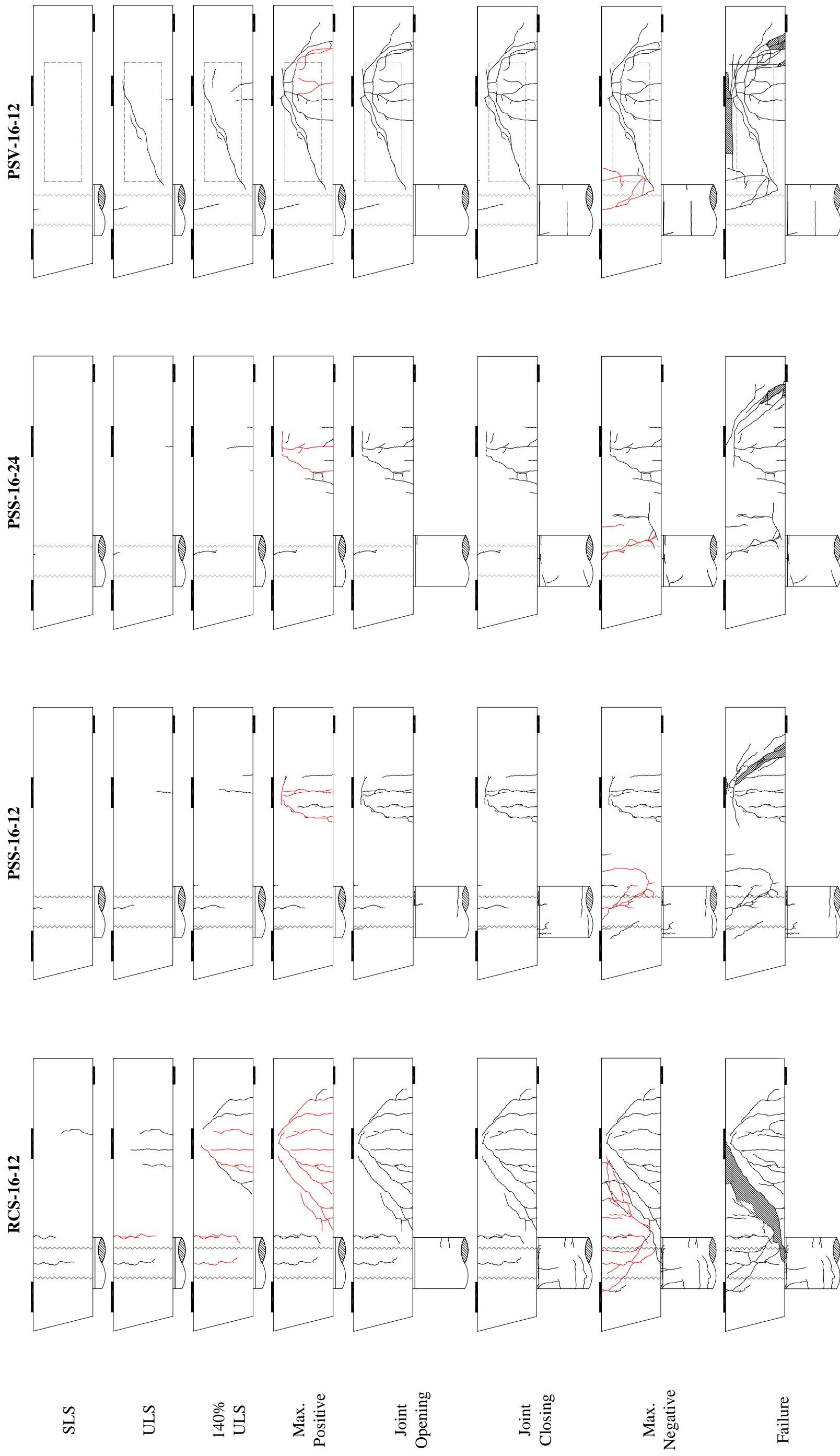


(e) PSV-28A



(f) PSV-28B

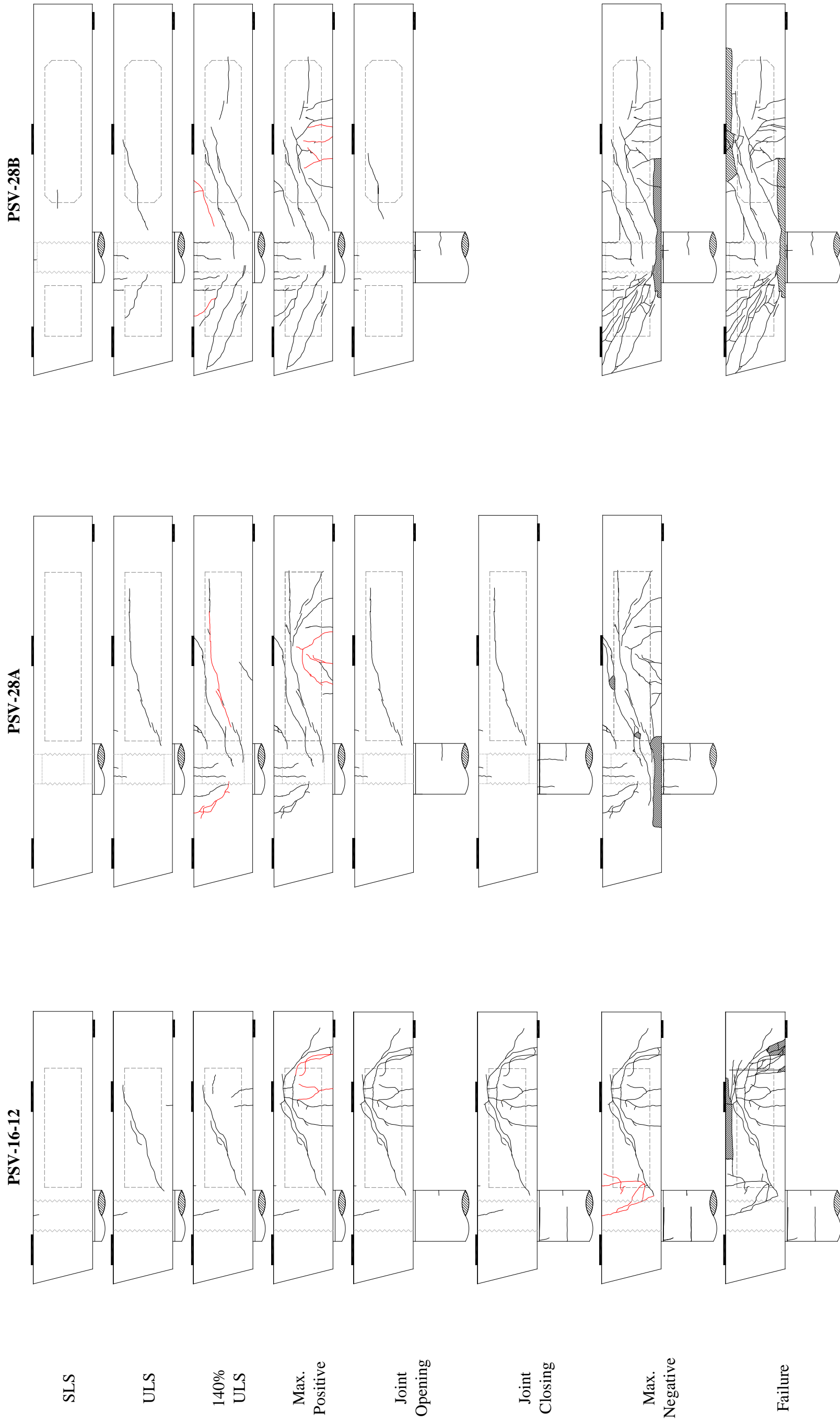
**Figure 5.5. Visual Observation at Failure (Failed region).**



\* Note: Crack width exceeding AASHTO crack width limit colored in red

Figure 5.6. Crack Maps of Phase 1 Specimens.





\* Note: Crack width exceeding AASHTO crack width limit colored in red; Phase 2 specimens failed during max. negative demand; Additional failure load was applied to PSV-28B

**Figure 5.7. Crack Maps of Voided Specimen Crack Damage Summary.**

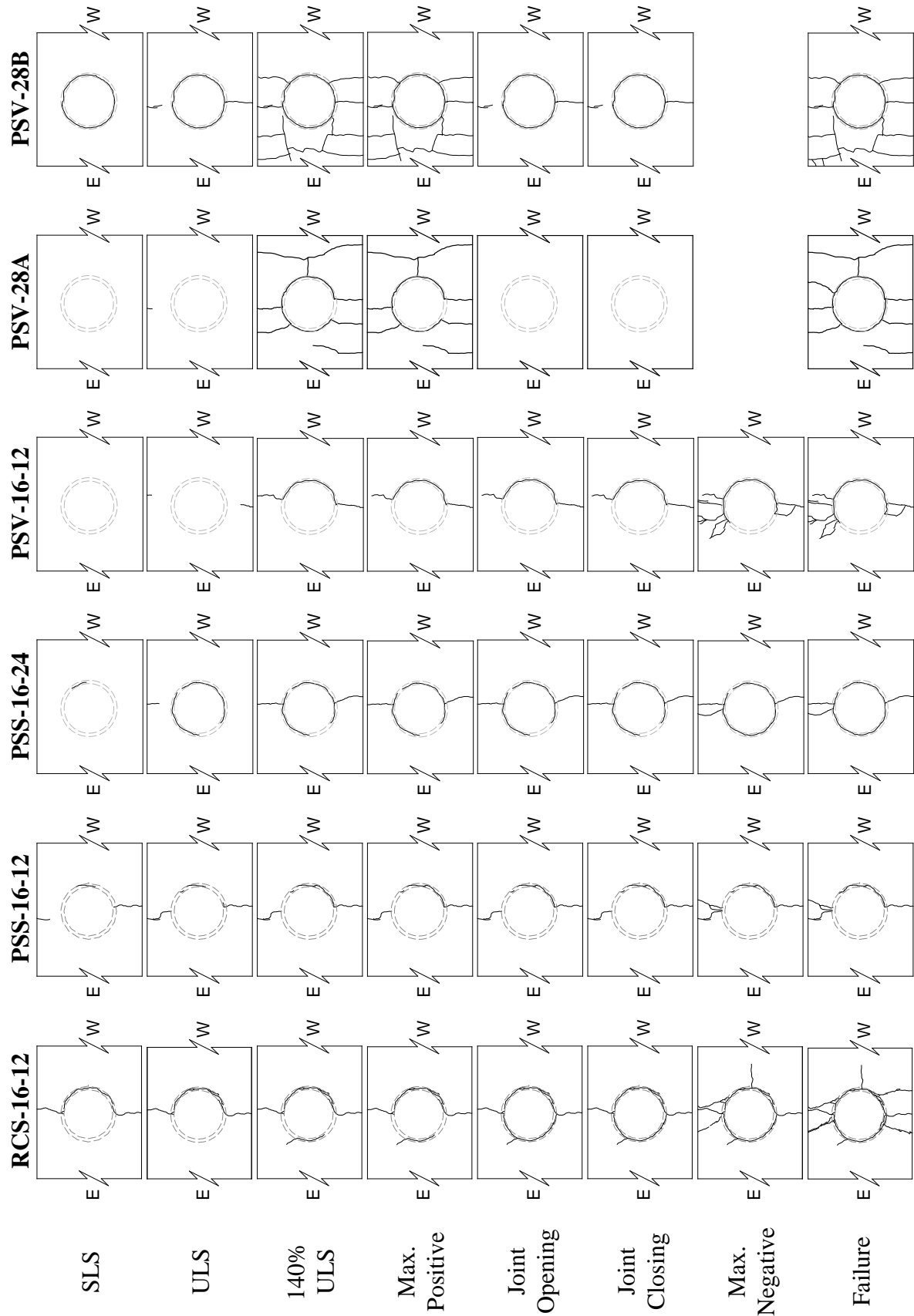


**Figure 5.8. Pocket Crack Propagation.**

Cracks are categorized with reference to the AASHTO Standard Specifications Section C.5.7.3.4 crack width limit of 0.017-in. (Class 1 exposure). Damage progressions of Phases 1 and 2 are presented, respectively, in Sections 5.2.1 and 5.2.2 with overall description.

Table 5.2 and Table 5.3 include crack formation in each region, maximum crack width, and comparison of the crack width to the AASHTO crack limit by each load case.

### **5.2.1. Phase 1**

All specimens had no cracks under dead load. At SLS demands ( $P1\&P2 = 270$  kips), the negative and positive moment regions cracked in the RC bent cap. The maximum width was 0.01-in. Only the negative moment region cracked in PSC bent caps (PSS-16-12, PSS-16-24, and PSV-16-12). All cracks were hairline cracks.

While loading to ULS demands, a diagonal shear crack appeared between the column face and P2 actuator in PSV-16-12 specimen. This type of shear crack was not observed in the other bent cap specimens with a solid section at this load stage.

Under ULS demands, crack extension and new crack formation were observed in the negative and positive moment regions in all specimens. The maximum crack width of RCS-16-12 (0.02-in.) exceeded AASHTO crack limit while that of PSC bent cap specimens were below the limit. The shear crack of PSV-16-12 specimen was along the interior void following the compression strut path between the column and P2 actuator.

During the creep test, crack length and width growth was observed in the RC bent cap. Slight expansion or formation of new hairline cracks were noted in the PSC bent caps.

After unloading to dead load, hairline cracks were closed and large cracks were reduced to 0.01-in. width in RCS-16-12. All cracks were closed or reduced to hairline cracks in PSS-16-24 and PSV-16-12. PSS-16-12 was unloaded to an equivalent dead load following Pattern B, not Pattern A as in other PSC specimens, thus cracks did not close as much.

At 140 percent ULS demands, diagonal shear cracks formed in RCS-16-12 between the column and P2 actuator, and P2 actuator and V actuator. Significant extension of existing cracks and new flexural cracks formation on both moment regions were also detected. The maximum crack width

was 0.04-in., well beyond the AASHTO crack limit. All PSC bent caps showed new crack formations in both moment regions and length extension following slight width growth in common. PSV-16-12 displayed shear crack extension with a horizontal crack formation below the P2 actuator. The maximum crack widths of PSC specimens ranged from 0.008-in. to 0.016-in., and those were still within AASHTO crack limit.

Under maximum positive moment demands, all specimens showed significant crack length and width extension with the formations of new cracks in the positive moment region. Additional diagonal cracks formed between the column face and P2 actuator in RCS-16-12, and between P2 and V actuators in PSV-16-12. Maximum crack widths for all specimens exceeded AASHTO crack limit in this stage. For PSS-16-12, the load was unloaded to equivalent dead load in span, and all cracks were closed or reduced to hairline cracks.

Significant crack growth was noted in all specimens under maximum negative moment demands. For RCS-16-12, diagonal shear cracks were present in both the overhang and span extending from both P1 and P2 to the interior face of the column. These shear cracks were similar to the shape of a compression strut and extended along the whole depth of the bent cap. For PSC specimens, no diagonal crack formed along the compression strut but a flexural-shear crack extended along the almost whole bent cap depth. Measured maximum crack widths for all specimens were 0.2-in. regardless a type of concrete, substantially exceeding AASHTO crack limit. These large cracks showed evidence that significant yielding of both mild steel and strand longitudinal reinforcement had occurred.

Load Pattern B and Pattern C applied joint opening and closing demands, respectively, to test the performance of the bedding layer and dowel bars in the connection of the column and the bent cap. Figure 5.9 shows the crack formation during joint closing and joint opening for both RCS-16-12 and PSS-16-12.

Joint opening demands created cracks at the interior face of the column of RCS-16-12 with a maximum width of 0.012-in. No cracks were observed in the bedding layer. During PSS-16-12, cracks in the column and the bedding layer formed with a maximum measured width of 0.004-in. Joint closing demands during RCS-16-12 created hairline cracks in the exterior face of the column and 0.026-in. cracks in the bedding layer that propagated both horizontally and vertically. During

PSS-16-12, hairline cracks formed on the exterior face of the column and the bedding layer, which also propagated horizontally and vertically. No signs of pull out from the dowel bars were observed during either joint opening or joint closing demands on either specimen. Results of joint opening and joint closing tests were consistent for the subsequent pretensioned specimens.

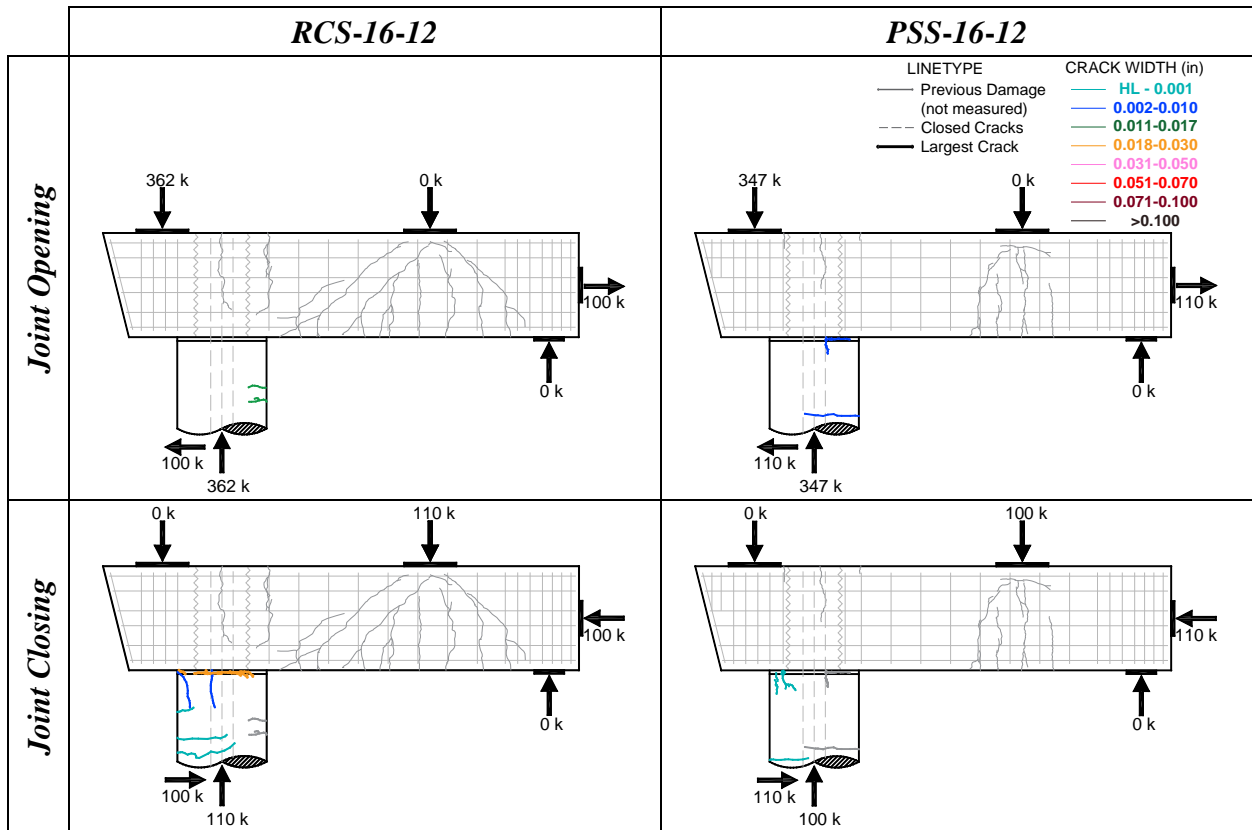


Figure 5.9. Crack Patterns – Joint Opening and Joint Closing Demands.

**Table 5.2. Summary of Crack Formation and Crack Widths in Phase 1 Specimens.**

	<b>RCS-16-12</b>	<b>PSS-16-12</b>
<b>Dead</b>	<ul style="list-style-type: none"> <li>No cracks</li> </ul>	<ul style="list-style-type: none"> <li>No cracks</li> </ul>
<b>SLS</b>	<ul style="list-style-type: none"> <li>Both negative and positive moment region cracked</li> <li>Max. crack: 30-in. long with 0.01-in. width</li> </ul>	<ul style="list-style-type: none"> <li>Negative moment region cracked</li> <li>Hairline cracks</li> </ul>
<b>ULS</b>	<ul style="list-style-type: none"> <li>New cracks in both regions</li> <li>Significant length and width growth in both regions</li> <li><b>Maximum crack width (0.02-in.) &gt; AASHTO limit</b></li> <li>Crack extension under creep (Maximum width = 0.024-in.)</li> <li>Cracks closed or reduced to 0.01-in. after unloading to dead load</li> </ul>	<ul style="list-style-type: none"> <li>Negative moment cracks extended</li> <li>Positive moment region cracked</li> <li>New hairline crack and crack extension under creep</li> <li>No unloading to dead load in this step</li> </ul>
<b>140% ULS</b>	<ul style="list-style-type: none"> <li>New crack in both regions</li> <li>Significant length and width expansion</li> <li><b>Maximum width (0.04-in.) &gt; AASHTO limit</b></li> <li>Diagonal crack between the column and P2</li> <li>Diagonal crack between P2 and V actuators</li> </ul>	<ul style="list-style-type: none"> <li>Both region cracks extended along with slight width growth</li> <li>New crack in both regions</li> <li>Maximum width (0.008-in.) &lt; AASHTO crack limit</li> </ul>
<b>Max. Positive</b>	<ul style="list-style-type: none"> <li>Additional diagonal cracks between the column and P2 actuator</li> <li>Significant crack length and width extension</li> <li><b>Maximum crack width in the span (0.1-in.) &gt; AASHTO limit</b></li> </ul>	<ul style="list-style-type: none"> <li>New cracks in the positive moment region</li> <li>Significant crack length and width extension</li> <li><b>Maximum crack width in the span (0.06-in.) &gt; AASHTO limit</b></li> <li>Equivalent dead load → All cracks closed or reduced to hairline cracks</li> </ul>
<b>J/O</b>	<ul style="list-style-type: none"> <li>East face of the column and bedding layer cracked</li> </ul>	<ul style="list-style-type: none"> <li>East face of the column and bedding layer cracked</li> </ul>
<b>J/C</b>	<ul style="list-style-type: none"> <li>West face of the column and bedding layer cracked</li> </ul>	<ul style="list-style-type: none"> <li>West face of the column and bedding layer cracked</li> </ul>
<b>Max. Negative</b>	<ul style="list-style-type: none"> <li>New flexural cracks in negative moment region</li> <li>Significant crack length and width growth</li> <li>New diagonal crack between the overhang</li> <li>Additional diagonal cracks in the span region</li> <li><b>Maximum crack width in the joint region (0.2 in.) &gt; AASHTO limit</b></li> </ul>	<ul style="list-style-type: none"> <li>New flexural cracks in negative moment region</li> <li>Significant crack length and width growth</li> <li><b>Maximum crack width in the joint region (0.2 in.) &gt; AASHTO limit</b></li> </ul>

*Note: Bold indicates when AASHTO limit of 0.017-in. exceeded*

**Table 5.2. Summary of Crack Formation and Crack Widths in Phase 1 Specimens (Cont.).**

	<b>PSS-16-24</b>	<b>PSV-16-12</b>
<b>Dead</b>	<ul style="list-style-type: none"> <li>• No cracks</li> </ul>	<ul style="list-style-type: none"> <li>• No cracks</li> </ul>
<b>SLS</b>	<ul style="list-style-type: none"> <li>• Negative moment region cracked</li> <li>• Hairline cracks</li> </ul>	<ul style="list-style-type: none"> <li>• Negative moment region cracked</li> <li>• Hairline cracks</li> </ul>
<b>ULS</b>	<ul style="list-style-type: none"> <li>• Negative moment cracks extended</li> <li>• Positive moment region cracked</li> <li>• New hairline crack and crack extension under creep</li> <li>• All cracks closed after unloading to dead load</li> </ul>	<ul style="list-style-type: none"> <li>• Shear crack along the interior void at 370 kips</li> <li>• Negative moment cracks extended</li> <li>• New cracks at the interface of the column</li> <li>• Positive moment region cracked</li> <li>• Cracks closed or reduced to hairline cracks after unloading to dead load</li> <li>• No significant changes under creep</li> </ul>
<b>140% ULS</b>	<ul style="list-style-type: none"> <li>• Flexural cracks extended with no significant width growth</li> <li>• New crack in the positive moment region</li> <li>• Maximum width (0.008-in.) &lt; AASHTO crack limit</li> </ul>	<ul style="list-style-type: none"> <li>• All flexural and shear cracks extended</li> <li>• New cracks in both moment regions</li> <li>• New horizontal crack below the P2 actuator</li> <li>• Maximum width (0.156-in.) &lt; AASHTO crack limit</li> </ul>
<b>Max. Positive</b>	<ul style="list-style-type: none"> <li>• New flexural cracks in the positive moment region</li> <li>• Significant crack length and width extension</li> <li>• <b>Maximum crack width in the span (0.04-in.) &gt; AASHTO limit</b></li> </ul>	<ul style="list-style-type: none"> <li>• New flexural cracks in the positive moment region</li> <li>• New shear crack between P2 and V actuators</li> <li>• <b>Maximum crack width in the span (0.04-in.) &gt; AASHTO limit</b></li> </ul>
<b>J/O</b>	<ul style="list-style-type: none"> <li>• East face of the column and bedding layer cracked</li> </ul>	<ul style="list-style-type: none"> <li>• East face of the column and bedding layer cracked</li> </ul>
<b>J/C</b>	<ul style="list-style-type: none"> <li>• West face of the column and bedding layer cracked</li> </ul>	<ul style="list-style-type: none"> <li>• West face of the column and bedding layer cracked</li> </ul>
<b>Max. Negative</b>	<ul style="list-style-type: none"> <li>• New flexural cracks in negative moment region</li> <li>• Significant crack length and width growth</li> <li>• <b>Maximum crack width in the joint region (0.2 in.) &gt; AASHTO limit</b></li> </ul>	<ul style="list-style-type: none"> <li>• New flexural cracks in negative moment region</li> <li>• Significant crack length and width growth</li> <li>• <b>Maximum crack width in the joint region (0.2 in.) &gt; AASHTO limit</b></li> </ul>

*Note: Bold indicates when AASHTO limit of 0.017-in. exceeded*

### 5.2.2. Phase 2

No cracks were observed under dead load in both specimens. At SLS, the first hairline cracks formed in the negative moment region in both specimens. PSV-28B showed a horizontal crack in the span region that was not observed in PSV-28A.

A shear crack was first observed while loading to ULS demands in both specimens. At ULS demands, negative moment cracks were extended, and additional flexure crack formations were noted in both specimens. Maximum crack widths were 0.049-in. and 0.033-in. for PSV-28A and PSV-28B, respectively, exceeding AASHTO crack limit. Additionally, shear cracks were observed in the overhang along the interior void, and horizontal cracks became prominent in PSV-28B specimen. After unloading to dead load, the majority of flexure cracks were closed or reduced to no more than 0.006-in.

Flexure cracks first occurred in the positive moment region in both specimens after applying maximum positive moment demand. This was accompanied by significant extension of existing shear cracks. A new diagonal shear crack occurred between P2 and V actuators in PSV-28A. Maximum crack width was 0.035-in. for both specimens, exceeding the AASHTO crack limit.

New flexural cracks developed in joint regions at maximum negative moment demands. While PSV-28A had no damage in the overhang region, PSV-28B had significant diagonal cracks in that region. As load increased, both specimens failed by showing crushing and spalling of concrete in the negative moment region.

After the maximum negative moment demands, PSV-28B was subjected to maximum positive moment demand again with excessive tension force on horizontal actuator to fail the positive moment region. The specimen failed by concrete crushing beneath the P2 actuator.



**Table 5.3. Summary of Crack Formation and Crack Widths in Phase 2 Specimens.**

	<b>PSV-28A</b>	<b>PSV-28B</b>
<b>Dead</b>	<ul style="list-style-type: none"> <li>• No cracks</li> </ul>	<ul style="list-style-type: none"> <li>• No cracks</li> </ul>
<b>SLS</b>	<ul style="list-style-type: none"> <li>• Negative moment region cracked</li> <li>• Hairline crack</li> </ul>	<ul style="list-style-type: none"> <li>• Negative moment region cracked</li> <li>• Horizontal crack observed in the span region</li> <li>• Hairline cracks</li> </ul>
<b>ULS</b>	<ul style="list-style-type: none"> <li>• Shear crack along the interior void at 263 kips</li> <li>• Negative moment cracks extended</li> <li>• Additional flexure cracks in the negative moment region</li> <li>• Cracks closed or reduced to hairline after unloading to dead load</li> </ul>	<ul style="list-style-type: none"> <li>• Shear crack along the interior void</li> <li>• Negative moment cracks extended</li> <li>• Additional flexure cracks in the negative moment region</li> <li>• Shear crack formed in overhang</li> <li>• Horizontal cracks more prominent</li> <li>• Flexure cracks closed or reduced to hairline after unloading to dead</li> <li>• Horizontal cracks reduced to 0.008-in. after unload to dead load</li> </ul>
<b>140% ULS</b>	<ul style="list-style-type: none"> <li>• All flexural and shear cracks extended</li> <li>• New cracks formed in negative region</li> <li>• Additional shear crack formed</li> <li>• Hairline positive moment crack formed</li> <li>• <b>Maximum crack width (0.049-in.) &gt; AASHTO limit</b></li> <li>• Majority of cracks closed or reduced to hairline after unload to dead</li> </ul>	<ul style="list-style-type: none"> <li>• All flexural and shear cracks extended</li> <li>• New cracks formed in negative region</li> <li>• Additional shear cracks formed in span and overhang</li> <li>• Hairline positive moment crack formed</li> <li>• <b>Maximum crack width (0.033-in.) &gt; AASHTO limit</b></li> <li>• Majority of cracks closed or reduced to 0.006-in. after unload to dead</li> </ul>
<b>Max. Positive</b>	<ul style="list-style-type: none"> <li>• Extension of existing shear and flexure cracks</li> <li>• New flexural cracks in the positive moment region</li> <li>• New shear crack between P2 and V actuators</li> <li>• <b>Maximum crack width (0.035-in.) &gt; AASHTO limit</b></li> </ul>	<ul style="list-style-type: none"> <li>• Extension of existing shear and flexure cracks</li> <li>• New flexural cracks in the positive moment region</li> <li>• <b>Maximum crack width (0.035-in.) &gt; AASHTO limit</b></li> </ul>
<b>J/O</b>	<ul style="list-style-type: none"> <li>• East face of the column and bedding layer cracked</li> </ul>	<ul style="list-style-type: none"> <li>• East face of the column and bedding layer cracked</li> </ul>
<b>J/C</b>	<ul style="list-style-type: none"> <li>• West face of the column and bedding layer cracked</li> </ul>	<ul style="list-style-type: none"> <li>• West face of the column and bedding layer cracked</li> </ul>
<b>Max. Negative</b>	<ul style="list-style-type: none"> <li>• New flexural cracks in negative moment region</li> <li>• Significant crack length and width growth</li> <li>• Crushing/spalling of concrete in negative moment region</li> </ul>	<ul style="list-style-type: none"> <li>• New flexural cracks in negative moment region</li> <li>• Significant crack length and width growth</li> <li>• Crushing/spalling of concrete in negative moment region and overhang</li> </ul>

*Note: Bold indicates when AASHTO limit of 0.017-in. exceeded*

### 5.3. COMPARISON OF DESIGN PARAMETERS

The impact of design parameters is compared in this section based on damage observation. Parameters include a) types of concrete (RC vs. PSC), b) shear reinforcement spacing, c) existence of an interior void, d) a number of strands, e) void details, f) pocket connection details, and g) overhang details.

#### 5.3.1. Impact of Prestressing

The results of RC (RCS-16-12) and PSC (PSS-16-12) bent caps are compared in this section. Both specimens have the same flexural steel layout (#8 bar for RCS-16-12; and 0.6-in. diameter strand for PSS-16-12), and the same shear reinforcement spacing (12-in.). Although different types of transverse reinforcement were used (#5 closed hoop for RCS-16-12; and #5 S-Bar pairs for PSS-16-12), both had two legs with same area of steel ( $A_v = 0.62 \text{ in.}^2$ ). Concrete strengths were different for both specimens, and this was taken into account in the expected strength calculations.

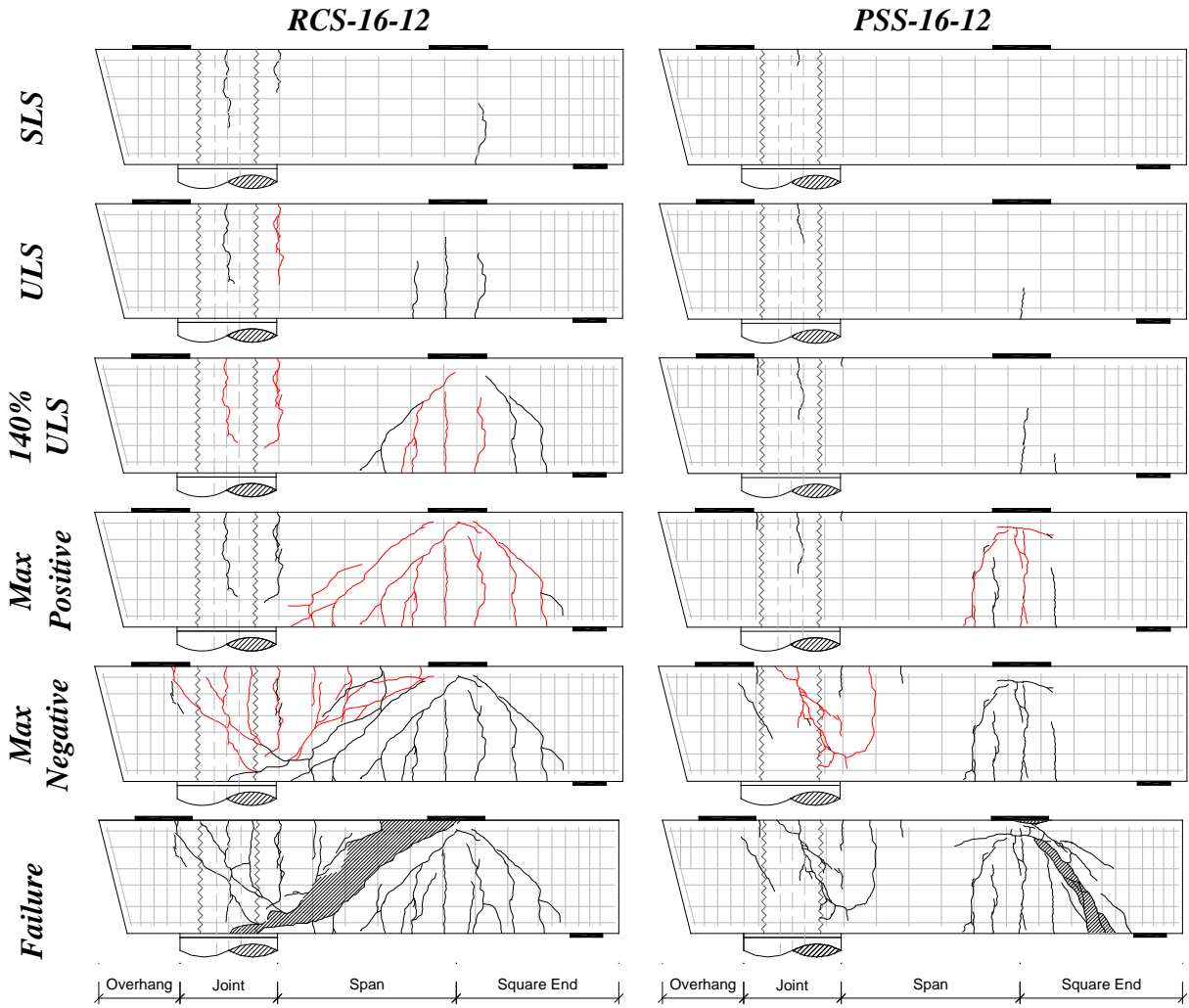
Table 5.4 summarizes the cracking moments. The table provides predicted cracking moment ( $M_{cr,pred}$ ), observed cracking moment ( $M_{cr,test}$ ), and ratio of predicted and observed moment values. The observed cracking moment were greater than predicted values except the negative moment region in PSS-16-12. This might be caused by the nature of the pocket connection, given that the cross-section was hollow in that region. The cracking moment of RCS-16-12 was normalized by multiplying  $\sqrt{f_{t,PSC}}/\sqrt{f_{t,RC}}$  to consider the difference of concrete tensile strength. PSS-16-12 displayed 16 percent and 32 percent higher cracking moment in negative and positive moment regions, respectively, compared to RCS-16-12.

**Table 5.4. Flexure Cracking Summary (RCS-16-12 vs. PSS-16-12).**

Specimen	Region	$f'_c$ (ksi)	$f_r$ (ksi)	$M_{cr,test}$ (k-ft)	$M_{cr,pred}$ (k-ft)	$M_{cr,test} /$ $M_{cr,pred}$	$M_{cr,PSC} /$ $*M_{cr,RC}$
RCS-16-12	Negative	5.94	0.30	400	317	1.26	-
	Positive			518	317	1.63	-
PSS-16-12	Negative	8.01	0.36	540	697	0.77	1.16
	Positive	7.46	0.35	768	684	1.12	1.32

$*M_{cr,RC}$  : Normalized cracking moment of RC specimen by multiplying  $\sqrt{f_{t,PSC}}/\sqrt{f_{t,RC}}$  to consider the difference of concrete strength;

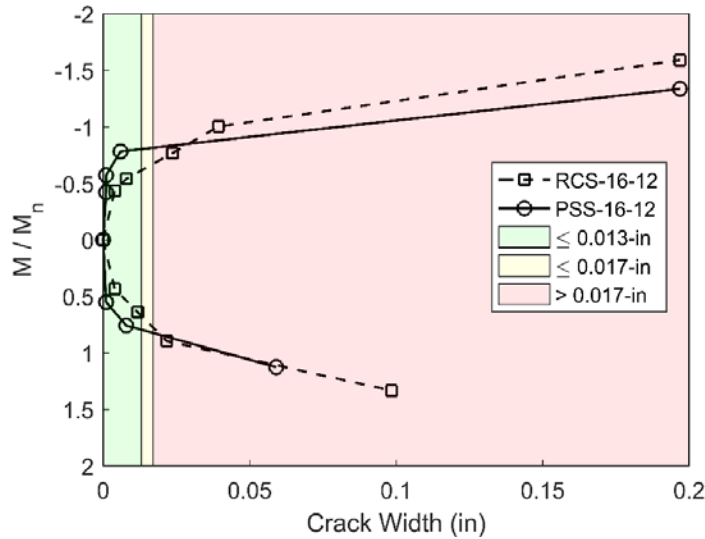
Figure 5.10 presents an overall summary of the front face crack progression. At ULS demands, PSS-16-12 exhibited fewer and finer cracks during the whole duration of the test. RCS-16-12 exhibited cracks wider than the AASHTO limit, but PSS-16-12 did not exceed the crack limit at 140 percent ULS demands. Flexure-shear failure was observed in both specimens; however, RCS-16-12 failed in the span region while PSS-16-12 failed in the square end region.



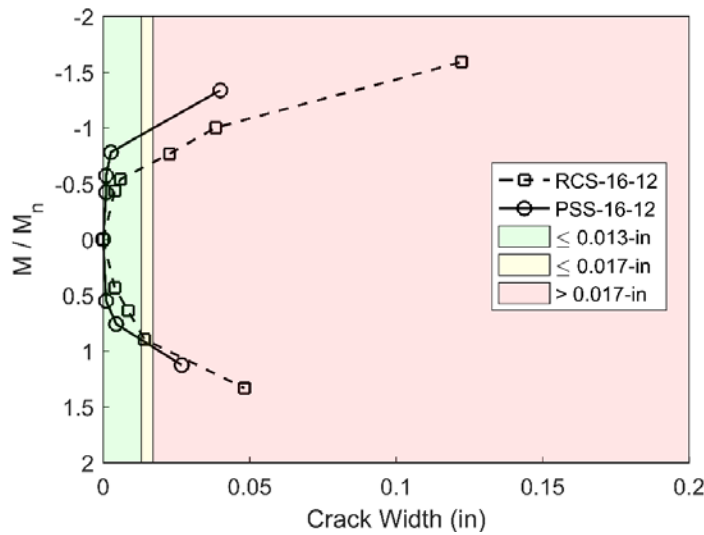
**Figure 5.10. Crack Progression Comparison for RC (RCS-16-12) and PSC (PSS-16-12).**

Figure 5.11 provides the (a) maximum and (b) average crack width envelopes for both specimens plotted against the normalized nominal moment ( $M_u/M_n$ ) in the positive and negative moment regions. The limits for the AASHTO LRFD Class 1 (0.017-in.) and Class 2 (0.013-in.) exposure limits are marked in the figure using different colors. The green region represents crack widths lower than the Class 2 exposure limit, the yellow regions represent cracks widths between the Class 1 and 2 exposure limits, and the red region represents crack widths greater than the Class 1

exposure limit. PSS-16-12 shows most cracks remain within the Class 2 exposure limit at demands below the expected nominal strength capacity while RCS-16-12 had widths greater than the Class 1 exposure limit before reaching its expected nominal moment strength. The widest positive and negative moment crack widths seen in the figure correspond to the maximum negative and positive moment demands for both specimens.



(a) Maximum Crack Widths



(b) Average Crack Widths

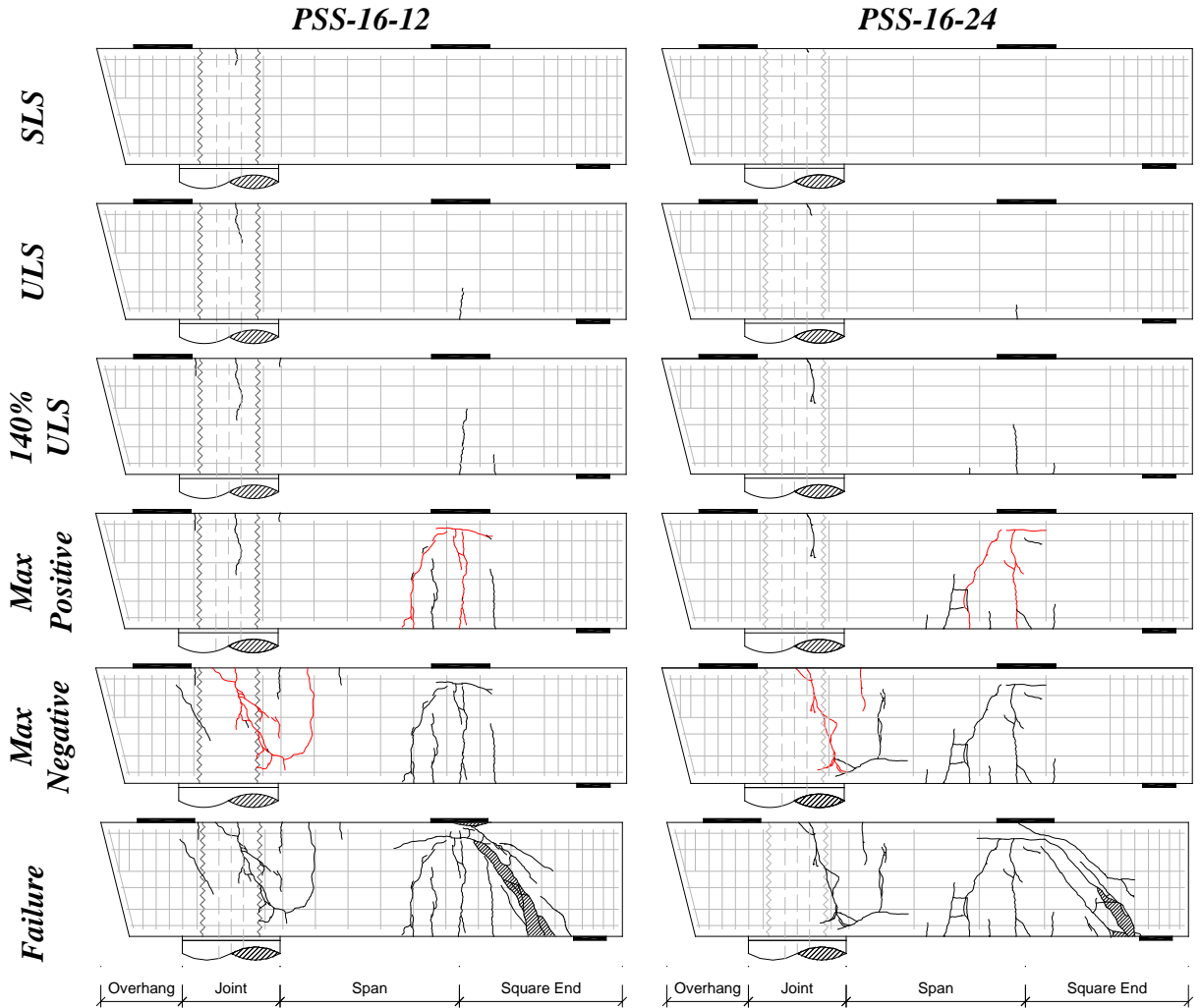
**Figure 5.11. Crack Width Envelopes (RCS-16-12 vs. PSS-16-12).**

### 5.3.2. Impact of Shear Reinforcement

This section compares the results of specimens with different transverse reinforcement spacing. As discussed in Section 4.2.3.1, no steel and 24-in. spacing of #5 transverse reinforcement were required to provide the necessary strength to satisfy strength requirement ( $\phi V_n > V_u$ ) for 32-ft and 40-ft prototype bridges, respectively, in the shear design of Phase 1 prestressed bent caps. However, 12-in. spacing was required to meet AASHTO provisions considering requirements of minimum transverse reinforcement (AASHTO-5.8.2.5) and maximum spacing limit (AASHTO-5.8.2.7).

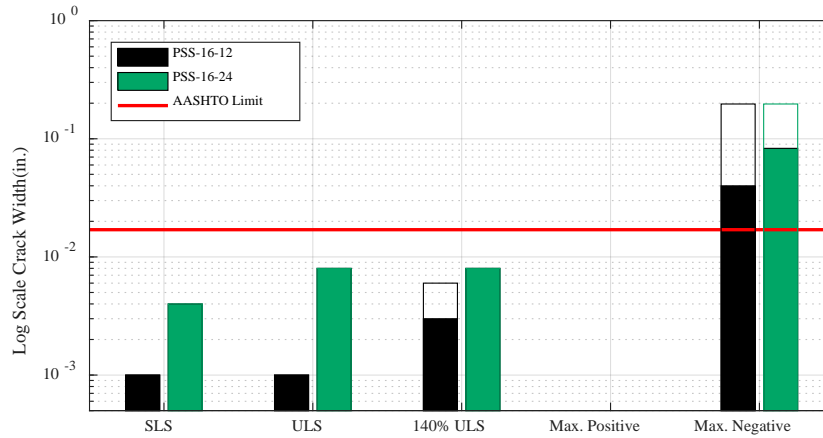
To reveal if this additional transverse reinforcement by AASHTO requirements improves the shear resistance, two specimens were designed with different transverse reinforcement spacing; a) PSC bent cap with 12-in. spacing (PSS-16-12); and b) PSC bent cap with 24-in. spacing (PSS-16-24). The two specimens had the same strand layout and transverse reinforcement detailing (#5 S-Bar). End region detailing and concrete compressive strengths were slightly different but the major variable was transverse reinforcement spacing.

Figure 5.12 compares the crack propagations by various load stages in both specimens. As shown in the figure, the two specimens displayed a similar crack pattern for all loading stages in terms of a number of formed cracks and propagated length. This similar crack pattern was maintained at the end of the test, and both specimens had flexural-shear failure in the square end region. Thus, no significant differences were observed in crack progression between PSS-16-12 and PSS-16-24.

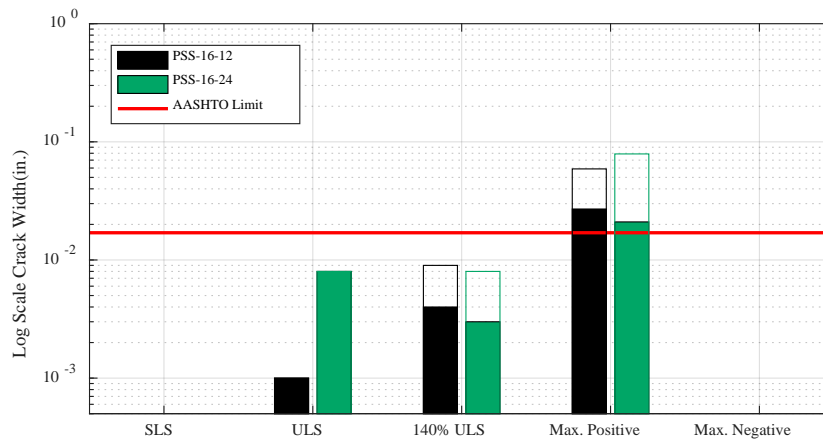


**Figure 5.12. Crack Progression Comparison of PSC Bent Caps with Different Shear Spacing; 12-in. Spacing (PSS-16-12) and 24-in. Spacing (PSS-16-24).**

Flexural crack widths in negative and positive moment regions are compared in Figure 5.13. In the figure, the hollow bars indicate the maximum crack width, and solid bars show the average crack width. As shown in the figure, both maximum and average flexural crack widths in PSS-16-24 tended to be slightly wider than those of PSS-16-12 generally, revealing that additional shear reinforcement can prevent cracks from being wider. Shear crack width is not presented here since no shear cracks appeared until failure demands, when measuring crack widths was not conducted for safety.



(a) Negative moment region



(b) Positive moment region

Note: Hollow bar and solid bar indicate maximum crack width and average crack width, respectively

**Figure 5.13. Log Scale Crack Width Comparison (PSS-16-12 vs. PSS-16-24).**

Cracking and nominal shear strengths of PSS-16-12 and PSS-16-24 in the span and square end are summarized Table 5.5 and Table 5.6, respectively. Data are presented for ULS demands and maximum demands through the full test. Test data were used for demands of shear, moment, and axial load to calculate a nominal shear strength as per AASHTO provisions. Measured crack widths and  $V_u/V_n$  and  $V_u/V_{cr}$  ratios are also presented in the tables. As shown in the tables, for both specimens no shear cracks appeared when  $V_u/V_n$  ratio was between 0.78–0.81, but shear failure occurred when the ratio was close to 1.0; however,  $V_u/V_{cr}$  was 0.63–0.67 even after specimen failed, revealing the theoretical cracking shear strength was overestimated. Figure 5.14 visualizes the tables.

**Table 5.5. Summary of Shear Strength and Damage in Span (PSS-16-12 vs. PSS-16-24).**

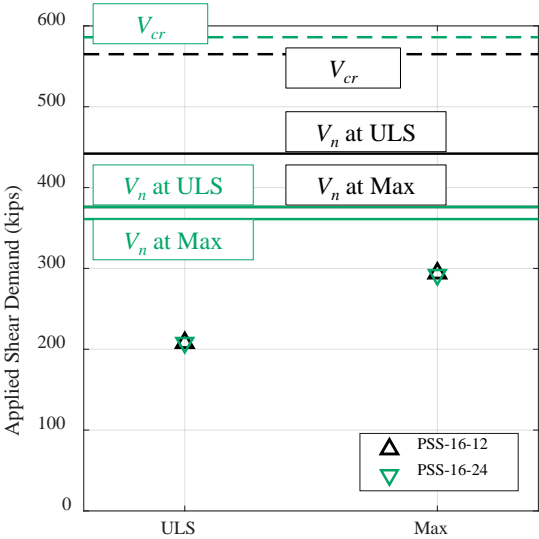
		Demands				AASHTO Design			Result		
		$V_{cr}$ (kips)	$V_u$ (kips)	$N_u$ (kips)	$M_u$ (k-ft)	$V_c$ (kips)	$V_s$ (kips)	$V_n$ (kips)	$V_u/V_n$	$V_u/V_{cr}$	$w$ (in.)
PSS-16-12	ULS	565	208	0	488	286	156	442	0.47	0.37	-
	Max*	565	294	-1	543	249	127	376	0.78	0.52	-
PSS-16-24	ULS	586	208	0	488	297	79	376	0.55	0.35	-
	Max*	586	292	-4	539	258	64	361	0.81	0.50	-

$V_u$ : Shear demand at span;  $V_n$ : Shear strength at span in accordance with AASHTO using demands given in the table; Max\*: Maximum shear demand in span during the test (140% ULS)

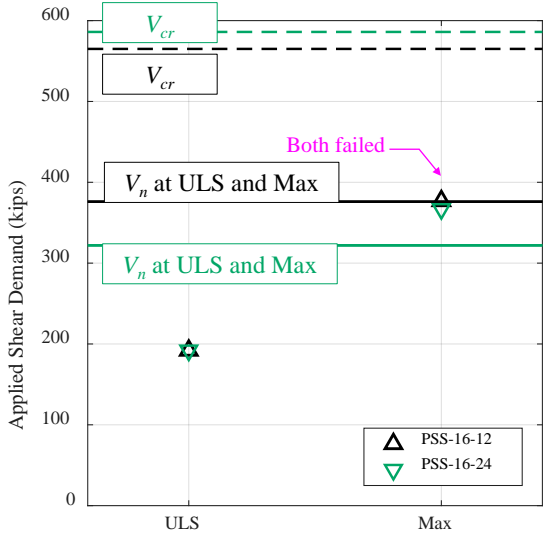
**Table 5.6. Shear Strength and Damage in Square End (PSS-16-12 vs. PSS-16-24).**

		Demands				AASHTO Design			Result		
		$V_{cr}$ (kips)	$V_u$ (kips)	$N_u$ (kips)	$M_u$ (k-ft)	$V_c$ (kips)	$V_s$ (kips)	$V_n$ (kips)	$V_u/V_n$	$V_u/V_{cr}$	$w$ (in.)
PSS-16-12	ULS	565	192	0	768	249	127	376	0.51	0.34	-
	Max*	565	377	105	1,508	249	127	376	1.00	0.67	Failed
PSS-16-24	ULS	586	192	0	768	258	64	322	0.78	0.33	-
	Max*	586	367	109	1,468	258	64	322	1.14	0.63	Failed

$V_u$ : Shear demand at square end;  $V_n$ : Shear strength at square end in accordance with AASHTO using demands given in the table; Max\*: Maximum shear demand in square end during the test (Failure load demand)



(a) Span Region



(b) Square End Region

**Figure 5.14. Shear Strength and Shear Damage Summary of PSS-16-12 and PSS-16-24.**



### 5.3.3. Impact of Interior Void.

To evaluate the impact of an interior void, the test results of PSS-16-12 and PSV-16-12 specimens are compared in this section. PSV-16-12 was designed in this experimental program to examine if PSC bent caps with a void can resist shear and moment demands, and control the cracking as effective as solid PSC bent caps. For this reason, all design detailing such as strand layout, shear reinforcement spacing, and end region detailing were the same for these two specimens, and the only difference was the existence of the interior void. Thus, it was thought that any differences in the results of both specimens were caused due to the interior void. Figure 5.15 provides the comparisons of crack progression in the bent caps.

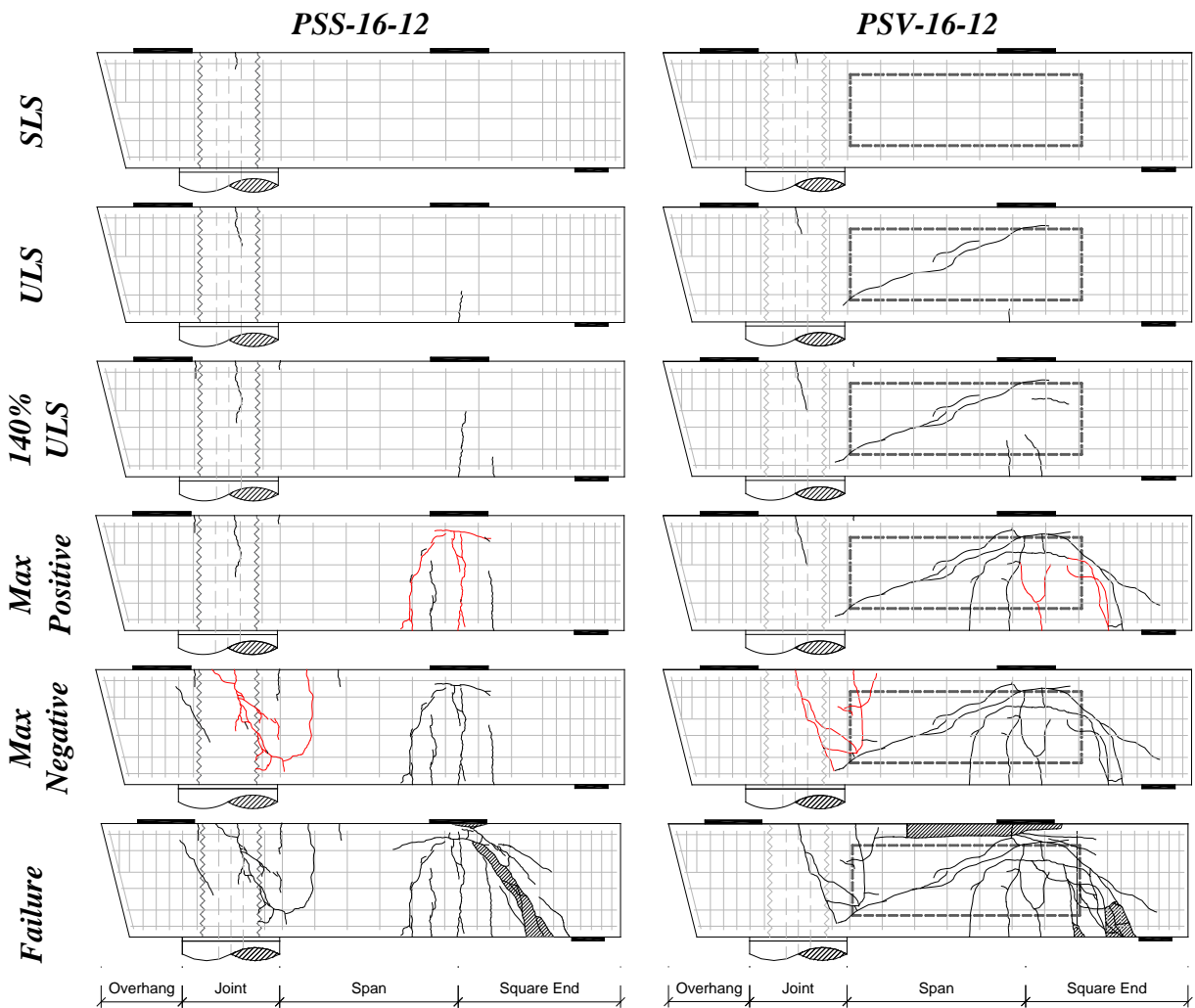


**Figure 5.15. Crack Progression Comparison for Specimens with No Void (PSS-16-12) and Void (PSV-16-12).**

As shown in the figure, both specimens showed similar pattern of flexural cracking, but shear cracks formed along the interior void in PSV-16-12. The shear cracks were developed following the diagonal compression strut in both the span and square end regions as the applied load increased. Both specimens exhibited similar peak load carrying capacities under failure load, even though the square end regions were both severely damaged. At failure, concrete crushing occurred in the square end region in both specimens, but additional concrete crushed along the interior void line in PSV-16-12, resulting in a more abrupt decrease of load carrying capacity. Figure 5.16 shows details of damages at failure.

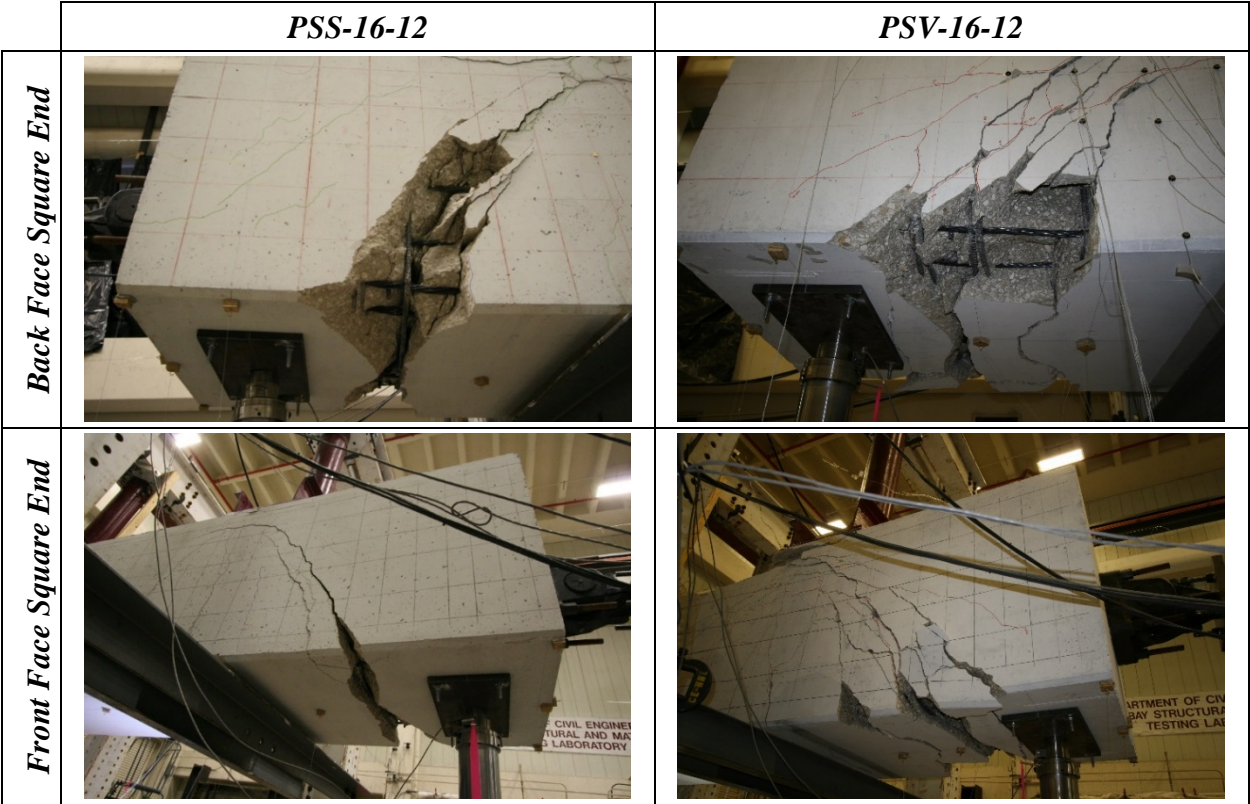
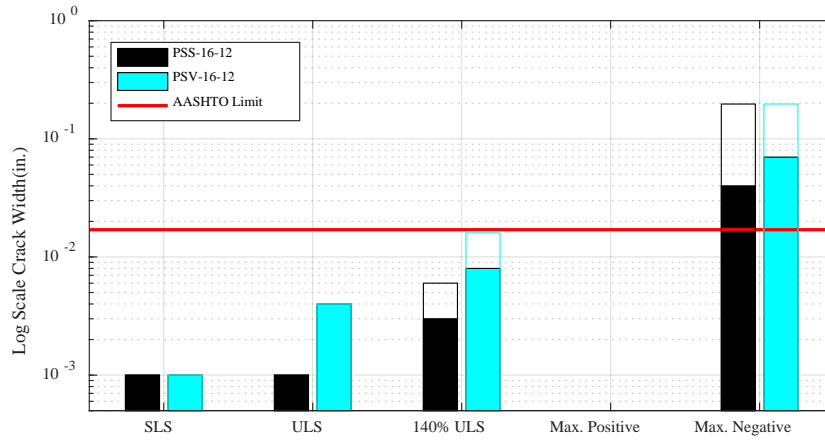
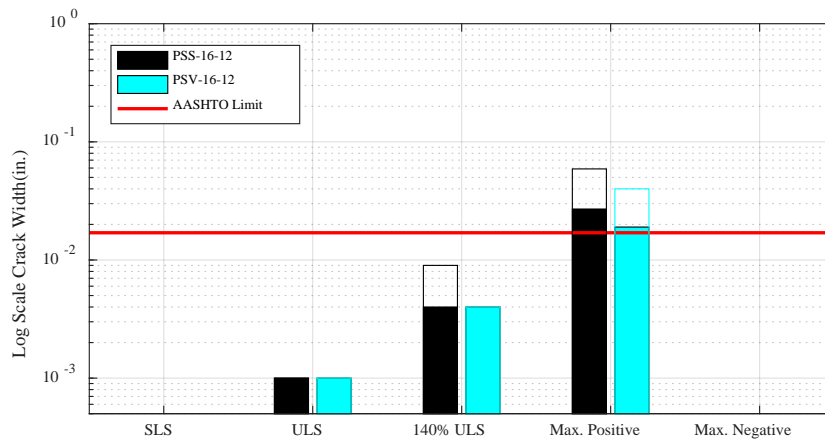


**Figure 5.16. Damage at Failure (PSS-16-12 vs. PSV-16-12).**

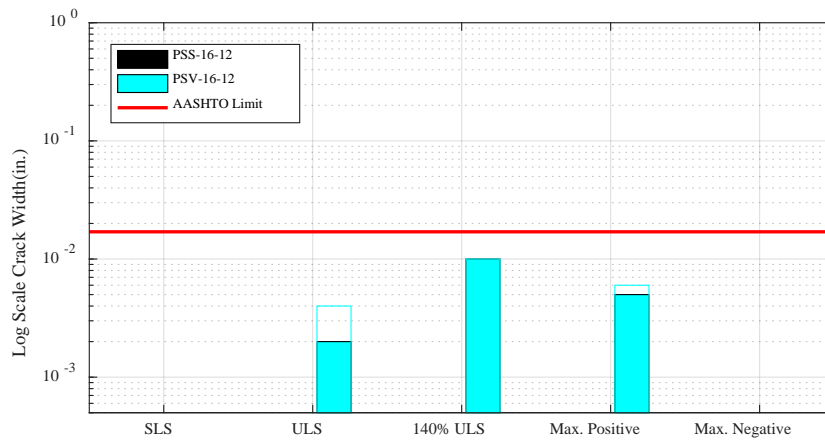
Crack width comparisons were made based on the type and location of cracks a) flexural crack in negative moment region; b) flexural crack in positive moment region; and c) shear cracks. Figure 5.17 summarizes each load case. In the figure, similar flexural crack formation, and average and maximum crack widths were observed in both specimens.



(a) Negative Moment Region



(b) Positive Moment Region

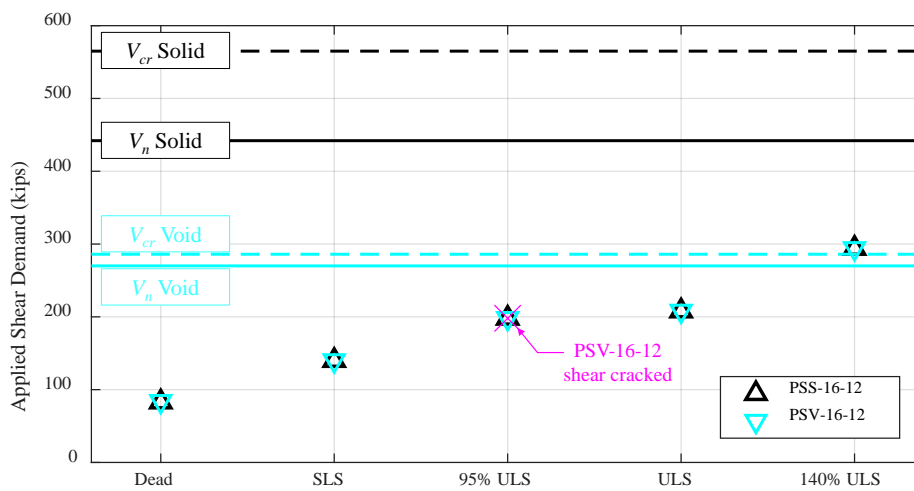


(c) Shear crack

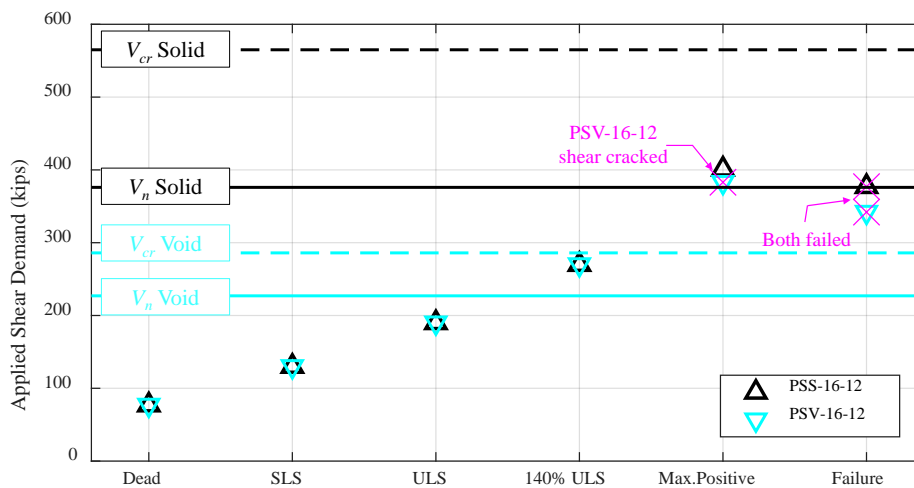
Note: Hollow bar and solid bar indicate maximum crack width and average crack width, respectively

**Figure 5.17. Crack Width Comparison (PSS-16-12 vs. PSV-16-12).**

Figure 5.18 shows applied shear demands during each load stage with nominal and cracking shear strengths of span and square end region for PSS-16-12 and PSV-16-12, respectively. Here, the nominal shear strength was calculated in accordance with AASHTO using ULS demands. As shown in Figure 5.18(a), in the span region shear crack was first observed at 95 percent ULS (P1&P2=262 kips) in PSV-16-12 (voided section) but no shear crack was found in PSS-16-12 (solid section) even after 140 percent ULS demands. In the square end region, first shear crack formed at the maximum positive moment demand in PSV-16-12, and then both specimens experienced flexure-shear failure at the failure demand.



(a) Span Region



(b) Square End Region

**Figure 5.18. Shear Strength and Shear Damage Summary of PSS-16-12 and PSV-16-12.**

#### 5.3.4. Impact of Number of Strands

To assess the impact of the number of strands, the initial cracking of Phase 1 and 2 specimens is compared. Since Phase 2 specimens have voids, a comparison was only made to PSV-16-12 in Phase 1. All voided specimens had the same size interior void (26-in. square). Each voided specimen had different void detailing; the effect of void details are discussed in Section 5.3.5.

Since Phases 1 and 2 test setups had different geometries, the shear and moment demands were not consistent between phases. Thus, it is not appropriate to compare damage directly by load case. For this reason, quick pauses were made during Phase 2 tests at loads generating equivalent demands to Phase 1 major events. These quick pauses included corresponding moment and shear demands at dead, SLS, ULS, and 140 percent ULS loads in regions subjected to negative moment, positive moment, and critical shear, respectively. Quick pauses also included the observed cracking shear demand in PSV-16-12.

Details of quick pause and observation at each quick pause were compared and summarized in Table 5.7 through Table 5.9 for negative moment, positive moment, and span regions, respectively. A target demand for each event in Phase 1 is provided in the first column. Required actuator forces to generate the target demand in Phase 1 and Phase 2 test setups are given in columns 2 and 4, respectively. The control actuator generating the target demand is P1 for negative moment and span regions, and V for positive moment region so that loads those actuators were in the column 2. While conducting the test, horizontal actuators acted as reactions; the recorded forces are provided in Columns 3 and 5. The remainder of the tables shows whether the region cracked, and if cracked, the crack width. The cracking  $M / M_{cr}$  or  $V / V_n$  ratio depending on the considered demand. As shown in Table 5.7 and Table 5.8, no flexural cracks formed in PSV-28A and PSV-28B after applying equivalent 140 percent ULS demand, unlike PSV-16-12, which displayed flexural cracks in the negative region at SLS and in the positive region at ULS. This observation proved that use of a greater number of strands significantly improves flexural capacity and delays onset of a crack formation.

However, cracking shear strength was not enhanced to the degree expected. The first shear cracks were observed when shear demand at the span region was 198 kips in PSV-16-12 and 208 kips in PSV-28A and PSV-28B. From this observation, a possibility arises that additional compression on

the bent cap by prestressing force may not be an appropriate option to increase the cracking shear strength.

**Table 5.7. Comparison of Voided Specimens at Equivalent Load (Negative Moment Region).**

Negative Moment Demand	PSV-16-12		PSV-28A (PSV-28B)		Test and Predicted Ratio and Crack width					
	P1*	HT†	P1*	HT†	PSV-16-12 ( $M_{cr} = 784$ k-ft)		PSV-28A ( $M_{cr} = 1,148$ k-ft)		PSV-28B ( $M_{cr} = 1,168$ k-ft)	
					$M/M_{cr}$	w (in.)	$M/M_{cr}$	w (in.)	$M/M_{cr}$	w (in.)
<i>M</i> Dead (320 k-ft)	160	-13	64	11 (9)	0.41	-	0.28	-	0.27	-
<i>M</i> SLS (540 k-ft)	270	-10	108	18 (16)	0.69	0.001	0.47	-	0.46	-
<i>M</i> ULS (800 k-ft)	400	-6	160	25 (22)	1.02	0.004	0.70	-	0.68	-
<i>M</i> 140% ULS (1,170 k-ft)	563	-2	225	30 (26)	1.49	0.016	1.02	-	1.00	-

\* Req'd actuator force to generate moment demand corresponding to Phase I event in the negative moment region;

† Recorded horizontal actuator force as a reaction; (+) tension and (-) compression;

**Table 5.8. Comparison of Voided Specimens at Equivalent Load (Positive Moment Region).**

Positive Moment Demand	PSV-16-12		PSV-28A (PSV-28B)		Test and Predicted Ratio and Crack width					
	V*	HT†	V*	HT†	PSV-16-12 ( $M_{cr} = 705$ k-ft)		PSV-28A ( $M_{cr} = 891$ k-ft)		PSV-28B ( $M_{cr} = 882$ k-ft)	
					$M^+/M_{cr}$	w (in.)	$M^+/M_{cr}$	w (in.)	$M^+/M_{cr}$	w (in.)
<i>M</i> Dead (308 k-ft)	76	-14	44	22 (21)	0.44	-	0.35	-	0.35	-
<i>M</i> SLS (518 k-ft)	130	-10	74	34 (31)	0.73	-	0.58	-	0.59	-
<i>M</i> ULS (768 k-ft)	192	-7	110	44 (48)	1.09	0.001	0.86	-	0.87	-
<i>M</i> 140% ULS (1,124 k-ft)	270	-2	156	-18 (-14)	1.59	0.004	1.26	-	1.27	-

\* Req'd actuator force to generate moment demand corresponding to Phase I event in the negative moment region;

† Recorded horizontal actuator force as a reaction; (+) tension and (-) compression;

**Table 5.9. Comparison of Voided Specimens at Equivalent Load (Span Region).**

Shear Demand	PSV-16-12		PSV-28A (PSV-28B)		Test and Predicted Ratio and Crack width					
	P1*	HT†	P1*	HT†	PSV-16-12 ( $V_{cr} = 288$ kips)		PSV-28A ( $V_{cr} = 333$ kips)		PSV-28B ( $V_{cr} = 326$ kips)	
	(kips)	(kips)	(kips)	(kips)	$V/V_{cr}$	$w$ (in.)	$V/V_{cr}$	$w$ (in.)	$V/V_{cr}$	$w$ (in.)
V at Dead (83 kips)	160	-13	105	18 (16)	0.29	-	0.25	-	0.25	-
V at SLS (140 kips)	270	-10	178	27 (23)	0.49	-	0.42	-	0.43	-
V Crack (198 kips)	380	-7	250	32 (27)	<b>0.69</b>	H.L	0.59	-	0.61	-
V at ULS (208 kips)	400	-6	263	33 (28)	0.72	H.L	<b>0.62</b>	H.L	<b>0.64</b>	H.L
V at 140% ULS (293 kips)	563	-2	370	38 (34)	1.02	0.004	0.88	0.004	0.90	0.004

\* Req'd actuator force to generate moment demand corresponding to Phase I event in the negative moment region;

† Recorded horizontal actuator force as a reaction; (+) tension and (-) compression;  $V_{cr}$  is calculated using  $0.126\sqrt{f'_c}$  considering horizontal forces

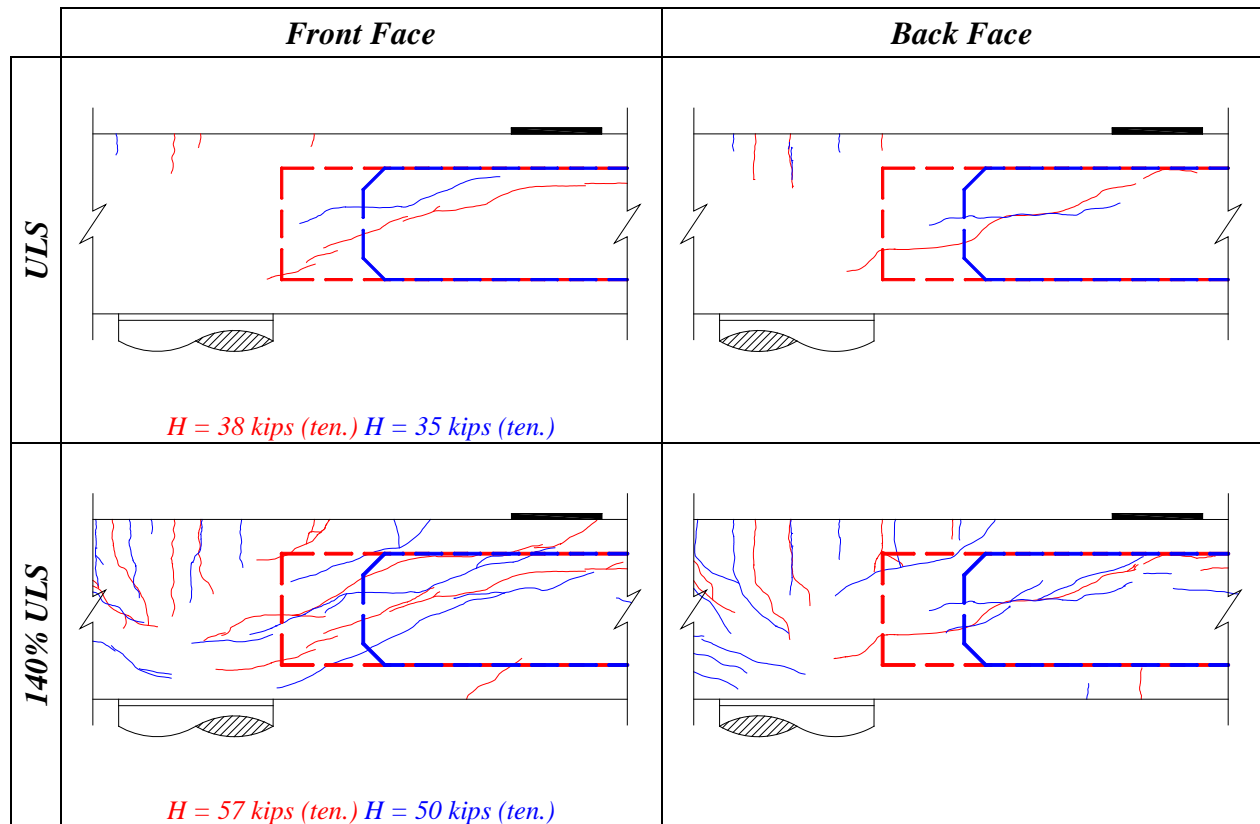
### 5.3.5. Impact of Void Details

This section discusses the results of the different interior void geometries and details investigated during Phase 2. During Phase 1, shear cracking formed along the length of the interior void (in the span region) under ULS and 140 percent ULS demands. Investigation of the interior void details in Phase 2 anticipated highlighting impact on the onset of shear cracking, crack angle, crack propagation, and the effect of the hollow/solid cross section in the critical shear locations.

Figure 5.19 compares the cracking in the span region of PSV-28A and PSV-28B under ULS and 140 percent ULS demands. The cracks and interior void outlines are shown in red and blue for PSV-28A and PSV-28B, respectively. Vertical loads were nearly identical for both PSV-28A and PSV-28B during ULS and 140 percent ULS demands, with slight differences due to the initial position, specimen weight, and horizontal forces applied. Horizontal tension force applied by the HT/HB actuators had minor differences; these differences are noted in Figure 5.19. During ULS loading, the initial shear crack angle for PSV-28B was shallower than for PSV-28A, and did not travel toward the corner of the interior void. The initial shear crack that formed on the front face of PSV-28B appeared to incorporate a preexisting horizontal crack, which was likely missed during pretesting inspection. Under 140 percent ULS loading, the differences in angle and direction of new shear cracks were not apparent. The extent of shear cracking in the span region

on the back face of PSV-28B, even under shear and moment demands greater than 140 percent ULS, did not reach to the interior face of the column like that of PSV-28A.

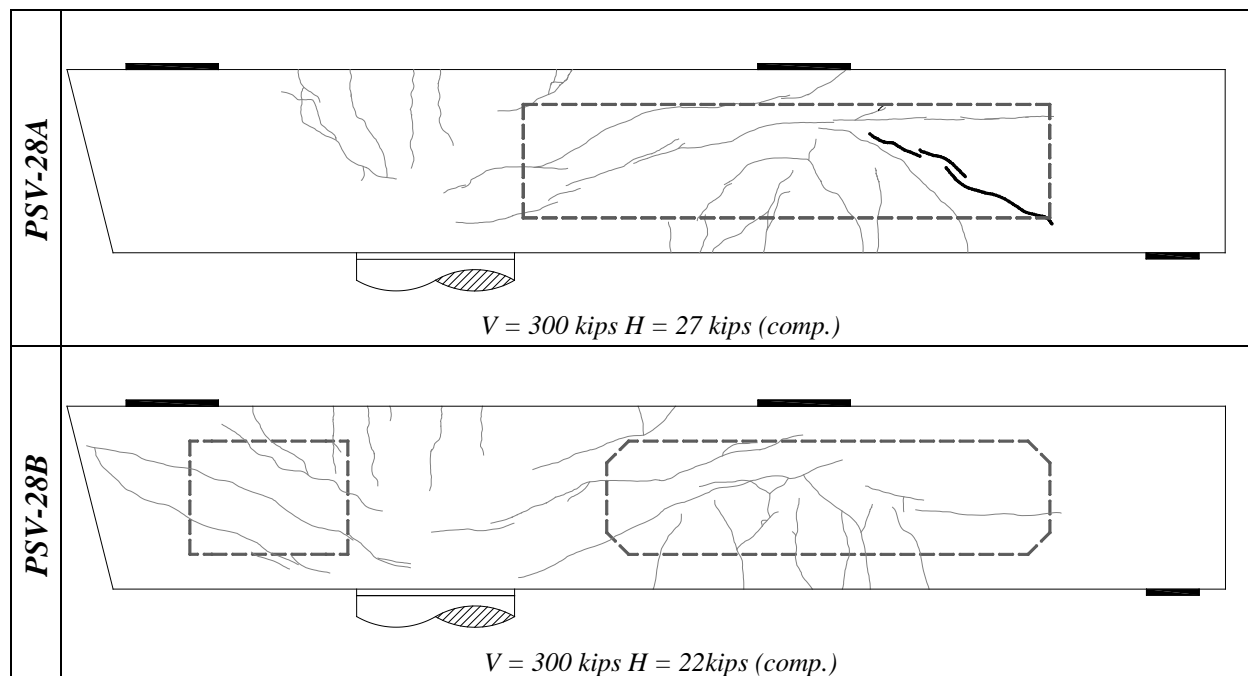
Differences in shear cracking in the square end of PSV-28A and PSV-28B were observed under maximum shear demands ( $V_{max}$ ) in the square end region. Figure 5.20 compares the formation of shear cracks under equivalent shear demands in the square ends of both specimens, noting the force in the V actuator ( $V_{max}$ ) and difference in horizontal compression. PSV-28A displayed a shear crack (on both faces) that traveled to the corner of interior void, stopping at the solid region of the cross-section. This crack is highlighted with a thick line in the figure. PSV-28B did not display a shear crack of the same nature.



*Red = PSV-28A Blue = PSV-28B*

**Figure 5.19. Comparison of Shear Cracks in Span Region of PSV-28A and PSV-28B at ULS and 140 Percent ULS Demands.**





Note: Thick line highlights shear cracks in square end

**Figure 5.20. Comparison of Formation of Shear Cracks in Square End of PSV-28A and PSV-28B under  $V_{max}$  of Square End.**

Both specimens failed in the negative moment region during Pattern E (maximum negative moment). Shown in Figure 5.21, the loss of concrete appears to be associated with the concentration of compressive stress at the corner of the interior void in both specimens. Differences in the loading conditions are noted. Although PSV-28B also had extensive shear damage in the overhang, the spalling and crushing of the concrete on the interior (span) side of the column happened first similar to the failure of PSV-28A.

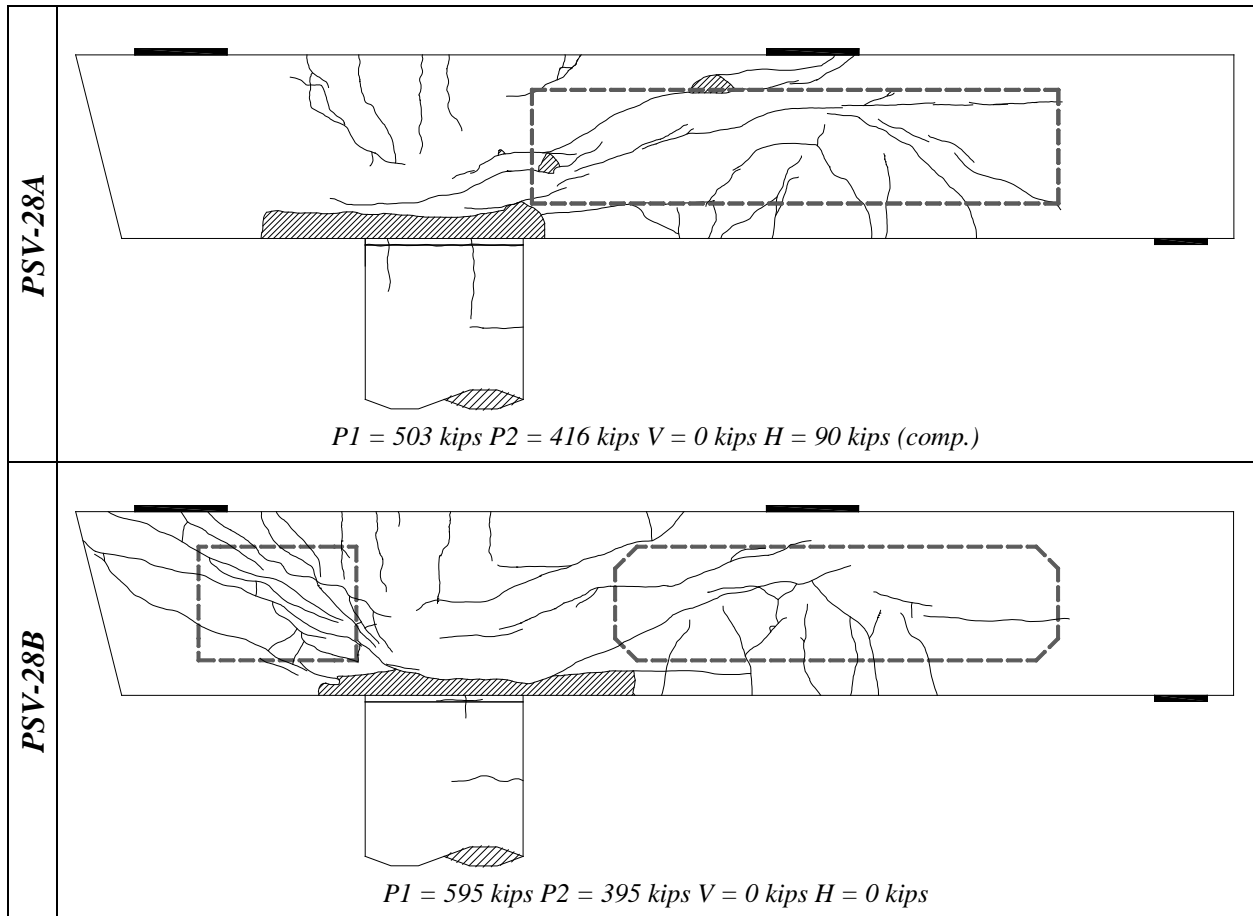
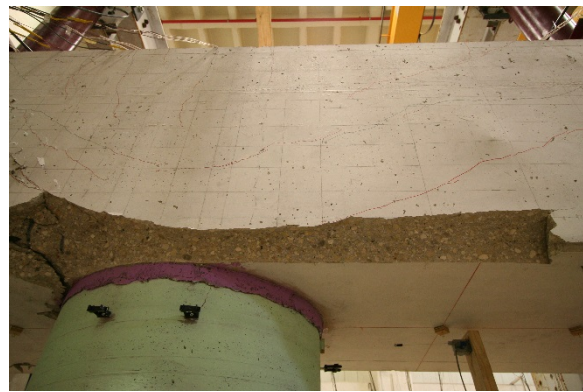


**Figure 5.21. Comparison of Damage at Failure in Negative Moment Region of PSV-28A and PSV-28B.**



(a) PSV-28A

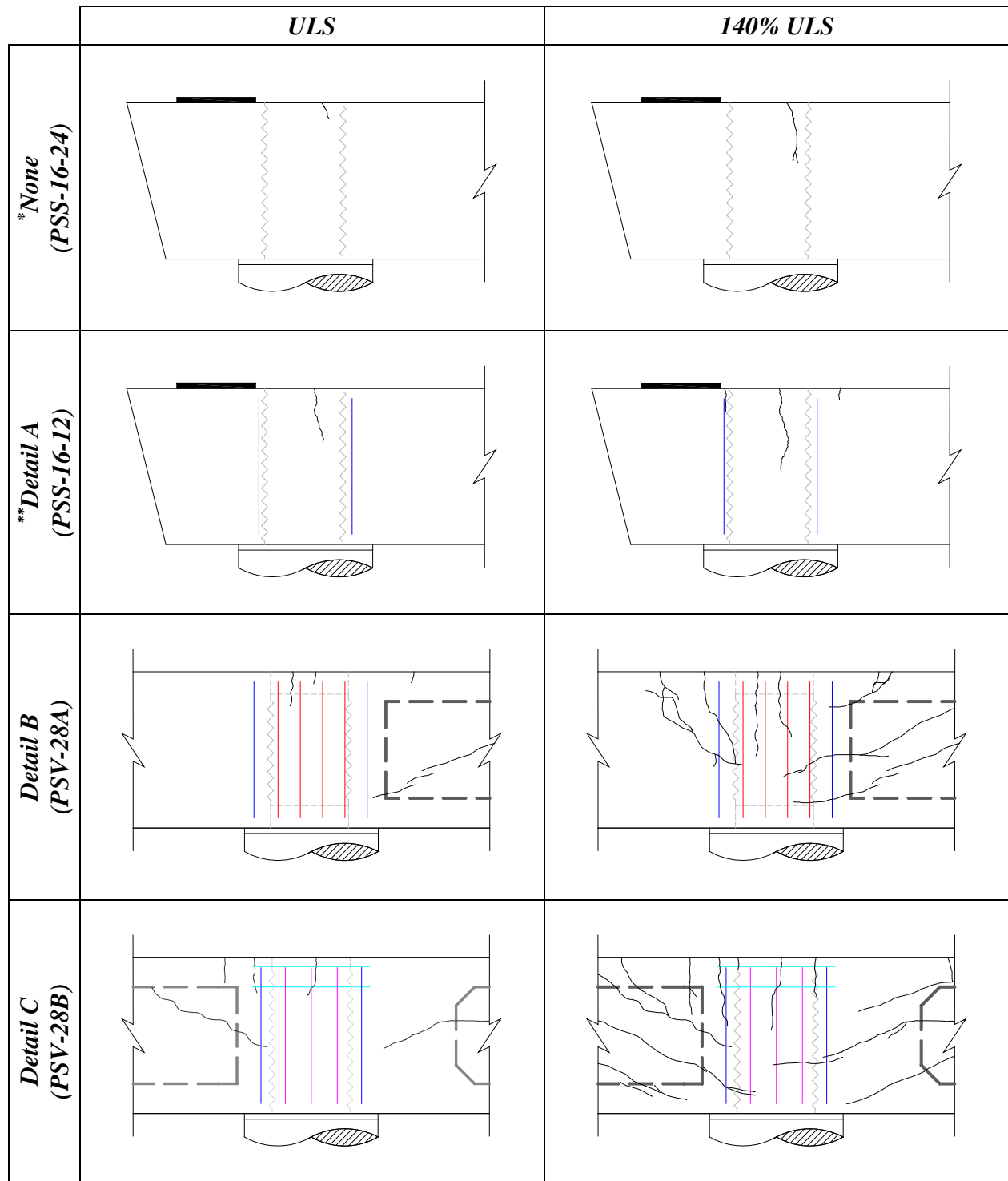


(b) PSV-28B

**Figure 5.22. Loss of Concrete in Negative Moment Region of Phase 2 Specimens during Maximum Negative Moment Demands.**

### **5.3.6. Impact of Pocket Connection Details**

Figure 5.23 shows the cracking in the negative moment region of the pretensioned specimens. While forces at ULS and 140 percent ULS demands are similar in both Phase 1 and Phase 2, the longer overhang of Phase 2 specimens induced a larger moment in the joint region. Due to the increased moment in the joint compared to Phase 1, a direct comparison of the damage between Phase 1 details and Phase 2 details are not feasible. However, comparisons of joint region detailing investigated in Phase 2 are possible. The maximum width of flexure cracks in the joint region of PSV-28A (0.014-in.) were larger than that of PSV-28B (0.010-in.), leading one to conclude that the additional mild steel hoops included at the top of the pocket connection were effective at limiting the expansion of flexure cracks at increased loads. No significant differences in the performance of the connection were observed with the varied corrugated pipe embedment depth. No significant differences in the onset or propagation of cracking in the joint region was observed with the variation in shear reinforcement between Detail B and Detail C.



\* Additional reinforcement also not included in RCS-16-12

\*\* Detail A is present in both PSS-16-12 and PSV-16-12

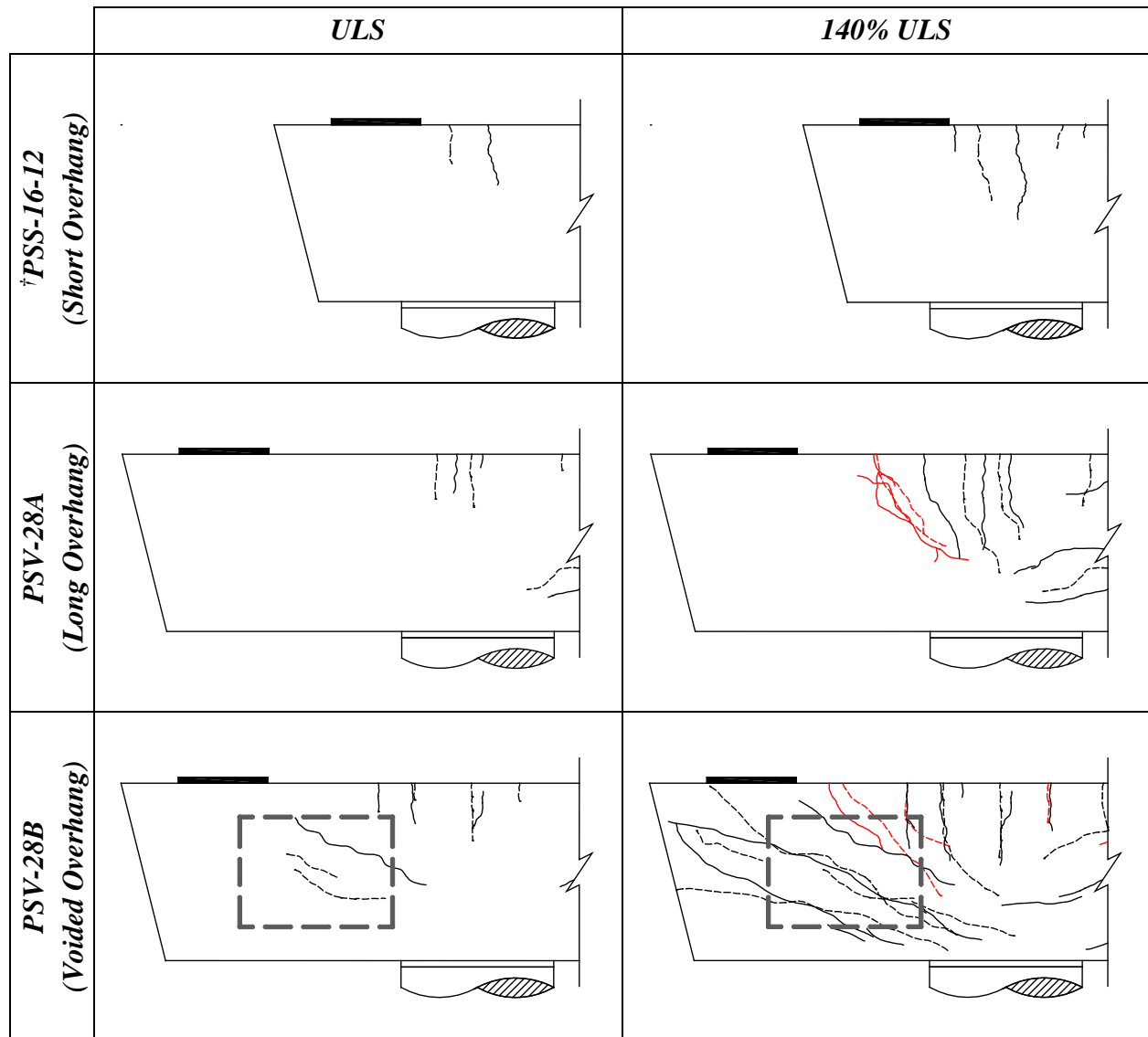
† Pocket connection details are discussed in section

**Figure 5.23. Comparison of Cracking in Negative Moment Region of Pretensioned Specimens with Different Pocket Connection Details<sup>†</sup> under ULS and 140 percent ULS Demands.**

### 5.3.7. Impact of Overhang Geometry and Details

The geometry and detailing of the overhang region was varied in Phase 2. Figure 5.24 compares the damage that occurred in pretensioned specimens that had the standard (short, solid) overhang in Phase 1 to that of the two Phase 2 overhangs (long, with and without void). Due to similarities in damage in Phase 1 pretensioned specimens, only PSS-16-12 is represented in the figure. Under ULS demands, the solid overhangs, both short and long, showed similar results. Cracking was limited to the flexure region within the joint. However, in the voided overhang (PSV-28B) shear cracking along the interior void was observed on both faces at ULS demands. Shear cracking was expected after ULS demands ( $P1$  and  $P2 = 380$  kips), when  $P1$  reached  $V_{cr}$  of the overhang (330 kips). These shear cracks were measured in the range of 0.002–0.010-in., which is below the AASHTO limit. Under 140 percent ULS demands, the standard overhang showed limited crack progression with the damage mainly isolated to the flexure region within the joint. Both longer overhangs showed crack propagation and the onset of additional cracking. In PSV-28A, flexure-shear cracks formed between the  $P1$  actuator and the exterior face of the column, and the widths exceeded the AASHTO limits. In PSV-28B, extensive shear cracking was observed with similar flexure-shear cracks present.

Figure 5.25 compares the damage in the solid and voided longer overhangs of PSV-28A and PSV-28B at the time of failure in the negative moment region. While failure in both specimens occurred in the compression zone of the negative moment region, PSV-28B also crushed along the compression strut from the  $P1$  actuator to the exterior face of the column.



*† Representative of Phase I specimens. Negligible differences in overhang cracking of other Phase I specimens*

*Red = Crack exceeds AASHTO limits.*

*- - - = Cracks on back face*

**Figure 5.24. Comparison of Damage in Overhangs with Different Lengths and Void Details under ULS and 140 Percent ULS Demands.**

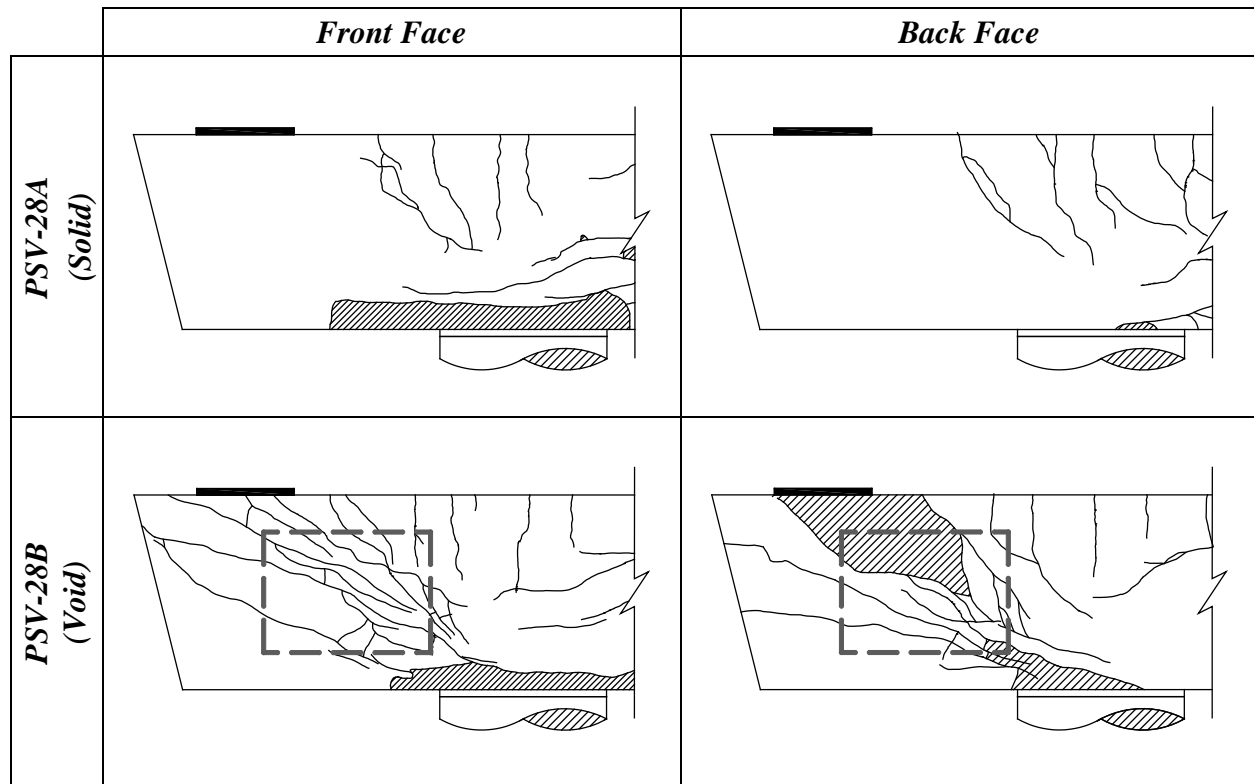


**Figure 5.25. Comparison of Overhang Damage of Solid (PSV-28A) and Voided (PSV-28B) Overhang at Negative Moment Region Failure.**

#### 5.4. EVALUATION OF CRACKING IN PRETENSIONED BENT CAPS

During the tests, both flexural and diagonal shear cracks initiated earlier than they were expected for most of the specimens, resulting in a need for better understanding and evaluation of cracking moment and shear.

As the cracking moment and shear are dependent on the tensile strength of concrete ( $f_t$ ), it is important to define the appropriate values. The demands at the first observed cracking were used to back calculate the associate tensile stresses using Equations (4-3) for flexure and (4-4) for shear. The stresses were then defined as a factor alpha ( $\alpha$ ) of the  $\sqrt{f'_c}$ :

$$f_t = \alpha \sqrt{f'_c} \quad (5-1)$$

where  $f_t$  = tensile strength of concrete;  $\alpha$  = coefficient multiplier for determining tensile strength of concrete; and  $f'_c$  = specified compression strength of the concrete.

Table 5.10 and Table 5.11 provide the results for flexure. Concrete compressive strength used the measured test day properties for the batch of concrete in the tension region. For negative bending,

a reduced cross-section was used to account for the pocket. Transformed cross-sections accounted for the longitudinal reinforcement and the pocket pipe (negative bending only). The concrete tensile stress at flexural cracking ranged from  $0.131-0.145\sqrt{f'_c}$  ( $4.1-4.6\sqrt{f'_c}$  in psi) for negative bending, and  $0.119-0.152\sqrt{f'_c}$  ( $3.8-4.8\sqrt{f'_c}$  in psi) for positive bending. Table 5.12 provides the results for shear cracking in the span region. Only the specimens with voids (PSV-16-12, PSV-28A, and PSV-28B) are considered as the solid specimens did not crack in the span region. Concrete compressive strength used the measured test day properties for the batch of concrete at mid-depth. The concrete tensile stress at shear cracking ranged from  $0.061-0.075\sqrt{f'_c}$  ( $1.9-2.3\sqrt{f'_c}$  in psi). In the solid bent caps, the maximum shear demand applied corresponded to a tensile stress of  $0.039-0.043\sqrt{f'_c}$  ( $1.32-1.36\sqrt{f'_c}$  in psi).

**Table 5.10. Cracking Moment Summary in Negative Moment Region.**

Specimen	$^*f'_c$ (ksi)	$n$	$S_x$ (in. <sup>3</sup> )	$M_{cr,test}$ (k-ft)	$\alpha$ in ksi (in psi)
PSS-16-12	8.01	16	6,662	-540	0.134 (4.2)
PSS-16-24	8.34	16	6,662	-540	0.131 (4.2)
PSV-16-12	8.38	16	6,662	-540	0.131 (4.1)
PSV-28A	7.19	28	6,784	-800	0.145 (4.6)
PSV-28B	8.01	28	6,784	-800	0.145 (4.6)
Avg.	—	—	—	—	0.137 (4.3)

Note:  $^*f'_c$  at the top layer in the bent cap was considered;  $\alpha$  is the coefficient back calculated to correspond to the test results,  $M_{cr,test}$

**Table 5.11. Cracking Moment Summary in Positive Moment Region.**

Specimen	$^*f'_c$ (ksi)	$n$	$S_x$ (in. <sup>3</sup> )	$M_{cr,test}$ (k-ft)	$\alpha$ in ksi (in psi)
PSS-16-12	7.46	16	12,703	768	0.152 (4.8)
PSS-16-24	8.27	16	12,703	768	0.145 (4.6)
PSV-16-12	8.82	16	10,889	768	0.119 (3.8)
PSV-28A	8.28	28	11,022	1,120	0.147 (4.6)
PSV-28B	7.81	28	11,022	1,120	0.131 (4.2)
Avg.	—	—	—	—	0.139 (4.4)

Note:  $^*f'_c$  at the bottom layer in the bent cap was considered;  $\alpha$  is the coefficient back calculated to correspond to the test results,  $M_{cr,test}$ ;



**Table 5.12. Cracking Shear Summary**

Specimen	$*f'_c$ (ksi)	$V_{cr,test}$ (kips)	$n$	$\alpha$ in ksi (in psi)
PSV-16-12	8.60	198	16	0.072 (2.3)
PSV-28A	8.03	208	28	0.061 (1.9)
PSV-28B	7.50	208	28	0.063 (2.0)
Avg.	–	–	–	0.065 (2.1)

Note:  $*f'_c$  at the mid-depth in the bent cap was considered;  $\alpha$  is the coefficient back calculated to correspond to the test results,  $V_{cr,test}$ ;

## 5.5. GENERAL FINDINGS

The experimental tests of full-scale sub-assemblages resulted in the following findings:

- **RC versus PSC Performance:** In general, the PSC specimen delayed the onset of shear and flexural cracking and limited crack formation and crack width compared to the traditional RC counterpart. After removal of service loads, the pretensioned specimens led to the predominant closure of the previously open cracks. The reduction of cracks and crack widths were not as prevalent for the RC specimen.
- **RC versus PSC Failure:** The RC specimen (RCS-16-12) displayed shear-flexure failure in the span region, while the PSC specimen (PSS-16-12) displayed flexure-shear failure in the square end region. Shear damage was limited in the span region of the PSC specimen compared to that of the RC specimen.
- **Impact of Shear Reinforcement Spacing:** Similar patterns of cracks were observed in both PSS-16-12 ( $s = 12$ -in.) and PSS-16-24 ( $s = 24$ -in.). Significant differences in crack formation at the various loading stages were not apparent. However, slightly smaller crack widths were observed in PSS-16-12, revealing that the additional shear reinforcement might be effective to limit the crack widths. Both specimens displayed shear failure in the square end region, showing significant damage along the compression strut from the P2 actuator to the V actuator. From observations of both specimens under prototype bridge demands, the 24-in. transverse reinforcement spacing (AASHTO maximum) performed satisfactory.
- **Impact of Interior Void:** Similar flexure cracking patterns were observed in PSS-16-12 and PSV-16-12 under bridge demands. Shear cracking was observed in PSV-16-12 in the

span region, along the interior void, under ULS demands. Significant shear damage was observed in the square end under failure demands for both specimens; however, PSV-16-12 exhibited additional concrete crushing in the region below the P2 actuator. Peak load carrying capacities were similar for both specimens, but post-peak behavior was more brittle for the voided specimen (PSV-16-12).

- Impact of Number of Strands: Pretensioned Phase 1 specimens displayed hairline cracking in the negative moment region under service demands and positive moment under ULS demands. Under equivalent moment demands, specimens with a greater number of strands showed no cracking. Cracking and nominal flexural capacity was improved with the use of more prestressing strands. However, shear cracking was observed in both Phase 1 and Phase 2 voided specimens under essentially equivalent shear demands. This leads one to conclude that the shear capacity was not significantly improved with the additional prestressing.
- Impact of Void Details: Under ULS demands, slight differences in the onset of shear cracking in the span region were observed. However, under increased loading any differences were no longer apparent. Shear cracking in the square end under maximum shear demands was noted in PSV-28A, but not present in PSV-28B. Both specimens displayed failure in the negative moment region near the face of the column.
- Impact of Pocket Connection Details: In the Phase 1 pretensioned specimens, the additional transverse reinforcement adjacent to the corrugated steel pipe did not appear to markedly improve the performance of the connection. The additional transverse reinforcement over the joint region during Phase 2 did not show significant improvement or difference compared to Phase 1 details. These observations are due, in part, to the fact that joint shear loading demands were modest. Therefore, under joint opening and closing demands, no significant damage was observed in the joint region.
- Impact of Overhang Geometry and Details: The longer, solid overhang of PSV-28A resulted in similar performance to that of the shorter overhang of Phase 1 pretensioned specimens under ULS demands. Under 140 percent ULS demands, the longer overhang exhibited flexure-shear cracking extending outside of the joint region that was not present within the Phase 1 specimens. Under ULS demands, shear cracking was observed along the interior void of the overhang of PSV-28B; this cracking did not occur in either the short

or long solid overhang. PSV-28B displayed concrete crushing along the compression strut from the P1 actuator to the exterior face of the column along the interior void, which was not present in PSV-28A.

## **6. SUMMARY AND CONCLUSIONS**

### **6.1. SUMMARY**

Precast RC bent caps have been used in the construction of many Texas bridges to enable accelerated construction. Standards available for connection of the bent caps to columns provide contractors the option of CIP or precast construction. Precast bent caps can offer greater flexibility in construction options with the use of prestressing, which provides the additional benefit of improving performance through reduced or eliminated cracking. To enable use of pretensioned bent caps, this research explored design considerations and tested full-scale bent caps under indeterminate demands.

To achieve the project objectives, four tasks were conducted. In Task 1, a comprehensive review of the state-of-the-practice and the relevant research was conducted, with a focus on connections to enable design. In Task 2, design objectives for pretensioned bent caps were identified, preliminary design procedures were recommended and applied to a suite of standard bridges, and recommendations were made for connection and end region detailing. In Task 3, six full scale bent caps, including one RC cap, were tested to assess the behavior of pretensioned caps. Tests included bent caps with voids to reduced shipping and construction weight. The results of Tasks 1 to 3 are presented in this document (Volume 1). Task 4, which uses the findings of the previous tasks to develop design recommendations for bent caps, along with design examples are documented separately (Volume 2).

### **6.2. CONCLUSIONS**

#### **6.2.1. Detailing and Fabrication**

Conclusions regarding bent cap detailing and fabrication:

1. To account for bursting and spalling stresses in the end regions, transverse reinforcement is required in the full overhang length. Additional reinforcement provided at the ends may provide additional restraint of cracks, although the specimens fabricated with this reinforcement did not experience cracking sufficient to assess these details.
2. Chamfers on internal voids provided less surface area to secure the void in place, resulting in movement of the void during concrete placement.

3. The spliced transverse reinforcement on the voided bent caps were difficult to tie as access to the top and bottom were impacted by the void and the strand distribution that restricted access to the bottom splice.
4. Pre-existing pre-test cracks formed in the newly cast pretensioned bent caps. For the 16-strand designs, when the bent caps were moved to an indoor laboratory environment hairline cracks appeared; these cracks were attributed to the low humidity and drying shrinkage. For the 28-strand designs, larger cracks appeared several days after strand release prior to delivery to the lab.

### **6.2.2. Pocket Connection Construction and Behavior**

Conclusions regarding pocket construction and behavior:

1. Movements during concrete pouring occurred when the pipe forming the pocket was not properly secured. The use of transverse steel and strands adjacent to the pipe provided assistance in securing the pocket.
2. Hoops around the top of the pocket were effective in restraining longitudinal cracks that occurred at the pocket in the Phase 2 bent caps.
3. The cluster of dowel bars at the center of the column and the open pocket at the bottom (no bars or strands through the opening) enables rapid and accurate placement of the bent cap on the column.
4. Proper placement and consolidation of the pocket concrete in the bedding layer was enabled by pre-wetting the concrete surface at the top of the column and the use of highly workable concrete with aggregate no larger than one-half the bedding layer thickness. Holes in the bedding layer formwork were sufficient to allow the air within the bedding layer to escape; special vent tubes were not needed.
5. Shrinkage of pocket concrete appeared to be successfully avoided without the use of shrinkage compensating admixtures. However, the connection was formed and tested in a laboratory under tightly controlled conditions.
6. Notwithstanding the overall tight appearance of the concrete within the pocket connection, early cracking at the top of the cap beam concrete at the narrowest cross-section of the prestressed cap occurred. This cracking strength can only be

explained if a void is assumed for the pocket and a transformed PSC section modulus is adopted for the cracking calculations.

7. The pocket connection provided adequate transfer of moment between the bent cap and column under design loads.
8. Cracks formed at the connection region due to negative bending. The flexural cracks traced the outline of the pocket, with the pocket concrete remaining uncracked.
9. Cracks and openings in the bedding layer occurred under joint opening and joint closing loading.
10. The performance of the pocket connection under collision or seismic loads is not known since the test setup was unable to generate demands simulating these conditions.

### **6.2.3. Flexure Design and Behavior**

Regarding flexure design and behavior:

1. Design for flexure using the concept of zero tension under dead load was applied to a suite of standard TxDOT bridges and was found to result in designs that had adequate strength and were expected to have no cracks under AASHTO Service 1 demands. In most of these designs, the bent cap was also expected to have no cracks under Strength 1 demands.
2. The pretensioned bent caps cracked at higher loads than did the counterpart RC bent cap. Once the cracks formed, the cracks in the RC bent cap were more extensive and wider than in the pretensioned bent cap specimens.
3. Upon removal of live loads, cracks that formed in the pretensioned bent caps closed if the reinforcement had not previously yielded; for RC bent cap, the cracks did not fully close. If yielding had occurred prior to unload, residual cracks were present in pretensioned and RC bent caps, but were small in the pretensioned bent caps.
4. The use of interior voids had minimal impact on the flexural cracking of bent caps, but shear cracks formed at service loads and extended over the full depth of the void at service loads. Increasing the amount of prestressing significantly increased the load at which flexural cracking occurred but had only a minor impact on when shear cracks formed.

#### **6.2.4. Shear Design and Behavior**

Regarding shear design and behavior:

1. Preliminary design for shear of TxDOT standard bridges with AASHTO LRFD provisions indicated that while the simplified method of 5.8.3.4.2 was more conservative than the method of Appendix B5, most designs were controlled by the minimum area of steel requirements.
2. For pretensioned bent caps, AASHTO LRFD design provisions may result in crack angles that are physically inadmissible within the geometry of bent caps.
3. Solid pretensioned bent caps had a higher cracking shear capacity than the RC bent cap. In the region between the column and interior girder, the shear span ratio was sufficiently large that a shear crack did not form in the pretensioned bent caps. Flexure-shear cracks formed beneath the bearing pad at the interior girder.

#### **6.3. RESEARCH NEEDS**

Based on the findings of the experimental studies, the following research needs are identified:

1. Guidelines should be developed for flexure and shear design of pretensioned bent caps for multicolumn substructures.
2. Experimental tests should be conducted on solid bent caps with moderate shear span ratios to establish shear behavior and enable development of revisions for shear strength design.
3. Research is needed to monitor the fabrication of future bent caps to better understand end region cracking and provide recommendations for avoidance or restraint of cracks. Inspection for cracks should occur after strand release and at regular intervals in the months following. Along with visual inspection, concrete internal temperature, formwork temperature, and ambient temperature should be monitored. Data collection should be supplemented by computational modeling to better understand the mechanisms leading to cracking and to provide recommendations for avoidance of cracks, or restraint in the event cracks may occur.
4. Pocket connections should be tested under more extreme lateral loads to assess appropriateness of such connections for collisions or earthquakes.

5. The use of smaller pockets should be explored, including essentially eliminating the pocket and providing a single duct that can accommodate a strand to post-tension the connection, leading to a completely dry-jointed connection. In this way, one trade would potentially be removed from the job site, leading to significant economy.
6. An alternative to interior voided specimens should be explored to enable weight reduction but that would inhibit the formation of the diagonal flexure-shear cracks. One such option may be the use of U-shaped shell beams that are infilled with site concrete to provide increased shear resistance.
7. To provide further options for accelerated construction of bridge substructures, the use of precast columns should be explored along with appropriate connections to the adjoining bent caps.





## REFERENCES

- AASHTO LRFD Bridge Design Specification, 1st edition (1994). Washington, DC, American Association of State Highway and Transportation Officials. Including interim revisions for 1996 through 2007.
- AASHTO LRFD Bridge Design Specification, 2nd edition (1998). Washington, DC, American Association of State Highway and Transportation Officials. Including interim revisions for 1999 through 2003.
- AASHTO LRFD Bridge Design Specifications, 7th edition (2014). Washington, DC, American Association of State Highway and Transportation Officials.
- AASHTO Standard Specifications for Highway Bridges, 16th edition (1996). Washington, DC, 722 pp. Including interim revisions for 1997 through 2002.
- AASHTO Standard Specifications for Highway Bridges, 17th edition (2002). Washington, DC, American Association of State Highway and Transportation Officials.
- ACI Committee 318 (1965). “Commentary on Building Code Requirements for Reinforced Concrete (ACI 318 63),” SP 10, American Concrete Institute, Farmington Hills, MI, pp. 78-84.
- ACI Committee 318 (2014). “Building Code Requirements for Structural Concrete (ACI 318-14) and Commentary of Building Code Requirements for Structural Concrete (ACI 318R-14).” American Concrete Institute.
- Avendaño, A.R. and Bayrak, O. (2013). “Efficient Shear Reinforcement Design Limits for Prestressed Concrete Beams,” *ACI Structural Journal*, V. 108 (6), pp. 689-697.
- Avendaño, A.R., Hovell, C., Moore, A., Dunkman, D., Nakamura, E., Bayrak, O., and Jirsa, J. (2013). “Pretensioned Box Beams: Prestress Transfer and Shear Behavior,” Rep. No. HWA/TX-13/0-5813-3. CTR.
- Barooah, U.R. (2016). “The Flexural Design of Pretensioned Bent Caps,” M.S. Thesis, Department of Civil Engineering, Texas A&M University, College Station, TX
- Bentz, E. C., Vecchio, F. J., and Collins, M. P. (2006). “Simplified Modified Compression Field Theory for Calculating Shear Strength of Reinforced Concrete Elements,” *ACI Structural Journal*, V. 103(4), pp. 614-624.
- Billington, S., Barnes, R., and Breen, J. (1998). “A Precast Substructure Design for Standard Bridge Systems,” Report No. FHWA/TX-98/1410-2F, Center for Transportation Research, University of Texas at Austin.
- Bracci, J.M., Keating, P.B., and Hueste, M.B.D. (2001). “Cracking in RC Bent Caps,” Rep. No. FHWA/TX 01/1851, Texas Transportation Institute, Texas A&M University.

- Brenes, F., Wood, S., and Kreger, M. (2006). "Anchorage Requirements for Grouted Vertical-Duct Connectors in Precast Bent Cap Systems," Report No. FHWA/TX-06/0-4176-1, Center for Transportation Research, University of Texas at Austin.
- Brown, M.D, Sankovich, C.L., Bayrak, O., Jirsa, J.O., Breen, J.E., and Wood, S.L. (2006). "Design for Shear in Reinforced Concrete Using Strut-and-Tie Models," Report No. FHWA/TX-06/0-4371-2. CTR.
- Bent Cap Analysis, CAP18, Bent Cap Program User Manual*, Texas State Department of Highways and Public Transportation, Bridge Division, Austin, Texas, 1978.
- CAP18 Version 6.2.2, Texas Department of Transportation. [Computer Software]
- Chalioris, C.E. (2013). "Steel Fibrous RC Beams Subjected to Cyclic Deformations under Predominant Shear," *Engineering Structures*, V. 49, pp. 104-118.
- Chalioris, C.E., and Karayannis, C.G. (2013). "Experimental Investigation of RC Beams with Rectangular Spiral Reinforcement in Torsion," *Engineering Structures*, V. 56, pp. 296-297.
- Cheok, G. S.; Stone, W. C.; and Kunnath, S. K. (1998). "Seismic Response of Precast Concrete Frames with Hybrid Connections," *ACI Structural Journal*, V. 95(5), 527-539.
- Choi, K. K., Park, H., and Wight, J. K. (2007). "Unified Shear Strength Model for Reinforced Concrete Beams – Part I: Development," *ACI Structural Journal*, V. 104(2), pp. 142-152.
- Collins, M. P., and Kuchma, D. (1999). "How Safe Our Large, Lightly Reinforced Concrete Beams, Slabs, and Footings?," *ACI Structural Journal*, V. 96 (4), pp. 482-490.
- Collins, M. P., and Mitchell, D. (1986). "A Rational Approach to Shear Design – The 1984 Canadian Code Provisions," *ACI Structural Journal*, V. 83(6), pp. 925-933.
- Collins, M.P. and Mitchell, D. (1991). *Prestressed Concrete Structures*. Prentice-Hall, Inc.
- Collins, M. P., Mitchell, D., Adebar, P., and Vecchio, F. J. (1996). "A General Shear Design Method," *ACI Structural Journal*, V. 93(1), pp. 36-45.
- Cook, W.D. and Mitchell, D. (1988). "Studies of Disturbed Regions near Discontinuities in Reinforced Concrete Members," *ACI Structural Journal*, V. 85(2), pp. 206-216.
- CSA Committee A23.3 (2004). "Design of Concrete Structures, (CSA A23.3-04)," Rexdale, ON, Canada, 240 pp.
- Culmo, M. P. (2009). "Connection Details for Prefabricated Bridge Elements and Systems," Report FHWA-IF-09-010, Federal Highway Administration.
- De Corte, W. and Boel, V. (2013). "Effectiveness of Spirally Shaped Stirrups in Reinforced Concrete Beams," *Engineering Structures*, V. 52, pp. 667-675.

- Deschenes, D.J., Bayrak, O., and Folliard, K.J. (2009). "ASR/DEF-Damaged Bent Caps: Shear Tests and Field Implications" Technical Report No. 12-8XXIA006. Ferguson Structural Engineering Laboratory, University of Texas at Austin.
- Dhonde, H.B., Mo, Y.L., and Hsu, T.T.C. (2005). "Fiber Reinforcement in Prestressed Concrete Beams," Report No. FHWA/TX-06/0-4819-1. University of Houston.
- Dinh, H.H., Parra-Montesinos, G.J., and Wight, J.K. (2011). "Shear Strength Model for Steel Fiber Reinforced Concrete Beams without Stirrup Reinforcement," *Journal of Structural Engineering*, V. 137(10), pp. 1039- 1051.
- Dutta, A., Mander, J.B., Eeri, M., and Kokorina, T. (1999). "Retrofit for Control and Repairability of Damage." *Earthquake Spectra*, V. 15(4), pp. 657-679.
- Dutta, A., and Mander, J.B. (2001). "Energy based methodology for ductile design of concrete column," *Journal of Structural Engineering*, V. 127(12), pp. 1374-1381.
- Ferguson, P.M. (1964). "Design Criteria for Overhanging Ends of Bent Caps – Bond and Shear," Research Report 3-5-63-52. Center of Highway Research, University of Texas, Austin.
- Filippou, F. C., Popov, E. G., and Bertero, V. V. (1983). "Effects of bond deterioration on hysteretic behavior of reinforced concrete joints," Report No. UCB/EERC-83/19. Earthquake Engineering Research Center. University of California. Berkeley, California.
- Fonseca, F., and Rowe, M.D. (2003). "Flexural Performance of Deteriorated Reinforced Concrete Cantilevered Bent Caps – Part 1," Technical Report UT-03.33, Utah Department of Transportation.
- Freeby, G., Hyzak, M., Medlock, R.D., Kenneth, O., Vogel, J., and Wolf, L.M. (2003). "Design and Construction of Precast Bent Caps at TxDOT," Texas Department of Transportation.
- Freeby, Gregg A., P.E. (2015). "Chapter 2: Damage Assessment and Repair Types," Concrete Repair Manual: Damage Assessment and Repair Types. Texas Department of Transportation, 4 Apr. 2015. Web. 12 Aug. 2016.
- Garber, D., Gallardo, J., Deschenes, D., Dunkman, D., Bayrak, O. (2013). "Effect of New Prestress Loss Estimates on Pretensioned Concrete Bridge Girder Design," Center for Transportation Research, Research Project 0-6374-2, University of Texas at Austin.
- Hawkins, N. M., and D. A. Kuchma. (2006). "Simplified Shear Design of Structural Concrete Members," NCHRP Report 549. Transportation Research Board, National Research Council, Washington, DC.
- Heiber, D.G., Stanton, J.F., Eberhard, M.O., and Wacker, J. M. (2005). "State-of-the-Art Report on Precast Concrete Systems for Rapid Construction of Bridges," Washington State Transportation Center, Washington State Department of Transportation, University of Washington, Seattle, Washington.

- Higgs, A., Barr, P.J., and Halling, M.W. (2015). "Comparison of measured and AASHTO LRFD-Predicted residual prestress forces, shear and flexural capacities of high-strength prestressed-concrete bridge girders," *Journal of Bridge Engineering*, V. 20(1), pp. 05014009-1-9.
- Kani, G. N. J. (1964). "The Riddle of Shear Failure and Its Solution," *Journal of the American Concrete Institute*, V 61(4), pp. 441-467.
- Kani, G. N. J. (1966). "Basic Facts Concerning Shear Failure," *ACI Journal*, V. 63(6), pp. 675-692.
- Kani, G. N. J. (1967). "How Safe Are Our Large Reinforced Concrete Beams," *ACI Journal*, V. 64 (3), pp. 128-141.
- Kapur, J., Yen, W.P., Dekelbab, W., Bardow, A., Keever, M., Sletten, J., Tobias, D., and Saiidi, M.S. (2012). "Best Practices Regarding Performance of ABC Connections in Bridges Subjected to Multihazard and Extreme Events," NCHRP Project 20-68A Scan 11-02, Arora and Associates P.C., American Association of State Highway and Transportation Officials, Lawrenceville, New Jersey.
- Karayannis, C.G. and Chalioris, C.E. (2013). "Shear Tests of Reinforced Concrete Beams with Continuous Rectangular Spiral Reinforcement," *Construction and Building Materials*, V. 46, pp. 86-97.
- Khaleghi, B., Schultz, E., Seguirant, S.J., Marsh, M.L., Haraldsson, O.S., Eberhard, M.O. and Stanton, J.F. (2012). "Accelerated Bridge Construction in Washington State: From Research to Practice," *PCI Journal*, V. 57(4), pp. 34-49.
- Kim, J.H. and Mander, J.B. (1999). "Truss Modeling of Reinforced Concrete Shear-Flexure Behavior." Technical Report MCEER-99-0005, University at Buffalo.
- Kim, J.H. and Mander, J.B. (2005). "Theoretical Shear Strength of Concrete Columns Due to Transverse Steel." *Journal of Structural Engineering*, V.131 (1), pp. 197-199.
- Kim, S.Y., Yang, K.H., Byun, Y, and Ashour, A.F. (2007). "Tests of Reinforced Concrete Beams Strengthened with Wire Rope Units," *Engineering Structures*, V. 29 (10), pp. 2711-2722.
- Kwak, Y.-K., Eberhard, M.O., Kim, W.-S., and Kim, J. (2002). "Shear Strength of Steel Fiber-Reinforced Concrete Beams without Stirrups," *ACI Structural Journal*, V. 99 (4), pp. 530-538.
- Lequesne, R., Parra-Montesinos, G.J., and Wight, J.K. (2013). "Seismic Behavior and Detailing of High-Performance Fiber-Reinforced Concrete Coupling Beams and Coupled Wall Systems," *Journal of Structural Engineering*, V. 139 (8), pp. 1362-1370.
- Li, L., Mander, J.B., and Dhakal, R.P. (2008). "Bidirectional Cyclic Loading Experiment on a 3D Beam-Column Joint Designed for Damage Avoidance," *Journal of Structural Engineering*, V. 134 (11), pp. 1733-1742.

- Mander, J.B., Bracci, J.M., and Hurlebaus, S. (2015). "Structural Assessment of "D" Regions Affected by Premature Concrete Deterioration: Technical Report," FHWA/TX-15/0-5997-2, TTI.
- Mander, J.B., and Cheng, C-T. (1997). "Seismic Resistance of Bridge Piers Based on Damage Avoidance Design," Technical Report NCEER-97-0014, National Center for Earthquake Engineering Research, University at Buffalo SUNY, Federal Highway Administration, Buffalo, New York.
- Mander, J.B., and Cheng, C-T. (1999). "Replaceable Hinge Detailing for Bridge Columns," American Concrete Institute, Special Publication SP – 187 Seismic Response of Concrete Bridges.
- Mander, J.B., Bracci, J.M., Hurlebaus, S., Grasley, Z., Karthik, M.M., Liu, S., and Scott R.M. (2012). "Structural Assessment of "D" Regions Affected by Premature Concrete Deterioration: Technical Report," Report No. FHWA/TX-12/0-5997-1, TTI.
- Mansur, M.A. and Ong, K.C.G. (1991). "Behavior of reinforced fiber concrete deep beams in shear," *ACI Structural Journal*, V. 88 (1), pp. 98-105.
- Mansur, M.A., Lee, C.K., and Lee, S.L. (1987). "Deformed Wire Fabric as Shear Reinforcement in Concrete Beams," *ACI Structural Journal*, V. 84 (5), pp. 392-399.
- Marsh, M.L., Wernli, M., Garrett, B.E., Stanton, J.F., Eberhard, M.O., and Weinert, M.D. (2011). "Application of Accelerated Bridge Construction Connections in Moderate-to-High Seismic Regions," Report 698, National Cooperative Highway Research Program, Transportation Research Board, Washington, D.C.
- Matlock, H., Ingram, W.B. (1996). "A computer program to analyze bending of bent caps," Summary Report 56-2 (S). Center for Highway Research, Project 3-5-63-56, University of Texas at Austin.
- Matsumoto, E. E. (2009). Emulative Precast Bent Cap Connections for Seismic Regions: Component Test Report-Cap Pocket Limited Ductility Specimen (Unit 4). Sacramento, CA: California State University, Sacramento, 149 pp.
- Matsumoto, E. E., Waggoner, M. C., Sumen, G., Kreger, M. E., Wood, S. L., and Breen, J. E. (2001). "Development of a Precast Bent Cap System," Report No. FHWA/TX-0-1748-2, Center for Transportation Research, Texas Department of Transportation, The University of Texas at Austin.
- Mehta, P. K., and Monteiro, P. J. M. (2004). *Concrete: Microstructure, Properties, and Materials*, McGraw Hill, New York, 659 pp.
- Miller, C., Holt, J., and McCammon, V. (2014). "Precast, Pretensioned, Bent Caps," Bridge Division, Texas Department of Transportation.

- Nakamura, E., Avendano, A.R., and Bayrak, O. (2013). "Shear Database for Prestressed Concrete Members," *ACI Structural Journal*, V.110 (6), pp. 909-919.
- O'Callaghan M.R., and Bayrak, O. (2008). "Tensile stresses in end regions of pretensioned I-beams at release," Technical report: IAC-88-5DD1A003-1, University of Texas at Austin.
- OpenSees. Open System for Earthquake Engineering Simulation. [Computer Software] Pacific Earthquake Engineering Research Center, University of California. Berkeley, California.
- Pang, J. B. K., Steuck, K. P., Cohagen, L., Stanton, J. F., and Eberhard M. O. (2008). "Rapidly Constructible Large-Bar Precast Bridge-Bent Seismic Connection." Report No. WA-RD 684.2, Washington State Transportation Center, Washington State Transportation Commission, University of Washington, Seattle, Washington.
- Pang, J., B. K., Eberhard, M. O. and Stanton, J. F. (2010). "Large-Bar Connection for Precast Bridge Bents in Seismic Regions." *Journal of Bridge Engineering*, V. 15 (3), pp. 231-239.
- Park, R. (1995). "A Perspective on the Seismic Design of Precast Concrete Structures in New Zealand," University of Canterbury Christchurch, New Zealand, *PCI Journal*, V. 40 (3), pp. 40-60.
- Parra-Montesinos, G. J. (2006). "Shear Strength of Beams with Deformed Steel Fibers." *Concrete International*, V. 28 (11), 57-66.
- Pincheira, J.A., Rizkalla, S.H., and Attiogbe, E.K. (1989). "Performance of Welded Wire Reinforcement as Shear Reinforcement under Cyclic Loading," *ACI Structural Journal*, V. 86 (6), pp. 728-735.
- Reineck, K., Kuchma, D.A., Kim, K.S., Marx, S. (2003). "Shear Database for Reinforced Concrete Members Without Shear Reinforcement." *ACI Structural Journal*, V.100 (2), pp. 240-249.
- Restrepo, J. I., Tobolski, M. J., and Matsumoto, E. E. (2011). "Development of a Precast Bent Cap System for Seismic Regions," NCHRP Report 681, Transportation Research Board, Washington, D.C., 116 pp.
- Robertson, I.N., and Durani, A.J. (1987) "Shear Strength of Prestressed Concrete T-beams with Welded Wire Reinforcement as Shear Reinforcement," *PCI Journal*, V. 32 (2), pp. 46-59.
- Runzell, B., Shield, C., and French, C. (2007). "Shear Capacity of Prestressed Concrete Beams," Rep. No. MN/RC 2007 47, Minnesota Department of Transportation, University of Minnesota.
- SAP 2000 Version 17.1.0. (2014). Computer and Structures, Inc., Berkeley, CA. [Computer Software].
- Scott, R.M., Mander, J.B., and Bracci, J.M. (2012a). "Compatibility Strut-and-Tie Modeling: Part I – Formulation." *ACI Structural Journal*, V.109 (5), pp. 635-644.

- Scott, R.M., Mander, J.B., and Bracci, J.M. (2012b). "Compatibility Strut-and-Tie Modeling: Part II – Implementation," *ACI Structural Journal*, V. 109 (5), pp. 645-653.
- Shioya, T., Iguro, M., Nojiri, Y., Akiyama, H., and Okada, T. (1990). "Shear Strength of Large Reinforced Concrete Beams, Fracture Mechanics: Application to Concrete." *ACI SP-118*, V. 118 pp. 25-279.
- Stanton, J., Eberhard, M., Marsh, M. L., Khaleghi, B., Haraldsson, O. S., Janes, T. M., Tran, H. Viet and Davis. P. (2012). "Accelerated Bridge Construction: Bent on Safety. New Design Toughens ABC During Seismic Events." *Roads and Bridges*.
- Stanton, J., Eberhard, M., Sanders, D., Thonstad, T., Schaefer, J., Kennedy, B., Haraldsson, O., and Mantawy, I. (2014). "A Pre-Tensioned, Rocking Bridge Bent for ABC in Seismic Regions," *Proceedings of the 10<sup>th</sup> National Conference in Earthquake Engineering, Earthquake Engineering Research Institute, Anchorage, Alaska*.
- SHRP (2013). "Innovative Bridge Design for Rapid Renewal: ABC Toolkit," SHRP 2 Report S2-RO4-RR-2, The Second Strategic Highway Research Program, Transportation Research Board.
- Steuck, K., Pang, J.B.K, Stanton, J.F. and Eberhard, M.O. (2007). "Anchorage of Large-Diameter Reinforcing Bars Grouted into Ducts," WA-RD 684.1, Department of Environmental and Civil Engineering University of Washington, Washington State Transportation Commission, Seattle, Washington.
- Stone, W. C., Cheok, G. S., and Stanton. J. F., (1995). "Performance of Hybrid Moment Resisting Precast Beam-Column Concrete Connections Subjected to Cyclic Loading," *ACI Structural Journal*, V.92, No.2, pp. 229-249
- Taylor, A. W., Rowell, R. B., and Breen, J. E. (1995). "Behavior of Thin Walled Concrete Box Piers," *ACI Structural Journal*, V. 92(3), pp. 319 333.
- Texas Department of Transportation (TxDOT). (2010). "Rectangular Bent Cap Design Example," Bridge Division, Texas Department of Transportation.
- Texas Department of Transportation (TxDOT). (2015a). "Precast Concrete Bent Cap Option for Round Columns," Bridge Division, Texas Department of Transportation.
- Texas Department of Transportation (TxDOT). (2015b). "TxDOT Bridge Manual-LRFD," Bridge Division, Texas Department of Transportation.
- Tobolski, M. J., Ralls, M. L., Matsumoto, E. E., and Restrepo, J. I. (2006). "State-of-Practice of Precast Bent Cap Systems," *Structures Congress 2006, ASCE Journal*, pp. 1-10.
- Tobolski, M. J. (2010). "Improving the Design and Performance of Concrete Bridges in Seismic Regions," Ph.D. Dissertation, University of California, San Diego.



- Tuan, C.Y., Yehia, S.A., Jongpitaksseel, A., Tadros, M.K. (2004). "End Zone Reinforcement for Prestensioned Concrete Girders," *PCI Journal*, V. 49 (33), pp. 62-82.
- Ueda, T., and Stitmannathum, B. (1991). "Shear Strength of Precast Prestressed Hollow Slabs with Concrete Topping," *ACI Structural Journal*, V. 88(4), pp. 402-410.
- Uijl, den J.A. (1983), "Tensile Stresses in the Transmission Zones of Hollow-Core Slabs Prestressed with Prestensioned Strands," Delft University of Technology Report 5-83-10 (Stevin Laboratory Report SR-49), 110 pp.
- Vecchio, F. J., and Collins, M. P. (1986). "The Modified Compression Field Theory for Reinforced Concrete Elements Subjected to Shear," *ACI Structural Journal*, V. 83(2), pp. 219-231.
- Vecchio, F. J., and Collins, M. P. (1988). "Predicting the Response of Reinforced Concrete Beams Subjected to Shear Using Modified Compression Field," *ACI Structural Journal*, V. 85(3), pp. 258-268.
- WisDOT (2014). "Precast Pier Cap and Column Details," Standard Detail Drawings Structures Development Section, State of Wisconsin Department of Transportation.
- Xuan, X., Rizkalla, S., and Maruyama, K. (1988). "Effectiveness of Welded Wire Fabric as Shear Reinforcement in Prestensioned Prestressed Concrete T-Beams," *ACI Structural Journal*, V. 85 (6), pp. 429-436.
- Yassin, M. H. M. (1994). "Nonlinear analysis of prestressed concrete structures under monotonic and cyclic load," Dissertation. University of California. Berkeley, California.
- Young, B. S., Bracci, J. M., Keating, P. B., and Hueste, M. B. D. (2001). "Cracking in Reinforced Concrete Bent Caps," *ACI Structural Journal*, V. 99(4), pp. 488-498.
- Zararis, P. D., and Papadakis, G. C. (2001). "Diagonal Shear Failure and Size Effect in RC Beams without Web Reinforcement," *Journal of Structural Engineering*, V. 127(7), pp. 733-742.
- Zhenqiang, L. and Leiva, J.D. (2010). "Prestensioned, Precast Concrete Hollow-Core Units Used for Interchanged Bridge Project in Honduras" *PCI Journal*, V. 55 (2) pp.71-81.
- Ziehl, P.H., Caicedo, J.M., Rizos, D., Mays, T., Larosche, A., ElBatanouny, M., and Mustain, B. (2011). "Testing of Connections between Prestressed Concrete Piles and Precast Concrete Bent Caps," Department of Civil and Environmental Engineering, University of South Carolina, South Carolina Department of Transportation.

## **APPENDIX A: CONSTRUCTION TIMELINE**

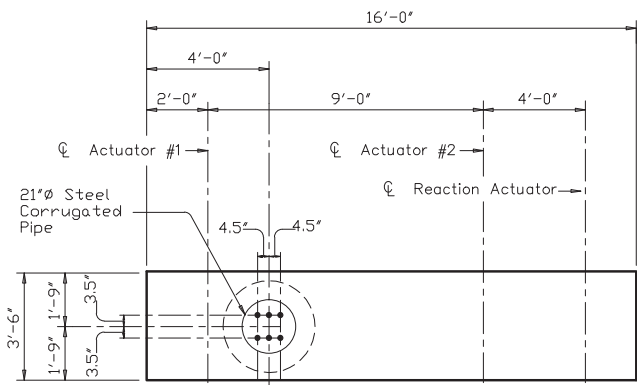


<b>Specimen</b>	<b>Activity</b>	<b>Date</b>
RCS-16-2	Cap Pour	6/2/2016
	Column Base Pour	6/3/2016
	Column Pour	6/6/2016
	Specimen Assembly	7/14/2016
	Pocket Connection Pour	7/18/2016
PSS-16-12	Cap Pour	8/26/2016
	Strand Release	8/29/2016
	Column Base Pour	8/11/2016
	Column Pour	8/12/2016
	Delivery	11/3/2016
	Specimen Assembly	11/3/2016
	Pocket Pour	11/7/2016
PSS-16-24	Cap Pour	8/26/2016
	Strand Release	8/29/2016
	Column Base Pour	11/18/2016
	Column Pour	11/22/2016
	Delivery	1/18/2017
	Specimen Assembly	1/18/2017
	Pocket Pour	1/26/2017
PSV-16-12	Cap Pour	8/26/2016
	Strand Release	8/29/2016
	Column Base Pour	11/18/2016
	Column Pour	11/22/2016
	Delivery	12/15/2016
	Specimen Assembly	12/15/2016
	Pocket Pour	12/19/2016
PSV-28A	Cap Pour	5/16/2017
	Strand Release	5/19/2017
	Column Base Pour	4/20/2017
	Column Pour	4/24/2017
	Delivery	6/7/2017
	Specimen Assembly	6/7/2017
	Pocket Pour	6/8/2017
PSV-28B	Cap Pour	5/16/2017
	Strand Release	5/19/2017
	Column Base Pour	4/20/2017
	Column Pour	4/24/2017
	Delivery	7/12/2017
	Specimen Assembly	7/12/2017
	Pocket Pour	7/13/2017

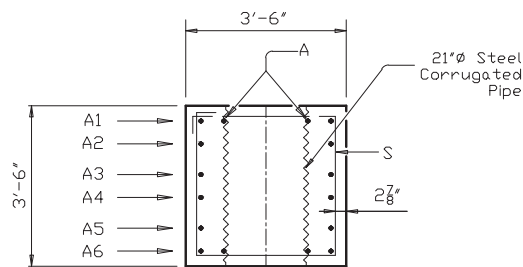


## **APPENDIX B: DESIGN DRAWINGS**

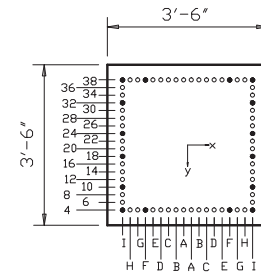




**PLAN**

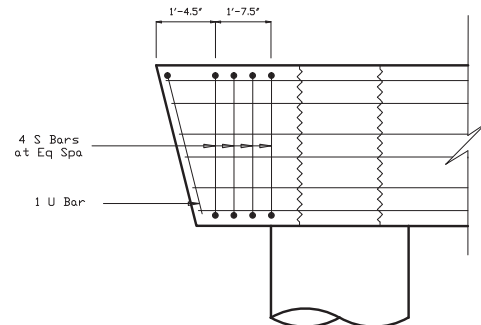
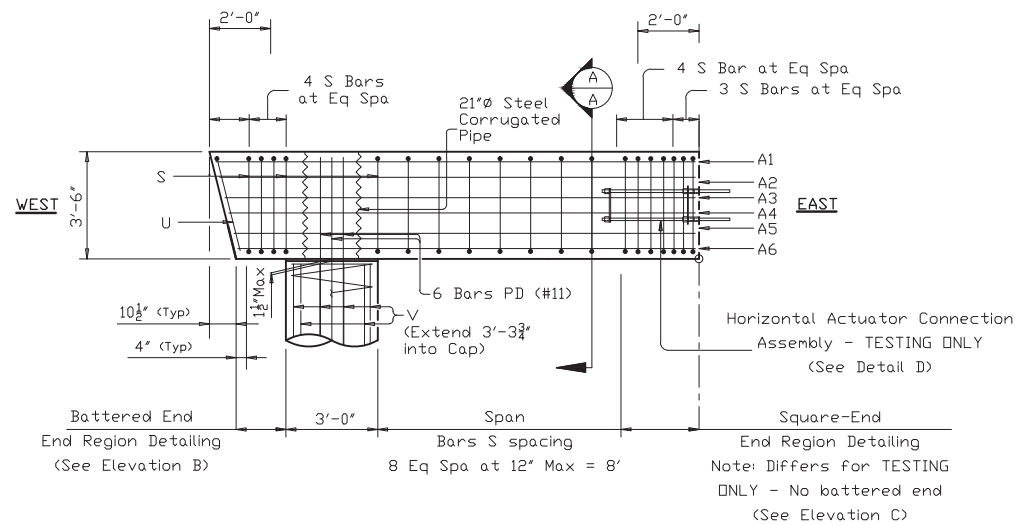


**REBAR LAYOUT**



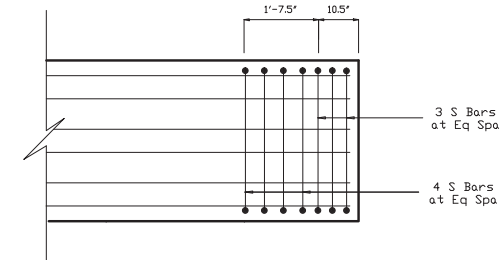
**REBAR PATTERN**

TABLE OF ESTIMATED REBAR QUANTITIES				
Bar	No.	Size	Length	Weight
A1	4	#8	15'-8"	
A2	2	#8	15'-6 1/2"	
A3	2	#8	15'-4 1/2"	
A4	2	#8	15'-3"	
A5	2	#8	15'-1"	
A6	4	#8	14'-11 1/2"	
PD	6	#11	8'-11 1/2"	
S	20	#5	13'-1"	
U	1	#5	9'-8"	
V	10	#9	6'-3 1/4"	
Z	1	#4	105'-1"	
Reinforcing Steel			Lb	
Class 'C' Concrete (Cap)			CY	
Class 'C' Concrete (Col)			CY	



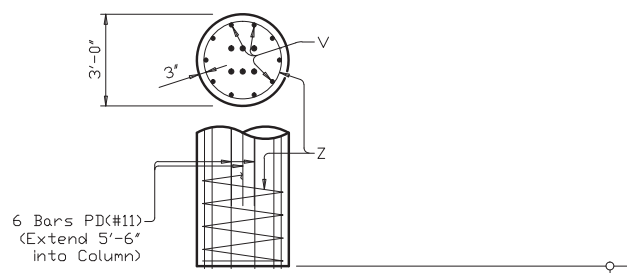
**ELEVATION B**

**BATTERED END - END REGION DETAILING**

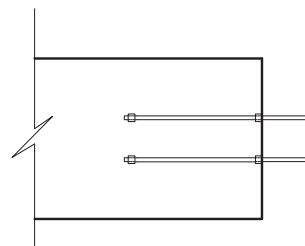


**ELEVATION C**

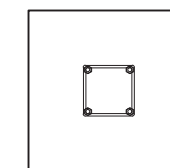
**DEAD-END END REGION DETAILING**



**ELEVATION A**



**SIDE VIEW**

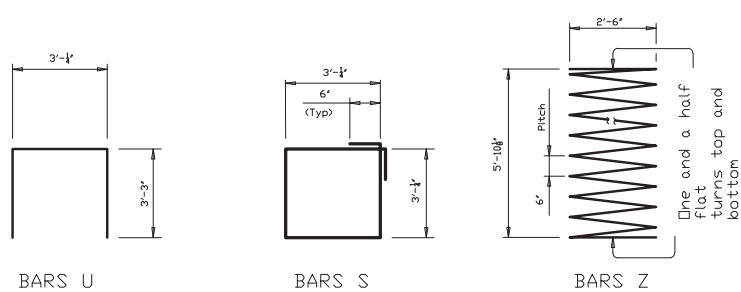


**FRONT VIEW**



**DETAIL D**

**WOOD FORMWORK HORIZONTAL ACTUATOR CONNECTION ASSEMBLY**



**BARS U**

**BARS S**

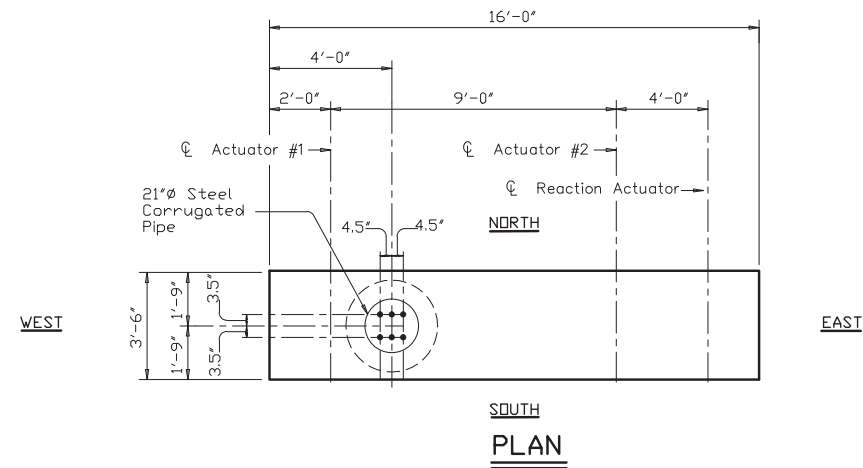
**BARS Z**

SCALE:  $\frac{3}{16}'' = 1.0'$

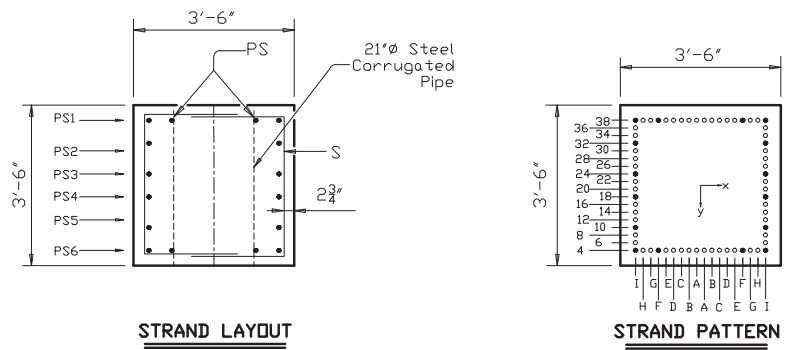
TxDOT 0-6863  
Precast Pretensioned  
Bent Caps  
RCS-16-12

DATE: Aug 28, 2017 - 2:33pm  
FILE:





**SOUTH PLAN**

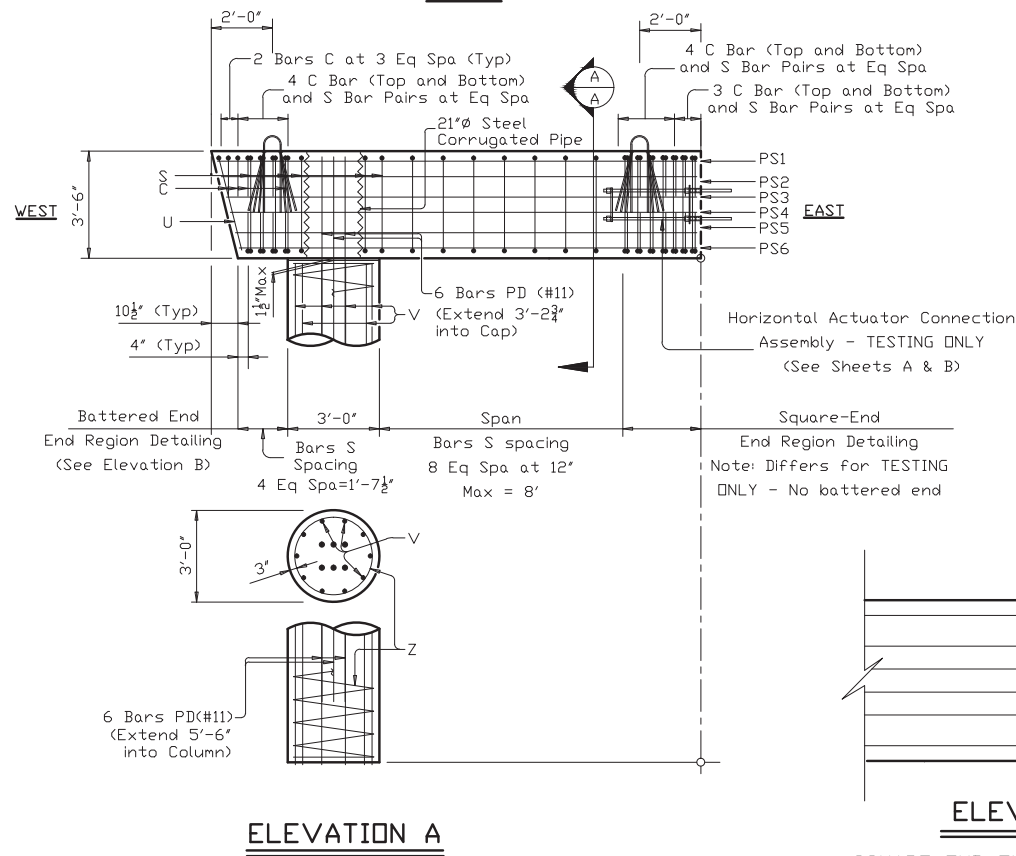


**STRAND LAYOUT**

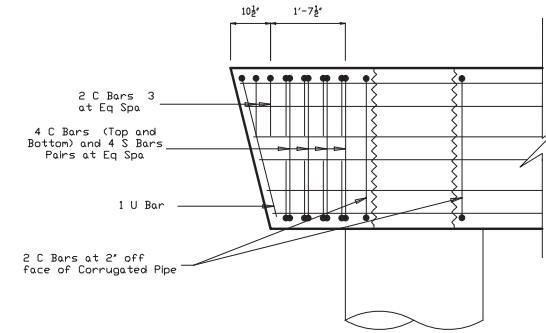
**STRAND PATTERN**

**SECTION A-A**

TABLE OF ESTIMATED BAR QUANTITIES				
Bar	No.	Size	Length	Weight
PD	6	#11	8'-11½"	
C	24	#5	5'-6½"	
S	18	#5	14'-2"	
B	12	#5	5'-4"	
U	1	#5	9'-3½"	
V	10	#9	6'-3½"	
Z	1	#4	105'-1"	
Reinforcing Steel			Lb	
Class "H" Concrete (Cap)			CY	
Class "C" Concrete (Col)			CY	



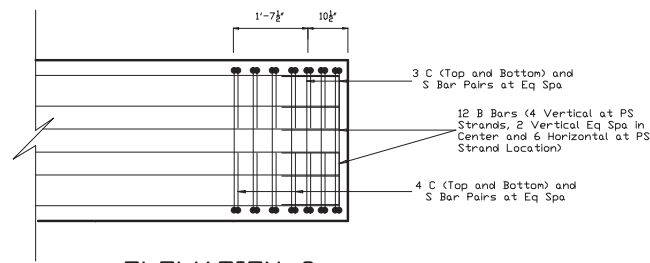
**ELEVATION A**



**ELEVATION B**

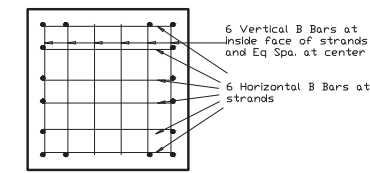
**BATTERED-END END REGION DETAILING**

TABLE OF ESTIMATED PRESTRESSING STRAND QUANTITIES				
Bar	No.	Size	Length	Weight
PS1	4	0.6	15'-8"	
PS2	2	0.6	15'-6"	
PS3	2	0.6	15'-4½"	
PS4	2	0.6	15'-3"	
PS5	2	0.6	15'-1½"	
PS6	4	0.6	14'-11½"	
PRESTRESSING STRGTH (ksi)				270
CONCRETE RELEASE STRGTH f'ci (ksi)				4.00
MIN. 28-DAY COMP STRGTH f'c (ksi)				5.00
MAX. 28-DAY COMP STRGTH f'c (ksi)				7.00



**ELEVATION C**

**SQUARE-END END REGION DETAILING**

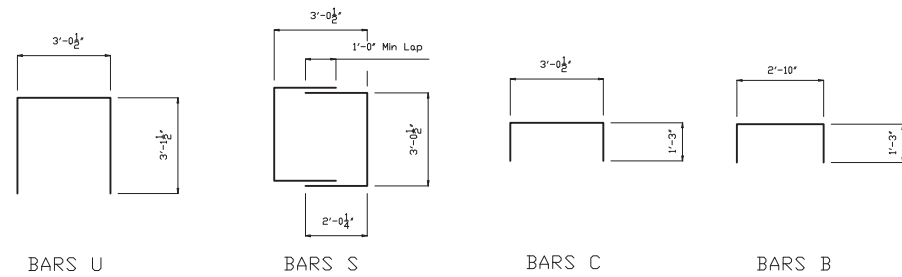


**SECTION D-D**

**SQUARE-END END REGION DETAILING**

SCALE:  $\frac{3}{16}'' = 1.0''$

DATE: Aug 28, 2017 - 2:14pm  
FILE:

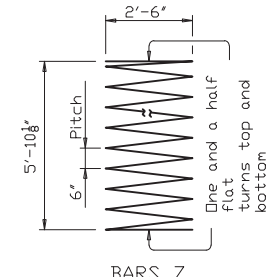


BARS U

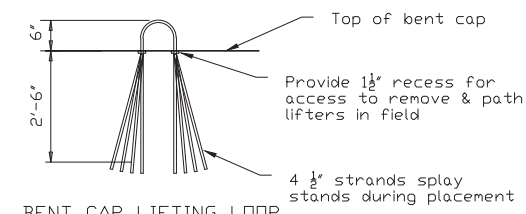
BARS S

BARS C

BARS B

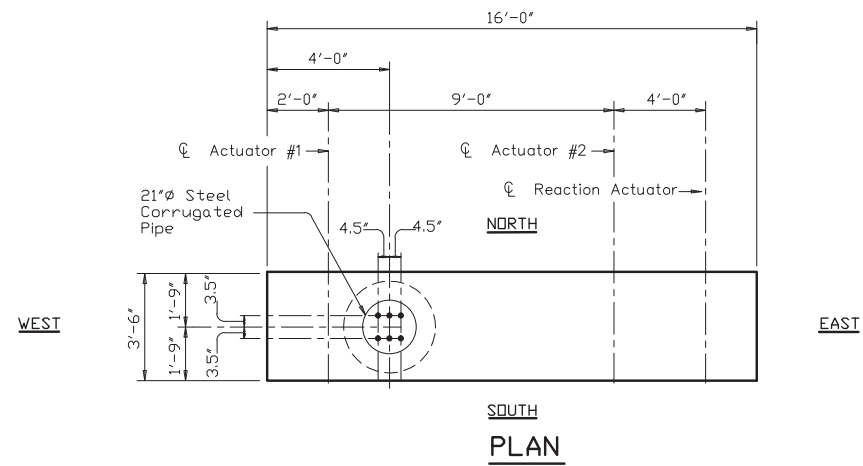


BARS Z

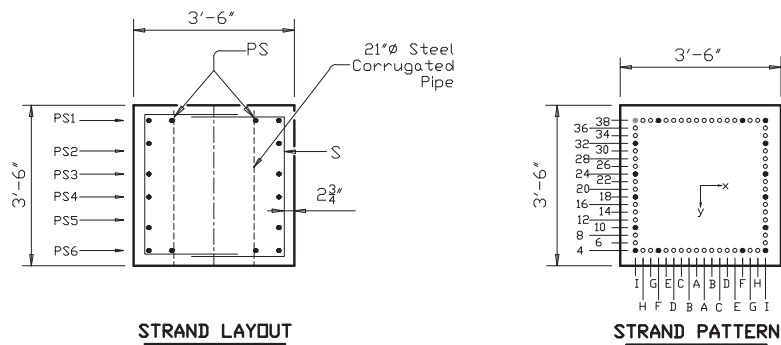


BENT CAP LIFTING LOOP

TxDOT 0-6863  
Precast Pretensioned  
Bent Caps  
PSS-16-12



**SOUTH PLAN**

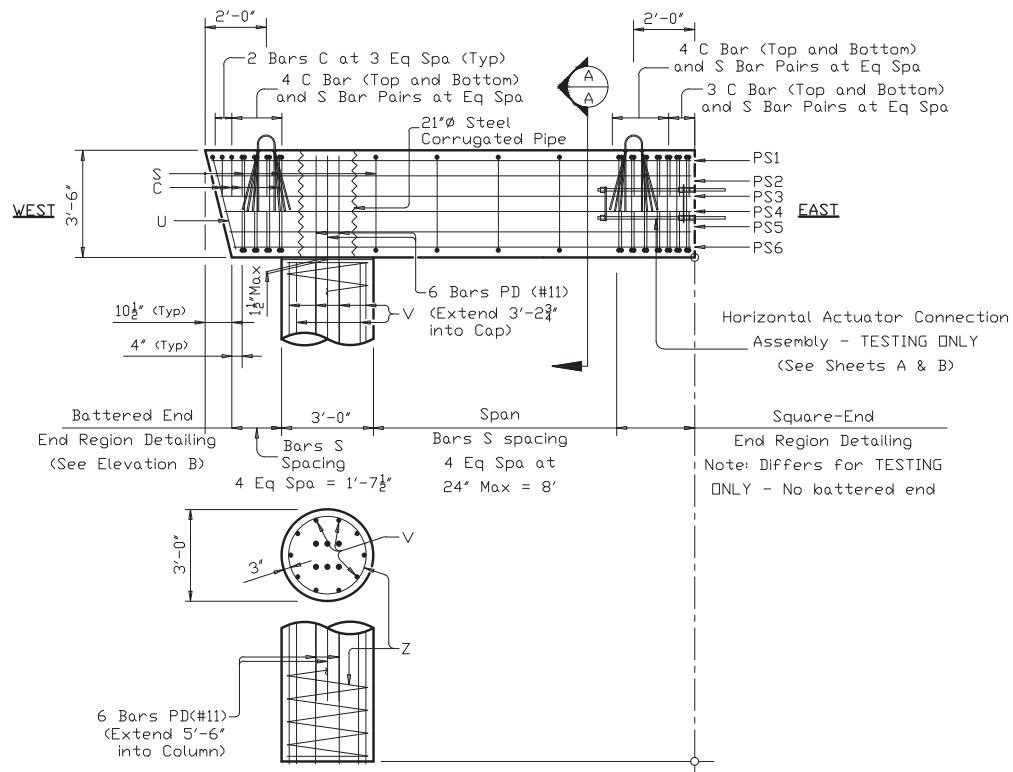


**STRAND LAYOUT**

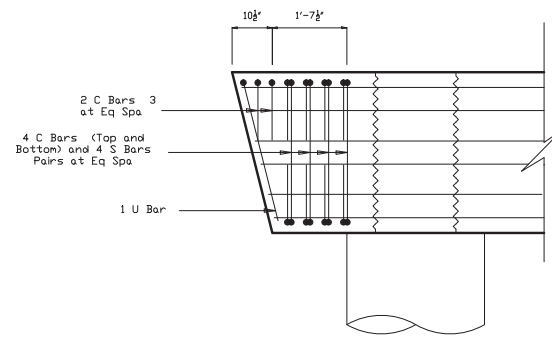
**STRAND PATTERN**

**SECTION A-A**

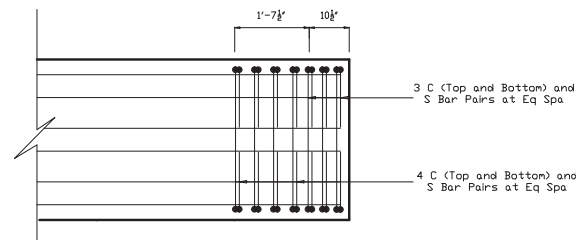
TABLE OF ESTIMATED BAR QUANTITIES				
Bar	No.	Size	Length	Weight
PD	6	#11	8'-11 1/2'	
C	24	#5	5'-6 1/2'	
S	14	#5	14'-2'	
U	1	#5	9'-3 1/2'	
V	10	#9	6'-3 1/2'	
Z	1	#4	105'-1'	
Reinforcing Steel			Lb	
Class 'H' Concrete (Cap)			CY	
Class 'C' Concrete (Col)			CY	



**ELEVATION A**



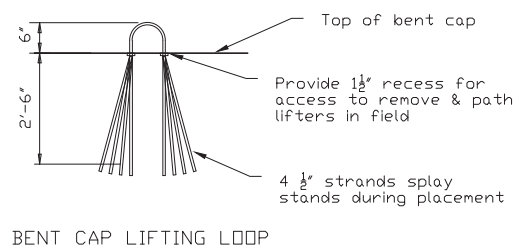
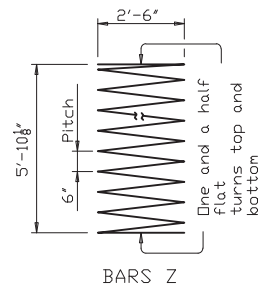
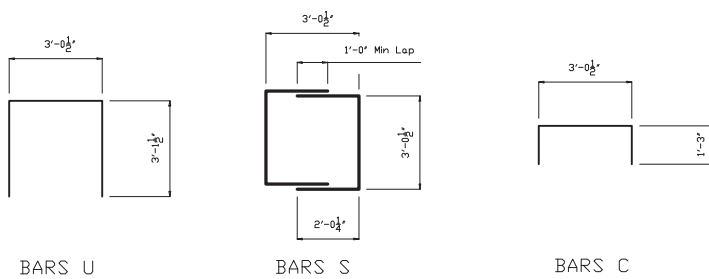
**ELEVATION B  
BATTERED-END END REGION DETAILING**



**ELEVATION C  
SQUARE-END END REGION DETAILING**

TABLE OF ESTIMATED PRESTRESSING STRAND QUANTITIES				
Bar	No.	Size	Length	Weight
PS1	4	0.6	15'-8"	
PS2	2	0.6	15'-6"	
PS3	2	0.6	15'-4 1/2"	
PS4	2	0.6	15'-3"	
PS5	2	0.6	15'-1 1/2"	
PS6	4	0.6	14'-11 1/2"	
PRESTRESSING STRGTH (ksi)				270
CONCRETE RELEASE STRGTH f'ci (ksi)				4.000
MIN. 28-DAY COMP STRGTH f'c (ksi)				5.000
MAX. 28-DAY COMP STRGTH f'c (ksi)				7.000

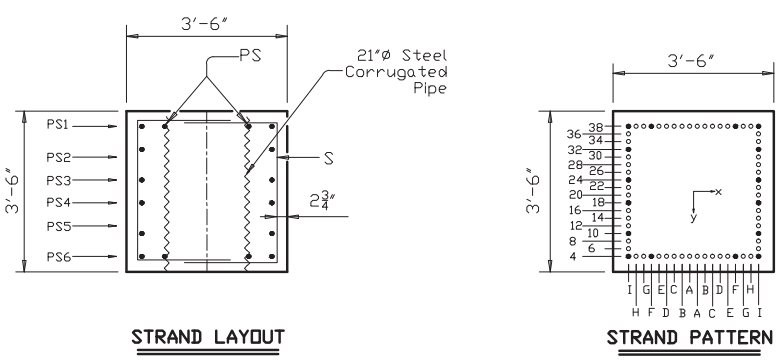
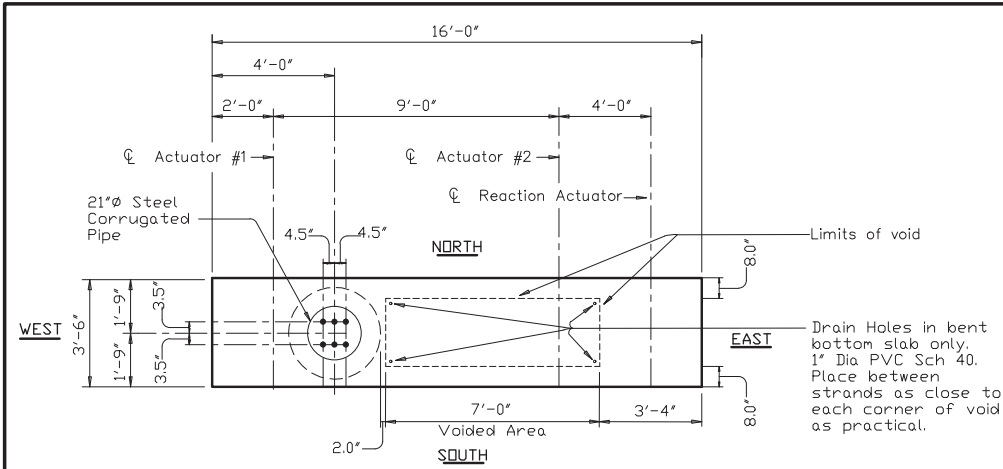
SCALE: 3/16" = 1.0"



**BENT CAP LIFTING LOOP**

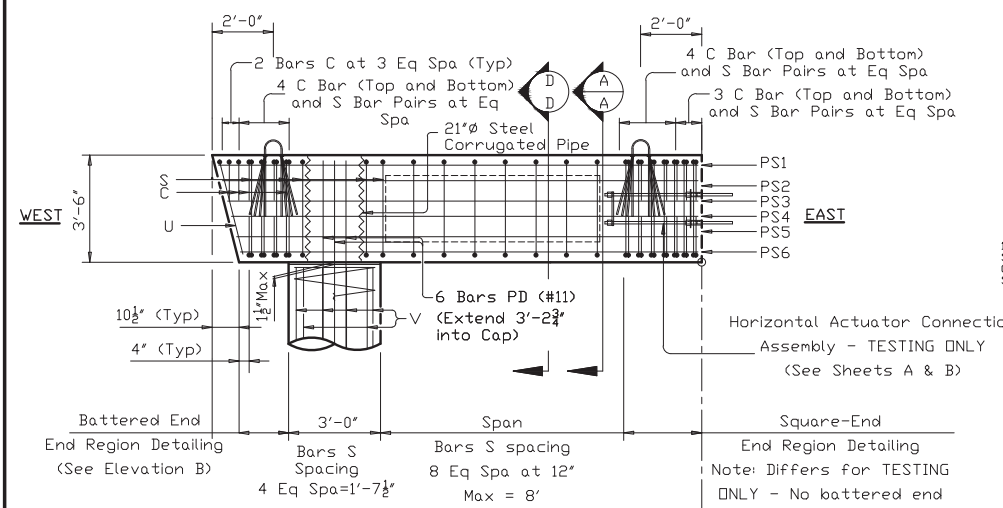
TxDOT 0-6863  
Precast Pretensioned  
Bent Caps  
PSS-16-24

DATE: Aug 28, 2017 - 2:14pm  
FILE:

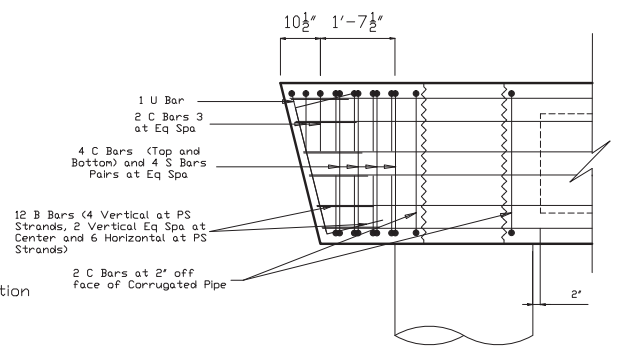


SECTION A-A

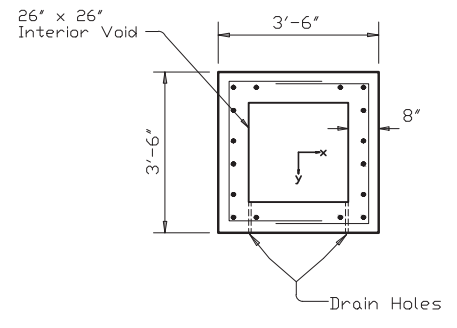
Bar	No.	Size	Length	Weight
PD	6	#11	8'-11½"	
C	24	#5	5'-6½"	
S	18	#5	14'-2"	
B	24	#5	5'-4"	
U	1	#5	9'-3½"	
V	10	#9	6'-3½"	
Z	1	#4	105'-1"	
Reinforcing Steel				Lb
Class 'H' Concrete (Cap)				CY
Class 'C' Concrete (Col)				CY



ELEVATION A

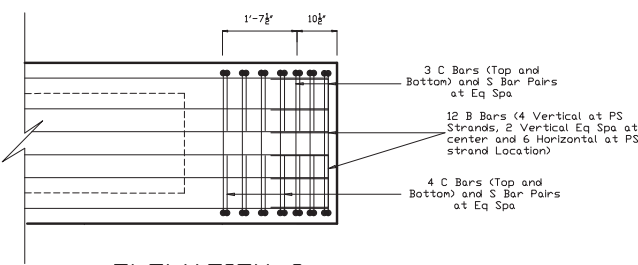


BATTERED-END END REGION DETAILING

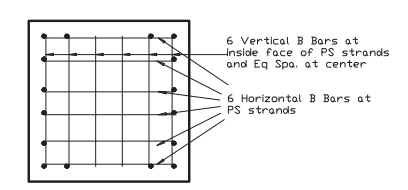


SECTION D-D  
VOIDED SECTION DETAILING

Bar	No.	Size	Length	Weight
PS1	4	0.6	15'-8"	
PS2	2	0.6	15'-6"	
PS3	2	0.6	15'-4½"	
PS4	2	0.6	15'-3"	
PS5	2	0.6	15'-1½"	
PS6	4	0.6	14'-11½"	
PRESTRESSING STRGTH (ksi)				270
CONCRETE RELEASE STRGTH F'ci (ksi)				4.00
MIN. 28-DAY COMP STRGTH F'c (ksi)				5.00
MAX. 28-DAY COMP STRGTH F'c (ksi)				7.00



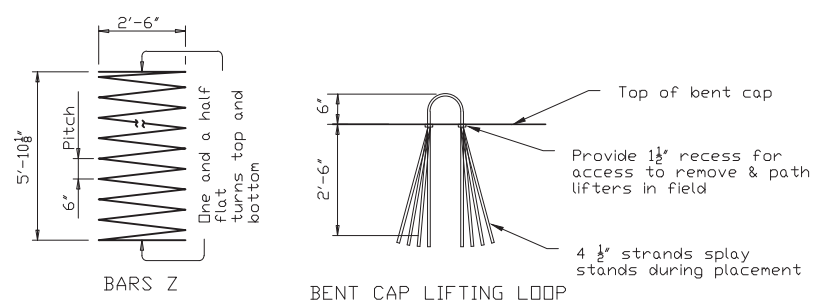
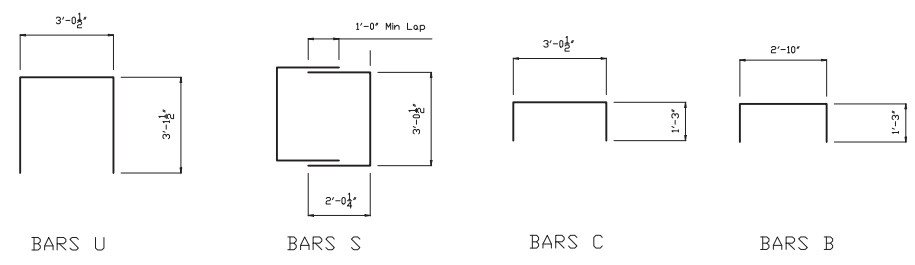
ELEVATION C  
SQUARE-END END REGION DETAILING



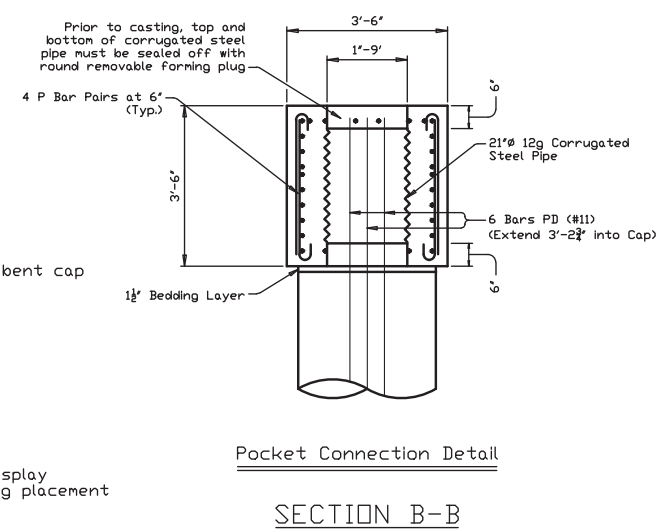
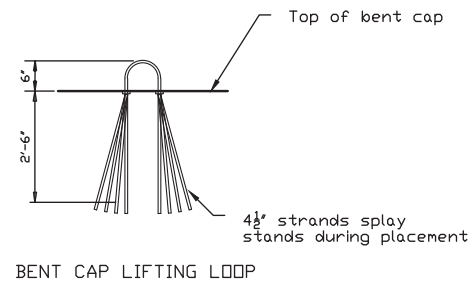
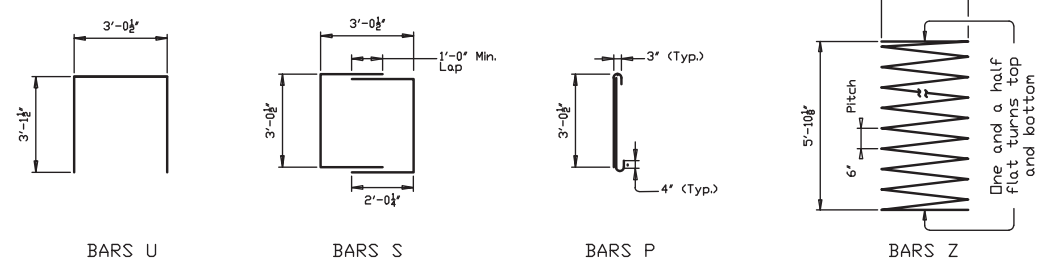
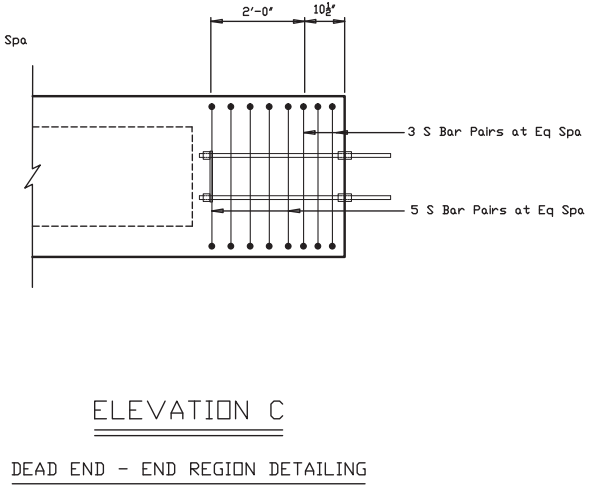
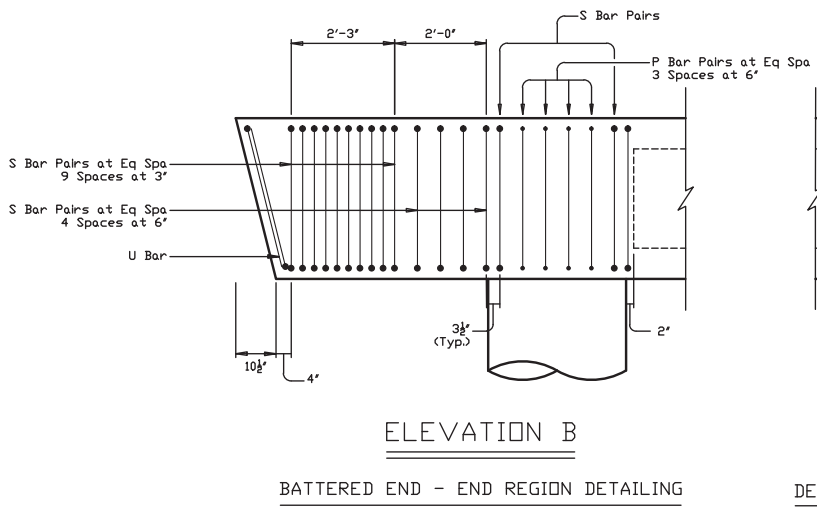
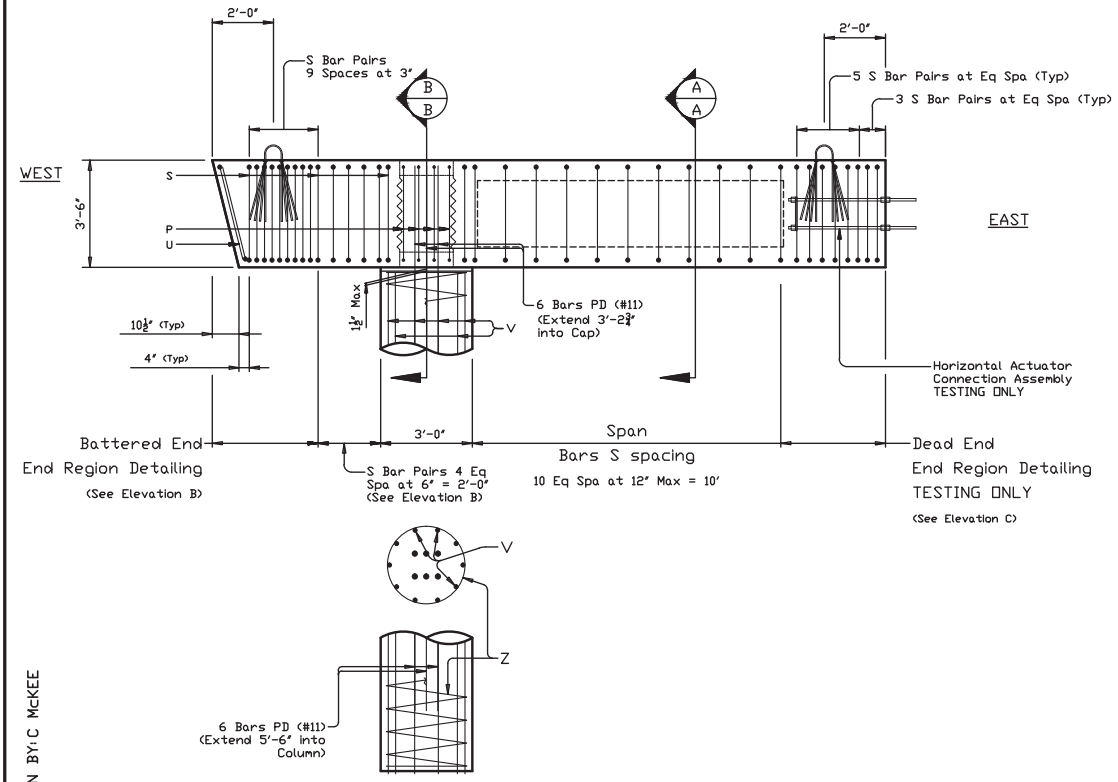
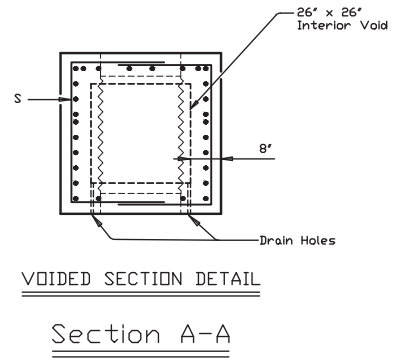
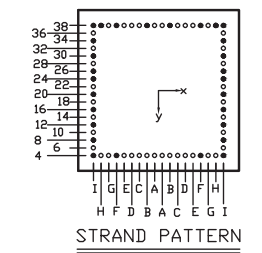
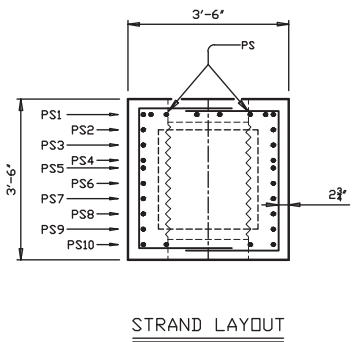
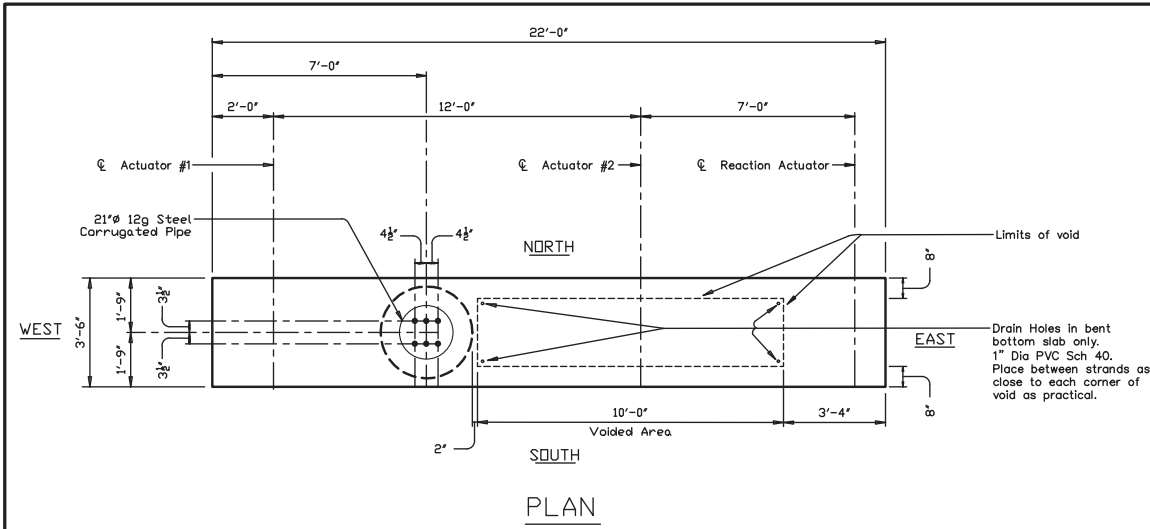
SECTION E-E  
SQUARE & BATTERED ENDS END REGION DETAILING

SCALE: 3/16" = 1.0"

DATE: Aug 28, 2017 - 2:16pm  
FILE:



TxDOT 0-6863  
Precast Prestressed  
Bent Caps  
PSV-16-12



SCALE: 3/16" = 1.0"

TxDOT 0-6863

Precast Pretensioned

Bent Caps

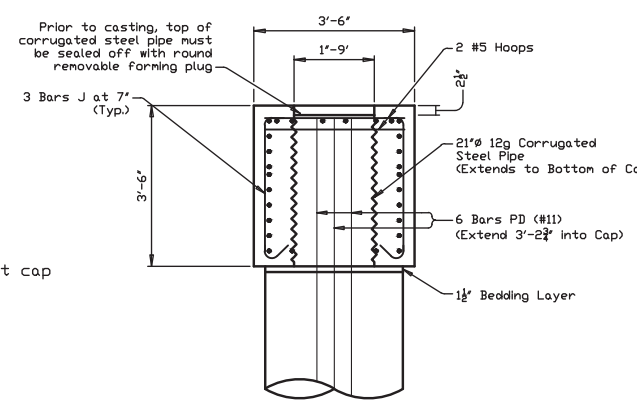
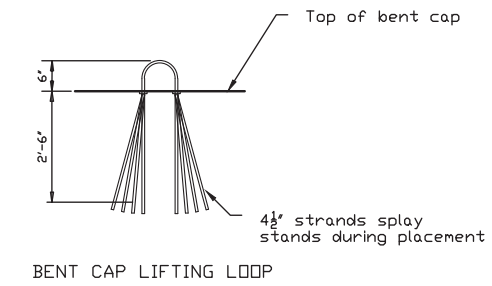
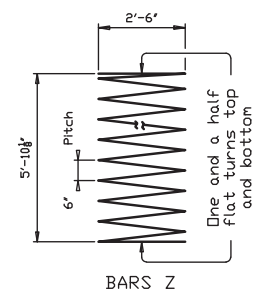
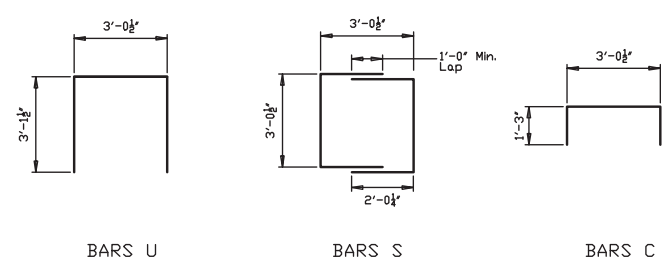
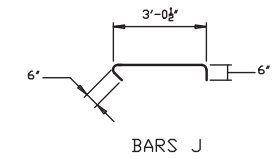
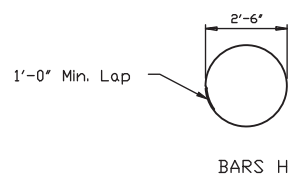
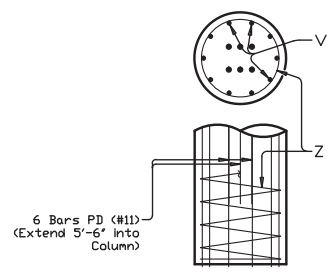
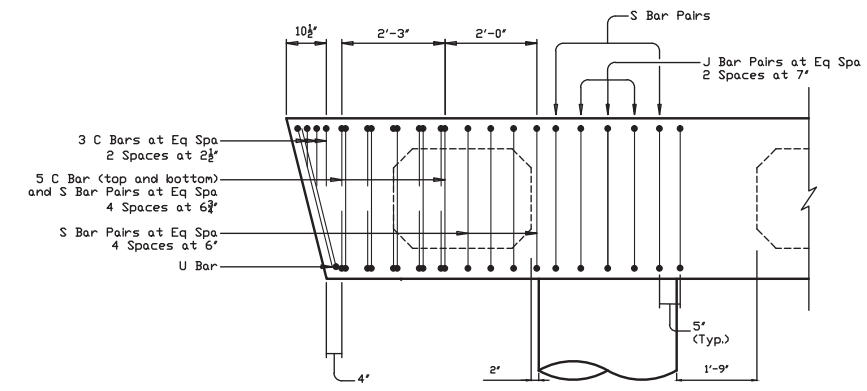
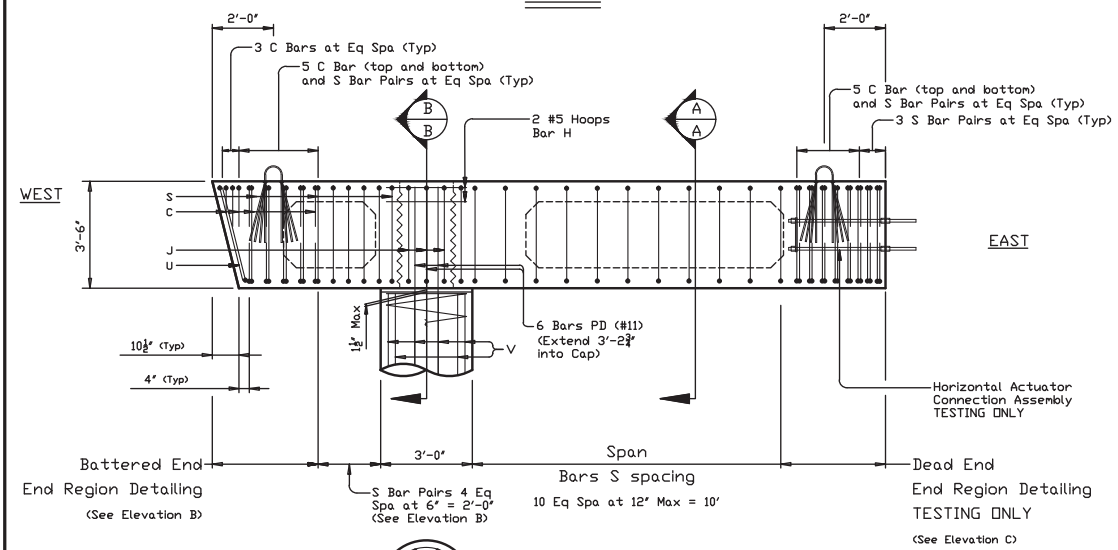
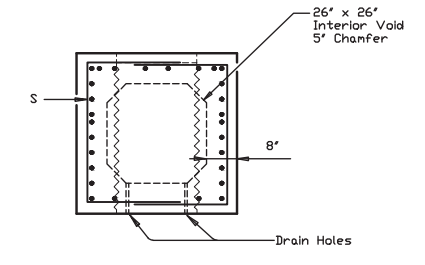
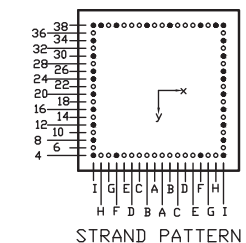
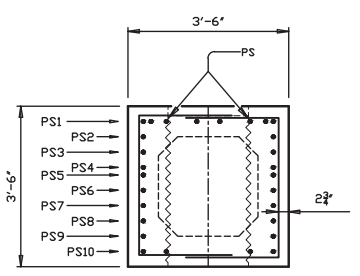
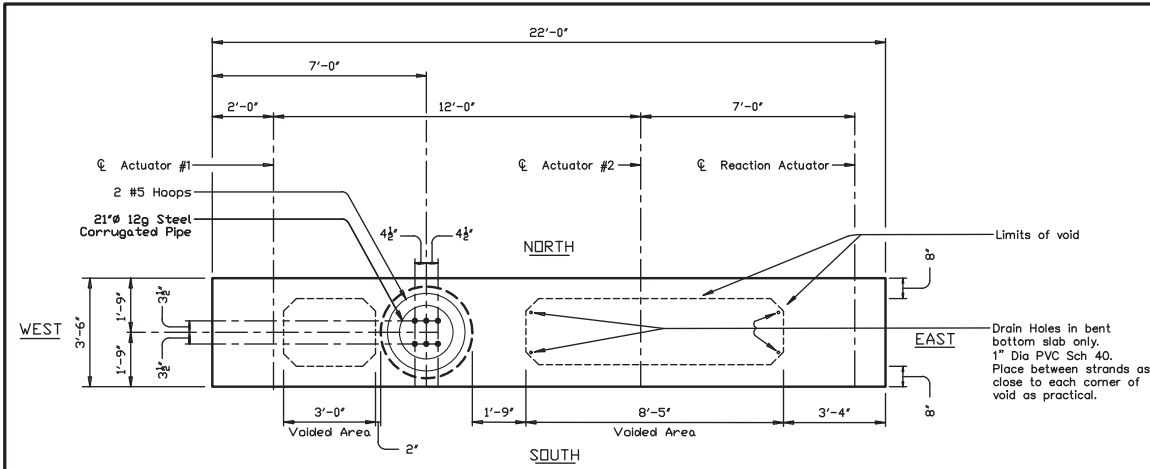
PSV-28A

AS-BUILT

DATE: May 24, 2017 - 3:58pm

FILE:

DRAWN BY: C McKEE



SCALE: 3/16" = 1.0"

TxDOT 0-6863  
Precast Pretensioned  
Bent Caps  
PSV-28B  
AS-BUILT

DATE: May 24, 2017 - 3:58pm  
DRAWN BY: C McKEE  
FILE:

## **APPENDIX C: THERMOCOUPLE AND TEMPERATURE DATA**



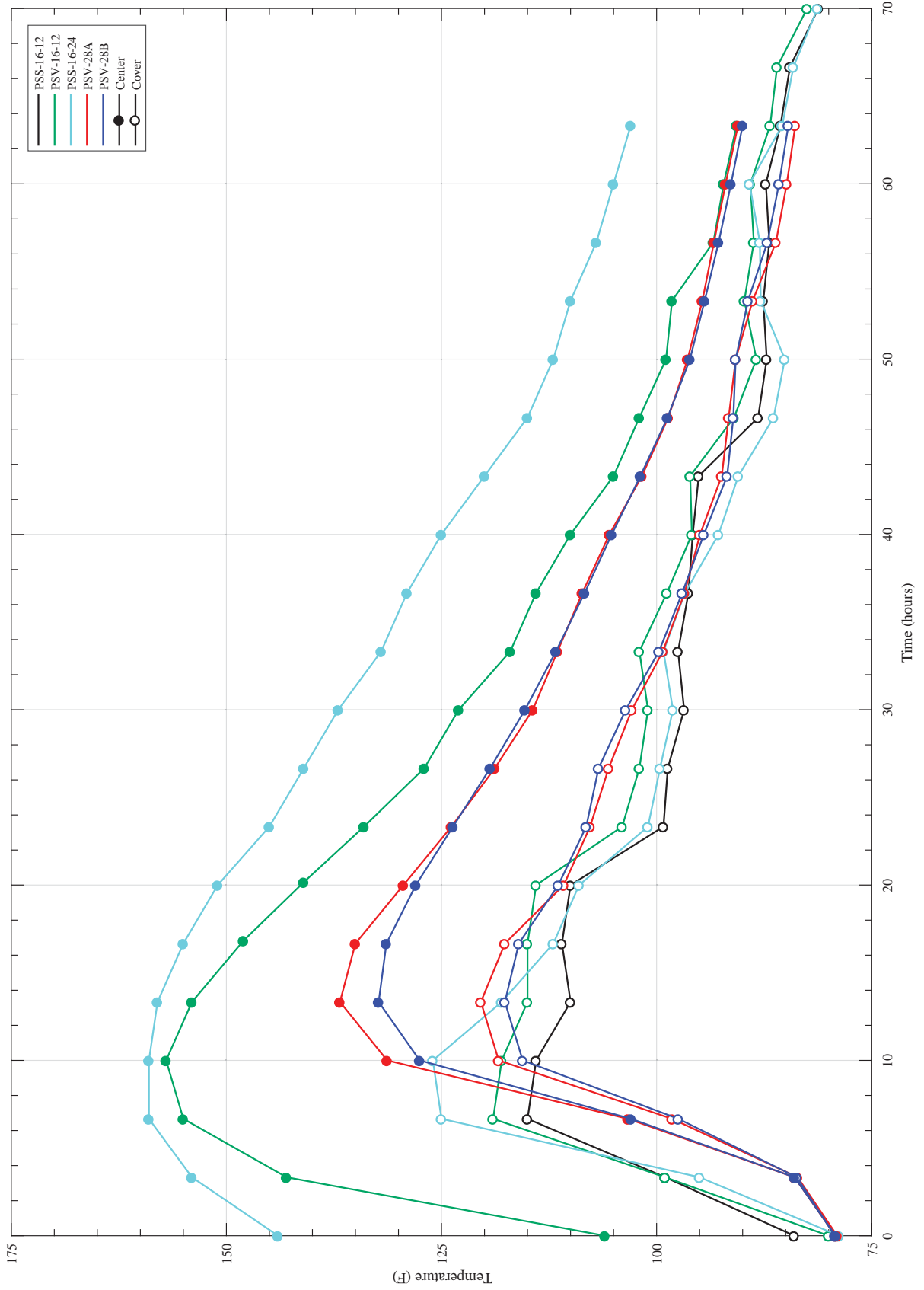
**Table C.1. Measured Surface Temperature of Phase 1 PSC Specimens.**

Specimen	Location	Time	South		North	
			Concrete (°F)	Steel (°F)	Concrete (°F)	Steel (°F)
PSS-16-12	Center	8/26/2016 09:15 (Concrete pour)	82.6	80.8	80.9	83.5
		8/26/2016 11:00 (+ 2 hours)	87.2	83.2	87.3	94.6
		8/26/2016 17:00 (+ 8 hours)	87.6	96.4	84.3	98.1
		8/27/2016 10:30 (+ 25 hours)	83.5	82.4	84.9	88.4
		8/29/2016 09:00 (+ 72 hours)	74.8	71.8	75.0	74.4
PSS-16-24	Center	8/26/2016 09:15 (Concrete pour)	80.8	80.6	80.4	79.3
		8/26/2016 11:00 (+ 2 hours)	91.3	86.4	90.6	96.8
		8/26/2016 17:00 (+ 8 hours)	92.6	98.7	87.6	100.4
		8/27/2016 10:30 (+ 25 hours)	86.6	82.1	88.3	104.2
		8/29/2016 09:00 (+ 72 hours)	74.4	72.5	76.6	75.1
PSV-16-12	Near pipe	8/26/2016 09:15 (Concrete pour)	78.1	78.7	80.9	84.1
		8/26/2016 11:00 (+ 2 hours)	92.4	85.1	89.8	94.8
		8/26/2016 17:00 (+ 8 hours)	89.7	98.0	86.6	97.8
		8/27/2016 10:30 (+ 25 hours)	85.3	83.4	86.8	101.9
		8/29/2016 09:00 (+ 72 hours)	74.2	73.1	75.1	78.9



**Table C.2. Measured Surface Temperature of Phase 2 Specimens.**

Specimen	Location	Time	South		North	
			Concrete (°F)	Steel (°F)	Concrete (°F)	Steel (°F)
PSV-28A	Battered end	5/16/2017 15:10 (Concrete pour)	74.4	79.3	75.2	79.4
	Pipe		74.5	79.4	74.4	78.9
	Dead end		74.3	79.0	73.6	78.7
	Battered end	5/19/2017 07:25 (+64 hours)	74.5	72.7	74.5	76.4
	Pipe		74.8	76.3	74.5	76.8
	Dead end		75.1	76.4	75.5	76.5
	Battered end	5/19/2017 11:00 (+68 hours)	80.8	77.0	83.6	80.0
	Pipe		85.2	78.2	85.3	79.9
	Dead end		85.6	77.6	82.6	78.1
	Battered end	5/19/2017 13:30 (+72 hours)	98.9	83.8	105.0	85.4
	Pipe		96.2	82.8	97.8	86.6
	Dead end		93.9	81.3	99.8	87.0
PSV-28B	Battered end	5/16/2017 15:10 (Concrete pour)	74.5	78.8	73.5	78.4
	Pipe		74.4	78.8	73.7	78.3
	Dead end		73.9	77.8	73.6	78.6
	Battered end	5/19/2017 07:25 (+64 hours)	74.2	76.1	75.3	77.2
	Pipe		74.1	77.6	75.9	78.8
	Dead end		72.6	74.6	74.4	75.4
	Battered end	5/19/2017 11:00 (+68 hours)	90.4	77.2	89.1	78.8
	Pipe		84.2	78.0	78.9	75.9
	Dead end		85.6	77.0	81.3	78.2
	Battered end	5/19/2017 13:30 (+72 hours)	91.9	86.9	93.5	83.3
	Pipe		92.6	83.1	93.1	83.3
	Dead end		93.4	82.3	93.9	80.6



*Note: Temperature data for PSV-28A and PSV-28B are displayed as an average of the temperature readings measured by both thermocouples.*



## **APPENDIX D: INSTRUMENTATION PLANS**



# Precast Prettensioned Bent Caps

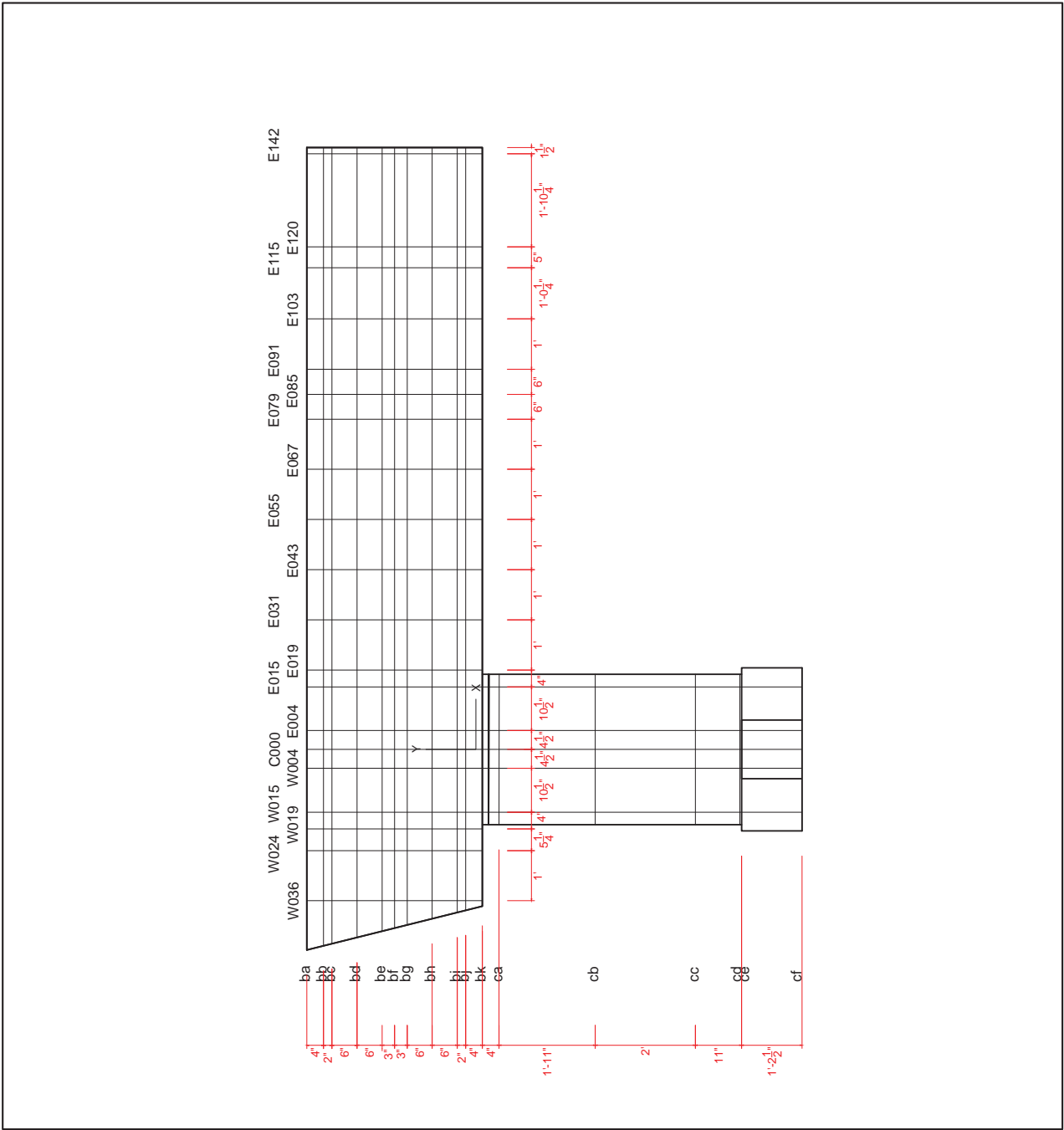
## Phase 1

<b>PROJECT NO:</b>	0-6863
<b>DATE:</b>	28-Aug-17
<b>VERSION:</b>	V-1
<b>DRAWN BY:</b>	J. LEE
<b>SCALE:</b>	N.T.S.
<b>TITLE:</b>	

## Phase 1 Instrumentation Plan Grid Line

<b>SHEET#:</b>	1 of 11
----------------	---------

F:\Kevin Yoelbem Cap Project\Kevin Yoelbem\CAD\Drawings\In KY Theses\Instrumentation 2\_15\_17\11x17.dwg August 28, 2017 - 4:35 PM





ZACHRY DEPARTMENT OF  
CIVIL ENGINEERING  
TEXAS A&M UNIVERSITY



TXDOT 0-6863  
Precast Prettensioned Bent Caps  
Phase 1

PROJECT NO: 0-6863

DATE: 28-Aug-17

VERSION: V-1

DRAWN BY: J. LEE

SCALE: N.T.S.

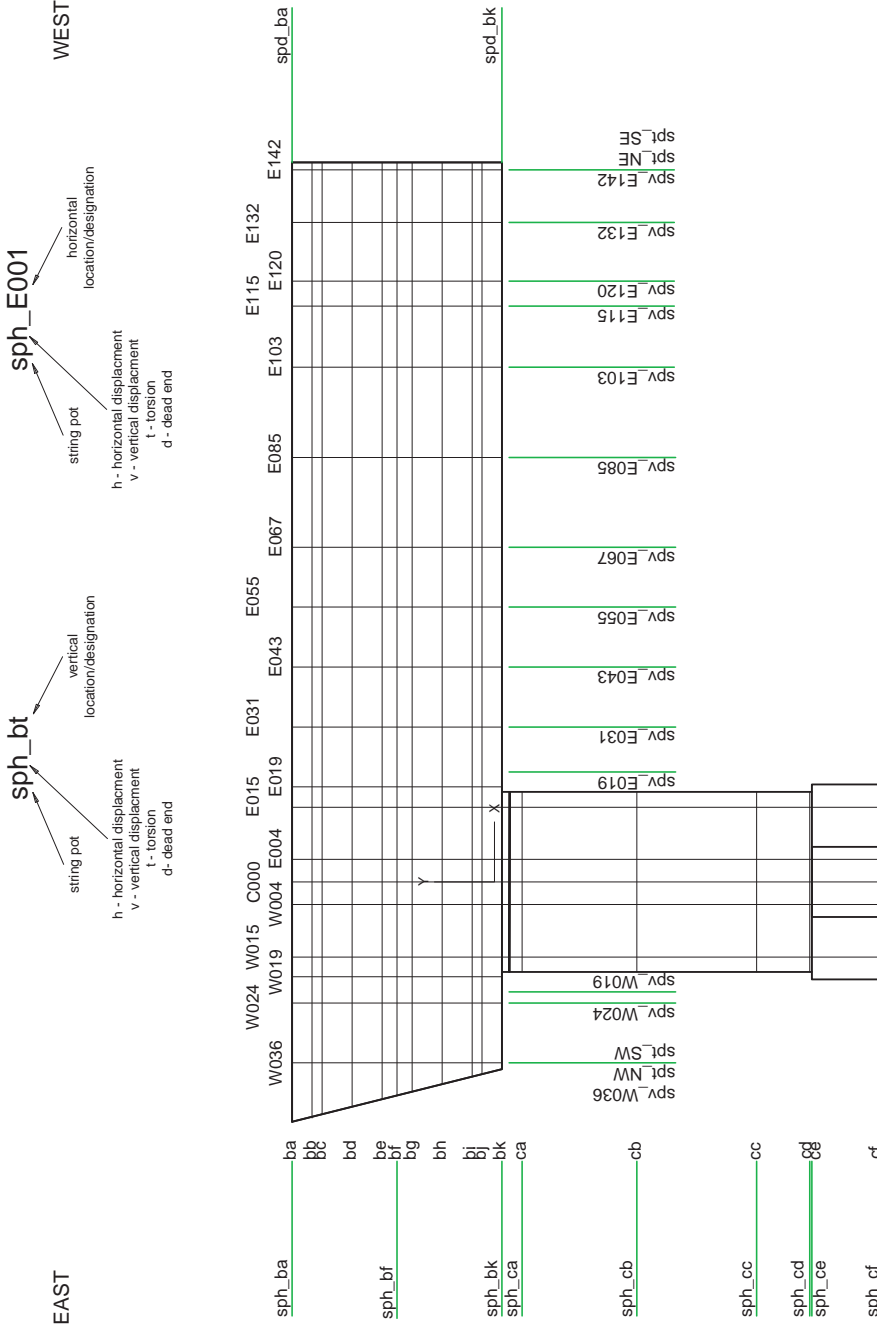
TITLE:

Phase 1  
Instrumentation Plan  
String Pot | S. Elev

SHEET#:

2 of 11

FRONT VIEW

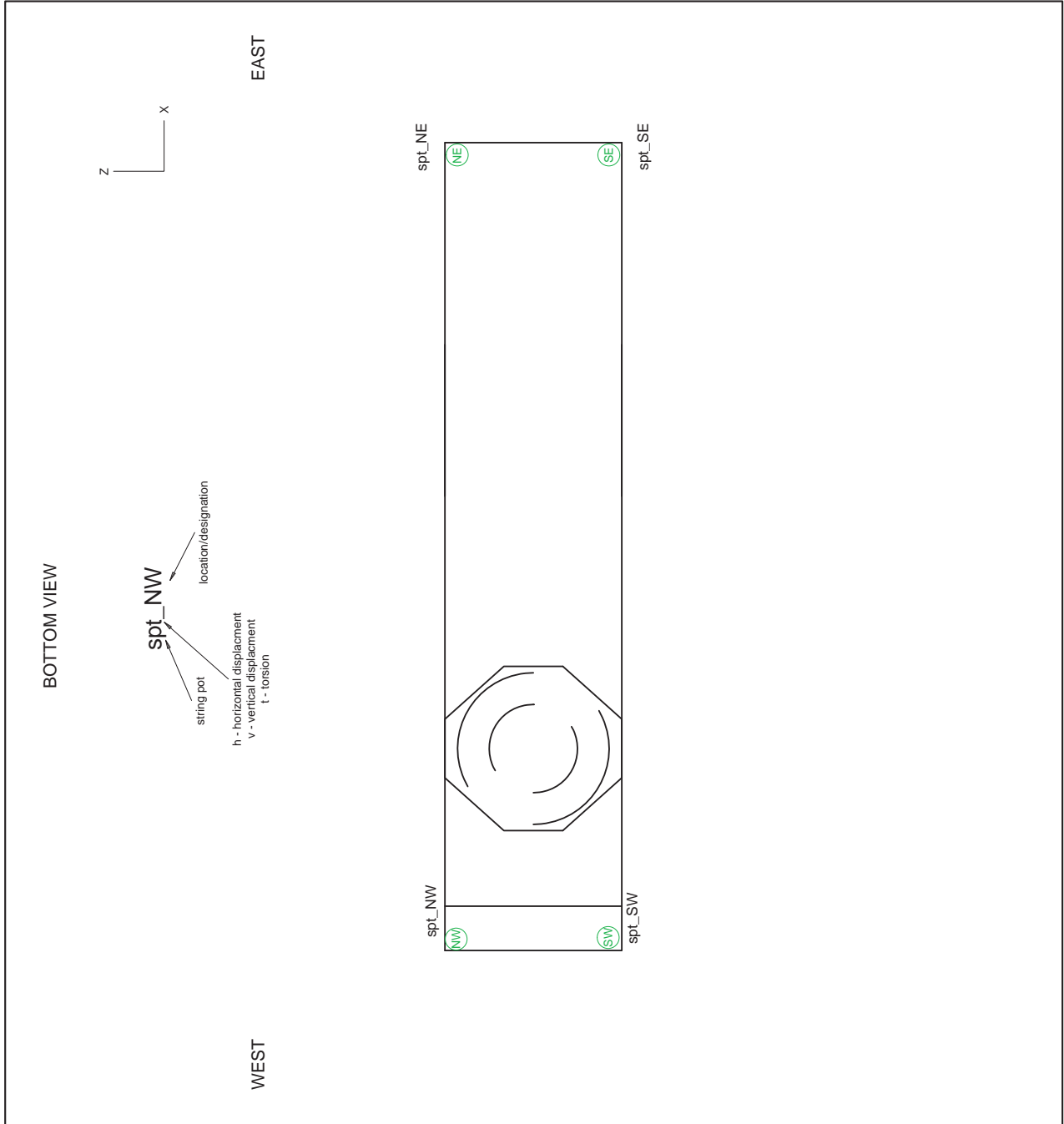






**TXDOT 0-6863  
Phase 1  
Precast Prestensioned Bent Caps**

PROJECT NO:	0-6863
DATE:	28-Aug-17
VERSION:	V-1
DRAWN BY:	J. LEE
SCALE:	N.T.S.
TITLE:	<b>Phase 1 Instrumentation Plan String Pot   Bottom</b>
SHEET#:	3 of 11

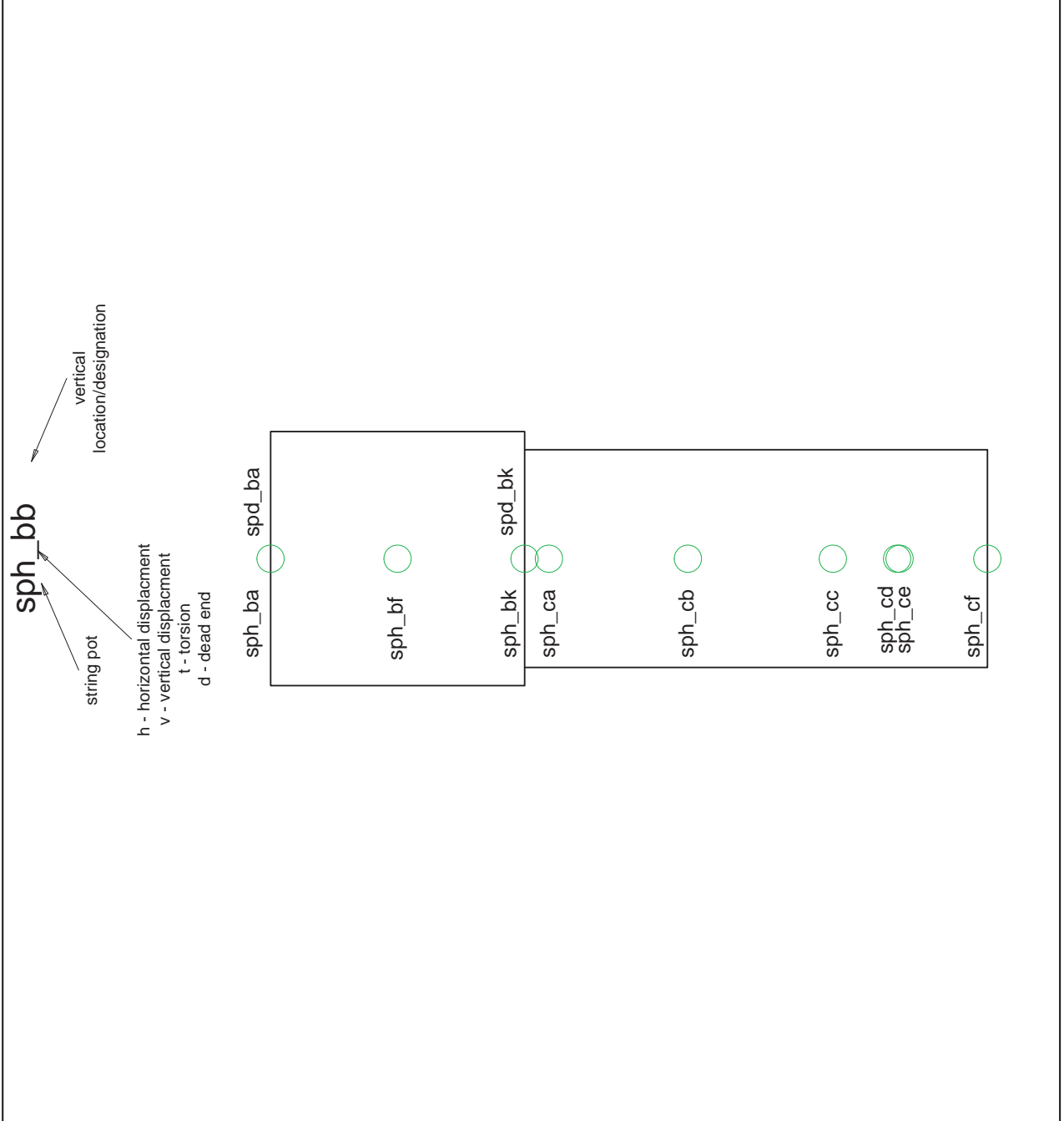
F:\Kevin Yeibem Cap Project\Kevin Yeibem\04\Drawings\in KY Thesis\Instrumentation 2\_15\_17 11x17.dwg August 28, 2017 4:35 PM





 <b>ZACHRY DEPARTMENT OF CIVIL ENGINEERING</b> TEXAS A&M UNIVERSITY	 <b>Texas A&amp;M Transportation Institute</b>	<b>Precast Prestensioned Bent Caps</b> <b>TXDOT 0-6863</b> <b>Phase 1</b>			
		PROJECT NO: 0-6863 DATE: 28-Aug-17 VERSION: V-1 DRAWN BY: J. LEE SCALE: N.T.S. TITLE:	<b>Phase 1</b> <b>Instrumentation Plan</b> <b>SP Battered End</b>		

August 28, 2017 - 4:35 PM  
 F:\Kevin Yoelbem Cap Project\Kevin Yoelbem\CAD\Drawings In KY Thesis\Instrumentation 2\_15\_17 11x17.dwg

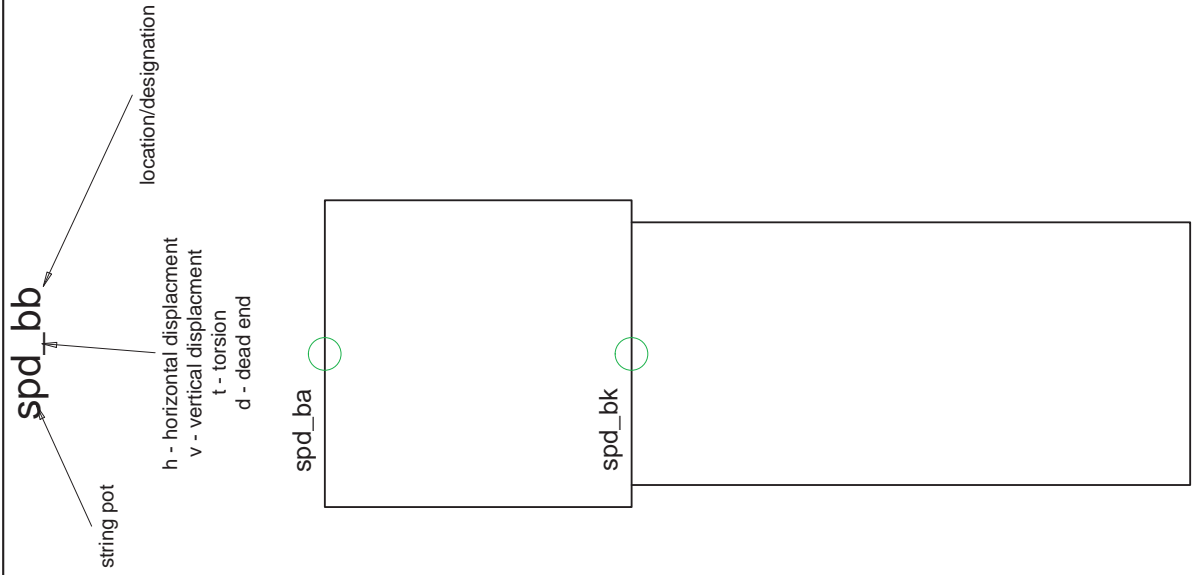




**TXDOT 0-6863  
Precast Prestensioned Bent Caps  
Phase 1**

PROJECT NO:	0-6863
DATE:	28-Aug-17
VERSION:	V-1
DRAWN BY:	J. LEE
SCALE:	N.T.S.
TITLE:	<b>Phase 1 Instrumentation Plan SP Square End</b>
SHEET#:	5 of 11

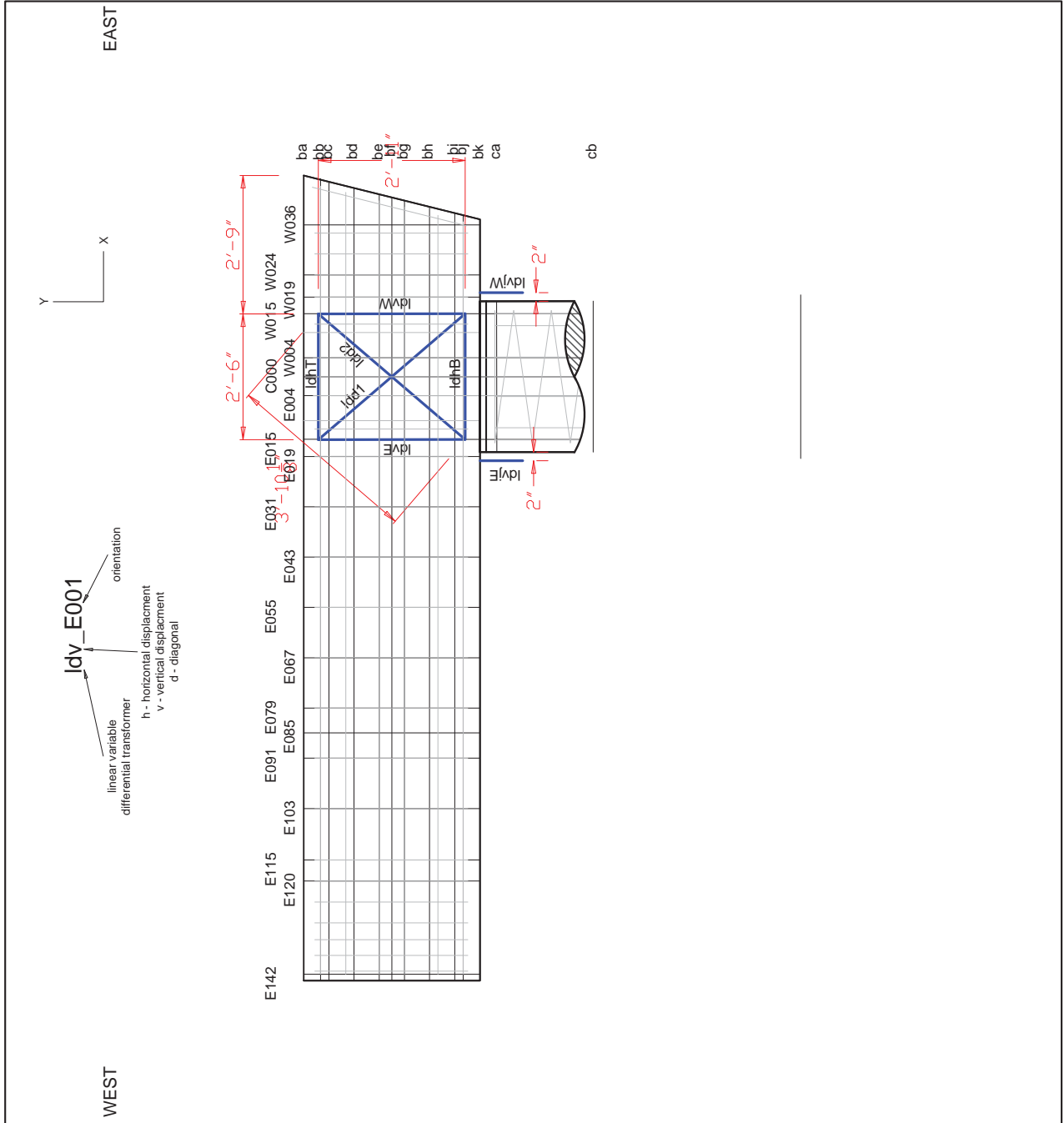
F:\Kevin Yoelbem Cap Project\Kevin Yoelbem\CAD\Drawings In KY Thesis\Instrumentation 2\_15\_17 11x17.dwg August 28, 2017 - 4:35 PM



TXDOT 0-6863  
Phase 1  
Precast Prestressed Bent Caps

PROJECT NO:	0-6863
DATE:	28-Aug-17
VERSION:	V-1
DRAWN BY:	J. LEE
SCALE:	N.T.S.
TITLE:	Phase 1 Instrumentation Plan LVDT
SHEET#:	6 of 11

F:\Kevin Yeibrem Cap Project\Kevin Yeibrem\AutoCAD\Drawings In KY Thesis\Instrumentation 2\_15\_17 11x17.dwg August 28, 2017 4:35 PM



Phase 1  
Precast Prestensioned Bent Caps  
TXDOT 0-6863

PROJECT NO: 0-6863

DATE: 28-Aug-17

VERSION: V-1

DRAWN BY: J. LEE

SCALE: N.T.S.

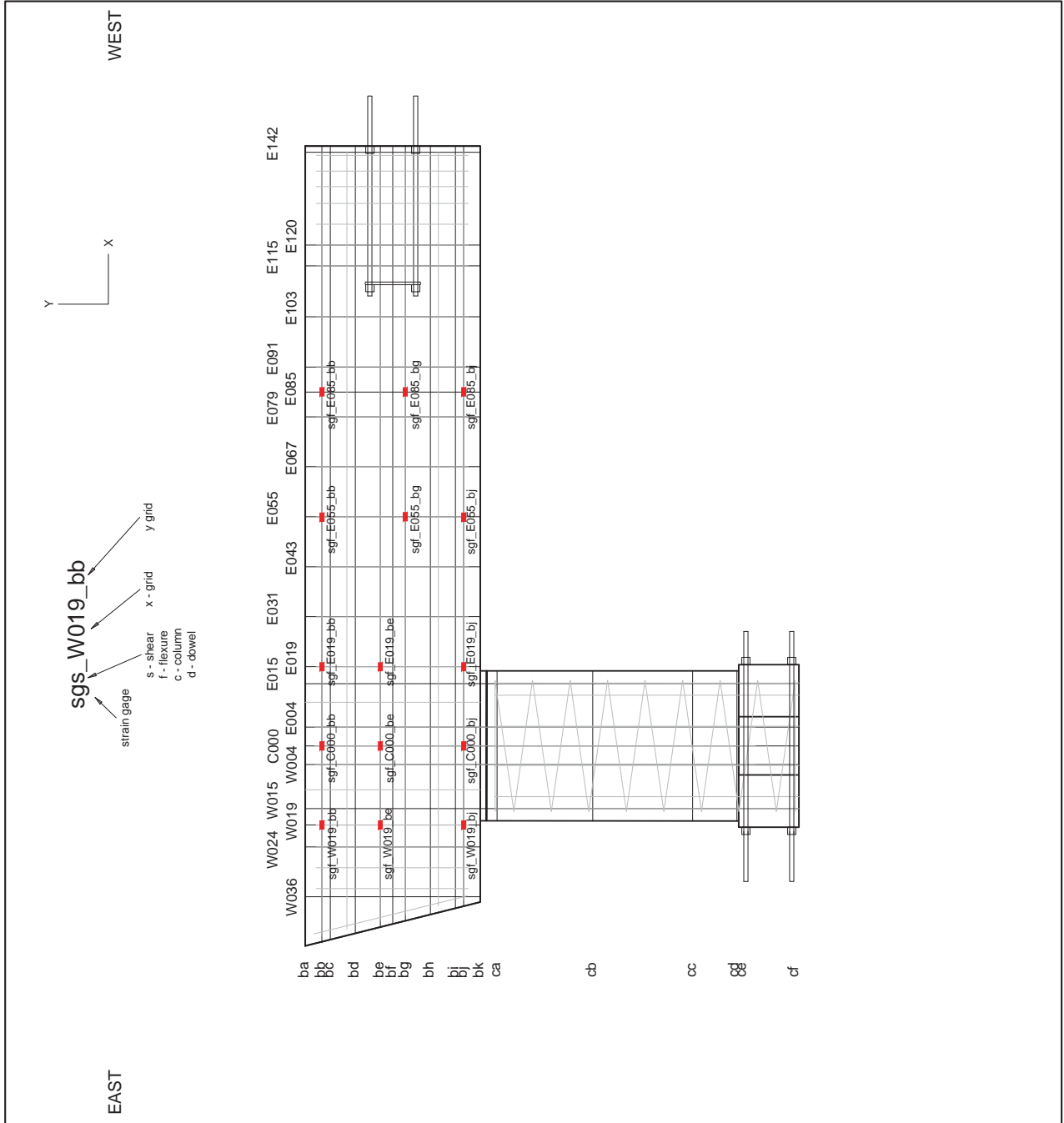
TITLE:

Phase 1  
Instrumentation Plan  
SG | Flex

SHEET#:

7 of 11

F:\Kevin Yeibem Cap Project\Kevin Yeibem\CAD\Drawings In KY\This\Instrumentation\_2\_15\_17\11x17.dwg August 28, 2017 4:35 PM



**TXDOT 0-6863**  
**Precast Prestensioned Bent Caps**  
**Phase 1**

PROJECT NO: 0-6863

DATE: 28-Aug-17

VERSION: V-1

DRAWN BY: J. LEE

SCALE: N.T.S.

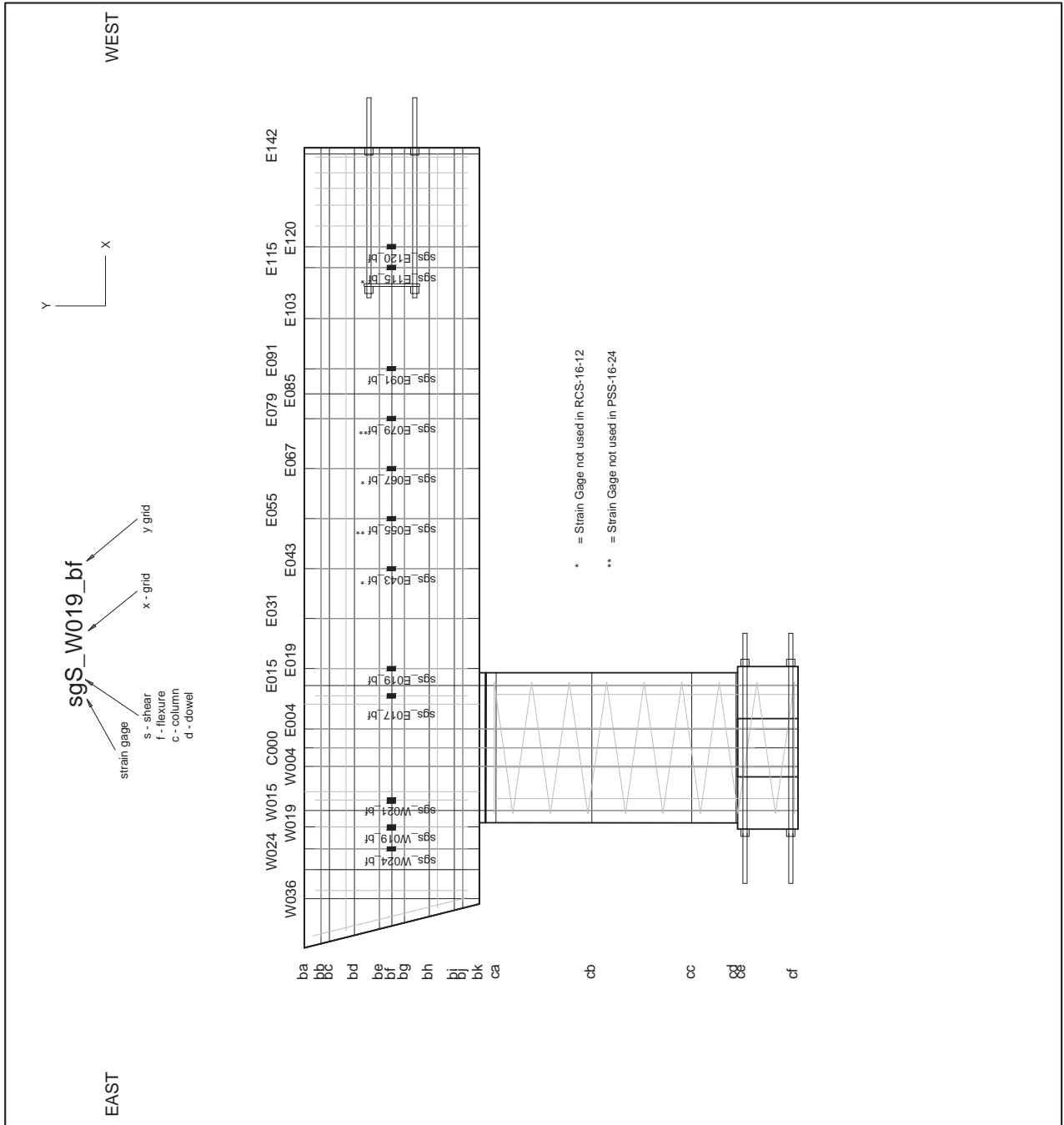
TITLE:

**Phase 1**  
**Instrumentation Plan**  
**SG | Shear**

SHEET#:

8 of 11

F:\Kevin Yeibem Cap Project\Kevin Yeibem\CAD\Drawings In KY Thesis\Instrumentation\_2\_15\_17 11x17.dwg August 28, 2017 - 4:35 PM

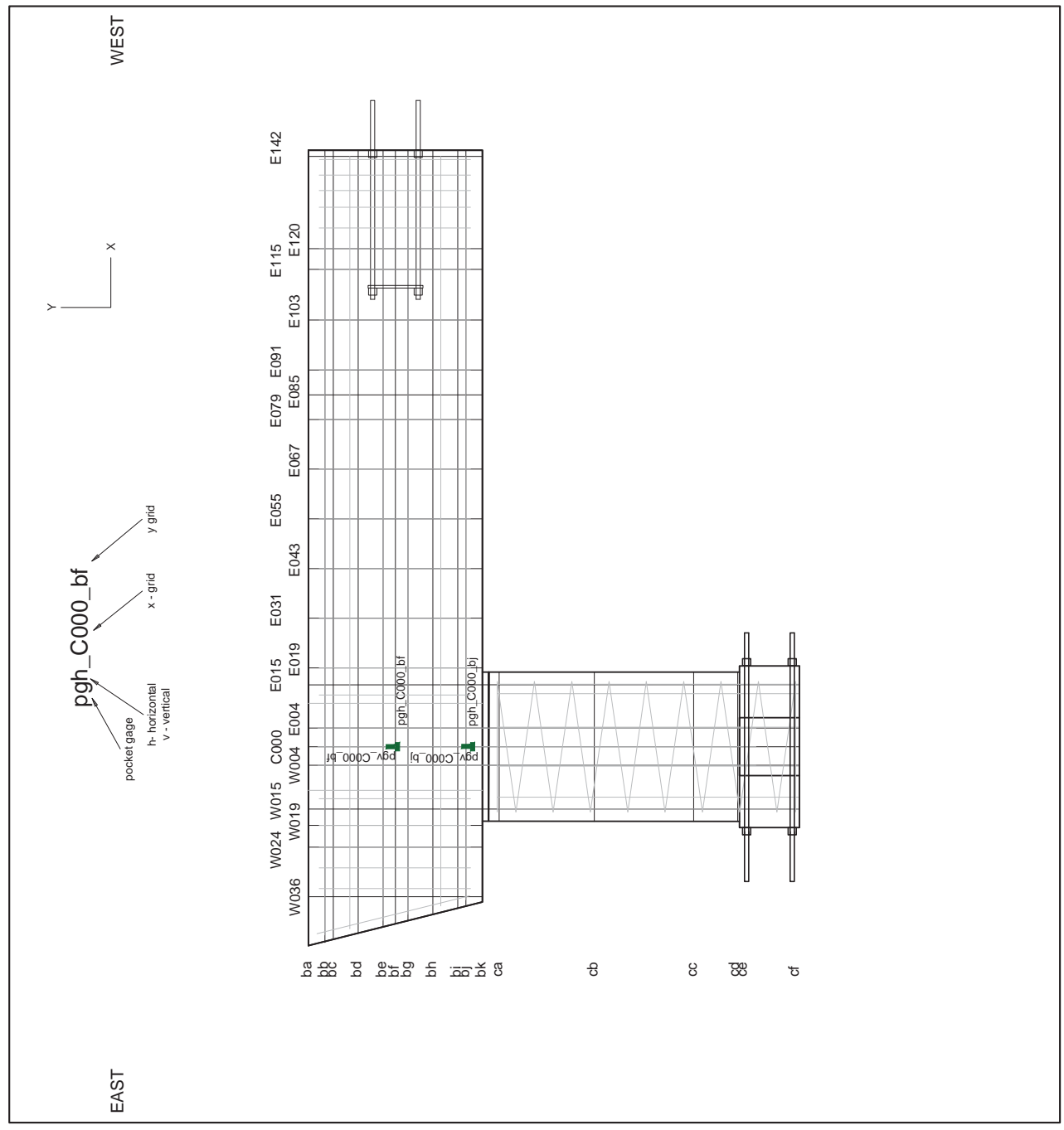




**Phase 1  
Precast Prestensioned Bent Caps  
TXDOT 0-6863**

PROJECT NO:	0-6863
DATE:	28-Aug-17
VERSION:	V-1
DRAWN BY:	J. LEE
SCALE:	N.T.S.
TITLE:	<b>Phase 1 Instrumentation Plan SG   Pocket</b>
SHEET#:	9 of 11

August 28, 2017 - 4:35 PM F:\Kevin Yeibem Cap Project\Kevin Yeibem\CAD\Drawings In KY Thesis\Instrumentation 2\_15\_17 11x17.dwg





ZACHRY DEPARTMENT OF  
CIVIL ENGINEERING  
TEXAS A&M UNIVERSITY



**Precast Prestensioned Bent Caps  
Phase 1  
TXDOT 0-6863**

PROJECT NO: 0-6863

DATE: 28-Aug-17

VERSION: V-1

DRAWN BY: J. LEE

SCALE: N.T.S.

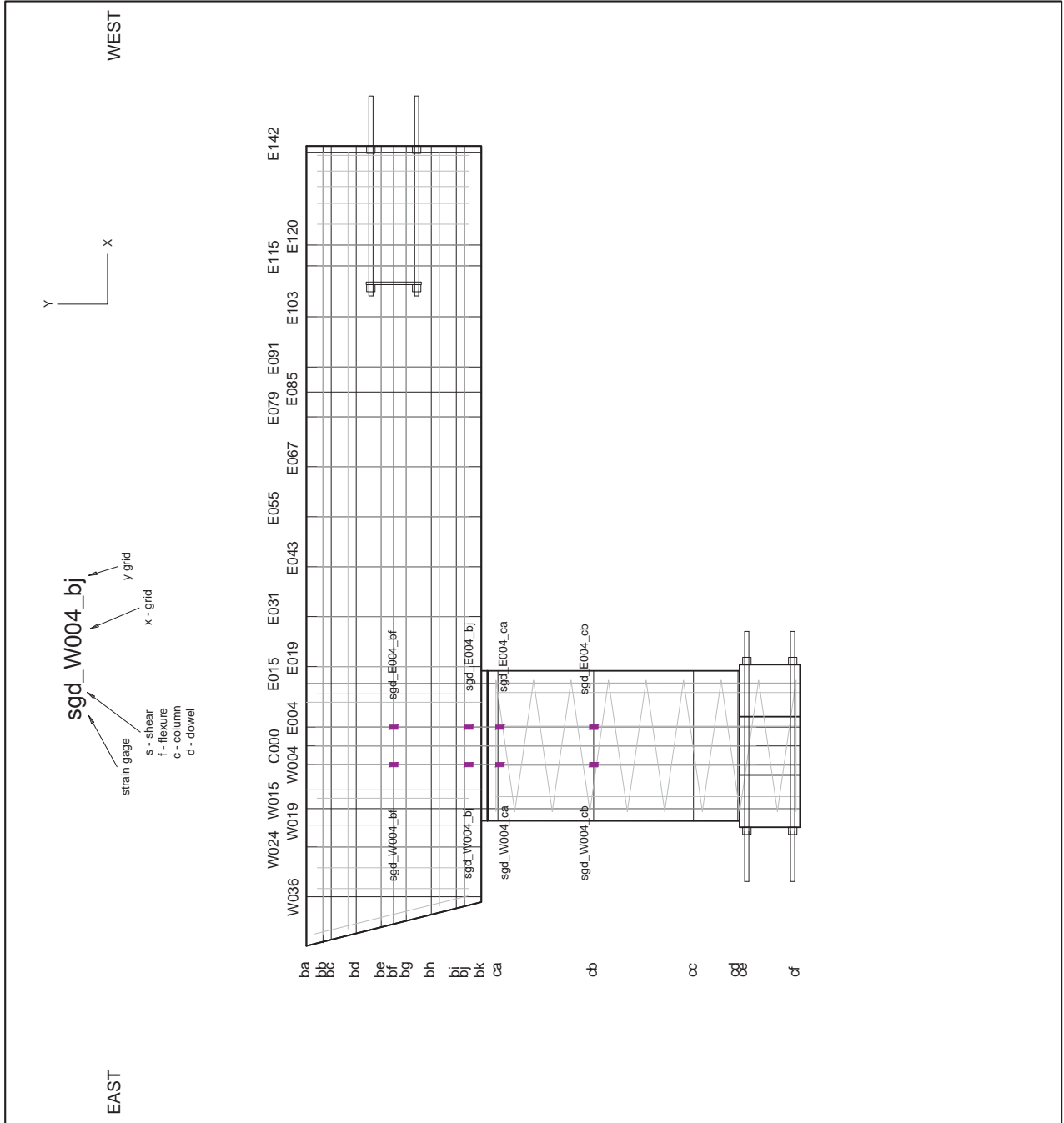
TITLE:

**Phase 1  
Instrumentation Plan  
SG | Dowel**

SHEET#:

10 of 11

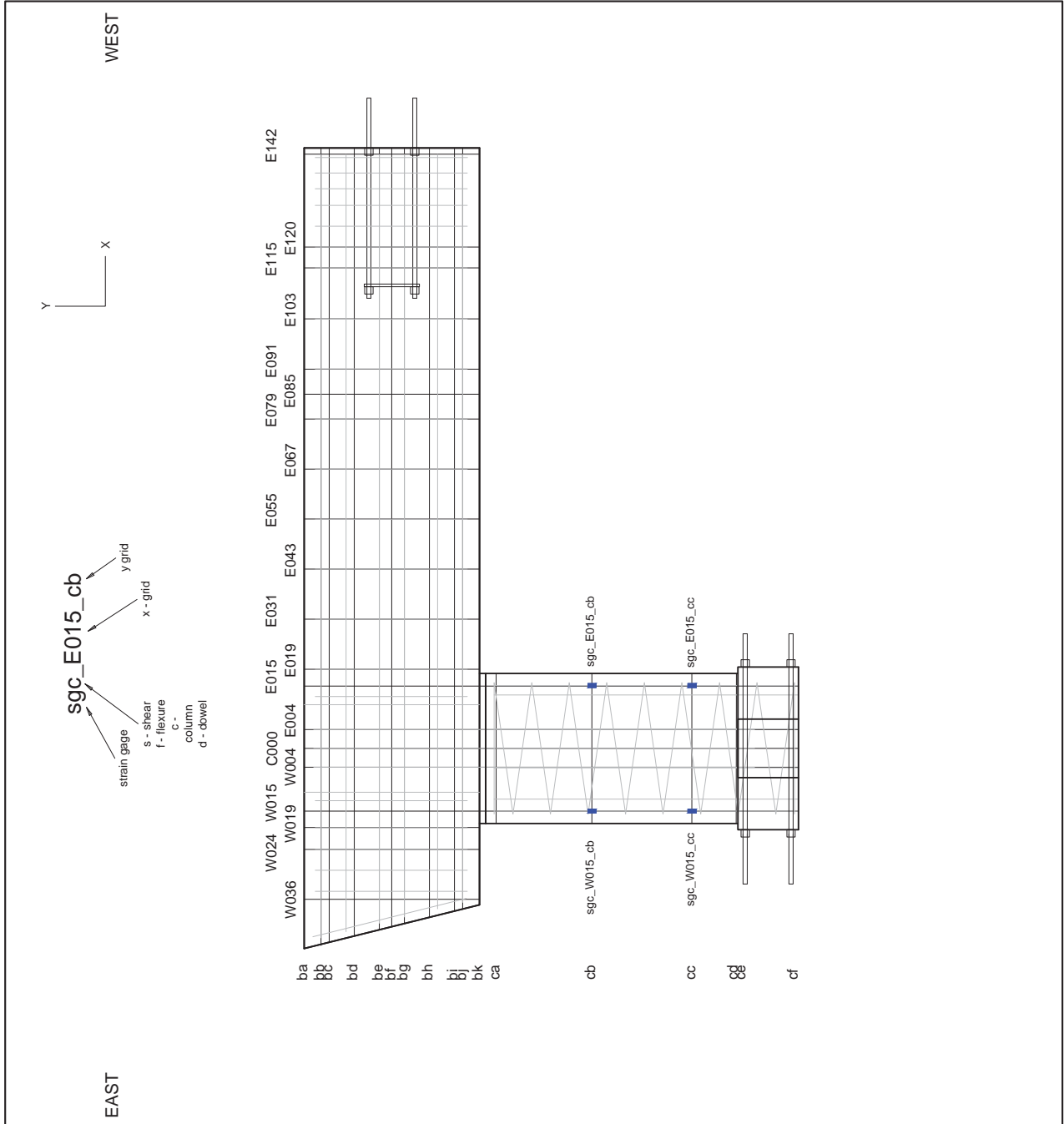
F:\Kevin Yeibrem Cap Project\Kevin Yeibrem\CAD\Drawings In\KT Thesis\Instrumentation\_2\_15\_17\11x17.dwg August 28, 2017 4:35 PM



**Phase 1**  
**Precast Prestensioned Bent Caps**  
**TXDOT 0-6863**

PROJECT NO:	0-6863
DATE:	28-Aug-17
VERSION:	V-1
DRAWN BY:	J. LEE
SCALE:	N.T.S.
TITLE:	Phase 1 Instrumentation Plan SG   Column
SHEET#:	11 of 11

F:\Kevin Yeibem Cap Project\Kevin Yeibem\CAD\Drawings\in\KT\Thesis\Instrumentation\_2\_15\_17\11x17.dwg August 28, 2017 4:35 PM







ZACHRY DEPARTMENT OF  
CIVIL ENGINEERING  
TEXAS A&M UNIVERSITY



# Precast Prestressed Bent Caps TXDOT 0-6863 Phase 2

PROJECT NO: 0-6863

DATE: 25-Aug-17

VERSION: V-1

DRAWN BY: J. LEE

SCALE: N.T.S.

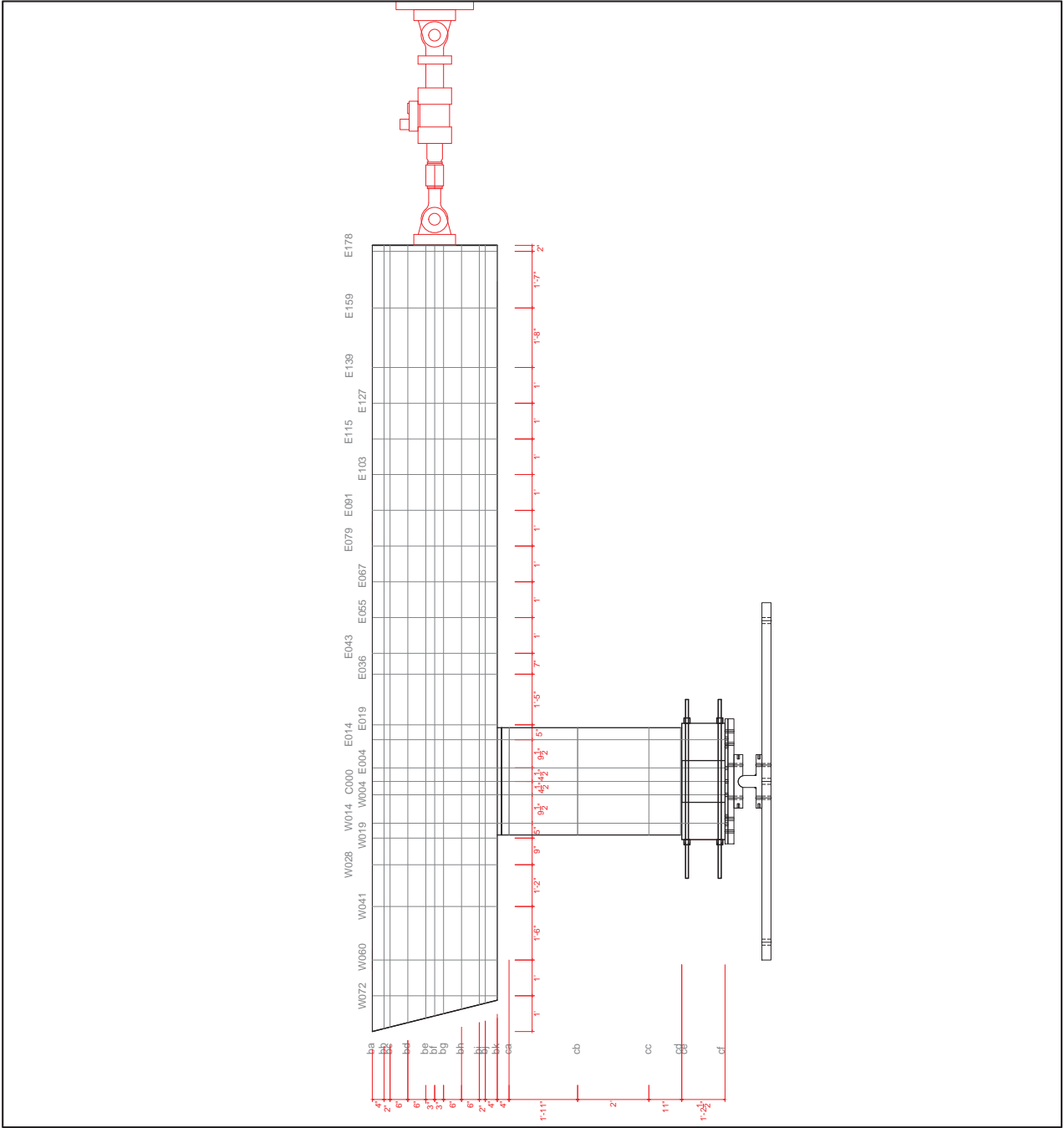
TITLE:

Phase 2  
Instrumentation Plan  
Grid Line

SHEET#:

1 of 9

C:\Users\jckee\Desktop\Texas A&M\Research\0-6863 Prestressed Bent Caps\CAD Final\Instrumentation 0\_13\_17.dwg August 25, 2017 - 9:55 AM





ZACHRY DEPARTMENT OF  
CIVIL ENGINEERING  
TEXAS A&M UNIVERSITY



**Precast Prestensioned Bent Caps  
Phase 2**

PROJECT NO: 0-6863

DATE: 25-Aug-17

VERSION: V-1

DRAWN BY: J. LEE

SCALE: N.T.S.

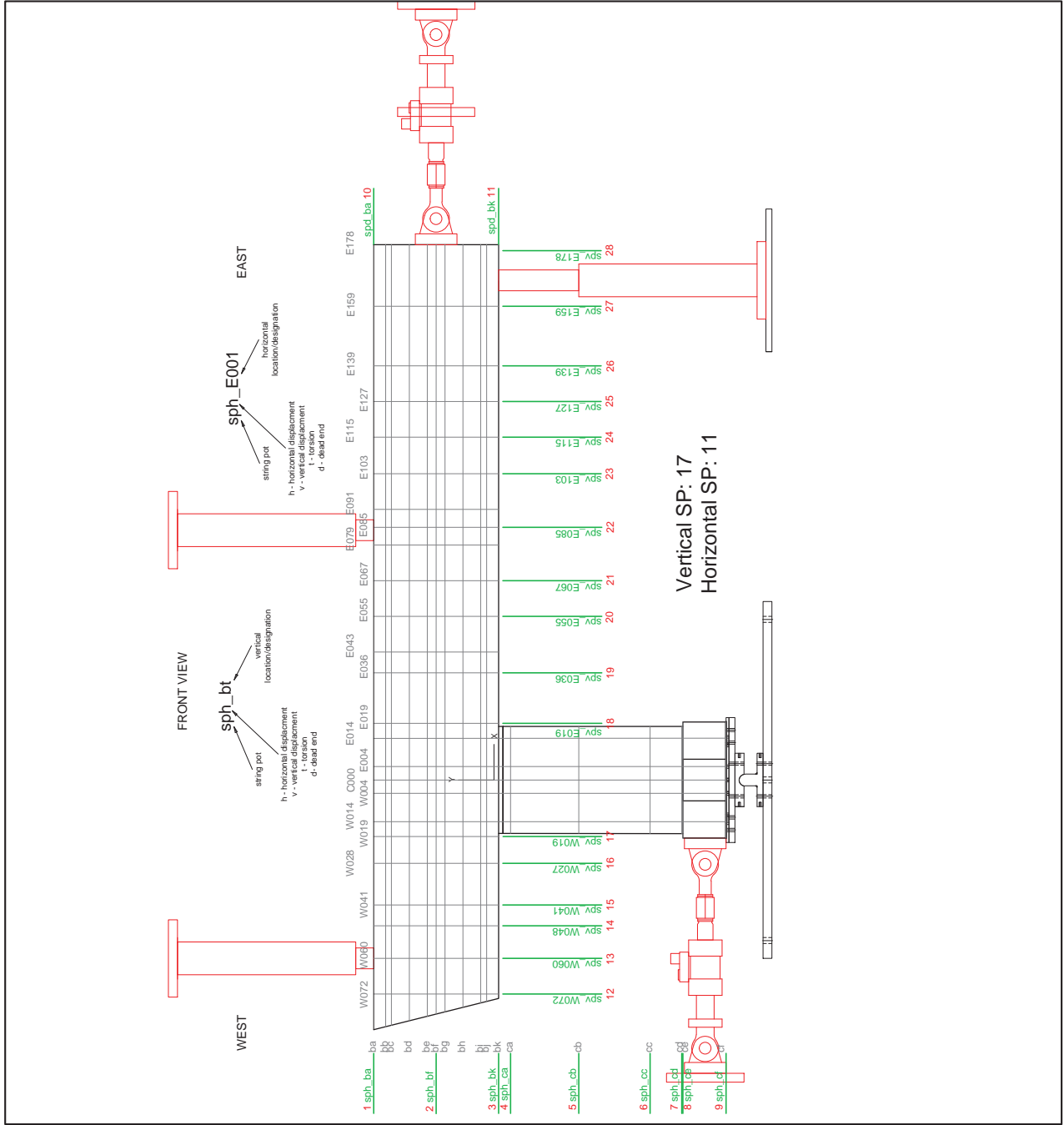
TITLE:

**Phase 2  
Instrumentation Plan  
String Pot | S. Elev**

SHEET#:

2 of 9

C:\Users\mckeet\Desktop\Texas A&M\Research\0-6863 Precressed Bent Caps\CAD Final\Instrumentation 0\_13\_17.dwg August 25, 2017 - 9:55 AM





ZACHRY DEPARTMENT OF  
CIVIL ENGINEERING  
TEXAS A&M UNIVERSITY



**TXDOT 0-6863  
Precast Prestensioned Bent Caps  
Phase 2**

PROJECT NO: 0-6863

DATE: 25-Aug-17

VERSION: V-1

DRAWN BY: J. LEE

SCALE: N.T.S.

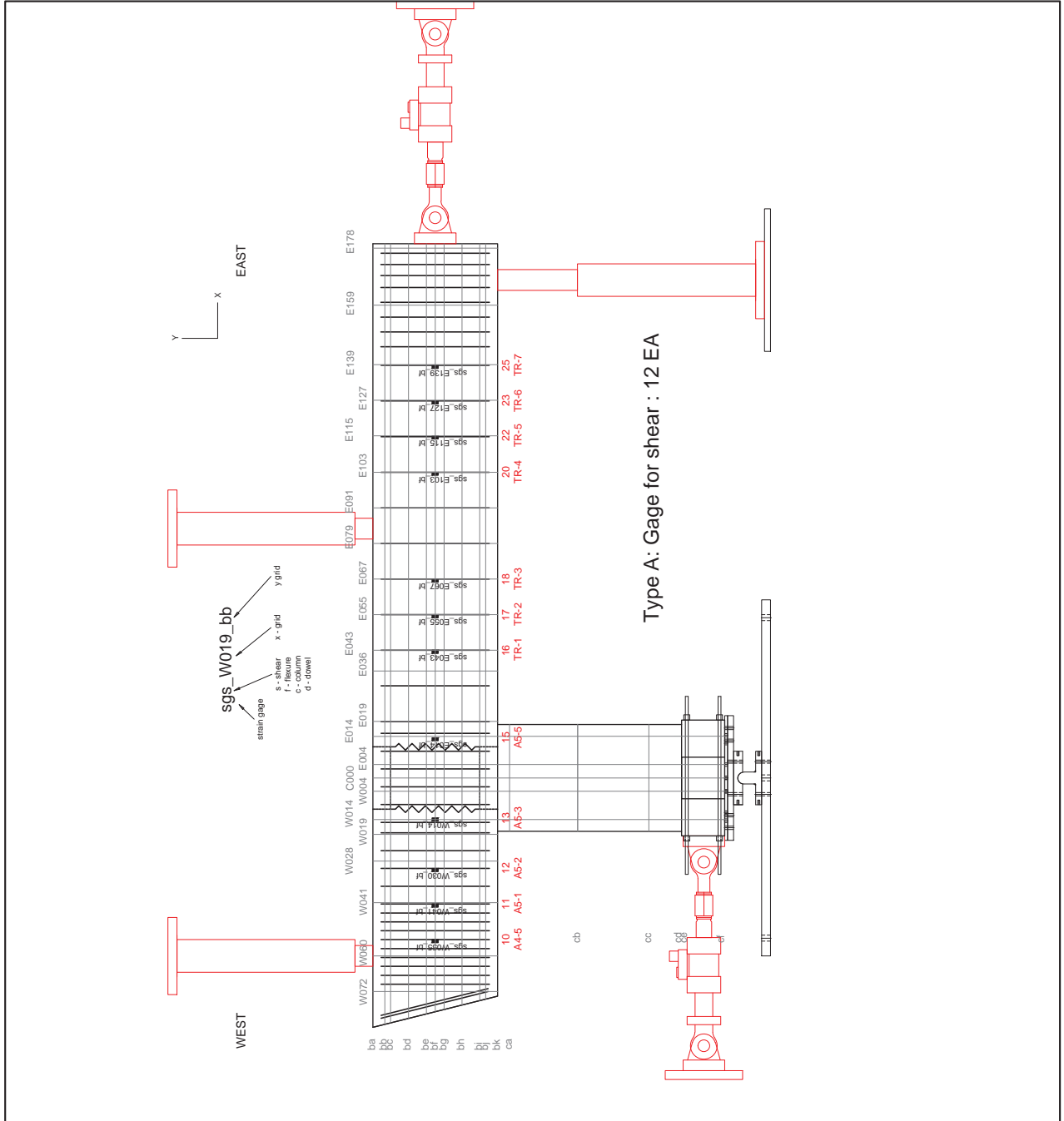
TITLE:

**Phase 2  
Instrumentation Plan  
PSV-28A SG Shear**

SHEET#:

3 of 9

C:\Users\mckeet\Desktop\Texas A&M\Research\0-6863 Prestressed Bent Caps\CAD Final\Instrumentation 0\_13\_17.dwg August 25, 2017 - 9:55 AM





ZACHRY DEPARTMENT OF  
CIVIL ENGINEERING  
TEXAS A&M UNIVERSITY



# Phase 2 Precast Prestressed Bent Caps TXDOT 0-6863

PROJECT NO: 0-6863

DATE: 25-Aug-17

VERSION: V-1

DRAWN BY: J. LEE

SCALE: N.T.S.

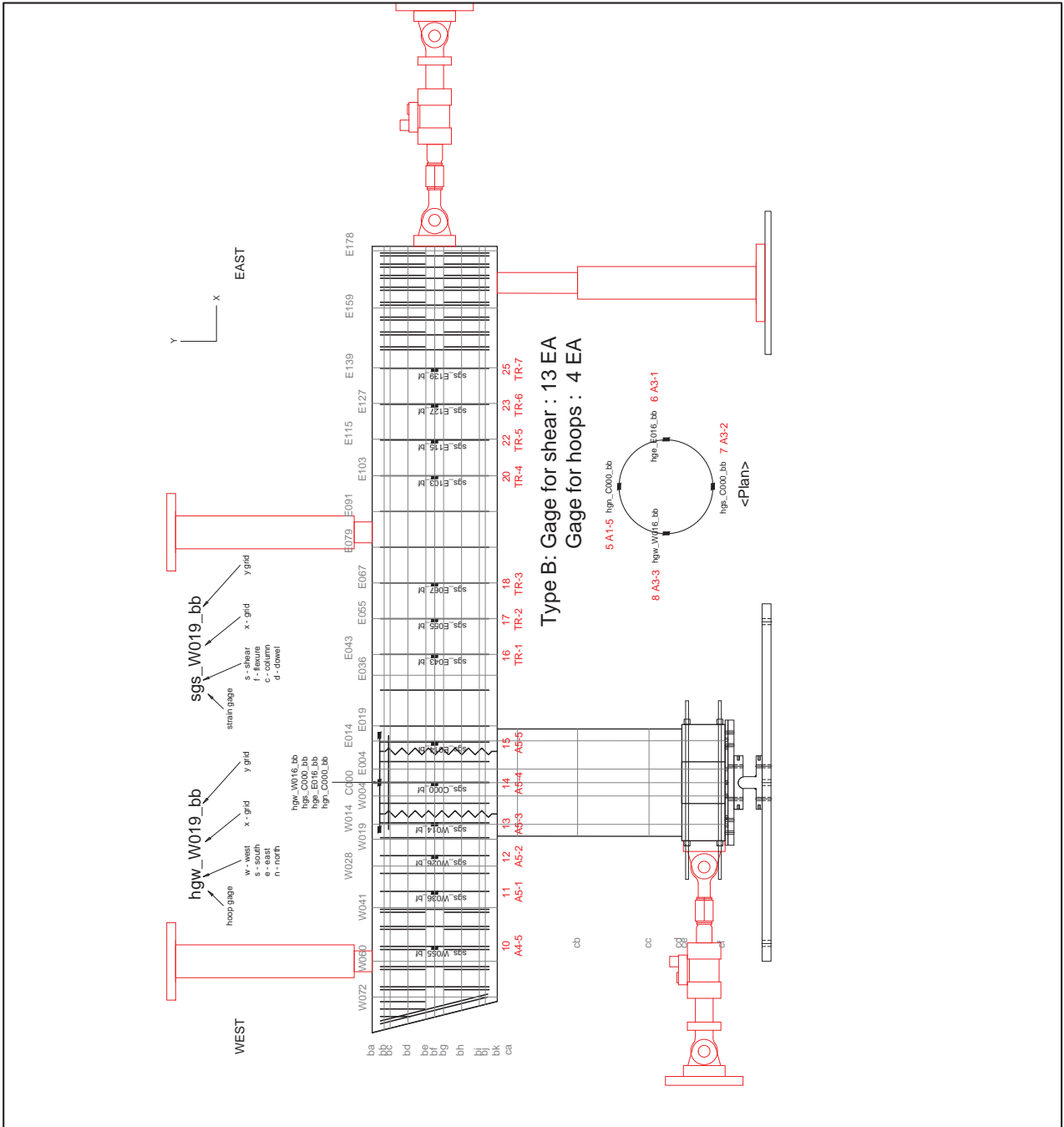
TITLE:

**Phase 2  
Instrumentation Plan  
PSV-28B SG Shear**

SHEET#:

4 of 9

C:\Users\j-mcke\Desktop\Texas A&M\Research\0-6863 Prestressed Bent Caps\CAD Final\Instrumentation 0\_13\_17.dwg August 25, 2017 - 9:55 AM





ZACHRY DEPARTMENT OF  
CIVIL ENGINEERING  
TEXAS A&M UNIVERSITY



## TXDOT 0-6863 Precast Prestensioned Bent Caps Phase 2

PROJECT NO: 0-6863

DATE: 25-Aug-17

VERSION: V-1

DRAWN BY: J. LEE

SCALE: N.T.S.

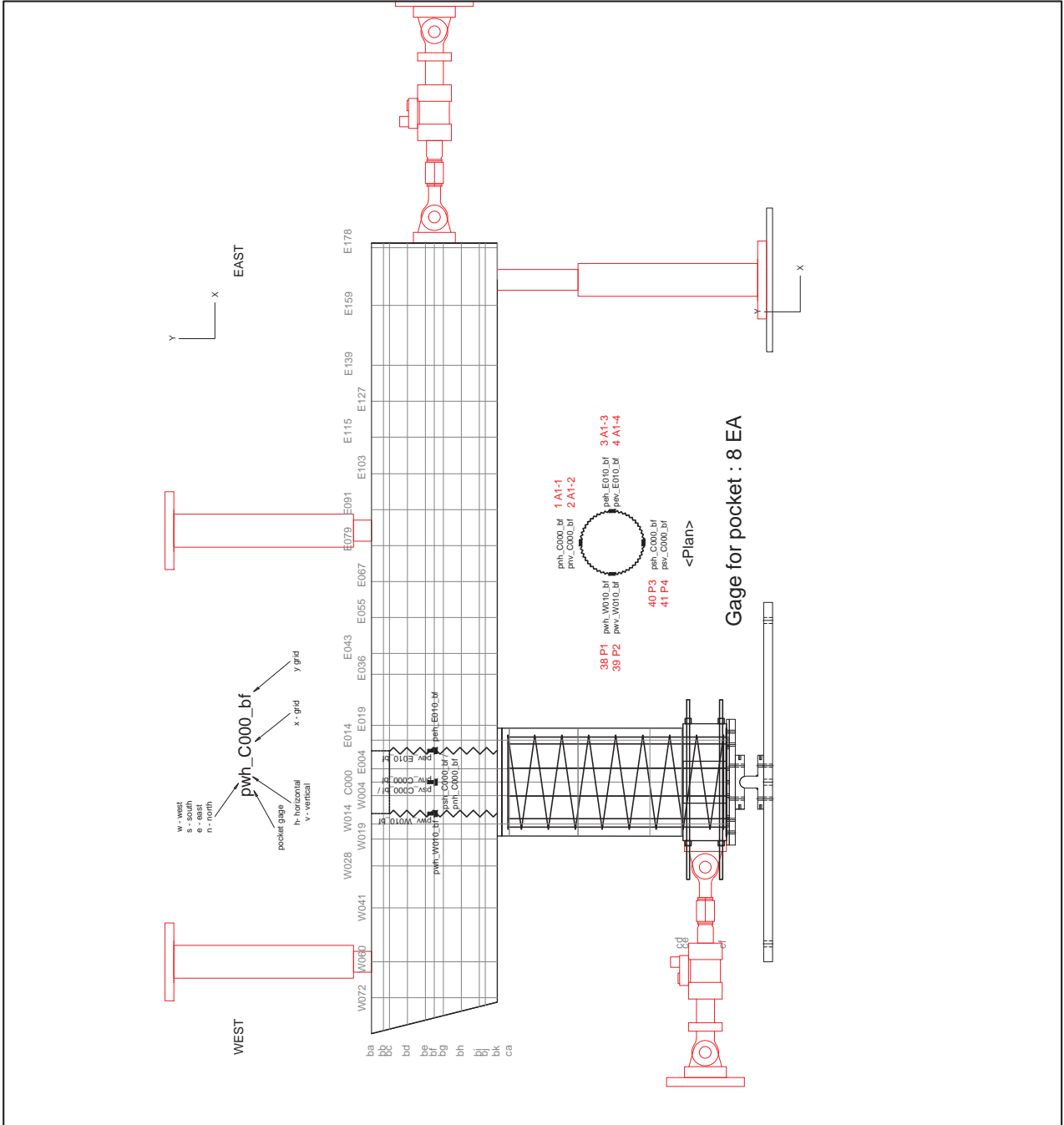
TITLE:

**Phase 2  
Instrumentation Plan  
SG Pocket**

SHEET#:

5 of 9

C:\Users\mckeet\Desktop\Texas A&M\Research\0-6863 Prestressed Bent Caps\CAD Final\Instrumentation 0\_13\_17.dwg August 25, 2017 - 9:55 AM





ZACHRY DEPARTMENT OF  
CIVIL ENGINEERING  
TEXAS A&M UNIVERSITY



**TXDOT 0-6863  
Precast Prestensioned Bent Caps  
Phase 2**

PROJECT NO: 0-6863

DATE: 25-Aug-17

VERSION: V-1

DRAWN BY: J. LEE

SCALE: N.T.S.

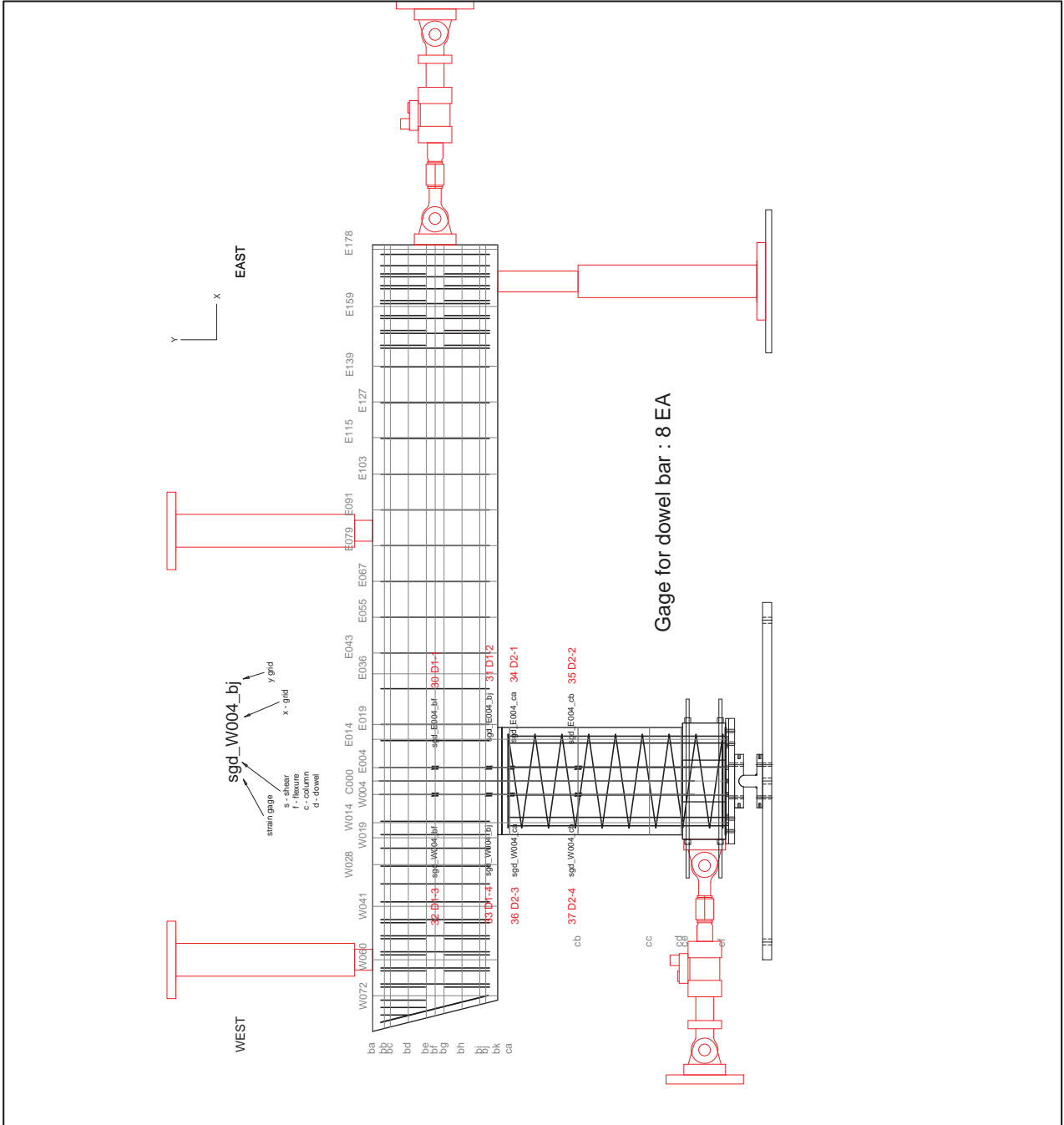
TITLE:

**Phase 2  
Instrumentation Plan  
SG Dowel Bars**

SHEET#:

6 of 9

C:\Users\mckee\Desktop\Texas A&M\Research\0-6863 Prestressed Bent Caps\CAD Final\Instrumentation 0\_13\_17.dwg August 25, 2017 - 9:55 AM





ZACHRY DEPARTMENT OF  
CIVIL ENGINEERING  
TEXAS A&M UNIVERSITY



**TXDOT 0-6863  
Precast Prestressed Bent Caps  
Phase 2**

PROJECT NO: 0-6863

DATE: 25-Aug-17

VERSION: V-1

DRAWN BY: J. LEE

SCALE: N.T.S.

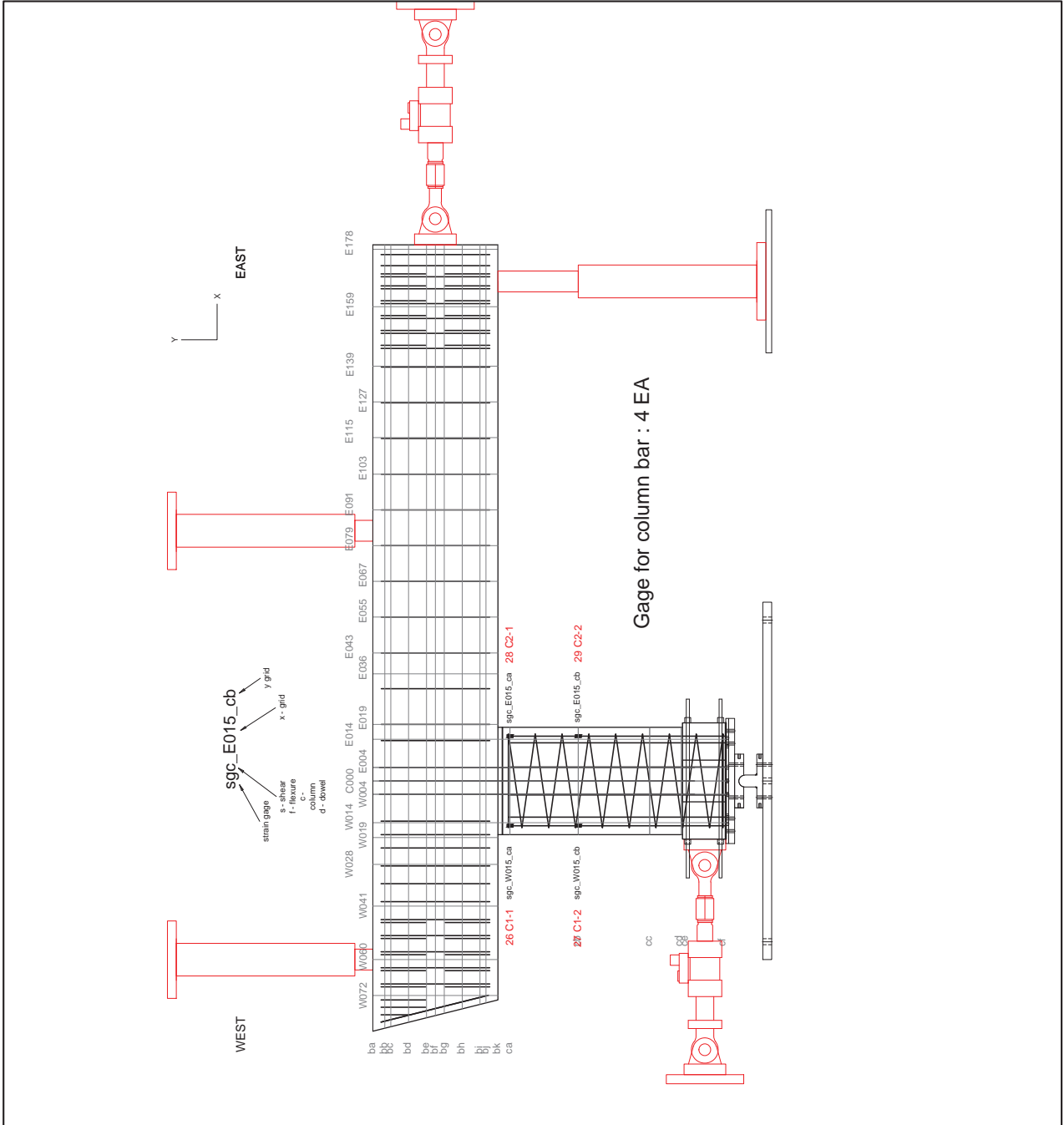
TITLE:

**Phase 2  
Instrumentation Plan  
SG Column**

SHEET#:

7 of 9

C:\Users\mckeet\Desktop\Texas A&M\Research\0-6863 Prestressed Bent Caps\CAD Final\Instrumentation 0\_13\_17.dwg August 25, 2017 - 9:55 AM



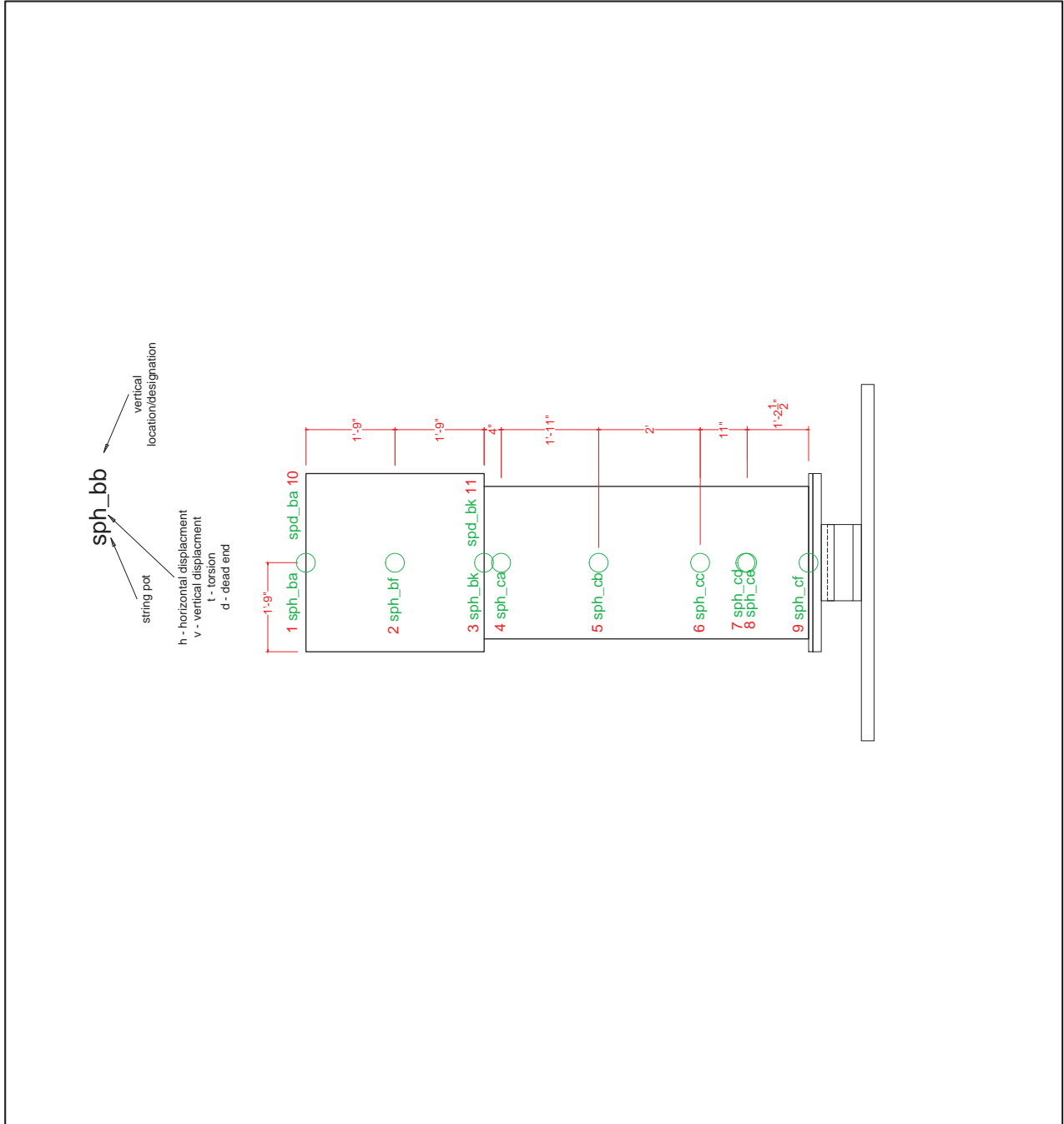
TXDOT 0-6863  
Phase 2  
Precast Prestensioned Bent Caps

PROJECT NO:	0-6863
DATE:	25-Aug-17
VERSION:	V-1
DRAWN BY:	J. LEE
SCALE:	N.T.S.
TITLE:	

Phase 2  
Instrumentation Plan  
SP Battered End

SHEET#:  
8 of 9

C:\Users\mckeet\Desktop\Texas A&M\Research\0-6863 Prestressed Bent Caps\CAD Final\Instrumentation 0\_13\_17.dwg August 25, 2017 - 9:55 AM



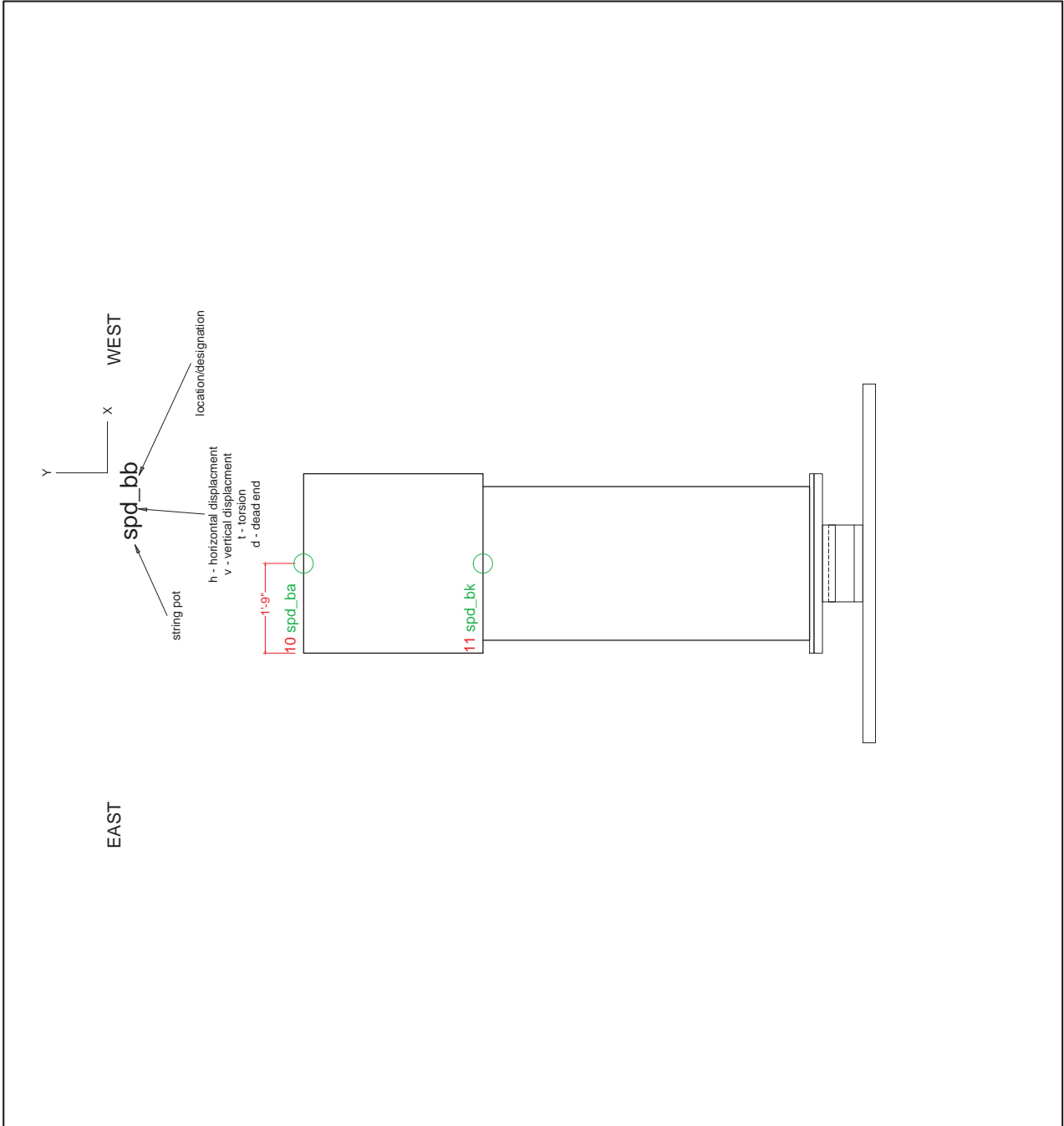




**TXDOT 0-6863  
Phase 2  
Precast Prestensioned Bent Caps**

PROJECT NO:	0-6863
DATE:	25-Aug-17
VERSION:	V-1
DRAWN BY:	J. LEE
SCALE:	N.T.S.
TITLE:	<b>Phase 2 Instrumentation Plan SP Square End</b>
SHEET#:	9 of 9

C:\Users\mckeet\Desktop\Texas A&M\Research\0-6863 Prestressed Bent Caps\CAD Final\Instrumentation 0\_13\_17.dwg August 25, 2017 - 9:55 AM



## **APPENDIX E: LOAD SEQUENCE**



**Table E-1. Loading Sequence – RCS-16-12**

<b>Dates</b>	<b>Loads</b>	<b>Cracks Measured</b>	<b>Creep (hrs)</b>	<b>Unload (kips)</b>
Day 1 10/10/2016	No loads (System check)			
Day 2 10/12/2016	Dead		1	
	SLS	✓		
	ULS	✓		0
Day 3 10/13/2016	SLS	✓		
	ULS	✓	6	270/160/0
Day 4 10/14/2016	Dead	✓		
	SLS	✓		
	ULS	✓		
	140% ULS	✓		
	Max Positive	✓		0
Day 5 10/17/2016	Joint Opening	✓		0
Day 6 10/28/2016	Joint Closing	✓		
	Max Negative	✓		0
	Joint Opening			
	Max Positive			
Day 7 10/31/2016	Failure			0

**Table E-2. Loading Sequence – PSS-16-24**

<b>Dates</b>	<b>Loads</b>	<b>Cracks Measured</b>	<b>Creep (hrs)</b>	<b>Unload (kips)</b>
Day 1 2/22/2017	Dead			
	SLS	✓		
	ULS	✓		
	ULS	✓	2.5	160
	140% ULS	✓		
Day 2 2/27/2017	Max Positive	✓		160 / 0
	Joint Opening	✓		0
	Joint Closing	✓		0
	Max Negative	✓		
	Failure			0

**Table E-3. Loading Sequence – PSS-16-12**

<b>Dates</b>	<b>Loads</b>	<b>Cracks Measured</b>	<b>Creep (hrs)</b>	<b>Unload (kips)</b>
Day 1 11/30/2016	Dead			
	SLS	✓		160
	ULS	✓	1	
	140% ULS	✓		
	Max Positive	✓		160/0
	Joint Opening	✓		
	Joint Closing	✓		
	Max Negative	✓		0
Day 2 12/2/2016	Dead	✓		
	SLS	✓		
	ULS	✓		
	140% ULS	✓		270/160
	Failure			0

**Table E-4. Loading Sequence – PSV-16-12**

<b>Dates</b>	<b>Loads</b>	<b>Cracks Measured</b>	<b>Creep (hrs)</b>	<b>Unload (kips)</b>
Day 1 1/6/2017	Dead			
	SLS	✓		
	ULS	✓		160 / 0
Day 2 1/9/2017	ULS	✓	1.5	
	140% ULS	✓		270 / 160 / 0
Day 3 1/12/2017	Max Positive	✓		160 / 0
	Joint Opening	✓		
	Joint Closing	✓		
	Max Negative	✓		
	Failure			

**Table E-5. Loading Sequence – PSV-28A**

<b>Dates</b>	<b>Loads</b>	<b>Cracks Measured</b>	<b>Creep (hrs)</b>	<b>Unload (kips)</b>
Day 1 6/29/2017	Dead			
	SLS	✓		
	ULS	✓		160 / 0
Day 2 6/30/2017	Joint Opening	✓		0
	Joint Closing	✓		0
	ULS	✓		
	140% ULS	✓		160 / 0
	Max. Positive	✓		0
	Max Negative / Failure			

**Table E-6. Loading Sequence – PSV-28B**

<b>Dates</b>	<b>Loads</b>	<b>Cracks Measured</b>	<b>Creep (hrs)</b>	<b>Unload (kips)</b>
Day 1 7/26/2017	Dead			
	SLS	✓		
	ULS	✓		160 / 0
	Joint Opening	✓		0
	Joint Closing			0
	SLS			0
Day 2 7/27/2017	ULS	✓		
	140% ULS	✓		160 / 0
	Max. Positive	✓		80 / 0
	Max Negative / Failure			
	Max Positive / Failure			

